UNIVERSIDADE FEDERAL DE MINAS GERAIS
INSTITUTO DE CIÊNCIAS BIOLÓGICAS
DEPARTAMENTO DE BIOQUÍMICA E IMUNOLOGIA
LABORATÓRIO DE GNOTOBIOLOGIA E IMUNOLOGIA

THE ROLE OF GP91^{PHOX}-DERIVED REACTIVE OXYGEN SPECIES IN THE INFECTION CAUSED BY *LEISHMANIA AMAZONENSIS*: IMPLICATIONS RELATIVE TO THE SITE OF INFECTION

Eric Henrique Roma de Lima

Orientadora: Prof. Dr. Leda Quercia Vieira

Co-orientadores: Dr. Nathan Peters
Dr. David Sacks

Outubro, 2013

UNIVERSIDADE FEDERAL DE MINAS GERAIS
INSTITUTO DE CIÊNCIAS BIOLÓGICAS
DEPARTAMENTO DE BIOQUÍMICA E IMUNOLOGIA
LABORATÓRIO DE GNOTOBIOLOGIA E IMUNOLOGIA

THE ROLE OF GP91^{PHOX}-DERIVED REACTIVE OXYGEN SPECIES IN THE INFECTION CAUSED BY *LEISHMANIA AMAZONENSIS*: IMPLICATIONS RELATIVE TO THE SITE OF INFECTION

Tese apresentada para o programa de pós-graduação em Bioquímica e Imunologia do departamentos de Bioquímica e Imunologia do Instituto de Ciências Biológicas da Universidade Federal de Minas Gerais como pré-requisito para obtenção do título de doutorado em Imunologia.

Eric Henrique Roma de Lima

Orientadora: Prof. Dr. Leda Quercia Vieira

Co-orientadores: Dr. Nathan Peters
Dr. David Sacks

Outubro, 2013

Dedicatória

Para minha mãe Lu, a qual devo tudo que sou hoje. Sempre ao meu lado com apoio e carinho... não importando o caminho e sacrifícios realizados sempre me ajudou a trilhar meus caminhos. Se estou aqui hoje é tudo devido a você. Terei por você gratidão eterna, pois nunca conseguirei retribuir o que sempre fez por mim.

Para minha esposa Juliana, minha companheira há 9 anos... sempre me apoiando tanto dentro como fora do laboratório. Com amor e carinho nas horas difíceis me ajudou a ultrapassar obstáculos e é responsável por grande parte da minha felicidade. Sem você ao meu lado, este trabalho seria bem mais difícil.

Para Leda, por me dar a oportunidade de realização deste trabalho e ter me acolhido em seu laboratório. Por ter confiado em mim e me ajudado em tudo que precisei. Por ter me dado a oportunidade de conhecer os EUA e vivenciar a ciência do jeito que ela deveria ser no Brasil. Obrigado Leda, por todo apoio dado neste tempo. Essa tese não existiria sem você.

A todas vocês, eu lhes dedico este trabalho!!!

Agradecimentos

Ao Dr. David Sacks por ter me aceitado em seu laboratório e ter fornecido todo suporte necessário para realização de grande parte deste trabalho, além dos ensinamentos sobre ciência os quais me ajudaram bastante a crescer como cientista.

Ao Dr. Nathan Peters, que acompanhou de perto meu trabalho nos EUA, com grandes contribuições técnicas e intelectuais, sendo de fato muito importante para a realização deste trabalho.

Ao NIH , por ter me dado a oportunidade de conhecer como é feito ciência de ponta no maior instituto de pesquisa do mundo.

À UFMG por ter sido responsável por toda minha formação como cientista, desde a graduação há dez anos atrás até os dias de hoje.

Aos integrantes do laboratório do Dr. David Sacks nos EUA, pelo apoio e a ótima convivência.

A todos os integrantes do LAGI pela ótima convivência nestes anos. Lugar este que com certeza foi um dos melhores ambientes nos quais vivi.

Aos amigos dos EUA, principalmente Helton e Ester, que me acolheram com carinho em sua casa no início da minha jornada fazendo com que eu me sentisse mais confortável mesmo longe da família.

Aos amigos da UFMG com os quais sempre pude contar. Sempre me trataram com carinho e por isso me sinto muito bem quando estou nessa universidade.

Aos amigos de bases, sempre bem dispostos e companheiros de ajuda mútua durante os tempos das disciplinas, fazendo com que aquele período fosse mais prazeroso mesmo tendo mais de 10 artigos para ler para no dia seguinte.

Aos amigos de 2003/02 pelos bons momentos que passamos juntos durante nossa graduação dentro e fora do ambiente acadêmico.

Aos meus familiares pelo incentivo, carinho e pelos momentos prazerosos que passamos juntos.

Aos familiares da Juliana, especialmente seus pais Namira e Márcio os quais também considero meus pais. Pelo acolhimento e por me tratarem como filho quando estou junto a eles.

Aos meus cães Raica, Julie, Princesa e Sadam por seu amor incondicional. Como disse Darwin: "O próprio homem não pode expressar o amor e humildade por sinais externos, tão claramente como um cachorro, quando ele encontra seu amado mestre". Por serem a válvula de escape de problemas através da demonstração do carinho que sempre estão dispostos a fornecer. Sempre que estou com eles me sinto bem e feliz. Afinal, você não precisa de psiquiatra se tem um cachorro.

A todos vocês, meu muito obrigado!!!

Table of Contents

List of Figures ..... **IX**
List of Tables ..... **XVIII**
List of Abbreviations ..... **XIX**
1. Resumo ..... **XXII**
1. Abstract ..... **XXIV**
2. Introduction **26**
3. Literature review **29**
3.1. Leishmania genus taxonomy **30**
3.2. Epidemiology **31**
3.3. Disease **34**
3.3.1. Etiological agent and clinical aspects 34
3.3.2. Biological cycle 35
3.3.3. Immune response 38
3.3.4. Evasion of immune response by the parasite 42
3.4. NADPH oxidases, production of ROS and inflammation **43**
3.5. ROS and Leishmania **48**
3.5.1. Production of ROS by host cells in *Leishmania* infections 48
3.5.2. Importance of ROS in the direct killing of *Leishmania* 50
3.5.3. Subversive mechanisms used by *Leishmania* to avoid damage by ROS 51
3.6. Relevance of the work and explanation of thesis structure **52**
4. Part one: subcutaneous inoculation with *L. amazonensis* in gp91$^{phox-/-}$ mice promote changes in inflammatory response to infection **55**
4.1. Objectives **56**
4.1.1. General objective 56
4.1.2. Specific objectives 56
4.2. Material and Methods **57**
4.2.1. Parasites 57
4.2.2. Mice 57
4.2.3. Luminometry assay 57
4.2.4. Infection with *L. amazonensis* 58
4.2.5. Euthanasia, collection of blood and organs 58
4.2.6. Parasite load quantification 58

4.2.7. Real time PCR 59
4.2.8. Generation of *L. amazonensis* antigen of (LA*La*) 61
4.2.9. ELISA for cytokine measurements 61
4.2.10. ELISA for anti-*Leishmania* IgG_1, IgG_{2a} and total IgG 61
4.2.11. Flow cytometry 62
4.2.12. Mieloperoxidase assay for neutrophil numbers inference 63
4.2.13. Phagocytic and microbicidal activity of macrophages in infections *in vitro* 64
4.2.14. Cytokine and chemokine production and nitrite measurements from peritoneal macrophages cultures 64
4.2.15. Statistical analysis 65
4.3. Results 65
4.3.1. *L. amazonensis* induces respiratory burst in macrophages from C57BL/6 mice 65
4.3.2. $Gp91^{phox-/-}$ mice show different lesion development, but present similar parasite loads in footpads and dLNs to those of WT mice. 66
4.3.3 WT mice express IL-1β in footpads at chronic phase of *L. amazonensis* infection when compared to $gp91^{phox-/-}$. 68
4.3.4. Mice lacking $gp91^{phox}$ induces a higher Th17 response in acute phase of *L. amazonensis* infection 70
4.3.5. Deficiency in ROS production is not compensated by increase in iNOS expression 72
4.3.6. ROS alter the influx of innate and adaptive immune cells to the site of infection and the dynamics of dLNS expansion in mice subcutaneously infected with *L. amazonensis* 73
4.3.7. ROS increased the migration and decreased clearance of neutrophils immediately after infection with *L. amazonensis* 78
4.3.8. ROS influence anti-*Leishmania* IgG antibodies secretion during *L. amazonensis* infection 79
4.3.9. Activated $gp91^{phox-/-}$ macrophages secrete higher levels of inflammatory cytokines in *L. amazonensis* infection *in vitro* 81
4.3.10. ROS promotes increased parasite loads in macrophages infected with *L. amazonensis in vitro* 85
5. Part two: Site of *L. major* infection determines dominant host cell phenotype 87
5.1. Objectives 88
5.1.1. General objective 88
5.1.2. Specific objectives 88
5.2. Material and Methods (the following text is taken from a manuscript in preparation) 88
5.2.1. Mice 88
5.2.2. Parasites 88

5.2.3. Parasite preparation and inoculations 89
5.2.4. Processing of tissues 90
5.2.5. Immunolabeling and flow cytometry 90
5.2.6. Statistical analysis 91
5.3. Results 91
5.3.1. The patterns of cell migration changes according to the site of *L. major* infection 91
5.3.2. The site of inoculation determines the cells involved in the initial uptake of *L. major* ... 99
5.3.3. Infection at the intradermal site elicited higher cell activation and inflammatory response in the acute phase of *L. major* infection 105
6. Part three: Reactive oxygen species (ROS) control the inflammation in *L. amazonensis* intradermal infection impairing neutrophil necrosis 110
6.1. Objectives 111
6.1.1. General objective 111
6.1.2. Specific objectives 111
6.2. Material and Methods 112
6.2.1. Mice 112
6.2.2. Parasites 112
6.2.3. Infection with *L. amazonensis* 113
6.2.4. Euthanasia and tissue processing 114
6.2.5. Parasite load quantification 114
6.2.6. Quantitative Real time PCR 115
6.2.6. Generation of *L. amazonensis* antigen (LA*La*) 116
6.2.8. Flow cytometry 116
6.2.9. Apoptosis assessment 117
6.2.10. Statistical analysis 118
6.3. Results 118
6.3.1. Intradermally inoculated gp91$^{phox-/-}$ mice exhibit higher inflammation in *L. amazonensis* infection 118
6.3.2. ROS do not influence the killing of *L. amazonensis in vivo* at the site of infection, but is required to control parasite loads in dLNs 120
6.3.3. ROS impairs neutrophil accumulation at the site of inoculation with *L. amazonensis* .. 121
6.3.4. Gp91$^{phox-/-}$ mice do not presented with alterations in T lymphocytes during *L. amazonensis* infection 126
6.3.5. Gp91$^{phox-/-}$ and WT mice produce similar levels of cytokines by T lymphocytes during *L. amazonensis* infection 128

6.3.6. ROS influence expansion of dLN cells during *L. amazonensis* infection 130

6.3.7. Gp91$^{phox-/-}$ mice *L. amazonensis* induces higher expression of CXCL2 at initial stages of infection in gp91$^{phox-/-}$ mice 137

6.3.8. In the absence of ROS neutrophils die by necrosis at the site of infection with *L. amazonensis* 138

6.3.9. Enhanced migration of inflammatory cells to the site of inoculation in gp91$^{phox-/-}$ during acute infection 143

6.3.10. The absence of gp91^{phox} changes the dynamics of *L. amazonensis* infected cells early during infection 146

6.3.11. Gp91$^{phox-/-}$ mice have deficiency in apoptotic neutrophil death at early stages of *L. amazonensis* infection 148

7. Discussion 150

8. Bibliographic references 171

List of Figures

Figure 1: Taxonomy of *Leishmania* genus (Banuls et al., 2007). Underlined species have had their taxonomic classification questioned. Twenty species of the thirty known are pathogenic for humans. 31

Figure 2: World distribution of tegumentar form of leishmaniasis. The blue-dotted areas indicate endemic zones between 2005 to 2009. WHO/CNTD. Map: Control of Neglected Tropical Diseases of the World Health Organization, 2010. 32

Figure 3: World distribution of visceral form of leishmaniasis. The blue-dotted areas indicate endemic zones between 2005 to 2009. WHO/CNTD. Map: Control of Neglected Tropical Diseases of the World Health Organization, 2010. 33

Figure 4: Distribution of *Leishmania* species causing cutaneous leishmaniasis in the Brazilian territory. *L. amazonensis* and *L. braziliensis* are responsible for the majority of cutaneous leishmaniasis cases in Brazil. Map: Ministry of Health of Brazil, Manual of leishmaniasis vigilance, 2007. 34

Figure 5: Biological cycle of *Leishmania major* (Peters and Sacks, 2009). (A) The cycle starts with the vector feeding on the blood from infected host. With the blood, the vector ingests amastigotes that are inside macrophages in the skin. In the insect gut, the amastigotes are released by macrophage lysis and differentiate into promastigote forms. They attach to the gut wall and start to replicate. (B) In the new blood meal, these metacyclic forms are inoculated in the skin of the host and (C) they are phagocyted majorly by neutrophils. (D) The neutrophils fail to kill phagocyted parasites, start the apoptotic process and (E) release the parasites together with apoptotic bodies into the extracellular environment. (D) Phagocytosis by the macrophages/DCs of these apoptotic bodies and parasites (F) induce the production of anti-inflammatory mediators such as TGF-β, which favor the survival of the parasite in the newly infected cells. (F and G) The fusion of phagosome membrane containing parasites with lysosomes in the host cells creates favorable environment to differentiation of the promastigotes into amastigotes, which start cycles of replication inside of the infected cells. (G) The amastigotes replicate indefinitely inside of macrophages until their lysis. Thus, many amastigotes are released in the extracellular environment and then are phagocyted by others phagocytic cells, enhancing the replication cycles. (A) Eventually, the vector might feed on contaminated host blood, re-initiating the cycle. 37

Figure 6: Models of immune responses in the infection caused by *L. major* (Gollob et al., 2008). $CD4^+$ T lymphocytes balance the activation of macrophages for *Leishmania* control. Classically, $CD4^+$ T cell subtypes Th1 and Th2 act controlling the anti-leishmanial activity in host macrophages. IL-12 and IFN-γ stimulate the differentiation of the immune response to Th1 subtype, which activate anti-leishmanial mechanisms in macrophages increasing nitric oxide ($^{\bullet}NO$) production by iNOS. IL-4, which differentiates the response into Th2, TGF-β and IL-10 inhibit the activation of macrophage promoting worsening in the disease. 38

Figure 7: Many ways of inhibition of microbicidal activities used by *Leishmania* spp. to immune response evasion. Adapted (Peters and Sacks, 2006). *Leishmania* evade the microbicidal activities of macrophages in many ways. The phagocytosis of *Leishmania* by specific CR1 and CR3, manose receptors and phosphatidylserine receptors promotes, among other responses, release of IL-10. The uptake by these receptors and IL-10 production induce downregulation of oxidative defenses by macrophages. Inside of macrophages, the *Leishmania* also inhibit the fusion with lysosomes with phagosomes via LPG and eventually gp63..... 43

Figure 8: Activation states of NADPH oxidase (Babior, 1999). On the left the inactivate state of the enzyme is represented, where the multimeric complexes are separated. Under appropriated signaling, there is a phosphorylation of p47, permitting the association of cytoplasmic complexes with transmembrane subunits to activate the enzyme, as represented on the right side..... 44

Figure 9. Production of reactive oxygen species by macrophages stimulated with *L. amazonensis*. Thioglycolate-elicited macrophages were harvested from the peritoneum of C57BL/6 mice in 3 days after stimulation. The macrophages were placed with luminol reagent and *L. amazonensis* metacyclic promastigotes (10 parasites per macrophage). The production of ROS was measured as relative light units generated by luminol oxidation, for 90 minutes. The basal production of ROS was obtained by incubating macrophages in medium. Data are from one representative experiment of 4, n=5 mice for each experiment..... 66

Figure 10. Lesion size and parasite loads in mice infected with *L. amazonensis*. Mice were infected with 1 x 10^6 metacyclic promastigote forms of *L. amazonensis* in the hind right footpad and followed for 16 weeks. (A) Footpad thickness measured weekly by, **$p<0.01$. (B) Parasite loads found in the footpads of infected mice 4, 8, 12 and 16 weeks post infection. (C) Parasite loads found in draining lymph nodes of infected mice 4, 8, 12 and 16 weeks post infection. Data are shown as mean plus/minus standard deviation (± SD) from one representative experiment of 3, n=5 for each experiment. 67

Figure 11. mRNA expression levels of cytokines in *L. Amazonensis*-infected footpads measured by qPCR. Mice were infected with 1 x 10^6 *L. amazonensis* metacyclic promastigotes in the right hind footpad and followed until 16 weeks. A, B, C, D, E, F, G and H represent the mRNA expression of IFN-γ, TNF-α, IL-4, IL-10, IL-1β, IL-6, IL-17 and CXCL1 respectively, normalized by 18S mRNA expression 4, 8, 12 and 16 weeks post infection. The results were expressed by mean ± SD, n=5, *$p<0.05$. 69

Figure 12. Cytokine production by re-stimulated dLNs of *L. amazonensis* infected mice performed by ELISA. The dLNs of infected mice were culture and re-stimulated with 50μg/ml of *L. amazonensis* antigen. After 72h, the supernatants were harvested and used to quantify cytokines by ELISA. A, B, C, D and E represent the IFN-γ, IL-12p70, IL-10, IL-6 and IL-17 secretion by dLNs of infected mice, respectively. The results were expressed by mean ± SD, n=5, *$p<0.05$ between WT and $gp91^{phox-/-}$. 71

Figure 13. iNOS mRNA expression levels in footpad and nitrite production by infected thioglycolate-elicited macrophages. (A) Mice were infected with 1 x 10^6 metacyclic promastigotes forms of *L. amazonensis* in the right hind footpad and followed for 16 weeks.

iNOS mRNA levels were normalized by 18S mRNA expression 4, 8, 12 and 16 weeks post infection. (B) Thioglycolate-elicited macrophages were harvested from WT or gp91$^{phox-/-}$ mice peritoneum 3 days after stimulation. Macrophages were infected with *L. amazonensis* metacyclic promastigotes at 10:1 for 4 hours, in the presence or absence of IFN-γ. After 48h of infection, the supernatants were collected and used to measure nitrite levels by Griess reaction. Data are shown as mean ± SD from one representative experiment of 4, n=5 for each experiment. 72

Figure 14. Flow cytometry of granulocytes present at the site of infection with *L. amazonensis*. (A) representative dot plots of the cell frequencies 4, 8, 12 and 16 weeks post infection. The figures represent the dot plots of events inside granulocyte and monocyte gate set by size and granularity of the cells. (B) graphic representation of the relative numbers of Ly6G$^+$F4/80$^-$ cells (mean ± SD, n=6 for each time point). * p<0.05 and ** p<0.01. 73

Figure 15. Flow cytometry of lymphoid cells present at the site of infection with *L. amazonensis*. (A) representative dot plots of the cell frequencies 4, 8, 12 and 16 weeks post infection. The figures represent the dot plots of events inside the lymphoid gate set by size and granularity of the cells. (B) and (C) graphic representation of the relative numbers of Ly6G$^+$F4/80$^-$ cells (mean ± SD, n=6 for each time point). *** p<0.001. 74

Figure 16. Total dLNs cell count during *L. amazonensis* infection. After 4, 8, 12 and 16 weeks of infection, dLNs were removed, macerated and the cells were resuspended in 1ml of complete RPMI medium and counted. The results are expressed as mean ± SD. *** p<0.001 (n=6 for each time point). 75

Figure 17. Flow cytometry of CD4$^+$ and CD8$^+$ cells in dLNs from mice during the *L. amazonensis* infection. After 4, 8, 12 and 16 weeks of infection, dLNs were removed, macerated and the cells were resuspended in 1ml of complete RPMI medium and counted. The cells were stained for CD4 and CD8 and read by flow cytometry. The figures represent the dot plots of events inside of lymphoid gate set by size and granularity (n=6 for each time point).. 76

Figure 18. Number of cells in white pulp of spleens during *L. amazonensis* infection. After 4, 8, 12 and 16 weeks of infection, the spleen from mice was removed, macerated with red blood cell lysis treatment and the immune cells were resuspended in 1ml of RPMI complete medium and counted. The results are expressed in average ± SD. *p<0.05 and **p<0.01 (n=6 for each time point). 77

Figure 19. Flow cytometry of CD4$^+$ and CD8$^+$ cells in spleen from mice during the *L. amazonensis* infection. After 4, 8, 12 and 16 weeks of infection, the spleen from mice was removed, macerated with red blood cell lysis buffer, the remaining cells were resuspended in 1ml of RPMI complete medium and counted. Cells were stained for CD4 and CD8 molecules and read in flow cytometry. The figures represent the dot plots of events inside of lymphoid gate set by size and granularity (n=6 for each time point). 78

Figure 20. MPO activity in mice infected with *L. amazonensis*. Mice were infected with 1 x 10^6 metacyclic promastigotes forms of *L. amazonensis* in the right hind footpad. After 6h or 72h of infection, mice were euthanized, the footpads were removed and used to perform MPO activity

assay to estimate the neutrophil numbers. Data are shown as mean ± SD from one representative experiment of 2, n=5 for each experiment, *p<0.05. 79

Figure 21. Production of anti-*Leishmania* IgG in NADPH oxidase deficient mice infected with *L. amazonensis*. Mice were infected with 1 x 10^6 metacyclic promastigote forms of *L. amazonensis* in the right hind footpad and followed until 16 weeks. After 4, 8, 12 and 16 weeks of infection, the serum was collected and ELISA to detect anti-*Leishmania* IgG was performed. A, B and C represent the absorbance found for anti-*Leishmania* IgG, IgG_1 and IgG_{2a}, respectively. The dotted lines represent the absorbance of serum of non-infected mice in dilution of 1:200, the same dilution used for the serum of the infected mice. Data are shown as mean ± SD from one representative experiment of 2, n=6 for each experiment. 81

Figure 22. Production of cytokines and chemokines in $gp91^{phox-/-}$ macrophages infected with *L. amazonensis*. Thioglycolate-elicited macrophages were infected with stationary-phase *L. amazonensis* promastigotes at 10 parasites per macrophage. Macrophages were activated 50U/ml of IFN-γ plus 100ng/ml of LPS. After 72h of infection with *L. amazonensis* or activation the supernatants were collected and ELISAs were performed to quantify cytokines and chemokines. For TNF-α assays, aliquots from cell cultures were collected at 24h of infection. Controls without stimuli and infection were used to quantify the basal levels of cytokines. A, B, C, D, E and F represent the concentration showed in pg/ml of the IL-6, TNF-α, IL-17, CXCL-1, MCP-1 and IL-10 respectively. Data are shown as mean ± SD from one representative experiment of 2, n=6 for each experiment. 84

Figure 23. Quantification of parasite loads in macrophages treated with ROS and nitric oxide inhibitors in infection caused by *L. amazonensis in vitro*. Peritoneal macrophages were infected with metacyclic promastigote forms of *L. amazonensis* in proportion 10 parasites per macrophage for 4h. During the infection, the cells were treated with several inhibitors (WT macrophages treated with L-NMMA alone; apocynin alone; L-NMMA plus apocynin; L-NMMA plus SOD; L-NMMA plus catalase; WT infection without treatment; and $gp91^{phox-/-}$ macrophages treated or not with L-NMMA. After 72h of infection the cells were stained counted under light microscope. 86

Figure 24. Flow cytometry gate strategy adopted to analyse the recruited cells after *L. major* infection. Mice ears or footpads were infected with 5 x 10^5 promastigote forms of *L. major* and 2h, 48h and 9 days post infection the tissues were processed and stained to surface markers. The same gate strategy was used in both tissues and all times. The red arrows indicate the pathways to split populations and identify subsequent sub-populations. The gates represent one sample of ears 48h post infection. A population that was $CD11b^+Ly6G^+Ly6C^-CD11c^+MHCII^-$ was suggested to be an immature dendritic cell population. 92

Figure 25. Percentage of subpopulations gated on $CD11b^+$ cells recruited to the inoculation site following *L. major* infection. Mouse ears or footpads were infected with 5 x 10^5 promastigote forms of *L. major* and 2h, 48h and 9 days post infection and the 0h time point represents the non-infected controls. The tissues were processed and stained to surface markers. A, B, C, D, E and F represent the kinetics of recruitment of neutrophils, inflammatory monocytes, macrophages, dendritic cells (DCs), activated macrophages and $CD11c^+MHCII^-$

cells, respectively. The data are represented as mean ±SD of one experiment representative of two performed, n=5 for each group. *=p<0.05, **=p<0.01 and ***=p<0.001. 96

Figure 26. Total cell numbers of subpopulations gated on CD11b$^+$ recruited to the inoculation site after *L. major* infection. Mouse ears or footpads were infected with 5 x 10^5 promastigote forms of *L. major* and 2h, 48h and 9 days post infection and the 0h time point represents the non-infected controls. The tissues were processed and stained to surface markers. A, B, C, D, E and F represent the kinetics of cell recruitment of neutrophils, inflammatory monocytes, macrophages, DCs, activated macrophages and CD11c$^+$MHCII$^-$ cells, respectively. The data are represented as mean ±SD of one experiment representative of two, n=5 for each group. *=p<0.05, **=p<0.01 and ***=p<0.001. 98

Figure 27. Flow cytometry gate strategy adopted to analyse the infected cells after *L. major* inoculation. Mouse ears or footpads were infected with 5 x 10^5 promastigote forms of *L. major* transfected with rfp gene and 2h, 48h and 9 days post infection the tissues were processed and stained for surface markers. The same gate strategy was used in both tissues and all times. The red arrows indicate the pathways to split populations and identify subsequent sub-populations. The gates represent one sample of ears 48h post infection. 99

Figure 28. Percentage of subpopulations gated on infected CD11b$^+$rfp$^+$ cells recruited to the *L. major* inoculation site. Mouse ears or footpads were infected with 5 x 10^5 *L. major* promastigote forms and 2h, 48h and 9 days post infection the tissues were processed and stained to surface markers. A, B, C, D, E and F represent the kinetics of phagocytic cells, neutrophils, inflammatory monocytes, macrophages, DCs and CD11c$^+$MHCII$^-$ cells, respectively. The data are represented as mean ±SD of 1 experiment representative of 2, n=5 for each group. *=p<0.05, **=p<0.01 and ***=p<0.001. 102

Figure 29. Total numbers of infected CD11b$^+$ cells recruited to the *L. major* inoculation site. Mouse ears or footpads were infected with 5 x 10^5 promastigote forms of *L. major* and 2h, 48h and 9 days post infection the tissues were processed and stained for surface markers. A, B, C, D, E and F represent phagocytic cells, neutrophils, inflammatory monocytes, macrophages, DCs and CD11c$^+$MHCII$^-$ cells, respectively. The data are represented as mean ±SD of 1 experiment representative of 2, n=5 for each group. *=p<0.05, **=p<0.01 and ***=p<0.001. 104

Figure 30. Mean fluorescence intensity (MFI) of MHCII on macrophages or DCs infected with *L. major*. Mouse ears or footpads were infected with 5 x 10^5 promastigote forms of *L. major* and 2h, 48h and 9 days post infection and the 0h time point represents the non-infected controls. The tissues were processed and stained for surface markers. A, B, C and D represent the MFI of MHCII$^+$ macrophages, DCs, infected macrophages and infected DCs, respectively. The data are represented as mean ±SD of 1 experiment representative of 2, n=5 for each group. **=p<0.01 and ***=p<0.001. 106

Figure 31. qRT-PCR of cytokines and chemokines expressed during acute phase of *L. major* infection. Mouse ears or footpads were infected with 5 x 10^5 promastigote forms of *L. major* and 2h, 48h and 9 days post infection the tissues were processed and a qRT-PCR was performed to verify the mRNA levels of cytokines and chemokines. A, B, C, D and D represent

the mRNA expression 2h, 48h and 9 days post infection of IL-1β, CXCL-1, IL-6, IL-10 and TNF-α, respectively and normalized by mRNA expression of the cytokines in naïve tissues. E and F represent the mRNA expression 2h, 48h and 9 days post infection of IFN-γ and IL-17, respectively and normalized by constitutive expression of 18S mRNA. N.D. indicates not determined. The data are represented as mean ±SD, n=5 for each group. *=p<0.05 and ***=p<0.001. 109

Figure 32. Lesion size of mice infected with *L. amazonensis*. Mice were infected with 5 x 10^3 *L. amazonensis* metacyclic promastigotes in pinna ears and followed until 16 weeks. (A) The lesion diameter was measured week by week with a calliper, *p<0.05, **p<0.01 and ***p<0.001 Data are shown as mean ± standard deviation (± SD). (B) Percentage of mice that had some tissue loss from 7 to 16 weeks post infection. (C) Representative pictures of ears from mice infected with *L. amazonesis* 4, 8, 12 and 16 weeks post infection. The figure represents one representative experiment of 2, n=5 for each experiment. 120

Figure 33. Parasite loads found in *L. Amazonensis*-infected mice 4, 8, 12 and 16 weeks post infection. Mice were infected with 5 x 10^3 *L. amazonensis* metacyclic promastigotes in pinna ears and followed for 16 weeks. (A) Parasite loads found in ears of infected mice 4, 8, 12 and 16 weeks post infection. (B) Parasite loads found in draining lymph nodes of infected mice 4, 8, 12 and 16 weeks post infection. Data are shown as mean ± SD from one representative experiment of 2, n=5 for each experiment. 121

Figure 34. Number of $CD11b^+$ cells recruited to the site of inoculation with *L. amazonensis* 4, 8 and 12 weeks post infection. Mice were infected with 5 x 10^3 *L. amazonensis* metacyclic promastigotes in pinna ears and followed for 16 weeks. The data represents the total numbers of CD11b+ cells in ears 4, 8 and 12 weeks post infection. Data are shown as mean ± SD from one representative experiment of 2, n=5 for each experiment. 122

Figure 35. $CD11b^+$ subpopulations recruited to the site of inoculation with *L. amazonensis* 4, 8 and 12 weeks post infection. The mice were infected with 5 x 10^3 of *L. amazonensis* metacyclic promastigotes in pinna ears and followed for 16 weeks. A, B C and D represent the total numbers of neutrophils, inflammatory monocytes, macrophages and dendritic cells in ears 4, 8 and 12 weeks post infection, respectively. Data are shown as mean ± SD from one representative experiment of 2, n=5 for each experiment. 123

Figure 36. Percentage of $CD11b^+$ subpopulations recruited to the site of inoculation with *L. amazonensis* 4, 8 and 12 weeks post infection. Mice were infected with 5 x 10^3 *L. amazonensis* metacyclic promastigotes in pinna ears and followed for 16 weeks. A represents the dot plots of the subpopulations gated on Ly6G and Ly6C markers. B C, D and E represent the percentage of neutrophils, inflammatory monocytes, macrophages and dendritic cells in ears 4, 8 and 12 weeks post infection, respectively. Data are shown as mean ± SD from one representative experiment of 2, n=5 for each experiment. 125

Figure 37. Total number of $CD4^+$ T cell sub-populations recruited to site of inoculation with *L. amazonensis* 4, 8 and 12 weeks post infection. Mice were infected with 5 x 10^3 *L. amazonensis* metacyclic promastigotes in pinna ears and followed for 16 weeks. A, B C, D and E represent the total numbers of $CD4^+$ T cells, activated $CD4^+$ T cells, regulatory $CD4^+$ T cells,

proliferating $CD4^+$ T cells and $CD8^+$ T cells in ears, respectively. T cell populations were analysed 4, 8 and 12 weeks post infection. Data are shown as mean ± SD from one representative experiment of 2, n=5 for each experiment. 127

Figure 38. Production of cytokines by $CD4^+$ T cells at the site of *L. amazonensis* inoculation 4, 8 and 12 weeks post infection. Mice were infected with 5 x 10^3 *L. amazonensis* metacyclic promastigotes in pinna ears and followed for 16 weeks. A represents $CD4^+$ T cells producing IFN-γ, B represents $CD4^+$ T cells producing TNF-α, C represents $CD4^+$ T cells producing IFN-γ and TNF-α, D represents $CD4^+$ T cells producing IL-2, E represents $CD4^+$ T cells producing IFN-γ, TNF-α and IL-2, F represents $CD4^+$ T cells producing IL-10 and G represents $CD4^+$ T cells producing IL-17 in ears 4, 8 and 12 weeks post infection. Data are shown as mean ± SD from one representative experiment of 2, n=5 for each experiment. 129

Figure 39. Total number of cells in draining lymph nodes in *L. amazonensis* infected mice 4, 8, 12 and 16 weeks post infection. Mice were infected with 5 x 10^3 *L. amazonensis* metacyclic promastigotes in pinna ears and followed for 16 weeks. At 4, 8, 12 and 16 the dLNs were harvested and cells counted. Data are shown as mean ± SD from one representative experiment of two, n=5 for each experiment. 130

Figure 40. Percentage phagocytic and T cells in draining lymph nodes in *L. amazonensis* infected mice 4, 8, 12 and 16 weeks post infection. Mice were infected with 5 x 10^3 *L. amazonensis* metacyclic promastigotes forms of in pinna ears and followed for 16 weeks. At 4, 8, 12 and 16 the dLNs were disrupted and the total cells counted. A, B and C represent the percentage of phagocytic, $CD4^+$ and $CD8^+$ T cells ranging from non-infected mice (week 0) until 16 weeks post infection. Data are shown as mean ± SD from one representative experiment of 2, n=5 for each experiment. 131

Figure 41. Percentage phagocytic subpopulations in draining lymph nodes in *L. amazonensis* infected mice 4, 8, 12 and 16 weeks post infection. Mice were infected with 5 x 10^3 *L. amazonensis* metacyclic promastigotes in pinna ears and followed for 16 weeks. At 4, 8, 12 and 16 the dLNs were harvested, disrupted and the total cells counted. A and B represent the percentage of neutrophils and inflammatory monocytes in lymph nodes from non-infected mice (week 0) until 16 weeks post infection. Data are shown as mean ± SD from one representative experiment of 2, n=5 for each experiment. 132

Figure 42. Percentage $CD4^+$ T cell subpopulations in draining lymph nodes in *L. amazonensis* infected mice 4, 8, 12 and 16 weeks post infection. Mice were infected with 5 x *L. amazonensis* 10^3 metacyclic promastigotes in pinna ears and followed until 16 weeks. At 4, 8, 12 and 16 the dLNs were harvested, disrupted and the total cells counted. A, B, C and D represent the percentage of activated, regulatory, proliferated and Th1 differentiated $CD4^+$ T cells, respectively, in DLNs from non-infected mice (week 0) until 16 weeks post infection. Data are shown as mean ± SD from one representative experiment of 2, n=5 for each experiment. 134

Figure 43. Percentage of $CD4^+$ T cells producing cytokines in draining lymph nodes in *L. Amazonensis*-infected mice 4, 8, 12 and 16 weeks post infection. Mice were infected with 5 x 10^3 metacyclic promastigotes forms of *L. amazonensis* in pinna ears and followed until 16

weeks. 4, 8, 12 and 16 the dLNs were disrupted and the total cells counted. A, B, C, D, E, F and G represent the percentage of IFN-γ, TNF-α, double (IFN-γ and TNF-α), IL-2, triple (IFN-γ, TNF-α and IL-2), IL-10 and IL-17 $CD4^+$ T producing cells, respectively, ranging from non-infected mice (week 0) until 16 weeks post infection. Data are shown as mean ± SD from one representative experiment of 2, n=5 for each experiment. 136

Figure 44. mRNA expression levels of CXCL1, CXCL2 and IL-1β from *L. amazonensis* infected ears measured by qPCR. Mice were infected with 5 x 10^3 metacyclic promastigotes forms of *L. amazonensis* in pinna ears and followed until 16 weeks. A, B and C represent the mRNA expression of CXCL1, CXCL2 and IL-1β, respectively, normalized to mRNA expression in naïve mice 4 and 8 weeks post infection. Data are shown as mean ± SD from one representative experiment of 2, n=5 for each experiment. 138

Figure 45. Percentage and total number of neutrophils recruited to the site of inoculation in *L. amazonensis* 8 weeks post infection. Mice were infected with 5 x 10^3 *L. amazonensis* metacyclic promastigotes transfected with rfp gene in pinna ears and followed for 8 weeks. A represents the dot plots of subpopulations gated on Ly6G and Ly6C markers. B and C represent the percentage and total numbers of neutrophils, respectively. Data are shown as mean ± SD from one experiment, n=13. 140

Figure 46. Percentage and total number of infected neutrophils at site of *L. amazonensis* inoculation 8 weeks post infection. Mice were infected with 5 x 10^3 *L. amazonensis* metacyclic promastigotes transfected with rfp gene in pinna ears and followed for 8 weeks. A represents the dot plots of the percentage of neutrophils gated on RFP. B and C represent the percentage and total numbers of infected neutrophils, respectively. Data are shown as mean ± SD from one experiment, n=13. 141

Figure 47. Percentage and total number of dying neutrophils at the site of inoculation with *L. amazonensis* 8 weeks post infection. Mice were infected with 5 x 10^3 *L. amazonensis* metacyclic promastigotes transfected with rfp gene in pinna ears and followed for 8 weeks. A represents the dot plots of the percentage of neutrophils in necrotic or apoptotic death process. B and C represent the percentage of apoptotic or necrotic cells, respectively, in total or infected neutrophils. D and E represent the total number of apoptotic or necrotic cells, respectively, in total or infected neutrophils. Data are shown as mean ± SD from one experiment, n=13..... 142

Figure 48. Total number of recruited phagocytic $CD11b^+$ cells at site of inoculation of *L. amazonensis* 10h, 36h and 60h post infection. Mice were infected with 5 x 10^5 *L. amazonensis* metacyclic promastigotes transfected with rfp gene in pinna ears. A, B, C, D and E represent the total number of phagocytic cells, neutrophils, inflammatory monocytes, macrophages and DCs, respectively, recruited to ears 10h, 36h and 60h post infection. Data are shown as mean ± SD from one representative experiment of 3, n=5 for each experiment..... 144

Figure 49. Percentage $CD11b^+$ subpopulations at site of inoculation of *L. amazonensis* 10h, 36h and 60h post infection. Mice were infected with 5 x 10^5 *L. amazonensis* metacyclic promastigotes transfected with rfp gene in pinna ears. A represents the dot plots of the percentage of $CD11b^+$ cells subpopulations during first hours of infection. B, C D and E represent the percentage of neutrophils, inflammatory monocytes, macrophages and DCs

present in ears 10h, 36h and 60h post infection. Data are shown as mean ± SD from one representative experiment of 3, n=5 for each experiment. 145

Figure 50. Percentage of infected CD11b^{+}RFP^{+} subpopulations at the site of inoculation with *L. amazonensis* 10h, 36h and 60h post infection. Mice were infected with 5 x 10^{5} metacyclic promastigotes forms of *L. amazonensis* transfected with rfp gene in pinna ears and followed since 10h to 60h post infection. A represents the dot plots of the percentage of infected CD11b^{+} cells subpopulations. B, C D and E represent the percentage of neutrophils, inflammatory monocytes, macrophages and DCs presented in ears. Data are shown as mean ± SD from one representative experiment of 3, n=5 for each experiment. 147

Figure 51. Percentage of dying neutrophils at the site of inoculation with *L. amazonensis* 36h and 60h post infection. Mice were infected with 5 x 10^{5} metacyclic promastigotes forms of *L. amazonensis* transfected with rfp gene in pinna ears and followed until 60h post infection. A represents the dot plots of the percentage of neutrophils in necrotic or apoptotic death process 36h and 60h post infection. B and C represent the percentage of apoptotic or necrotic cells, respectively, in total recruited neutrophils 36h or 60h post infection. D and E represent the percentage of apoptotic or necrotic cells, respectively, in infected neutrophils 36h or 60h post infection. Data are shown as mean ± SD from one representative experiment of 2, n=5 for each experiment. 149

List of Tables

Table 1. Primers used in qPCR to quantify the expression of mRNA from footpads in the infection. 60

Table 2. Primers used in qPCR to quantify the expression of mRNA from ears in the infection. .115

List of Abbreviations

7-AAD	7-aminoactinomycin D
ANOVA	Analysis of variance
APC	Antigen presenting cell
BOD	Biochemical Oxygen Demand
BSA	Bovine serum albumin
cDNA	Complementary DNA
CGD	Chronic granulomatous disease
CR1	Complement receptor 1
CR3	Complement receptor 3
DAMPs	Danger associated molecular patterns
DC	Dendritic cells
DETC	Diethyldithiocarbamate
dLNs	draining Lymph Nodes
DMEM	Dulbecco's Modified Eagle Medium
DNA	Deoxyribonucleic acid
DTH	Delayed type hypersensitivity
EDTA	Ethylenediamine tetraacetic acid
ELISA	Enzyme-Linked Immunosorbent Assay
FBS	Fetal bovine serum
FcR	Fc receptor
FCS	Fetal calf serum
FITC	Fluorescein isothiocyanate
GIPs	Glycoinositolphospholipids
HEPES	4-(2-hydroxyethyl)-1-piperazineethanesulfonic acid
HMGB1	High mobility group box protein 1
HO-1	Heme oxygenase 1
HTAB	Hexadecyltrimethylammonium bromide
IFN-β	Interferon β
IFN-γ	Interferon γ
IgG	Immunoglobulin G
IgG_1	Immunoglobulin G subtype 1

IgG_{2a}	Immunoglobulin G subtype 2a
IL-10	Interleukin 10
IL-12	Interleukin 12
IL-13	Interleukin 13
IL-17	Interleukin 17
IL-1β	Interleukin 1β
IL-4	Interleukin 4
IL-5	Interleukin 5
IL-6	Interleukin 6
IL-8	Interleukin 8
iNOS	inducible nitric oxide synthase
L-NMMA	L-NG-monomethyl Arginine citrate
LF	Lactoferrin
LPG	Lipophosphoglycan
LPS	Lipopolysaccharide
MCP-1	Monocyte chemoattractant protein 1
MHCII	Major histocompatibility complex class II
MPO	Mieloperoxidase
mRNA	messenger RNA
NAC	N-acetylcysteine
NADPH	Nicotinamide adenine dinucleotide phosphate-oxidase
OD	Optical density
OPD	o-phenylenediamine
PAMPs	Pathogen-associated molecular patterns
PBS	Phosphate buffer saline
PCR	Polymerase chain reaction
PE	Phycoerythrin
PEG-catalase	Polyethylene glycol linked catalase
PEG-SOD	Polyethylene glycol linked superoxide dismutase
PGE_2	Prostaglandin E2
PIP_3	Phosphatidylinositol (3,4,5)-triphosphate
PVs	Parasitophorous vacuoles
qPCR	quantitative PCR
RFP	Red fluorescent protein

RNS	Reactive nitrogen species
ROS	Reactive oxygen species
RPMI	Roswell Park Memorial Institute Medium
rRNA	ribosomal RNA
LA	*Leishmania* antigen
LA*La*	*Leishmania* antigen of *L. amazonensis*
LA*Lm*	*Leishmania* antigen of *L. major*
SOD	Superoxide dismutase
TGF-β	Transforming growth factor β
Th1	T helper response type 1
Th17A	T helper response type 17A
Th2	T helper response type 2
Th3	T helper response type 3
TLRs	Toll like receptor
TNF-α	Tumor necrosis factor α
T_{regs}	Regulatory T response
UCP2	Uncoupling protein 2
WT	Wild type

1. Resumo

As leishmanioses são um espectro de doenças causadas por parasitas do gênero *Leishmania.* Por ser um patógeno intracelular obrigatório, infectando principalmente macrófagos e neutrófilos, a produção de radicais de oxigênio e nitrogênio poderia ser importante fator na eliminação de parasitas. No caso específico da infecção causada por *Leishmania amazonensis,* uma importante espécie causadora de leishmaniose cutânea no Brasil, não há dados na literatura demonstrando o efeito desses radicais em infecções *in vivo*. Dados do nosso grupo confirmaram que o óxido nítrico possui um importante papel na eliminação dos parasitas em infecções causadas por *L. amazonensis in vivo*, porém o ânion superóxido e o peróxido de hidrogênio não parecem estar associados com a morte dos parasitas *in vivo.* Neste trabalho, nós mostramos que animais C57BL/6 deficientes da subunidade $gp91^{phox}$ da NADPH oxidase de fagócitos ($gp91^{phox-/-}$) infectados de forma subcutânea com *L. amazonensis* desenvolvem lesões maiores nas primeiras semanas de infeção e lesões menores na fase crônica da doença quando comparados a animais selvagens (WT). Entretanto, ambos camundongos WT e $gp91^{phox-/-}$ apresentaram a mesma carga parasitária. Nós detectamos altos níveis de IL-17 nos linfonodos drenantes 8 semanas pós infecção (p.i.) e baixos níveis de mRNA de IL-1β no sítio da lesão 12 e 16 semanas p.i. nos camundongos $gp91^{phox-/-}$. Há dados controversos na literatura sobre o papel dos neutrófilos nas infecções causadas por *Leishmania* principalmente quando diferentes rotas de inoculação são usadas. Considerando a relevância dessas células para produção de ROS e prevendo alterações importantes do efeito de ROS quando a rota de inoculação é alterada, nós comparamos a resposta imune inata gerada nas rotas de inoculação mais usadas no estudo da leishmaniose, as rotas subcutânea e intradérmica. Porém, usamos o modelo de infecção por *L. major* por este ser mais bem estabelecido na literatura. Duas horas p.i., a infecção intradérmica com *L. major* apresentou massivo recrutamento de neutrófilos e maiores níveis de expressão de mRNA de CXCL-1, seguido por um intenso recrutamento de monócitos inflamatórios $Ly6C^{hi}$ 48h e 9 dias p.i. quando comparados à infecção subcutânea. Este mais intenso perfil inflamatório observado no sítio intradérmico infectado também foi acompanhado por uma mais eficiente captura dos parasitas. Nós observamos um aumento de 10 vezes no número de células infectadas neste sítio nos tempos observados. Por outro lado, células dendríticas e macrófagos representaram a maioria das células infectadas no sítio subcutâneo. Devido à essa confirmada e importante participação de neutrófilos na infecção intradérmica, utilizamos essa rota de inoculação para determinar a influência de ROS em nosso modelo de infecção por *L. amazonensis.* Quando infectados de forma intradérmica com formas metacíclicas de *L. amazonensis*, os camundongos

gp91$^{phox-/-}$ apresentaram lesões maiores desde 4 semanas p.i. com grande inflamação, densas áreas necróticas e perda de tecido, porém sem apresentar diferenças na carga parasitária. Curiosamente, os níveis de citocinas inflamatórias não se alteraram durante o curso de infeção, porém nós detectamos uma extensa acumulação de neutrófilos no sítio intradérmico de infecção. O elevado número de neutrófilos em camundongos gp91$^{phox-/-}$ foi associado com alta frequência e números de neutrófilos necróticos em 8 semanas p.i. e isso pode ser o fator principal responsável pelo fenótipo inflamatório observado nestes camundongos. Estes experimentos sugerem que radicais de oxigênio têm um importante papel desde estágios iniciais da infecção causada por *L. amazonensis*, controlando o fluxo de neutrófilos para o sítio da lesão, impedindo a necrose inflamatória nestas células e consequentemente a inflamação dos tecidos infectados. Além disso, a rota de inoculação influencia profundamente o efeito das espécies reativas de oxigênio (ROS) na infecção por *L. amazonensis*, visto que as principais células produtoras de ROS, os neutrófilos, demonstram um papel proeminente somente na infecção intradérmica. Este é o primeiro trabalho a mostrar o efeito do ROS em *Leishmania* em um modelo aproximado em relação à infecção natural, indicando uma via mais fisiológica para o estudo de ROS em infecções causadas por *Leishmania*.

1. Abstract

Leishmaniasis are a wide spectrum of diseases caused by parasites of the genus *Leishmania*. Because these are obligatory intracellular pathogens, infecting mainly macrophages and neutrophils, oxygen and nitrogen radicals production could be important factors in parasite killing. In the specific case of infection caused by *Leishmania amazonensis*, an important species causing cutaneous leishmaniasis in Brazil, there is no data in the literature demonstrating the effect of these radicals on the infection *in vivo*. Data from our group confirmed that nitric oxide has an important role in parasite killing in *L. amazonensis* infection, but superoxide and hydrogen peroxide do not appear to be associated with parasite killing *in vivo*. In this work, we showed that C57BL/6 mice deficient in the $gp91^{phox}$ subunit of NADPH-dependent oxidase of phagocytes ($gp91^{phox-/-}$) infected subcutaneously with *L. amazonensis* develop larger lesions in the first weeks of infection and smaller lesions in the chronic phase of the disease when compared to wild type animals (WT). However, both WT and $gp91^{phox-/-}$ mice presented similar parasite loads. We detected higher levels of IL-17 in draining lymph nodes 8 weeks post infection (p.i.) and lower mRNA levels of IL-1β in the lesion site 12 and 16 weeks p.i. in $gp91^{phox-/-}$ mice. There are controversial data in the literature about the role of neutrophils in *Leishmania* infection, principally when different routes of inoculation are involved. Considering the relevance of these cells to ROS production and predicting important alterations of ROS effect when the inoculation route is changed, we compared the innate immune response generated on the most common used routes of parasite inoculation, the subcutaneous and the intradermal routes. However, we used the model of *L. major* infection, since this model is better established in the literature. Starting at 2h p.i., intradermal infection with *L. major* presented massive neutrophil recruitment and higher mRNA expression of CXCL-1 followed by intense recruitment of $Ly6C^{hi}$ inflammatory monocytes at 48h and 9 days p.i. compared to subcutaneous infection. This more intense inflammatory profile observed at the infected intradermal site also was accompanied by a more efficient parasite capture in this site. We observed a 10-fold increase in the number of infected cells at the times measured. In contrast, dendritic cells and macrophages represented the majority of infected cells in the subcutaneous site. Due this confirmed and important participation of neutrophils in the intradermal infection, we utilized this route of inoculation to determine the influence of ROS in our model of *L. amazonensis* infection. When infected intradermally, $gp91^{phox-/-}$ mice presented larger lesions starting at 4 weeks p.i. and a high degree of inflammation leading to a dense necrotic area and tissue loss without differences in parasite loads. Surprisingly, the levels of inflammatory cytokines did not change during the course

of infection, but we did detect a large accumulation of neutrophils at the intradermal site. Increased neutrophil numbers in gp91$^{phox-/-}$ mice was associated with higher numbers and frequencies of necrotic neutrophils at 8 weeks p.i. and may be the major factor responsible for the inflammatory phenotype observed in these mice. These experiments suggest that oxygen radicals have an important role in *L. amazonensis* infection, controlling neutrophil flux to the lesion, impairing necrotic inflammatory death in these cells and consequently the inflammation of infected tissue. Moreover, the route of inoculation greatly influences the effect of reactive oxygen species (ROS) in *L. amazonensis* infection, since the major cells producing ROS, the neutrophils, play a prominent role only in intradermal infection. This is the first report to show the effect of ROS in *Leishmania* model closest to natural infection, indicating a more physiological way to study ROS in *Leishmania* infections.

2. INTRODUCTION

Leishmaniasis are a spectrum of diseases caused by parasites of the genus *Leishmania*. They are endemic in 88 countries in the world and about 350 million people are at risk to contracting these diseases (WHO, 2013). Leishmaniasis are concentrated in developing countries, mainly Brazil and India, the African continent, and the Middle East. About 12 million people suffer from these diseases and it is estimated that 1.3 million new cases occur every year, with 20-30,000 deaths annually (WHO, 2013). The *Leishmania* genus includes 30 species and about 20 are pathogenic to humans (Cupolillo et al., 2000). The disease presents with high frequency in the visceral or tegumentary form, this latter presentation being subdivided in cutaneous, diffuse cutaneous or mucocutaneous leishmaniasis. There are estimated to be 0.7 to 1.3 million new cases of cutaneous disease and 0.2-0.4 million new cases of visceral disease every year (WHO, 2013). Consequently, leishmaniasis are considered one of the six major endemic diseases in the world.

The natural chronic persistence of leishmaniasis favors the development of a polarized immune response. In the most well studied model of leishmaniasis, the experimental infection of mice with *Leishmania major*, the immune response is polarized into Th1 or Th2 depending on the mouse strain, and the kind of immune response developed determines the course of infection (Heinzel et al., 1991; Reiner et al., 1994; Wilson et al., 2005). Progressive disease is observed in BALB/c mice due to the expansion Th2 cells, which are producers of IL-4, IL-5, IL-9, IL-10 and IL-13 (Gessner et al., 1993; Heinzel et al., 1991; Locksley et al., 1987; Matthews et al., 2000; Scott et al., 1988). In contrast, the expansion of Th1 cells producing IL-2 and IFN-γ in resistant mice, such as C3H and C57BL/6, promotes healing of lesions and control of *L. major* growth (Heinzel et al., 1991; Scott, 1993; Scott et al., 1988).

Reactive oxygen species (ROS) are a group of ions, radicals and highly reactive molecules derived from oxygen. They participate in many biological processes, from hormonal biosynthesis, cellular signaling, and killing of microbial pathogens. They can be generated in mitochondria as respiratory chain by products in an unspecific way (Rada and Leto, 2008). They are also one of major effector mechanisms against intracellular pathogens and can be induced by IFN-γ or via activation through toll like receptors (TLRs) (Calegari-Silva et al., 2009; Kavoosi et al., 2009; Pawate et al., 2004).

NADPH oxidase is an enzyme responsible for superoxide anion production. NADPH oxidase deficient animals develop granulomatous disease (Babior, 2004), due to an inability to resolve microbial infections, especially those caused by fungi and bacteria (Heyworth et al., 2003). The study of the role of ROS in *Leishmania* infections is not well studied since parasite control is attributed to nitric oxide, the major effector molecule in parasite killing (Green et al., 1990; Liew et

al., 1990). *In vitro* studies suggest an irrelevant role of ROS in parasite killing by *L. major* infected macrophages (Assreuy et al., 1994; Blos et al., 2003). *In vivo* studies also showed that ROS by phagocyte NADPH oxidase do not play a relevant role during infection with *L. major* of *L. donovani* (Blos et al., 2003; Carter et al., 2005; Murray and Nathan, 1999). However, *L. guyanensis* is highly susceptible to ROS (Sousa-Franco et al., 2006). This differential resistance of some species could be explained by differential antioxidant expression systems, making the study of ROS in infections caused by different species of *Leishmania* necessary.

Data from our group show that ROS from phagocyte NADPH-dependent oxidase did not alter parasite loads at the site of infection and draining lymph nodes, IFN-γ, IL-10 and nitric oxide levels in animals infected with *L. amazonensis*. However, an increase in lesion size was observed in animals deficient of phagocyte NADPH-dependent oxidase, which suggested an immunomodulatory role of ROS in disease, controlling the inflammation. Indeed, ROS have been attributes a role in the control of inflammatory responses in several systems. They activate transcriptional factors of inflammatory genes such as NFκB and AP-1 (Schmidt et al., 1995; Schreck and Baeuerle, 1991) and also contribute to induce apoptosis in neutrophils and T lymphocytes by oxidative stress (Purushothaman and Sarin, 2009; Sanmun et al., 2009; Spinner et al., 2010; Zhang et al., 2003). There are some controversial data in the literature about the anti-inflammatory or inflammatory activity of ROS. While some studies defend the induction of chemokine and cytokine production by ROS and subsequent cell recruitment (Hattori et al., 2010), others favor ROS having an anti-inflammatory role by inducing apoptosis of inflammatory cells such as neutrophils and macrophages (Marriott et al., 2008). Moreover, it was demonstrated that apoptotic bodies of neutrophils downregulate the immune response against *Leishmania sp.* (Afonso et al., 2008; Ribeiro-Gomes et al., 2012; Ribeiro-Gomes and Sacks, 2012). This could decrease the number of cells at the site of infection as well the inflammatory cytokine and chemokine production.

So, it would be important to evaluate the inflammatory role of ROS in infections caused by *Leishmania*, in view of the controversial data in the literature as well the shortage of studies relating ROS with infections caused by *Leishmania.*

3. LITERATURE REVIEW

3.1. *Leishmania* genus taxonomy

The taxonomy of the genus *Leishmania* (family: Trypanosomatidae, order: Kinetoplastida) started with its discovery in 1903 by Donovan and Leishman, who independently described the parasite isolated from the spleen of patients from India (Herwaldt, 1999). However, until today there is not a consensus about the taxonomic division due the different criteria used for classification (Hommel, 1999).

The classification of genus *Leishmania* was initially based on ecobiological criteria such as vectors, geographic distribution, tropism, antigenic properties and clinical manifestations (Bray, 1974; Lumsden, 1974; Pratt and David, 1981). However, biochemical and molecular analysis showed contradictory results for classifications based on geographic and pathological criteria. So, other criteria such as polymorphism patterns exhibited by kinetoplastic DNA markers, proteins or antigens are being used to classify the species of the genus *Leishmania* (Banuls et al., 2007).

The two species more frequently associated with visceral leishmaniasis are *Leishmania donovani* and *Leishmania infantum*. *Leishmania chagasi* is generally considered as synonymous of *L. infantum*, and these two species are practically indistinguishable (Mauricio et al., 2000), but the name *L. chagasi* is more commonly used in Latin American literature.

For epidemiological studies, the major tool for classification analysis is the analysis of isoenzymes. About 12 enzymes can be used to distinguish between all species. Each species can have a distinct zymodeme, each one characterized by a group of isoenzymes (Rioux et al., 1990). Figure 1 illustrates a modern classification scheme for the genus *Leishmania*.

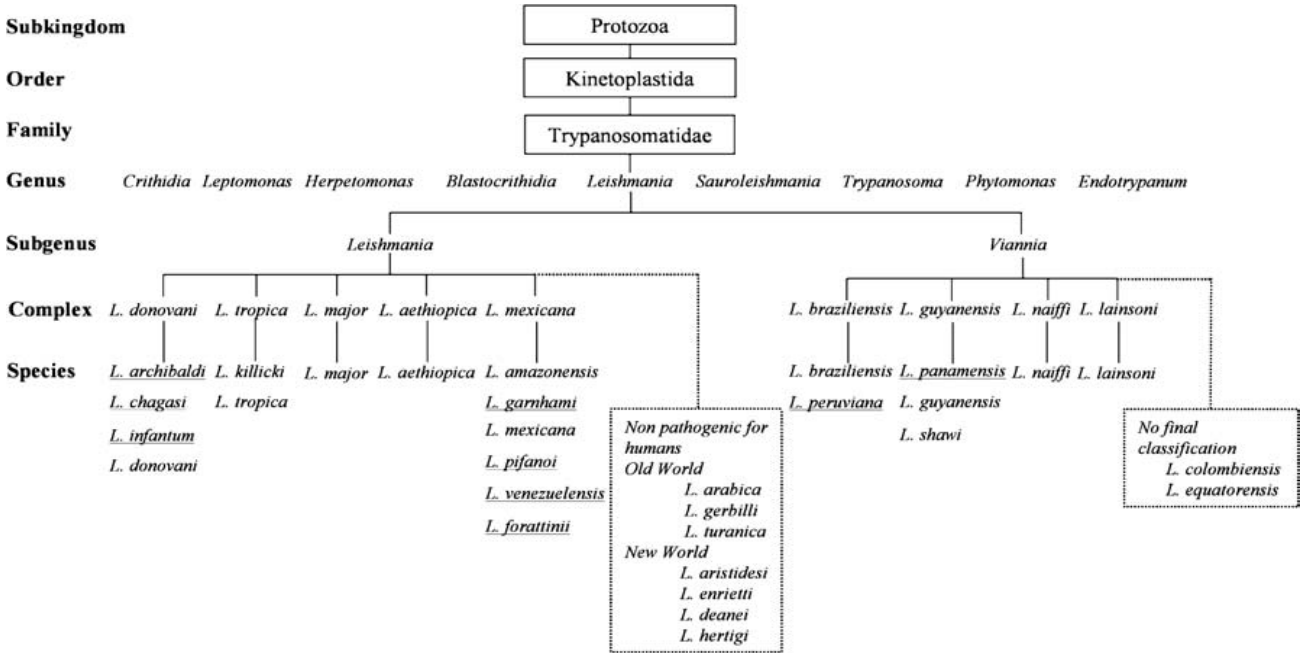

Figure 1: Taxonomy of *Leishmania* genus (Banuls et al., 2007). Underlined species have had their taxonomic classification questioned. Twenty species of the thirty known are pathogenic for humans.

3.2. Epidemiology

The leishmaniasis are endemic in more than 88 countries in the world, including countries in South of Europe, North of Africa, South and Central America, India and the Middle East (Murray, 2002). The areas with higher incidence of cutaneous and visceral leishmaniasis are marked in the maps of the figures 2 and 3, respectively.

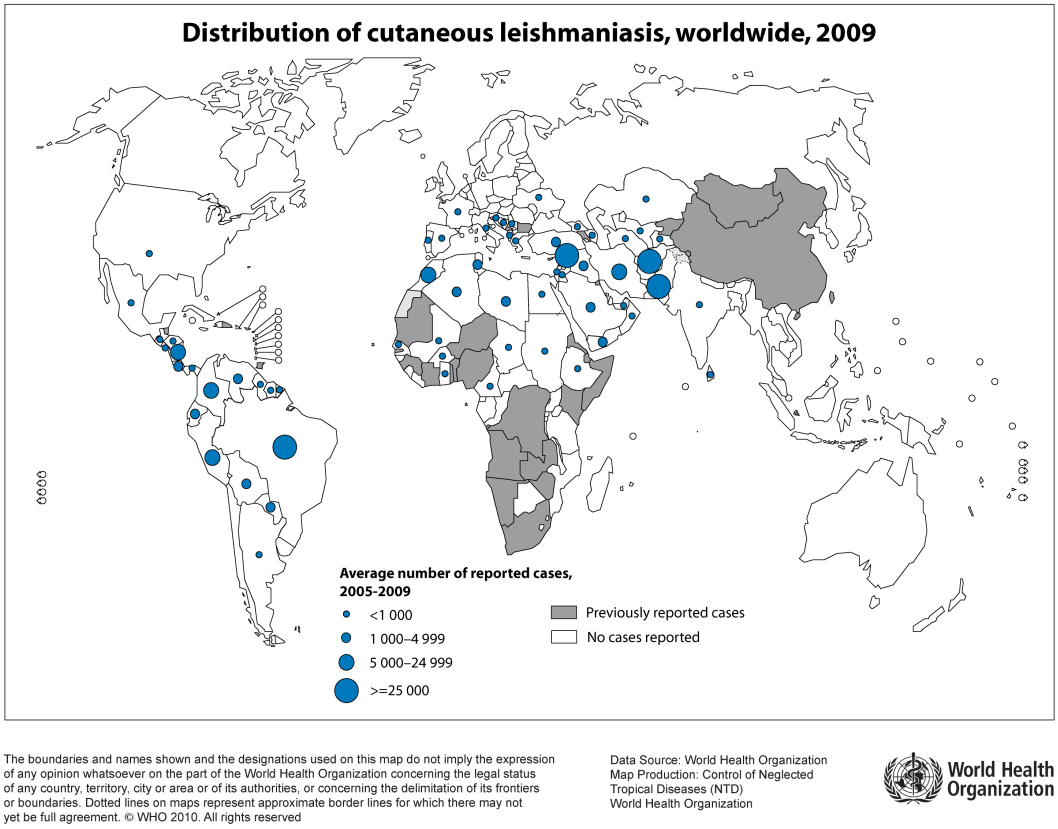

Figure 2: World distribution of tegumentar form of leishmaniasis. The blue-dotted areas indicate endemic zones between 2005 to 2009. WHO/CNTD. Map: Control of Neglected Tropical Diseases of the World Health Organization, 2010.

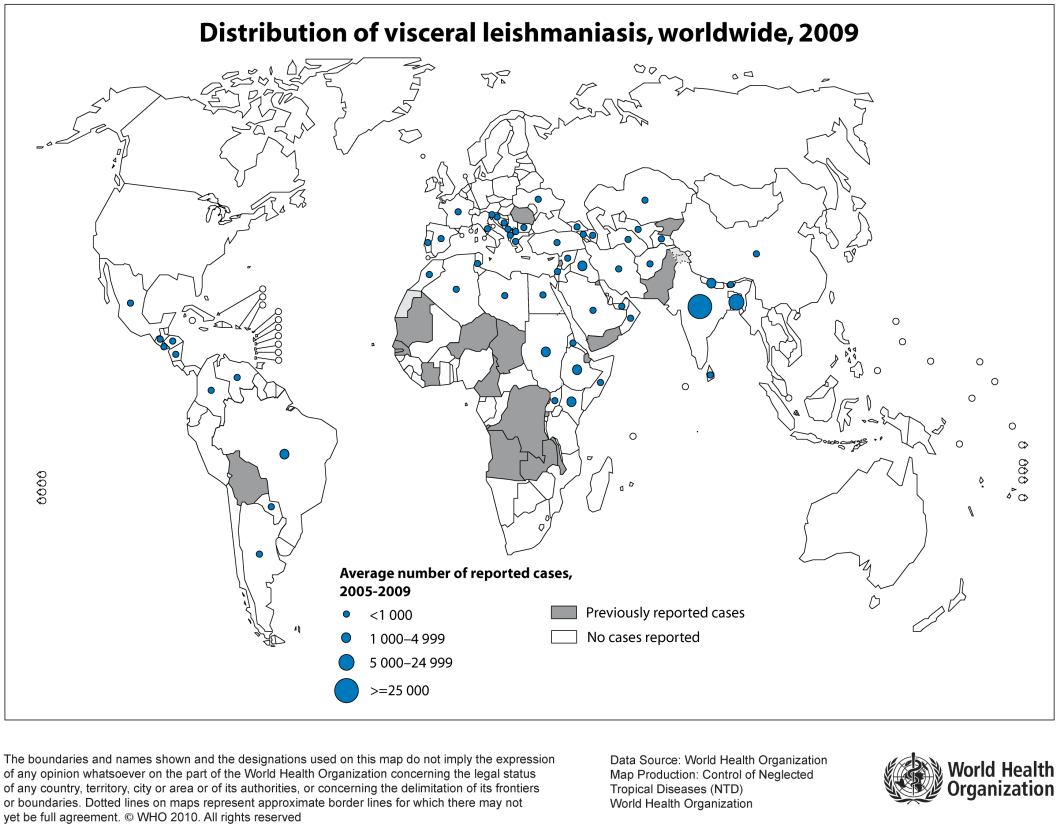

Figure 3: World distribution of visceral form of leishmaniasis. The blue-dotted areas indicate endemic zones between 2005 to 2009. WHO/CNTD. Map: Control of Neglected Tropical Diseases of the World Health Organization, 2010.

Recently, the number of cases reported and the prevalence of the disease are growing and there is a consensus that this is due to global awareness (Desjeux, 2001).

About 350 million people, distributed in 88 countries, are at risk to contract or in treatment for leishmaniasis (Kedzierski et al., 2006; WHO, 2013). In present, about 12 million people are infected with *Leishmania* and it is estimated that 1.3 million new cases occur every year, with 20-30,000 deaths per year (WHO, 2013). In addition, *Leishmania*-HIV co-infection is a major problem in affected areas (Sinha et al., 2005).

Data from the Brazilian Ministry of Health show the evolution of leishmaniasis in Brazilian territory. More than 123,000 cases were registered from 2007 to 2012, concentrated according to geographic region as follow: North (40.42%), Northeast (33.44%), Center-West (14.67%), Southeast (9.37%) and South (2.1%). The state of Minas Gerais contains 71.62% of all cases in the Southeast region. Particularly, there is a dense concentration of cases in the north of Minas Gerais, closest to the state of Bahia, which is the second most affected state in Brazil (about 19,200 cases).

The state of Pará, in the North region, leads the total number of cases registered in Brazil, reaching more than 19,900 people infected from 2007 to 2012.

In Brazil, two species are considered to deserve most public health attention: *L. amazonensis* and *L. braziliensis*. These two species are spread in all regions of the Brazilian territory, being responsible for the majority of cutaneous leishmaniasis registered cases, as shown in the map in figure 4.

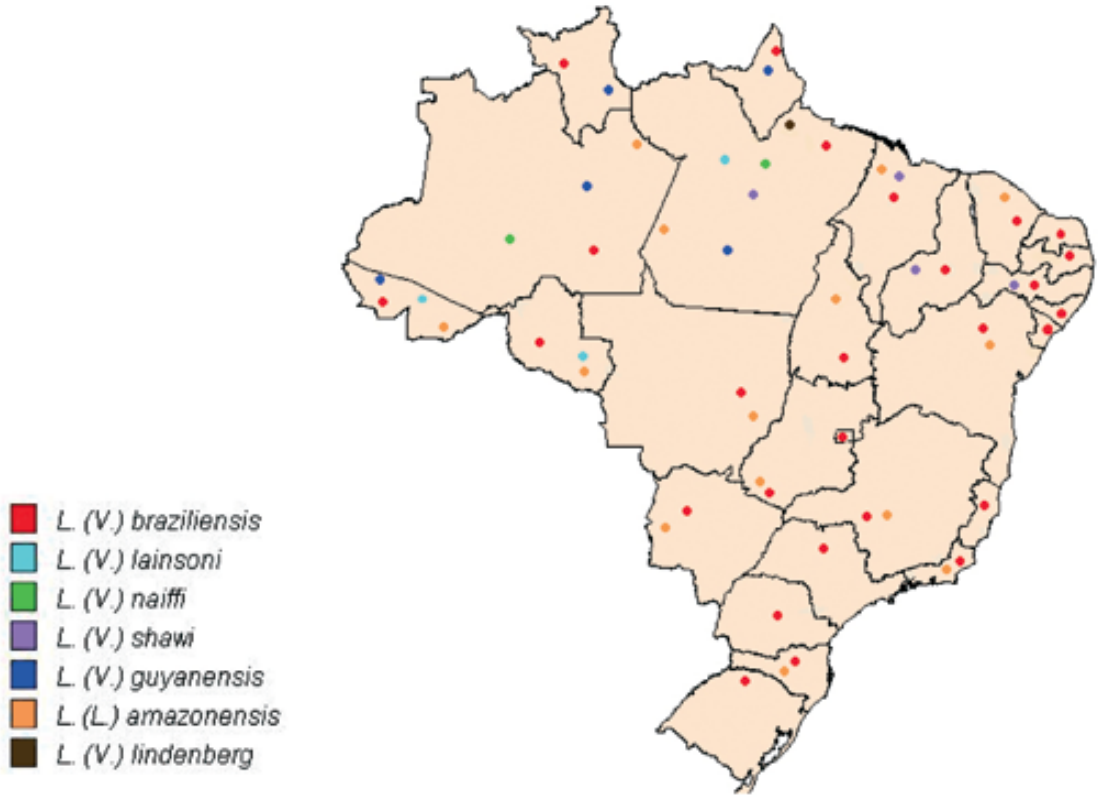

Figure 4: Distribution of *Leishmania* species causing cutaneous leishmaniasis in the Brazilian territory. *L. amazonensis* and *L. braziliensis* are responsible for the majority of cutaneous leishmaniasis cases in Brazil. Map: Ministry of Health of Brazil, Manual of leishmaniasis vigilance, 2007.

3.3. Disease

3.3.1. Etiological agent and clinical aspects

The leishmaniasis are traditionally divided in three major groups according to clinical outcomes: visceral, cutaneous and mucocutaneous (Evans, 1993).

The cutaneous form of the disease causes ulcers in skin, around the sand fly bite area, usually in exposed parts of body such as face, neck, arms and legs. The cutaneous form is caused by many species of *Leishmania*: *L. major, L. tropica, L. aethiopica, L. mexicana, L. braziliensis, L.*

panamensis, L. peruviana and *L. amazonensis*. Sick subjects generally heal spontaneously, but the time of healing changes according to the infecting specie and the host response. The disease can spread to other sites of the skin, being then known as diffuse cutaneous leishmaniasis. In this particular case, the disease might visceralize, being more aggressive, and when not properly treated can lead to death. The diffuse form of the disease is caused by *L. aethiopica, L. mexicana* and *L. amazonensis*, but occurs only when the host presents with impaired immunity (Kedzierski et al., 2006).

In mucocutaneous leishmaniasis, usually caused by *L. braziliensis*, the initial skin lesion can heal spontaneously, but over the years a lesion with partial or complete mucosal membrane destruction can develop. If not treated, affected subjects can develop serious deformities or even die.

The visceral leishmaniasis, also known as Kala-azar, is the most severe form of leishmaniasis and frequently leads to death if not treated. *L donovani, L. infantum* and *L. chagasi* are the major species responsible for this kind of illness. The parasites migrate to internal organs, principally liver and spleen, and can cause hepatosplenomegaly, fever, anemia and weight loss in the host. Some individuals can develop an uncommon syndrome named post-kala-azar dermal leishmaniasis, a few years after cure of visceral leishmaniasis. Patients committed by this syndrome are considered the major source of parasites for new infections due to the heavy parasite loads localized in the skin which are easily accessible to sand fly bites (Kedzierski et al., 2006).

3.3.2. Biological cycle

During its complex life cycle, parasites of the *Leishmania* genus are exposed to different extra and intracellular environments. These organisms are digenetic with two basic stages of life cycle: the extracellular in invertebrate host (sand fly) and the intracellular in vertebrate host (mammals). Hence, the parasites have two major forms: promastigotes, slender and flagellate, present in invertebrate host, and amastigotes, round and aflagellate, present in vertebrate host (Banuls et al., 2007).

The invertebrate host or vectors are tiny insects of the order Diptera, subfamily Phlebotominae. Two of six known geni are of medical importance: *Phlebotomus* in the Old World and *Lutzomya* in the New World. Thirty one of more than 500 phlebotomine species were confirmed as vectors for leishmaniasis (Killick-Kendrick, 1990 1999).

The *Leishmania* parasites are extremely efficient, and can infect several orders of mammals: Rodentia, Carnivora, Marsupialia, Primates, Edentata and Ungulata (Banuls et al., 2007). All these mammals are considered potential reservoirs of the disease.

The parasites are transmitted to vertebrate hosts by female sand flies, which inject a small number of metacyclic promastigotes into the skin. These forms are efficiently opsonized by complement components and phagocyted by neutrophils (major cells involved in the initial *Leihsmania* uptake), which turn on the apoptotic program releasing the parasites to the extracellular environment. The released *Leishmania* are phagocyted now by monocytes or macrophages, where they transform into replicating amastigotes inside of phagosomes. The replication of parasites lyses the membrane of macrophages and the infection spreads. The infected macrophages, present in the skin of the host, are ingested by sand flies when they feed on the host's blood and then are lysed, releasing the amastigote form. Because of changes in pH and temperature within the sand fly, the amastigote form rapidly transforms into replicating non-infecting promastigote forms. These promastigotes attach to the gut wall of the vector and replicate continuously. After replication, differentiated metacyclic promastigotes migrate to the anterior gut and are regurgitated into the host during the next blood meal. The life cycle is common to all parasitic *Leishmania* species (Figure 5).

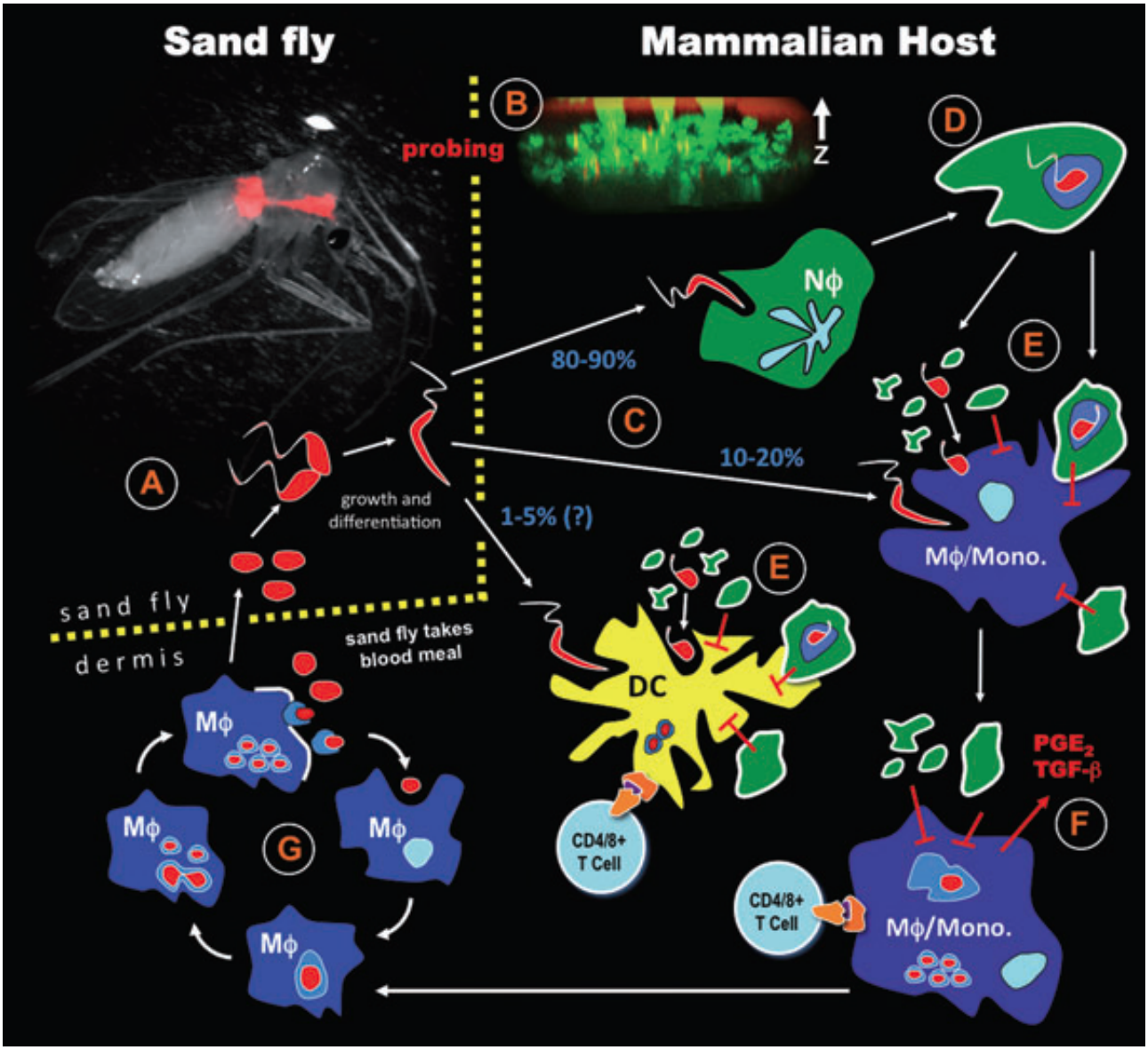

Figure 5: Biological cycle of *Leishmania major* (Peters and Sacks, 2009). (A) The cycle starts with the vector feeding on the blood from infected host. With the blood, the vector ingests amastigotes that are inside macrophages in the skin. In the insect gut, the amastigotes are released by macrophage lysis and differentiate into promastigote forms. They attach to the gut wall and start to replicate. (B) In the new blood meal, these metacyclic forms are inoculated in the skin of the host and (C) they are phagocyted majorly by neutrophils. (D) The neutrophils fail to kill phagocyted parasites, start the apoptotic process and (E) release the parasites together with apoptotic bodies into the extracellular environment. (D) Phagocytosis by the macrophages/DCs of these apoptotic bodies and parasites (F) induce the production of anti-inflammatory mediators such as TGF-β, which favor the survival of the parasite in the newly infected cells. (F and G) The fusion of phagosome membrane containing parasites with lysosomes in the host cells creates favorable environment to differentiation of the promastigotes into amastigotes, which start cycles of replication inside of the infected cells. (G) The amastigotes replicate indefinitely inside of macrophages until their lysis. Thus, many amastigotes are released in the extracellular environment and then are phagocyted by others phagocytic cells, enhancing the replication cycles. (A) Eventually, the vector might feed on contaminated host blood, re-initiating the cycle.

3.3.3. Immune response

Murine model studies have revealed differences in the immune response during visceral or cutaneous leishmaniasis.

The natural chronic persistence of leishmaniasis favors the development of a polarized immune response. In the more established model of disease, the infection caused by *Leishmania major*, there is a deep influence of Th1 and Th2 immune responses in disease course (Wilson et al., 2005). Progressive infection by *L. major* is observed BALB/c mice by expansion of Th2 cells producing IL-4, IL-10 and IL-13. In contrast, the IL-12-mediated expansion of Th1 cells in resistant mice, eg. C3H, and subsequent production IFN-γ, causes control of parasite growth (Heinzel et al., 1991; Scott, 1993; Scott et al., 1988) (Figure 6).

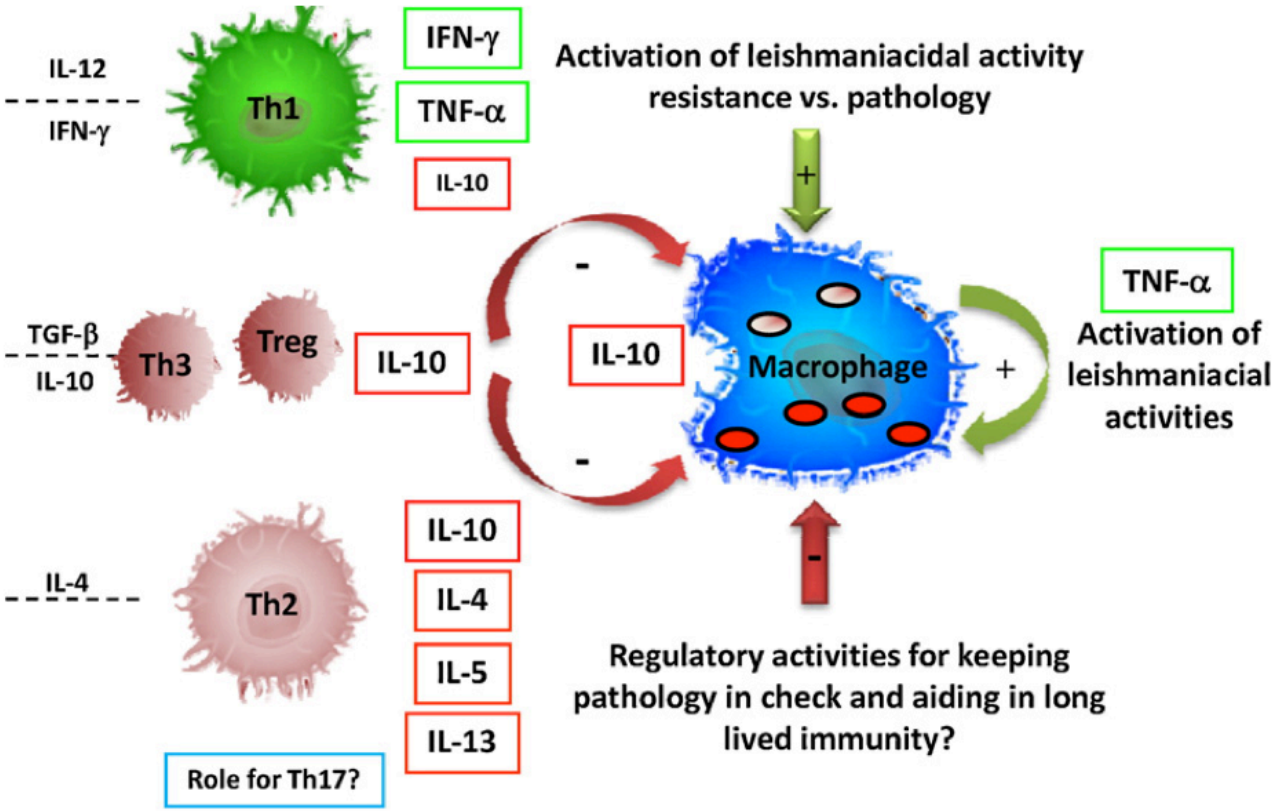

Figure 6: Models of immune responses in the infection caused by *L. major* (Gollob et al., 2008). $CD4^+$ T lymphocytes balance the activation of macrophages for *Leishmania* control. Classically, $CD4^+$ T cell subtypes Th1 and Th2 act controlling the anti-leishmanial activity in host macrophages. IL-12 and IFN-γ stimulate the differentiation of the immune response to Th1 subtype, which activate anti-leishmanial mechanisms in macrophages increasing nitric oxide (•NO) production by iNOS. IL-4, which differentiates the response into Th2, TGF-β and IL-10 inhibit the activation of macrophage promoting worsening in the disease.

The murine model of leishmaniasis has been widely used to better understand the life cycle, course of infection and parasite-host relationship. This model has the advantage of permitting a highly controlled study, potentially clarifying important immunological aspects of the disease (Pereira and Alves, 2008).

The course of infection caused by *L. amazonensis* changes remarkably in different isogenic strains of mice. BALB/c animals are highly susceptible presenting progressive lesion growth (Calabrese and da Costa, 1992). C57BL/10 also present with non-healing lesions and persistent parasite loads (Afonso and Scott, 1993). C3H, C57BL/6, BDA and CBA mice are less susceptible to infection, but they do not heal and do not decrease the parasite loads (Afonso and Scott, 1993; Barral et al., 1983; Cortes et al., 2010; Jones et al., 2002; Neal and Bray, 1983; Soong et al., 1997). Thus, contrary to the established model of Th1/Th2 dichotomy in infections caused by *L. major*, there is not a resistant model to *L. amazonensis* infection. The characterization of the type of immune response generated in this infection still presents controversial data in the literature (Pereira and Alves, 2008). The capacity to mount a Th1 response is still considered as resistance factor, but the susceptible phenotype is remarkably variable. Many factors such as a Th2 dominant response (Lemos de Souza et al., 2000), the absence of a Th1 response (Afonso and Scott, 1993), or a mixed Th1/Th2 response (Ji et al., 2002; Sacks and Noben-Trauth, 2002) influences the increased susceptibility to *L. amazonensis* infection.

IFN-γ, cytokine associated with a Th1 response, is downregulated in draining lymph nodes of C57BL/6 mice infected with *L. amazonensis*, when compared to infection caused by *L. braziliensis* (Maioli et al., 2004). This could suggest a regulator mechanism promoted by *L. amazonensis* differing from other *Leishmania* species, related with the capacity of this specific parasite to successfully infect many mouse strains. Moreover, mice lacking IFN-γ present similar lesions compared to wild type animals at the initial stages of infection, suggesting an irrelevant role of this cytokine in the beginning of the infection. However, 2 months post infection, IFN-γ deficient mice loose control of lesion growth, increase the production of IL-4 and decrease the production of IL-12 and TNF-α. These data suggest that production of IFN-γ is crucial for the establishment of Th1 response in the disease (Pinheiro and Rossi-Bergmann, 2007).

An ambiguous role was attributed to IFN-γ during *L. amazonensis* infection: it was observed that IFN-γ increases the replication of *L. amazonensis* in infected macrophages, but also activates the killing of promastigotes (Qi et al., 2004). On the other hand, the association of IFN-γ with LPS limits their growth and induces parasite death in infected macrophages.

The expression of IL-12, another important inflammatory cytokine during the Th1 response, has been shown to induce a significant reduction in parasitism during *L. amazonensis* infection. IL-12 is downregulated in infected C3H mice, and its expression is associated with the presence of the pathogen and it is independent of IL-4 expression (Jones et al., 2000). In addition to the reduction of IL-12 expression, those animals were also irresponsive to exogenous IL-12. This characteristic implies a deficiency in mRNA expression of IL-12b2 receptor, which is prevented somehow by the parasite (Jones et al., 2000).

The role of IL-4 during infection with *L. amazonensis* is very controversial. It was demonstrated that IL-4 deficient BALB/c mice express high levels of IFN-γ and anti-*Leishmania* IgG_{2a} antibodies 2 weeks post infections when compared to wild type. However, following infection with high dose of parasites (5 x 10^6 promastigotes/footpads), the lesions progress equally in IL-$4^{-/-}$ or WT BALB/c mice with no differences in parasite loads. In contrast, IL-$4^{-/-}$ develops smaller lesions and lower parasite loads when inoculated with 10^5, 10^4 or 10^3 parasites/footpads (Guimaraes et al., 2006). On the other hand, some studies suggest that IL-4 is not a predominant factor of susceptibility in the infection, since its production decreases 3 weeks post infection. Moreover, IL-4 deficient mice or C57BL/6 and BALB/c mice treated with anti-IL-4 are not capable of healing lesions (Afonso and Scott, 1993; Ji et al., 2003; Jones et al., 2000).

The regulatory cytokine IL-10 also has an obscure role in the infection caused by *L. amazonenis*. Despite its importance as a limiting factor of the Th1 response during the acute phase of the disease, this cytokine does not have a similar role in the chronic phase: both WT and IL-10 deficient C57BL/6 mice exhibit a decreased Th1 response in the chronic phase. Moreover, the IL-$10^{-/-}$ mice reduce 1-2 logs of parasite burden during the infection with parasite persistence and similar lesion development. Therefore, IL-10 has a partial influence in the *l. amazonensis* infection (Jones et al., 2002).

Experiments with IL-10 deficient BALB/c mice showed that these animals, although unable to control the lesion progression, upregulate the production of IFN-γ, nitric oxide and mRNA levels of IL-12p40 and IL-12Rb2 when compared to wild type animals (Padigel et al., 2003). However, after anti-IL-4 treatment, the IL-10 deficient mice can control the infection and have few parasites in the lesion site. This shows that IL-10 together with IL-4 modulate the susceptibility impairing the development of a protective Th1 immune response.

In case of the infection in humans, there are strong differences in the immune response and disease behavior with two major components involved in these phenotypes: the genetic inheritance of the individual and the specie of *Leishmania* causing the disease (Silveira et al., 2009). The *L. amazonensis*, as demonstrated in mice models, have a remarkable capacity to escape the immune

system and promote disease. As with other *Leishmania* species causing cutaneous disease, *L. amazonensis* presents with three clinical manifestations varying according to the genetic background of the patient and the efficiency of the T-cell response: localized cutaneous leishmaniasis (LCL), anergic diffuse cutaneous leishmaniasis (ADCL), and borderline disseminated cutaneous leishmaniasis (BDCL) (Silveira et al., 2009).

The LCL is the most common form the leishmaniasis (about 95% of the cases) caused by *L. amazonensis.* This form is characterized by one or more ulcerative lesion(s) with good response to traditional antimonial therapy (Silveira et al., 2009). More than 50% of the patients do not present delayed type hypersensitivity (DTH) and lymphocyte proliferation reactivity (Silveira et al., 1998; Silveira et al., 1991). Moreover, LCL patients produce higher expression of IL-4 mRNA, without a decrease in the expression of IFN-γ mRNA. Indeed, the augmented expression of IL-4 mRNA suggests a possible mechanism of downregulation of IFN-γ activity, which could explain the lack of DTH in these patients (Silveira et al., 2004).

In contrast to LCL, patients with ADCL present with more than one non-ulcerative cutaneous lesions containing heavily parasitized macrophages (Soong et al., 2012). All ADCL patients present as DTH negative. This suggests a strong inhibition of T-cell response, which could contribute with disease dissemination (Barral et al., 1995; Petersen et al., 1982). Moreover, there are low numbers of $CD4^+$ and $CD8^+$ T cells in the lesions as well as very low IFN-γ mRNA expression and very high IL-4 mRNA expression, which characterize this form of disease as a well defined Th2 immune response inducer. Because of this well-defined Th2 response in ADCL, frequent recrudescence of the disease is observed after antimonial therapy (Bomfim et al., 1996; Silveira et al., 2004).

The BDCL is an intermediary form of the disease between LCL and ADCL. BDCL patients affected by *L. amazonensis* infection present very slow dissemination of the disease, taking 1-2 years to develop about 5-10 infiltrated lesions in the skin (Silveira et al., 2009). Patients present incomplete T-cell immune suppression by the parasite, and while they are DTH negative their T-cell response is enough to avoid recrudesce of the disease after antimonial therapy (Carvalho et al., 1994; Costa et al., 1986; Turetz et al., 2002). Therefore, this capacity of the patients to recover after antimonial therapy imply a dominance of Th1 over Th2 response albeit it slight, contrary what happens in ADCL (Silveira et al., 2005).

3.3.4. Evasion of immune response by the parasite

Because of the lack of the necessary machinery to invade actively the host, the *Leishmania* are confined mostly to professional phagocytes. Although these parasites achieve invasion of many phagocytic cellular types, there is no evidence that the parasite can replicate in cells other than macrophages. These cells have primary defenses, including the activation of oxidative metabolism, by NADPH oxidase, iNOS, and synthesis and liberation of metabolites of arachidonic acid, which are induced by attachment and phagocytosis of microbial agents (Peters and Sacks, 2006). The microorganisms are endocyted through the plasma membrane of the phagocytic cells forming a vesicle in the cytoplasm called the phagosome. However, the phagosome does not have the machinery to digest and destroy the phagocyted intruder. So, there is a fusion of phagosome with lysosomes, a vesicle containing proteases, acid pH and ROS, capable to destroy and digest the microorganism.

The promastigote forms of *Leishmania* are covered by lipophosphoglycan (LPG) and a family of glycolipids named glycoinositolphospholipids (GIPs) (Naderer et al., 2004). LPG has a critical role in the infection of macrophages, protecting the promastigotes from reactive oxygen species (ROS) generated during the infection (Spath et al., 2003). Some studies showed that LPG could inhibit the fusion of the phagosome with the lysosome (Tuon et al., 2008), act as a ROS scavenger or inhibit the recruitment of NADPH oxidase to the phagosome membrane preventing damage to the parasite (Lodge et al., 2006). Another protein present on the surface of promastigotes, the gp63 protease, can inhibit the action of phagolysosome enzymes, favoring the persistence of the parasite inside the cell (Sorensen et al., 1994).

Complement receptors (CRs) also have a crucial role in the phagocytosis of promastigote forms by macrophages. The interaction of parasites with CRs occurs in three different ways: in the presence of the complement protein C3, present in serum, the iC3b fragment binds to complement receptor 3 (CR3/CD11b/Mac-1) on macrophage; by direct interaction between gp63 and CR3, independently of complement; and by the interaction of LPG interacting with lectin-like regions in CR3 and CR1 (Handman, 1999). The binding of parasite to these receptors does not trigger microbicidal mechanisms and increases the survival chances of the parasite in the host (Mosser and Edelson, 1987; Mosser et al., 1987). The phagocytic cells recognize microorganisms opsonized by the molecule C3b of the complement. The C3 molecule is abundant in the blood and is spontaneously hydrolyzed in bloodstream. This hydrolysis generates the C3b molecule that opsonizes the microorganisms and then can be phagocytosed more efficiently by the phagocytic cells.

Amastigotes do not express LPG and gp63, however, they also have evasion mechanisms to avoid the host immune response. The membrane of amastigotes has high numbers of phosphatidylserine on the external portion, which permits an entrance mechanism into macrophages that is similar to that of apoptotic cells. This strategy avoids microbicidal processes and inflammatory responses (Wanderley et al., 2006). Furthermore, the opsonization of amastigotes by IgG antibodies from the host promotes the uptake of amastigotes via FC receptors, which induces the release of IL-10 (Kane and Mosser, 2001).

Figure 7 illustrates the major ways that *Leishmania* enter macrophages without triggering inflammatory and microbicidal mechanisms.

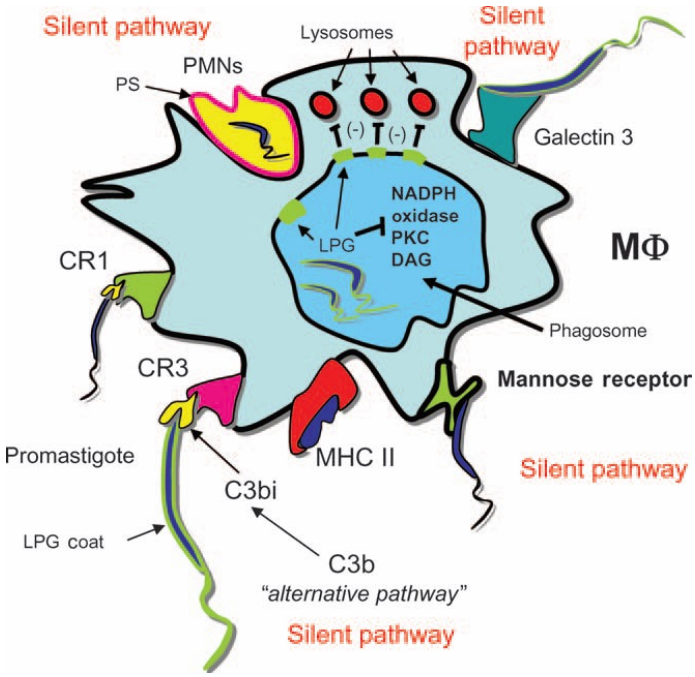

Figure 7: Many ways of inhibition of microbicidal activities used by *Leishmania* spp. **to immune response evasion.** Adapted (Peters and Sacks, 2006). *Leishmania* evade the microbicidal activities of macrophages in many ways. The phagocytosis of *Leishmania* by specific CR1 and CR3, manose receptors and phosphatidylserine receptors promotes, among other responses, release of IL-10. The uptake by these receptors and IL-10 production induce downregulation of oxidative defenses by macrophages. Inside of macrophages, the *Leishmania* also inhibit the fusion with lysosomes with phagosomes via LPG and eventually gp63.

3.4. NADPH oxidases, production of ROS and inflammation

The NADPH oxidases are a group of membrane-associated and cytoplasm proteins expressed by many cell types of mesodermic origin. The oxidases are enzymes involved in redox

reactions where the molecular oxygen (O_2) is the final acceptor of electrons. However, the majority of the studies about the NADPH oxidases are concentrated on B lymphocytes. They catalyze superoxide anion ($O_2^{\bullet -}$) production by reducing oxygen using NADPH as an electron donor in the following reaction: $NADPH + 2O_2 \rightarrow NADP^+ + 2O_2^{\bullet -} + H^+$ (Babior, 1999).

The superoxide generated by these enzymes is used as the initial molecule for the production of many ROS, including, free radicals and oxygen singlets, hydrogen peroxide, hydroxyl radicals and oxidized halogens. These oxidants generated are used by phagocytes to destroy invader microorganisms, but can also cause much tissue damage to the host. The damage caused by ROS is due to the spontaneous chemical reaction between ROS and cell components. There are oxidations by ROS of important proteins or even DNA, which promotes cell collapse and death. Because of this, the action of NADPH oxidase is highly regulated e activated just under certain stimuli (Babior, 1999).

The structure of the NADPH-dependent oxidase of phagocytes (also called Nox2 or $gp91^{phox}$) is composed by two transmembrane subunits ($gp91^{phox}$ and $p22^{phox}$), three cytosolic components ($p67^{phox}$, $p47^{phox}$ and $p40^{phox}$) and a small G protein (rac1 or rac2). The rac proteins are kept inactivated by interaction with an inhibitor of guanine nucleotide dissociation, which impairs the exchanges of guanine nucleotides (GDP by GTP) by racs. The activation of NADPH oxidase is associated to attachment of cytoplasmatic components to transmembrane subunits (Babior, 2004).

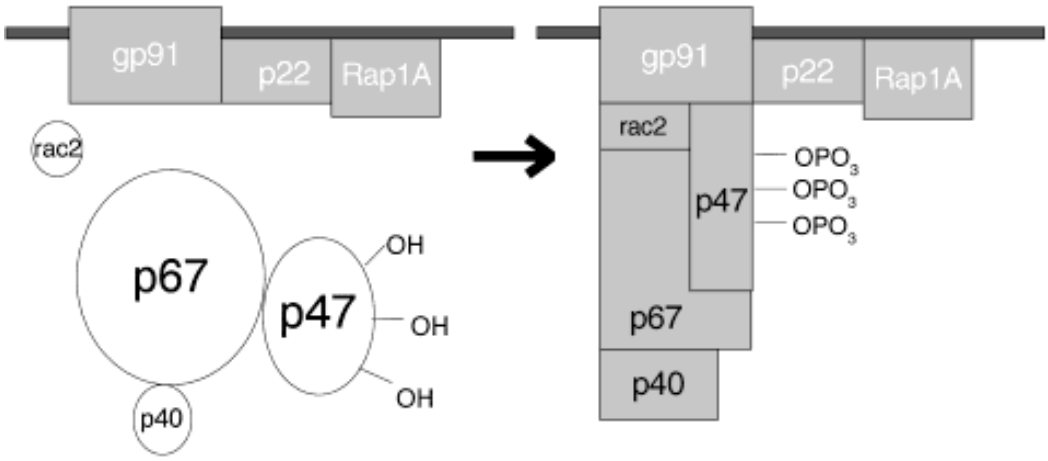

Figure 8: Activation states of NADPH oxidase (Babior, 1999). On the left the inactivate state of the enzyme is represented, where the multimeric complexes are separated. Under appropriated signaling, there is a phosphorylation of p47, permitting the association of cytoplasmic complexes with transmembrane subunits to activate the enzyme, as represented on the right side.

The superoxide anion is the product of the multimeric NADPH oxidase enzyme complex. The NADPH complex contains the membrane-bound cytochrome b_{558}, which two polypeptide chains ($gp91^{phox}$ and $p22^{phox}$) and two non-identical heme groups (associated to $gp91^{phox}$) are part of the membrane-linked complex (DeLeo et al., 2000; Nauseef, 2004). The gp91 subunit is expressed as a polypeptide of 58-kDa and after glycosylation in the endoplasmic reticulum becomes a 65-kDa subunit (Yu et al., 1999). After this subunit leaves the endoplasmic reticulum, it traffic trough the *trans*-Golgi network, where it is additionally glycosylated, acquiring also the heme group, which increases the mass of the molecule to the final 91-kDa (DeLeo et al., 2000; Nauseef, 2004; Yu et al., 1999). The process of maturation of $gp91^{phox}$ increases the affinity for the p22, the other membrane-linked subunit and both are anchored to the membrane. The other subunits of NADPH oxidase, p40, p47, p67, and Rac2 are located in the cell cytoplasm and associate with the membrane-bound components upon activation (Nauseef, 2004). The assembly of the subunits to active the enzyme on the target membrane is crucial for the local release of optimal amounts of superoxide, since this molecule is unable to transpose cellular membranes.

In the presence of appropriated stimuli such as phagocytosis triggered by pathogen-associated molecular patterns (PAMPs) binding to toll receptors, there is activation of p38 MAPK via MyD88. It was demonstrated that $Myd88^{-/-}$ peritoneal macrophages are inefficient in eliminating Gram-negative bacteria such as *Escherichia coli* or *Salmonella typhimurium*. This deficiency was correlated with decreased production of superoxide anion mediated by NADPH oxidase. Moreover, these $Myd88^{-/-}$ peritoneal macrophages have defective NADPH oxidase assembly due to impaired p38 MAPK activation and consequent $p47^{phox}$ phosphorylation (Laroux et al., 2005). Therefore, after p38 MAPK, $p47^{phox}$ is phosphorylated, which exposes the binding site to $p22^{phox}$ assembly (Laroux et al., 2005). The assembly of the three subunits ($p22^{phox}$, $p47^{phox}$ and $gp9^{phox}$) permits the recruitment of $p67^{phox}$ (Leto et al., 1994), which after interaction with rac, exposes the binding site to $gp91^{phox}$, activating the superoxide production (Mizrahi et al., 2006). The subunit $p40^{phox}$ seems to be an obligatory binding partner of $p67^{phox}$, but its role in the activation of NADPH oxidase is still unclear. However, animal models deficient to subunit $p40^{phox}$ (Ellson et al., 2006) and granulomatous disease patients presenting mutations in the PX domain of $p40^{phox}$ (Matute et al., 2009) established the importance of this subunit in the activity of the NADPH oxidase. The phosphorylation of the PX domain of $p40^{phox}$ is an important signal to activation of NADPH oxidase (Chessa et al., 2010).

The $gp91^{phox}$ subunit is essential for NADPH oxidase function. This subunit is responsible for oxygen reduction by donation of electrons provided from NADPH (Shatwell and Segal, 1996). $Gp91^{phox}$-deficient mice or humans with mutations in this gene present X-linked chronic

granulomatous disease (CGD) (Pollock et al., 1995). Patients with CGD have early recurrent infections that can lead to death as early as childhood. Although they show normal chemotaxis, degranulation and phagocytosis, the patients show deficiency in destruction of phagocyted microorganisms because of the lack of metabolites generated by superoxide anion. In addition to the symptoms found in humans, mice with CGD also show higher numbers of neutrophils after peritonitis caused by chemical components (Pollock et al., 1995) and an increase in polymorph nuclear cells, chemokines and inflammatory cytokines as well the global lung inflammation caused by experimental infection with *Pneumococcal pneumonia* (Marriott et al., 2008).

At the moment, there are seven isoforms of NADPH oxidase identified in mammals, the isoforms Nox-1 to 5, and Duox-1 and 2. Others variations in subunits of the complex, the $p47^{phox}$ isoform (Noxo1) and $p67^{phox}$ isoform (Noxa1) also were identified in mammalian cells (Banfi et al., 2003; Banfi et al., 2001; Cheng et al., 2001; De Deken et al., 2000; Dupuy et al., 1999; Geiszt et al., 2000; Suh et al., 1999). However, except for $gp91^{phox}$, the others isoforms do not seem to be involved in phagocytes defense.

Superoxide may associate with other ions to generate even more toxic products such as O_3, HOCl, HOBr, $ONOO^-$, $NO_2^{\bullet}$, $CO_3^{\bullet-}$, H_2O_2, $^{\bullet}OH$, etc. (Halliwell, 2006). However, because of its negative charge, superoxide is unable to transpose biological membranes. Among the cited molecules, hydrogen peroxide (H_2O_2) stands out as being formed by action of superoxide dismutase (SOD) on $O_2^{\bullet-}$ and H_2O. SOD is an antioxidant enzyme present in many organisms and is a hallmark of antioxidant defense in many systems. It catalyzes the formation of H_2O_2 by combination of $O_2^{\bullet-}$ and $2H^+$ ions. The SOD transforms the highly reactive superoxide anion in a lesser reactive hydrogen peroxide, which protect partially the proteins of the organism from oxidation. There are three isoforms of SOD presented in mammals: SOD1, localized in cytoplasm and dependent of Cu/Zn metals; SOD2, presented in mitochondrial matrix and dependent of Mn metal; and SOD3, a secreted isoform also dependent of Cu/Zn (Fukai and Ushio-Fukai, 2011). Mice deficient in SOD2, have uncontrolled oxidative stress and die a few days after the birth (Li et al., 1995), which illustrates the importance of SOD to protect the organism of superoxide action.

Differently from superoxide, hydrogen peroxide can easily transpose membranes and participate on killing, generating hydroxyl anion ($^{\bullet}OH$) by the Fenton reaction (Gutteridge and Halliwell, 1992; Repine et al., 1981). The Fenton reaction is the name given for the spontaneous oxidation of Fe^{2+} to Fe^{3+} through H_2O_2, represented by the equation: $Fe^{2+} + H_2O_2 \rightarrow Fe^{3+} + {}^{\bullet}OH + OH^-$ (Fenton, 1894). So, Fe-S centers are a target for H_2O_2. On the other hand, the death of microorganisms by conversion of H_2O_2 in $^{\bullet}OH$ inside of the phagosome (outside of the pathogen's membrane) is improbable. Peroxide is extremely reactive. Inside the phagosome, it can react with a

variety of compounds, and even if a few H_2O_2 molecules reach the pathogen's cell wall, for example, they will cause irrelevant damages. In neutrophils, lactoferrin, a Fe^{2+} binding protein, reduces the self-damage caused by $^{\bullet}OH$ avoiding the generation of $^{\bullet}OH$ by the Fenton reaction (Gutteridge and Halliwell, 1992; Segal, 2005).

Other remarkable process is the reaction between $^{\bullet}NO$ and $O_2^{\bullet-}$, forming $ONOO^-$, which in physiological pH and high concentration of CO_2, as in tissues, can form, among others, the radicals $^{\bullet}NO_2$ and $CO_3^{\bullet-}$ with high potential to cause damage in microorganism and host cells (Alvarez and Radi, 2003). However, the mammal cells seem to be prepared for such aggression with several antioxidant strategies (Evans and Halliwell, 2001). Although peroxynitrite can cause damage to host cells, the benefits for the host are irrefutable. The importance of both nitric oxide and superoxide, and subsequent formation of peroxynitrite is underscored by the fact that double knockouts for iNOS and NADPH oxidase are just viable in germ free conditions (Gyurko et al., 2003) or in specials cases (constant administration of antibiotics cocktail) (Murray et al., 2006).

In case of neutrophils, an important microbicidal mechanism is the formation hypochlorous acid (HOCl) by myeloperoxidase. This enzyme comprises 2 to 5% of all proteins of this cell and by the fusion of cytoplasmatic granules with phagosomes can promote the death of microorganisms (Winterbourn, 2002). The enzyme generates HOCl from H_2O_2 and Cl^-, therefore limitations in the capacity of superoxide production possibly lead to less activity of MPO.

Patients with CGD present high quantities of granulomas formed in many parts of the body, which indicate an exuberant inflammatory process in progression. So, as cited before, animals deficient in ROS production present high neutrophilia in some experimental infections and persistent inflammation. These data could indicate a role of ROS controlling the inflammation.

One of the mechanisms proposed for the hyperinflammation seen in phagocyte NADPH oxidase deficient animals would be a decrease in the degradation of phagocyted material by the cells. This material could accumulate in ROS deficient phagocytes leading to a persistent cellular activation (Schappi et al., 2008).

The attenuation of Ca^{2+}dependent signaling could be impaired in CGD, which would contribute to an increase of inflammation. This could happen by regulation of membrane potential in CGD granulocytes, which present a more negative membrane potential, and consequently an increase in Ca^{2+} influx. This higher intracellular Ca^{2+} concentration would promote a longer period of cell activation and increase in inflammatory response (Geiszt et al., 1997; Rada et al., 2003).

Recent discoveries have implicated ROS in intracellular signaling by oxidation of cysteine residues in phosphatases and transcriptional factors (Bedard and Krause, 2007). Therewith, it is possible that the absence of NADPH oxidase could create alterations in cellular signaling favoring

the inflammatory responses. Moreover, there are many data in the literature showing increased production of TNF-α and IL-8 (Geiszt et al., 1997; Hatanaka et al., 2004; Lekstrom-Himes et al., 2005; Rada et al., 2003) and decreased production of TGF-β and prostaglandin 2 (Brown et al., 2003) in neutrophils of patients with CGD.

There are solid evidences suggesting that ROS can induce apoptosis in neutrophils (Coxon et al., 1996; Gamberale et al., 1998; Hiraoka et al., 1998; Kasahara et al., 1997; Kobayashi et al., 2004; Ottonello et al., 2002; Yamamoto et al., 2002). Consequently, it was suggested that a decrease in the apoptosis of neutrophils would be the reason for the hyperinflammation seen in CGD (Brown et al., 2003; Hampton et al., 1998; Hampton et al., 2002; Kasahara et al., 1997; van de Loo et al., 2003).

3.5. ROS and *Leishmania*

3.5.1. Production of ROS by host cells in *Leishmania* infections

There are few papers in the literature addressing the direct role of ROS in infections caused by *Leishmania sp.* and the majority of them address their functions in *in vitro* systems.

In vitro studies show that neutrophils and macrophages produce ROS in response to *Leishmania*. However, the killing of *L. major* by IFN-γ-activated macrophages is dependent on $^{\bullet}NO$ production, but not on the production of superoxide or peroxynitrite (Assreuy et al., 1994). The lesions developed in mice deficient in NADPH-dependent oxidase of phagocytes (Nox2 or $gp91^{phox}$) infected with *L. major* are similar when compared to C57BL/6 mice. $Gp91^{phox}$ knockout mice control *L. major* at the site of infection at early time points, but display an unexpected reactivation of *L. major* infection after long periods of observation (more than 200 days of infection). Further, they show deficient control of parasite replication in draining lymph nodes and spleens, suggesting that $gp91^{phox}$ is important for the control of *L. major in vivo* at later times of infection by preventing visceralization of the disease (Blos et al., 2003).

The role of ROS in different models of infection with *Leishmania* changes according to the species. *L. guyanensis* (Sousa-Franco et al., 2006) and *L. braziliensis* (Scott and Sher, 1986) fail to establish infection and do not survive within non-activated peritoneal macrophages *in vitro*. In *in vitro* infection of BALB/c macrophages, *L. guyanensis* does not activate the production of $^{\bullet}NO$, however, the infection activates a respiratory burst markedly higher than that promoted by infection with *L. amazonensis*. The production of ROS is responsible for the elimination of *L. guyanensis* by

macrophages and *L. guyanensis* amastigotes die inside BALB/c macrophages through an apoptosis-like process mediated by parasite-induced ROS (Sousa-Franco et al., 2006). These findings demonstrate an important killing mechanism of *L. guyanensis* amastigotes. ROS are probably involved in resistance to infection in this species because mice that are unable to activate the respiratory burst by the regular administration of apocynin, an inhibitor of NADPH oxidase, do not control the infection as in untreated animals (Horta et al., 2012).

The participation of ROS in killing of *L. amazonensis* by mouse or human macrophages and their importance to parasite killing has been reported. The augmented SOD expression induced by IFN-β decreases the superoxide release interfering with killing of *L. amazonensis* and *L. braziliensis* (Khouri et al., 2009). Moreover, it has been shown that both superoxide and nitric oxide are required to parasite killing, *in vitro*, of *L. amazonensis* amastigotes within LPS/IFN-γ-activated bone marrow-derived macrophages generated from C3H mice (Mukbel et al., 2007).

Mouse peritoneal macrophages or J774 cell lineage treated with N-acetylcysteine (NAC) inhibits the leishmanicidal effect under hypoxia (Degrossoli et al., 2011). It is generally assumed that the action of NAC results from its antioxidative or free radical scavenging property (Sun, 2010). So NAC acts decreasing the concentrations of ROS making it possible to observe the behaviour of infected macrophages in the absence of ROS.

IFN-β dose-dependently increases parasite burden in *L. amazonensis* as well as *L. braziliensis* in infected human macrophages, independently of endogenous or exogenous $^{\bullet}NO$. In addition, IFN-β significantly reduces superoxide release in *Leishmania*-infected as well as uninfected human macrophages (Khouri et al., 2009), implying a possible involvement of *Leishmania* killing independent of nitric oxide, but dependent of superoxide anion.

The superoxide anion may combine with nitric oxide generating $ONOO^-$ and there are evidences in the literature that $ONOO^-$ is not involved in the killing of *L. major* (Assreuy et al., 1994; Blos et al., 2003). However, the specific role of this important oxidant has not been thoroughly explored. In contrast, the production of nitric oxide and $ONOO^-$ has been shown during infection with *L. amazonensis* in BALB/c (more susceptible to infection) and C57BL/6 mice (less susceptible to infection). The production of nitric oxide *in vivo* was detected as the nitrosyl hemoglobin complex in blood of infected mice. In parallel, infected footpads from mice, at several time points, present $ONOO^-$ formation detected as nitrotyrosine (Giorgio et al., 1996; Linares et al., 2001). C57BL/6 mice presented higher levels of nitrosyl complexes when compared to BALB/c mice at 6 weeks of infection. This coincides with the time where the lesions become chronic in C57BL/6 mice. Nitrosyl complexes also increase in BALB/c mice, but this effect is correlated with the lesion size. iNOS and nitrotyrosine-containing complexes co-localize in macrophages present in

the lesions from both mouse strains, and the most probable agent of protein nitration is $ONOO^-$ (Linares et al., 2001). Peroxynitrite kills *L. amazonensis* axenic amastigotes *in vitro* more efficiently than nitric oxide and it is proposed that, in BALB/c mice, $ONOO^-$ is involved in tissue damage (Linares et al., 2001). Since BALB/c is more susceptible despite the production of $^{\bullet}NO$, it is suggested that the delayed production of $ONOO^-$ impairs the capacity of these mice to control *L. amazonensis*. In addition, the treatment of C57BL/6 mice with Tempol, a stable cyclic nitroxide radical that protects cells from damage due to oxidative stress, promotes larger lesions, parasite growth, and lower levels of nitric oxide products and nitrotyrosine (Linares et al., 2008). Although transient, the effect of Tempol provides further evidence that $ONOO^-$ is involved in the control of *L. amazonensis in vivo*.

3.5.2. Importance of ROS in the direct killing of *Leishmania*

Several anti-leishmanial drugs have been tested and many of them exploit the redox system showing the importance of the oxidants agents derived from superoxide to eliminate the parasites.

Geranylgeraniol, a compound obtained from *B. orellana* seeds, increase ROS quantities in parasite membranes leading to permeabilization of these membranes followed by mitochondrial depolarization and increased mitochondrial ROS production. It was shown that this oxidative imbalance causes destructive effects on *L. amazonensis* DNA and that the promastigotes subsequently undergoes to apoptosis-like cell death (Lopes et al., 2012). Also, expanded porphyrins might generate oxygen singlets by light reaction promoting death of axenic amastigotes of *L. panamensis in vitro* by the same apoptosis-like cell death as described before (Hooker et al., 2012).

Another chemical reagent, the superoxide dismutase inhibitor diethyldithiocarbamate (DETC), induces *L. amazonensis* killing in human macrophages *in vitro*. Further, DETC induces superoxide production and the parasite killing. The effects of DETC are reverted by the addition of NAC, indicating that DETC-induced killing occurs through oxidative damage. In addition, DETC significantly induces parasite killing in *Leishmania* promastigotes in axenic cultures, increasing the production of ROS and killing of *L. braziliensis* in murine macrophages. The treatment with DETC also decreases the lesion size and parasite loads in BALB/c mice infected with *L. braziliensis* (Khouri et al., 2010).

Indeed, many papers in the literature show the direct effect of ROS, derived by chemical agents, in killing of *Leishmania* axenic cultures. The majority of those chemicals act in same way as

described as follows: chemicals stimulate ROS production by the parasites promoting lesions on DNA and consequently apoptosis.

3.5.3. Subversive mechanisms used by *Leishmania* to avoid damage by ROS

As mentioned before, ROS are important for parasite killing by causing severe lesions in DNA and promoting apoptosis of the parasite. So, *Leishmania* developed mechanisms to avoid the effects of ROS. These mechanisms mainly avoid ROS production by the host cells or promote the overexpression of antioxidant systems to neutralize the reactive ions.

SOD produced by *L. tropica* is a key enzyme that appears to act as first line defense against ROS generated by host cells. High levels of SOD are expressed in amastigote and promastigote forms of *L. tropica* suggesting a clear mechanism to decrease the ROS effects (Bahrami et al., 2011). In addition, SOD-deficient *L. tropica* are more sensitive to menadione (a ROS inducer) and hydrogen peroxide in axenic culture, and survive less in peritoneal BALB/c macrophages (Ghosh et al., 2003). These reports indicate that SOD is a major determinant of intracellular survival of *L. tropica*.

Fe-SOD from *L. chagasi* is expressed in high levels in the stationary promastigote and amastigote stages of infection. Parasites deficient in Fe-SOD have impaired growth in macrophages treated with paraquat (a ROS inducer) as the levels of intracellular $O_2^{\cdot -}$ increases Moreover, *in vitro* studies show decreased survival of these deficient parasites within the U937 human macrophage cell line, suggesting that Fe-SOD is important for the growth and survival of *L. chagasi* (Plewes et al., 2003).

Trypanothione reductase (TR) is the enzyme responsible for maintaining trypanothione in its reduced form and probably has a central role in the redox defense systems of trypanosomatids. Mutants of *L. donovani* and *L. major* possessing only one functional TR allele express less TR mRNA and have lower TR activity. Thus, these mutants present reduced infectivity and markedly less resistance to survive within macrophages stimulated to produce ROS (Dumas et al., 1997).

Besides the mechanisms cited, *Leishmania* can directly modify the ROS production of the host cells. Generally, these mechanisms involve the impairment of the NADPH oxidase complex assembly by amastigotes or promastigotes, the overexpression of antioxidant systems by host among others as described below.

The infection of macrophages with amastigote forms of *L. donovani* induce almost undetectable levels of superoxide release during phagocytosis, suggesting that the parasite influences the ability of the macrophages in produce ROS during phagocytosis. Indeed, *L. donovani*

amastigotes impair the phosphorylation of the NADPH oxidase component $p47^{phox}$, culminating on an ineffective assembly of the NADPH oxidase complex specifically in the recruitment of $p67^{phox}$ and $p47^{phox}$ (Lodge et al., 2006).

Immunoblots of subcellular fractions enriched with parasitophorous vacuoles (PVs) from *L. pifanoi* amastigote-infected cells reveal only a premature form of $gp91^{phox}$ in these compartments, the 65-kDa form of $gp91^{phox}$ (Pham et al., 2005). Therefore, it has been suggested that only the non-active form of $gp91^{phox}$ is recruited to vacuoles containing amastigotes forms of *L. pifanoi*. In addition, since $gp91^{phox}$ maturation is dependent on a heme group, infections by *Leishmania* induce an increase in heme oxygenase 1 (HO-1) expression, which decreases the viability of heme for NADPH oxidase assembly. On the other hand, infection using *L. pifanoi* amastigotes plus metalloporphyrins (inhibitors of HO-1) increases superoxide release by the infected macrophages (Pham et al., 2005). Therefore, it is has been suggest that *L. pifanoi* amastigotes avoid superoxide production by increasing the expression of HO-1 and consequently heme degradation. Thus, there is a blockage of the maturation of $gp91^{phox}$ and interruption in the assembly of the NADPH oxidase enzyme complex (Pham et al., 2005).

L. donovani interferes with the expression of SOD in infected macrophages through the upregulation of this gene. This increase in SOD expression levels by the infected macrophages might be due the attachment of the parasite to the macrophage membrane. Thus, there is a NADPH oxidase activation culminating in respiratory burst, which promotes a considerable increased level of SOD in the infected cells (Mukherjee et al., 1988). This increase in SOD levels by the host cell might promote a reduction in the availability of the superoxide.

L. donovani infection is upregulates uncoupling protein 2 (UCP2), which is a negative regulator of mitochondrial ROS generation located at the inner membrane of mitochondria. The silencing of macrophage UCP2 by small interfering RNA is associated with increased ROS production in mitochondria, lower parasite survival, and induction of marked pro-inflammatory cytokine response (Basu Ball et al., 2011). So, the induction UCP2 expression during *Leishmania* infection downregulate mitochondrial ROS generation in the host, and consequently decreases the parasite damage.

3.6. Relevance of the work and explanation of thesis structure

As shown above, a number of studies on the role of ROS on the control of infection with *Leishmania* exist, but few reports really address the importance of ROS produced by phagocytes in *Leishmania* killing. Moreover, ROS play an important role in the immune response regulation in

several bacterial infections, but this role was not explored in the parasitic infections field until now. In face of the scarcity of studies on the link between ROS and *Leishmania* genus and the important role that ROS have in inflammation control, we set up to study these points. Therewith, we hope to have elucidated ROS importance in the control of infection caused by *L. amazonensis* and their role in immune regulation in parasitic infections.

The results presented in this thesis will be separated in three parts: in part one I will show the results on the role of ROS in subcutaneous infection with *L. amazonensis* in mice; in the second part I will compare intradermal and subcutaneous murine infections with *L. major* and in the third part I will show the effect of ROS in intradermal infection with *L. amazonensis*.

In the first part, we focused on the influence of ROS during subcutaneous *L. amazonensis* infection of the footpad. There studies should be highly informative as there are no reports in the literature demonstrating the effects of ROS in this important disease in Brazil. We employed subcutaneous infection of the mouse footpad as previous studies involving ROS and *Leishmania,* or infection by *L. amazonensis,* have employed this site.

There are some controversial results in the literature about the influence of innate immune cells such as neutrophils on *Leishmania* infection. Our data suggests that different routes of infection could play a role in these contradictory results. Therefore, in the secondary part of these studies, we investigated, at the cellular and molecular levels, the differences in the two main routes of infection used in leishmaniasis study: the subcutaneous infection of the footpad and intradermal infection of the ear, which is thought to more closely reproduce natural infection. For these studies we employed a more established model of *Leishmania* infection, the infection caused by *L. major* in mice.

We identified interesting differences in the infection course comparing intradermal and subcutaneous routes of inoculation. We observed a massive accumulation of inflammatory cells, especially neutrophils, and a more efficient capture of *Leishmania* by these cells at the intradermal site, promoting a much higher inflammation and parasite loads during early infection versus mice infected by the subcutaneous route. Because the massive neutrophils infiltration post infection observed at intradermal site and the low frequency of these cells after subcutaneous infection, we predicted this phenomenon could also be true in our *L. amazonensis*/ROS model. Moreover, neutrophils are the most important cells involved in oxidative stress induction through ROS production. These cells are the major ROS producers during the innate immune response and are a major source of these radicals. The exacerbated production of ROS by these cells during the immune response promotes damage and triggers apoptosis. Apoptosis contributes to the resolution of inflammation, since apoptotic bodies have anti-inflammatory actions (Haanen and Vermes,

1995). Therefore, there is a close relation between neutrophils and ROS. Because this relation and the massive accumulation of these cells at intradermal site of *L. major* infection, we decided, in the third part of this thesis, to determine the participation of ROS following intradermal infection with special attention to neutrophil behavior. We speculate that neutrophils could demonstrate some impairment in apoptotic/anti-inflammatory cell death, which could culminate in an uncontrolled inflammation in $gp91^{phox}$ deficient mice. Moreover, since we demonstrated that neutrophils have much more influence in the intradermal route of infection (and consequently higher ROS participation), and this site is closest to natural infection, we speculated that intradermal infection would be a better model to study the influence of ROS in *Leishmania* infection.

The first part of this work was performed at the Laboratory of Gnotobiology and Immunology of ICB/UFMG - Brazil, under the supervision of Dr. Leda Quercia Vieira. The second part was performed in collaboration with Dr. Flávia Ribeiro Gomes of the Laboratory of Parasitic diseases, NIAID/NIH - USA, under the supervision of Dr. David Sacks and Dr. Nathan Peters. The third part was developed at the Laboratory of Parasitic diseases under the supervision of Dr. Leda Quercia Vieira and Dr. Nathan Peters.

The aims, material and methods and results will be presented separately in each section. At the end a discussion will be made grouping all results as well as the conclusions.

4. PART ONE: SUBCUTANEOUS INOCULATION WITH *L. AMAZONENSIS* IN GP91$^{PHOX-/-}$ MICE PROMOTE CHANGES IN INFLAMMATORY RESPONSE TO INFECTION

4.1. Objectives

4.1.1. General objective

To evaluate the role of ROS in the inflammatory response and parasite control of C57BL/6 mice infected subcutaneously with *Leishmania amazonensis*.

4.1.2. Specific objectives

- To determine the production or ROS by peritoneal macrophages infected with *L. amazonensis*;
- To follow the development of dermal lesions in gp91$^{phox-/-}$ and C57BL/6 mice (WT) infected with *Leishmania amazonesis* until 16 weeks post-infection;
- To compare the parasite loads found in gp91$^{phox-/-}$ and WT mice at 4, 8, 12 and 16 weeks of infection;
- To analyze the phenotype of immune cells at several time points post-infection at the site of infection, the draining lymph node, and the spleen;
- To analyze the expression of inflammatory and anti-inflammatory cytokines, as well as chemokines (in protein or mRNA levels) at the site of infection and draining lymph nodes;
- To analyze the humoral response against *L. amazonensis* by anti-*Leishmania* antibodies (total IgG, IgG_1 and IgG_{2a}) present in serum;
- To compare the neutrophil migration profile to the lesion site from 6h to 72h post-infection with *L. amazonensis* in gp91$^{phox-/-}$ and WT mice;
- To evaluate separately the contribution of superoxide anion, hydrogen peroxide and nitric oxide in parasite killing;
- To measure the production of inflammatory cytokines, chemokines and nitrite in peritoneal macrophages (stimulated or not with IFN-γ/LPS) infected with *L. amazonensis in vitro*;

4.2. Material and Methods

4.2.1. Parasites

We utilized the PH8 strain of *Leishmania amazonensis* (IFLA/BR/1967/PH8). The promastigote forms were cultivated in BOD incubator at 25ºC in Grace's insect medium (Gibco, Invitrogen do Brasil S.A., São Paulo, SP, Brazil) diluted in bi-distilled water, plus 20% of fetal bovine serum (FBS, Cultilab, Campinas, SP, Brazil), 10,000U/ml of penicillin (Gibco) and 2mM of glutamine (Gibco). Parasites with less than 10 passages in culture were used for all experiments and new isolates were obtained form BALB/c mice lesions.

4.2.2. Mice

Mice (n=6 for all experiments for each repetition) which genes for the gp91^{phox} chain of NADPH oxidase were deleted by homologous recombination (C57BL/6.129S6-Cybb^{tm1Din}/J, here named gp91$^{phox-/-}$) were obtained from Jackson Farms (Glensville, NJ, USA) (Pollock et al., 1995). The control mice used in the experiments were C57BL/6 strain. BALB/c mice were periodically infected for the maintenance of *L. amazonensis*. These animals were supplied by the Center of Bioterism (CEBIO - ICB, UFMG, Belo Horizonte, MG, Brazil). Four to twelve-week-old animals were used in the experiments and kept in conventional animal facility with barriers, controlled 12h dark-light cycles and without food and water restrictions. The experimental protocol was approved by ethical committee of the UFMG (Protocol 031/09).

4.2.3. Luminometry assay

Mice were injected intraperitoneally with 2ml of thioglycolate 4% (BD Falcon, Franklin Lakes, NJ USA) in PBS. After 72h, the mice were euthanized and the peritoneum cells were harvested by repeated cycles of aspiration and re-injection with 10ml of cold PBS in 10ml syringe with 24G needle. After harvested, more than 80% of the cells of peritoneum are macrophages. The cells were centrifuged at 4^{o}C, 1,500 x *g* for 10 minutes. The cells were counted in a hemocytometer and the concentration was set up to 1x10^{6} cells/100µl of supplemented with 10% heat-inactivated fetal bovine serum (FBS) (Cultilab, Campinas, SP - Brazil), 100U/mL penicillin, 100µg/ml

streptomycin and 2mM L-Gglutamine (GIBCO BRL) (complete RPMI) without phenol red. The cells (1 x 10^6 cells/well) were plated in a 96 well opaque plates (NUNC, Rochester, NY, USA) together with 0.05mM of luminol (5-Amino-2,3-dihydro-1,4-phthalazinedione) (Sigma-Aldrich, Inc, St. Louis, MO, USA). Immediately before the measurement, metacyclic promastigote forms of *L. amazonensis* were added in the proportion of 10 parasites to 1 macrophage. The measurement was followed by 90 minutes with 1 minute interval between the measurements. The production of ROS was calculated by the light intensity generated by reaction between ROS and luminol and expressed as relative light units (Allen and Loose, 1976).

4.2.4. Infection with *L. amazonensis*

Mice were infected with 1 x 10^6 metacyclic promastigote forms of *L. amazonensis* diluted in 40µl of PBS in the hind right footpad. Metacyclic promastigote forms obtained by centrifugation in Ficoll gradient (Spath and Beverley, 2001). The course of infection was followed weekly for 16 weeks by measurements of the thickness of the footpads swelling using a digital micrometre (Starrett 727, Itu, SP, Brazil).

4.2.5. Euthanasia, collection of blood and organs

Mice were anesthetized intraperitoneally with a solution made with ketamine 130mg/kg and xylazine 0.3mg/kg of corporal weight diluted in PBS. After certification of unconsciousness, the blood was collected from the cutaneous plexus in the inguinal region. Subsequently, animals were euthanized by exsanguination and the death was confirmed by cervical dislocation. Blood was collected with Pasteur pipettes and the serum was separated by centrifugation at 3000 x *g* for 15 minutes. The serum samples were kept at -20ºC for the analysis. The draining lymph nodes, spleens and footpads were also removed and used for additional experiments.

4.2.6. Parasite load quantification

The quantification of the parasites was made by limiting dilution. After the euthanasia, the footpads were removed and washed in detergent and ethanol 70%. The tissues were triturated in

0,01M sodium phosphate buffered saline, pH 7.2 (PBS) containing 200μg/ml streptomycin and 200U/ml penicillin (Gibco). The suspension was centrifuged at 1000 x *g* for parasite sedimentation and the pellet was resuspended in 0.5ml of Grace's insect medium containing 20% FBS, 200μg/ml of streptomycin, 200U/ml of penicillin and 2mM of L-Glutamine (complete Grace's medium). Two hundred μl of parasite suspensions were added to 96-well sterile assay microplates, in duplicates. These samples were diluted 1:4 successively in complete Grace's medium. The draining lymph nodes were removed, triturated in 0.5ml of complete Grace's medium and plated as were the footpads. After 10 days of incubation at 25ºC in BOD incubator, the cultures were examined for parasite detection. The same procedure was performed for parasite determination in spleens, except that just one fragment (around 0.1g) was used for quantification. The results were expressed as titers as described (Santiago, Oliveira *et al.*, 2004).

4.2.7. Real time PCR

Total RNA, obtained from lesions at 4, 8, 12 and 16 weeks post-infection, was extracted using Trizol Reagent (Invitrogen, Carlsbad, CA, USA) according to the manufacturer's instructions. Next, 1 μg of total RNA obtained from the lesions or lymph nodes was reverse transcribed using Reverse Transcriptase (Promega, Southampton, UK) and oligo (dT) 15 nucleotide primers (Promega, Southampton, UK). PCR amplification was performed with a programmable thermal cycler (Perkin–Elmer 2400, USA) and the cDNA amplification protocol was as follows: 2 minutes at 50^{o}C, activation of AmpliTaq at 95^{o}C for 10 minutes, melting at 95^{o}C for 15 seconds. For the annealing and final extension, the samples were heated at 60^{o}C for 1 minute for 45 cycles. For dissociation curve, the samples were heated at 95^{o}C for 15 seconds, following by cooling at 60^{o}C for 5 seconds. Finally, the samples were cooled for 1 minute at 4^{o}C.

The amplification of cDNA was made using specific primers as represented in the table 1:

Table 1. Primers used in qPCR to quantify the expression of mRNA from footpads in the infection.

Gene	Primer	Sequence
IFN-γ	Forward	5' -TCAAGTGGCATAGATGTGGAAGAA- 3'
	Reverse	5' -TGGCTCTGCAGGATTTTCATG- 3'
IL-4	Forward	5' -ACAGGAGAAGGGACGCCA- 3'
	Reverse	5' -GAAGCCCTACAGACGAGCTCA- 3'
IL-10	Forward	5' -GGTTGCCAATTATCGGA- 3'
	Reverse	5' -ACCTGCTCCACTGCCTTGCT- 3'
TNF-α	Forward	5' -TTCTGTCTACTGAACTTCGGGGTGATCGGTCC- 3'
	Reverse	5' -GTATGAGATAGCAAATCGGCTGACGGTGTGGG- 3
IL1-β	Forward	5' -CAACCAACAAGTGATATTCTCCAT- 3'
	Reverse	5' -GATCCACACTCTCCAGCTGCA- 3
IL-6	Forward	5' -CAGAATTGCCATCGTACAACTCTTTTCTCA- 3'
	Reverse	5' -AAGTGCATCATCGTTGTTCATACA- 3'
IL-17	Forward	5' -ATCCCTCAAAGCTCAGCGTGTC- 3'
	Reverse	5' -GGGTCTTCATTGCGGTGGAGAG- 3'
CXCL1 (KC)	Forward	5' -TGTCCCCAAGTAACGGAGAAA- 3'
	Reverse	5' -TGTCAGAAGCCAGCGTTCAC- 3'
iNOS	Forward	5' -CCCTTCCGAAGTTTCTGGCAGCAGC- 3'
	Reverse	5' - GGCTGTCAGAGCCTCGTGGCTTTGG- 3'
18S rRNA	Forward	5' -TACCACATCCAAGAAGGCAG- 3'
	Reverse	5' -TGCCCTCCAATGGATCCTC- 3'

The reactions were developed in the ABI PRISM®7900HT (Applied Biosystems, Foster City, CA, USA) using 20% of reaction in cDNA volume and 15µl of total PCR mixture. All reactions were made in duplicates using SYBR Green Master Mix (Applied Biosystems) according manufacturer instructions. Finally, the samples were cooled by 1 minute at 4^{o}C. The specific cDNAs were normalized according the expression of ribosomal 18S gene based in ΔCT calculation.

4.2.8. Generation of *L. amazonensis* antigen of (LA*La*)

Antigens were prepared from log phase promastigotes, washed in PBS and submitted to seven cycles of freezing in liquid nitrogen and thawing in water bath (37ºC). Suspensions were adjusted to a final concentration of 1 mg of protein/ml and kept at -70ºC until use. Protein concentration was assessed by the Lowry method (Lowry et al., 1951).

4.2.9. ELISA for cytokine measurements

The draining lymph nodes (dLNs) of mice 8, 12 and 16 weeks post infection were macerated and resuspended in complete RPMI. Five million cells were plated in 24 well plates (NUNC) and stimulated or not with *L. amazonensis* antigen (LA*La*) (50µg/ml) for 48h at 37°C and 5% CO_2. Concanavalin A (Sigma-Aldrich, Inc, St. Louis, MO, USA) was used as positive control (10µg/ml) of cytokine production. The levels of IFN-γ, IL-10, IL-6 and IL-17 were measured in supernatants using appropriated cytokine assay kits BD OptEIA$_{TM}$ following manufacturer instructions. The detection levels were 15.625 picograms for IFN-γ, IL-10, IL-6 and 7.8125 picograms for IL-17.

4.2.10. ELISA for anti-*Leishmania* IgG_1, IgG_{2a} and total IgG

Mouse sera were collected as described in item 4.2.4. at 4, 8, 12 and 16 weeks post infection.

Nunc Maxisorp® 96-well plates (ThermoFisher Scientific Rochester, NY - USA) were coated with 5µg/ml of LA*La* (100µl of final volume) for 16h at 4^{o}C in 0.02M sodium bicarbonate, pH 9.6 (coating buffer). After incubation, the coating buffer was discarded and the plates were blocked with casein 2% in PBS (200µl of final volume) for 1h at 37^{o}C and then washed three times with PBS containing 0.05% Tween 20 (PBS-Tween). Following the blocking, the serum was placed in the plates in 1:2, serial dilution ranging from 1:50 to 1:400 (100µl of final volume). Sera were diluted in PBS containing 0.25% casein and 0.05% of tween 20 (incubator buffer) and incubated for 1h at 37^{o}C. The plates were washed five times with PBS-Tween and the respective secondary antibody (anti-total mouse IgG, anti- mouse IgG_1 or anti- mouse IgG_{2a}) conjugated to peroxidase

(Sigma-Aldrich, Inc.) were plated diluted in PBS containing 0.25% casein and 0.05% Tween 20 in their respective dilutions for 1h at 37°C. After incubation time, the plates were washed seven times with PBS-Tween and the next step was the colorimetric reaction.

The binding of specific antibodies to *Leishmania* antigens present in the serum of mice is indirectly revealed by the secondary antibody conjugated to horseradish peroxidase. For the colorimetric step, 100µl of *o*-phenylenediamine (OPD) solution (0.33mg/ml of OPD plus H_2O_2 0.04% in 0.1M citrate buffer pH 5.0) was added to plates for 15-20 min at room temperature in dark environment. The OPD is oxidized by horseradish peroxidase donating electrons to H_2O_2 and forming 2,3-diaminophenazine plus H_2O. The product formed, 2,3-diaminophenazine, is orange-brown in color and can be read spectrophotometrically at 450 nm (Bovaird et al., 1982). The OPD reaction was stopped with 2N H_2SO_4 solution, and read at 492 nm in an ELISA microplate reader TITERTEK multiscan (Rockville, Maryland, USA). The intensity of the color is correlated with the quantity of specific anti-*Leishmania* antibodies presented in the assay. The results were expressed as the absorbance value given in the reader.

4.2.11. Flow cytometry

The footpads were cut into small parts and placed in RPMI (GIBCO BRL) containing 100U/ml penicillin, 100µg/mL streptomycin (GIBCO BRL) and 125U/mL collagenase A (Sigma-Aldrich, Inc) for 2h at 37ºC in a humidified atmosphere containing 5% CO_2. After incubation the pieces of footpads were filtered with 40µm cell strainer filter (BD Falcon, USA) and washed with 10ml of RPMI containing 0.05% DNAse (Sigma-Aldrich, Inc). The homogenates were centrifuged at 50 x *g* for 4 min. to remove large tissue debris and the supernatants were collected and centrifuged at 1,500 x *g* for 15 min. The sediment was resuspended in 1ml of complete RPMI.

The draining lymph nodes were excised from the animals, smashed in 40µm cell strainer filter (BD Falcon, USA) and washed by 10ml of RPMI 0.05% DNAse (Sigma-Aldrich, Inc, St. Louis, MO, USA). The homogenates were centrifuged at 1,500 x *g* for 15 min. and the pellet was resuspended in 1ml of complete RPMI. The spleens had the same procedure as the lymph nodes to cell collection. However, some extra steps to lysate red blood cells were performed. After the organ smashing, the suspension was washed with PBS and then centrifuged at 1,500 x *g* for 15 min. The pellet was resuspended in 4ml of ACK Lysing Buffer (Life Technologies, Grand Island, NY - USA) for 4 min. at room temperature. The reaction was stopped adding 10ml of PBS and the suspension

was centrifuged at 1,500 x *g* for 15 min. Finally the pellet was resuspended in 1ml of complete RPMI and counted in a hemocytometer.

The phenotypic analysis of cell by flow cytometry was made according as follow: the cells, after of isolation, were resuspended in 100µl of PBS pH 7.4 containing 0.2% bovine serum albumin (BSA) and 0.1% de NaN_3, incubated for 30 min. at 4ºC with anti-phenotypic markers monoclonal antibodies conjugated with fluorescein isothiocyanate (FITC), phycoerythrin (PE) or PerCP-Cy5.5 in v-bottom plates. Plates were centrifuged at 1,500 x *g* for 15 min, 4^{o}C, washed with PBS-BSA-NaN_3 and re-centrifuged at 800 x *g* for 2 min, 4^{o}C. The supernatant was discarded and the cells were resuspended in 100µl of PBS-BSA-NaN_3 buffer. The acquisition of the samples was made in a three colors FACScan cytometer (Becton Dickinson, Mountain View, California, USA) using the software CellQuest (Becton Dickinson, Mountain View, California, USA). The percentage of positive cells and the median of fluorescence intensity were analyzed with the software FlowJo (Tree Star, Ashland, Oregon, USA).

The antibodies used were organized and described as follow: tube 1 (anti-CD4 PerCP-cy5.5, anti-CD8 FITC, anti-CD44 PE) and tube 2 (anti-F4/80 PE-Cy5, anti-Ly6G PE, anti-CD80 FITC), all acquired from Pharmingen (Becton Dickinson, Mountain View, California, USA).

4.2.12. Mieloperoxidase assay for neutrophil numbers inference

The neutrophil accumulation in the infected footpads at acute phase (6h and 72h) was measured by assaying myeloperoxidase activity (MPO). Briefly, the footpads were infected as described in item 4.2.4. Six and 72 h post infection, the mice were euthanized, the footpads were removed and snap-frozen in liquid nitrogen. On thawing, the tissue (100mg of tissue per 1.9ml of buffer) was homogenized in pH 4.7 buffer (0.1mol/L NaCl, 0.02mol/L NaH_2PO_4, 0.015mol/L sodium ethylenediaminetetraacetic acid), centrifuged at 260 x *g* for 10 minutes and the pellet subjected to hypotonic lyses (15ml of 0.2% NaCl solution followed 30 seconds later by the addition of an equal volume of a solution containing NaCl 1.6% and glucose 5%). After a further centrifugation, the pellet was resuspended in 0.05M NaH_2PO_4 buffer (pH 5.4) containing 0.5% hexadecyltrimethylammonium bromide (HTAB) and re-homogenized. One-milliliter aliquots of the suspension were transferred into 1.5ml tubes followed by three freeze-thaw cycles using liquid nitrogen. The aliquots were then centrifuged for 15 minutes at 10,000 × *g*, the pellet was resuspended to 1ml. Myeloperoxidase activity in the resuspended pellet was assayed by measuring

the change in optical density (OD) at 450nm using tetramethylbenzidine (1.6mM) and H_2O_2 (0.5mM) as substrates. Results were expressed as OD.

4.2.13. Phagocytic and microbicidal activity of macrophages in infections *in vitro*

Two hundred thousand peritoneal macrophages were collected as described in item 4.2.3 and placed in 8-well Lab-Tek® chamber slides for 16h. After incubation, the cells were washed to remove the non-adherent cells and infected with 1 x 10^6 metacyclic promastigote forms of *L. amazonensis* for 4h at 34°C in 5% of CO_2 atmosphere. The cultures were washed three times with RPMI to remove non-phagocytized parasites and then the cultures were incubated for 72h at 34°C in 5% of CO_2 atmosphere. Cells were treated with inhibitors of ROS and nitric oxide production throughout the incubation period as follow: 300μM of apocynin, 1mM of L-NG-monomethyl arginine citrate (L-NMMA), 1000U/ml of polyethylene glycol conjugated catalase (PEG-catalase) and 100U/ml of polyethylene glycol conjugated superoxide dismutase (PEG-SOD) (all purchased from Sigma-Aldrich, Inc.). These inhibitors were used in combination to isolate specifically superoxide anion, peroxide of hydrogen and nitric oxide. So, we could verify the specific importance of these reactives in parasite killing.

After 72h the cells were washed and stained with Panótico (Panótico Rápido, Center Kit, Ribeirão Preto, SP - Brazil) according to manufacturer instructions. Following the staining, 100 cells were counted in three different spots for each sample, performed in triplicates.

4.2.14. Cytokine and chemokine production and nitrite measurements from peritoneal macrophages cultures

Two million peritoneal macrophages were placed in 24-well plates (TPP, Trasadingen, Switzerland) for 16h in complete RPMI at 37°C, 5% of CO_2 atmosphere and then washed three times to remove non-adherent cells. The infection and wash of non-internalized parasites was performed as described in item 4.2.13, but in this particular case we used *L. amazonensis* stationary phase promastigotes respecting the proportion of 10 parasites per 1 macrophage.

After 4h of infection, the cells were activated with LPS (100ng/ml) and IFN-γ (100U/ml). In these experiments, we utilized macrophages in culture media (basal), stimulated with LPS/IFN-γ,

infected with *L. amazonensis* or infected and stimulated with LPS/IFN-γ. After 48h, part of the supernatant was collected for nitrite measurement by Griess method (Green et al., 1982) and 72h post infection the supernatant was used the measure the cytokines and chemokines. Due the stability and peak of production, the TNF-α was collected 24h post infection.

4.2.15. Statistical analysis

The statistical analysis was performed by with two-tailed Student's *t*-test, Mann-Withney nonparametric test or two-way ANOVA with Bonferroni post-test depending on the experiment. The software GraphPad Prism 5.0 (GraphPad, La Jolla, CA, USA) was utilized for the analysis. Differences were considered significant if $p<0.05$, data are expressed as mean and standard deviation.

4.3. Results

4.3.1. *L. amazonensis* induces respiratory burst in macrophages from C57BL/6 mice

Because ROS are very important for the elimination of a variety of intracellular parasites, we first investigated if *L. amazonensis* was capable of triggering respiratory burst in macrophages from C57BL/6 mice. We followed ROS production for 90 minutes using the luminometry technique (Allen and Loose, 1976). ROS produced by macrophages in phagolysosomes acts as an oxidizing agent to luminol releasing light and N_2. The chemiluminescent reaction is detected by a luminometer, which quantifies the light in arbitrary light units.

One million peritoneal macrophages from C57BL/6 wild-type (WT) mice were infected with promastigote forms of *L. amazonensis* in stationary phase of growth (10 parasites per macrophage) and were immediately placed in the luminometer. Even after a few minutes, the macrophages produced ROS reaching the peak of production between 15 and 30 minutes post infection (Figure 9). Since *L. amazonensis* could stimulate ROS production by macrophages, we asked if this could have an effect in the infection development.

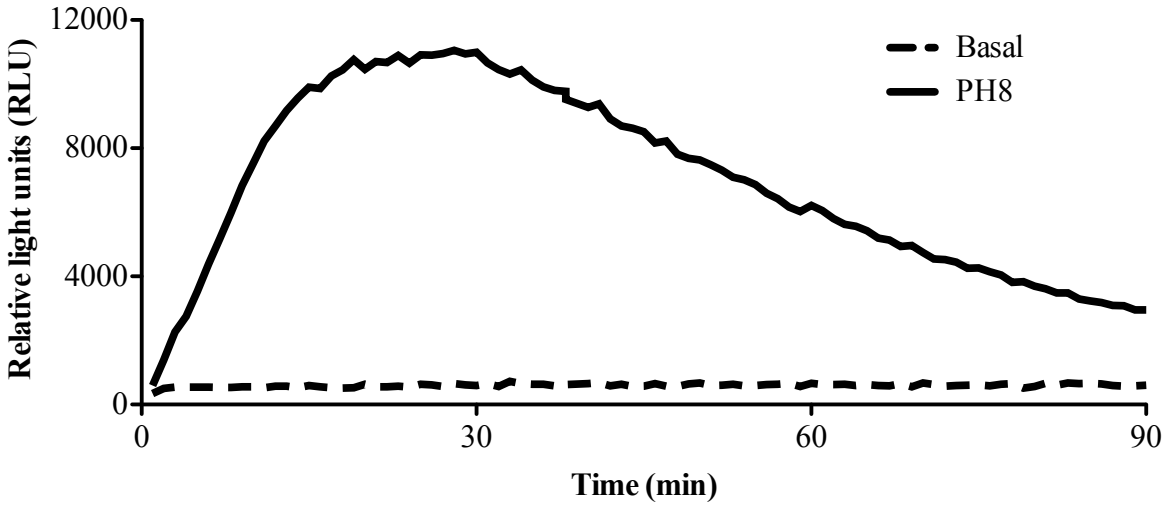

Figure 9. Production of reactive oxygen species by macrophages stimulated with *L. amazonensis*. Thioglycolate-elicited macrophages were harvested from the peritoneum of C57BL/6 mice in 3 days after stimulation. The macrophages were placed with luminol reagent and *L. amazonensis* metacyclic promastigotes (10 parasites per macrophage). The production of ROS was measured as relative light units generated by luminol oxidation, for 90 minutes. The basal production of ROS was obtained by incubating macrophages in medium. Data are from one representative experiment of 4, n=5 mice for each experiment.

4.3.2. Gp91$^{phox-/-}$ mice show different lesion development, but present similar parasite loads in footpads and dLNs to those of WT mice.

To address the importance of ROS in *L. amazonensis* infection, we used mice deficient in the subunit gp91^{phox} of NADPH-dependent oxidase of phagocytes enzyme (gp91$^{phox-/-}$). This subunit is responsible for transferring electrons from NADPH to oxygen in gp91^{phox}, generating the superoxide anion (Pollock et al., 1995). So, these mice cannot produce ROS dependent of gp91^{phox}.

WT and gp91$^{phox-/-}$ mice were infected with 1 x 10^6 metacyclic promastigote forms of *L. amazonensis* in the right hind footpad and the lesions were followed weekly by paw swelling measurements with a paquimeter until 16 weeks. In intervals of 4, 8, 12 and 16 weeks (5 animals per time point), the mice were euthanized and we used the footpad, draining lymph nodes and spleens to quantify the parasite loads by limiting dilution.

We observed larger lesions in gp91$^{phox-/-}$ mice five to seven weeks post infection. However, at 10 weeks, the lesions in gp91$^{phox-/-}$ started to decline, in contrast to WT animals. The WT mice still presented lesion growth after 10 weeks, lesions started to decline one week later. WT mice presented larger lesions compared to gp91$^{phox-/-}$ at weeks 11 to 14. The lesions in both groups

stabilized 13 weeks post infection and we could not detect differences in lesion sizes at weeks 15 and 16 post infection (Figure 10A).

Regardless of the observed differences in lesion size, we did not detect differences in parasite loads at the site of infection 4, 8, 12 and 16 weeks post infection (Figure 10B). The same was observed in draining lymph nodes (dLNs) (Figure 10C). Despite heavy parasite loads found in the footpads and draining lymph nodes, we could not find parasites in the spleens of either group (not shown).

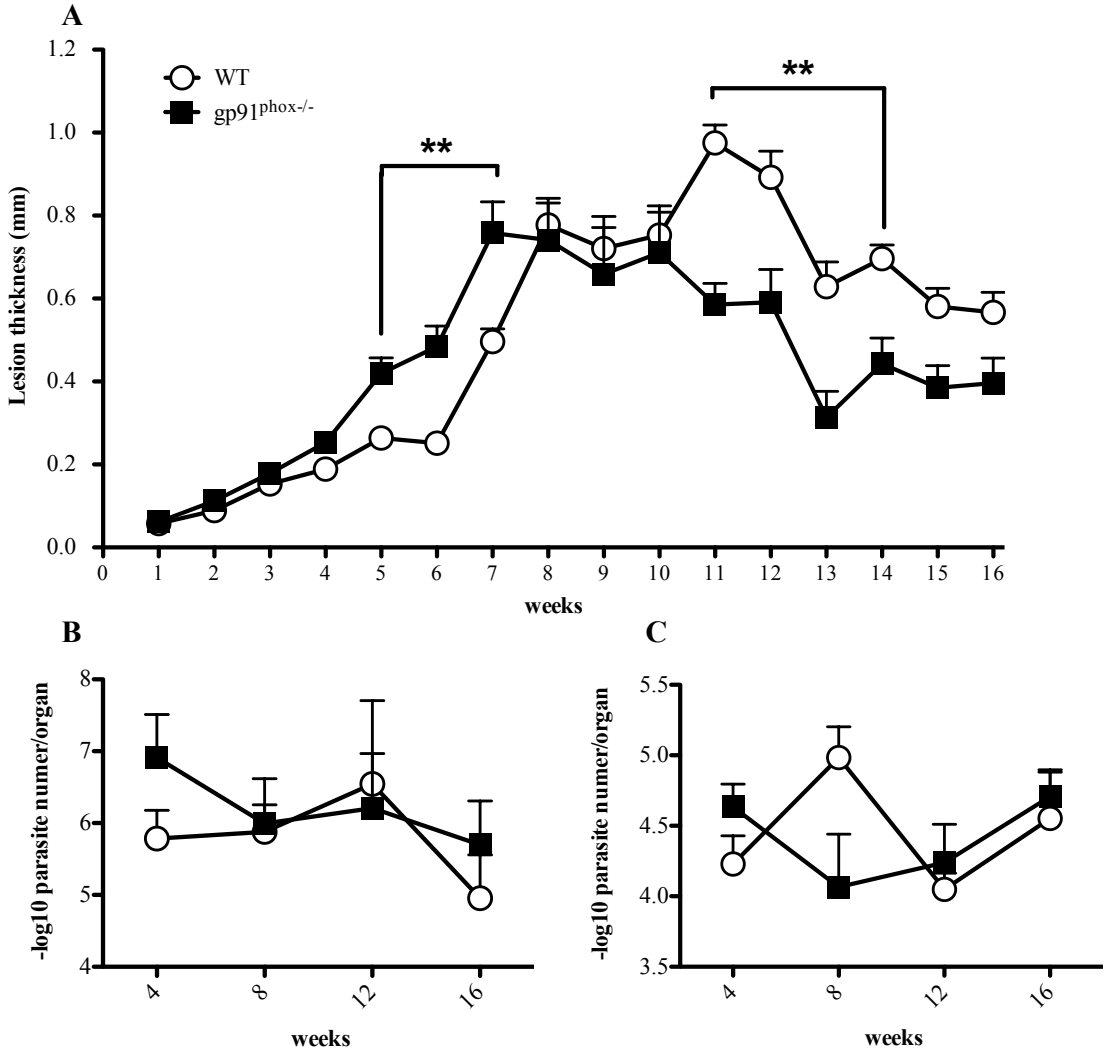

Figure 10. Lesion size and parasite loads in mice infected with *L. amazonensis*. Mice were infected with 1 x 10^6 metacyclic promastigote forms of *L. amazonensis* in the hind right footpad and followed for 16 weeks. (A) Footpad thickness measured weekly by, **p<0.01. (B) Parasite loads found in the footpads of infected mice 4, 8, 12 and 16 weeks post infection. (C) Parasite loads found in draining lymph nodes of infected mice 4, 8, 12 and 16 weeks post infection. Data are shown as mean plus/minus standard deviation (± SD) from one representative experiment of 3, n=5 for each experiment.

4.3.3 WT mice express IL-1β in footpads at chronic phase of *L. amazonensis* infection when compared to gp91$^{phox-/-}$.

Since IFN-γ and TNF-α are crucial to eliminate *Leishmania* in infected macrophages (Bogdan et al., 1990), we speculated a possible compensatory mechanism of cytokine production in gp91$^{phox-/-}$. So, we extracted mRNA 4, 8, 12 and 16 weeks post infection in footpad and performed a real time PCR to verify possible changes in mRNA levels of inflammatory cytokines and chemokines. We could not observe changes in mRNA levels of IFN-γ or TNF-α in footpads (Figure 11A and 11B). However, we found higher expression of IL-1β mRNA in WT in the chronic phase of the infection, as seen in 12 and 16 weeks post infection (Figure 11E) which agrees with higher swelling of footpads in these mice observed at 11 weeks after infection (Figure 10A). Moreover, the mRNA levels of IL-4 were higher in gp91$^{phox-/-}$ in the last time point measured (Figure 11C), which could indicate a signalling of anti-inflammatory response. Despite the unbalanced inflammatory response observed in WT mice, no changes in IL-10 mRNA levels were observed in either group until 16 weeks post infection (Figure 11D).

IL-17 is an important cytokine related to neutrophilic response to infection (Hoshino et al., 2000) and we decided to verify the expression levels of this cytokine during *L. amazonensis* infection in gp91$^{phox-/-}$ mice. However, we could not find differences in IL-17 mRNA expression at the time points analysed (Figure 11G).

IL-6 is produced by immune innate cells, especially neutrophils, and it is considered a hallmark of inflammation (Rose-John et al., 2007). So we also decided to analyse possible changes in the expression of this cytokine due to alterations observed in the footpad swelling in gp91$^{phox-/-}$ mice infected with *L. amazonensis*. However, we could not find differences in IL-6 mRNA levels 4, 8, 12 and 16 weeks post infection (Figure 11F).

In addition, CXCL1, one of the major chemokines, together with CXCL2, involved neutrophil recruitment (Kobayashi, 2006) was analysed based on mRNA expression. We could not observe alterations in CXCL1 mRNA expression in any of the times measured (Figure 11H).

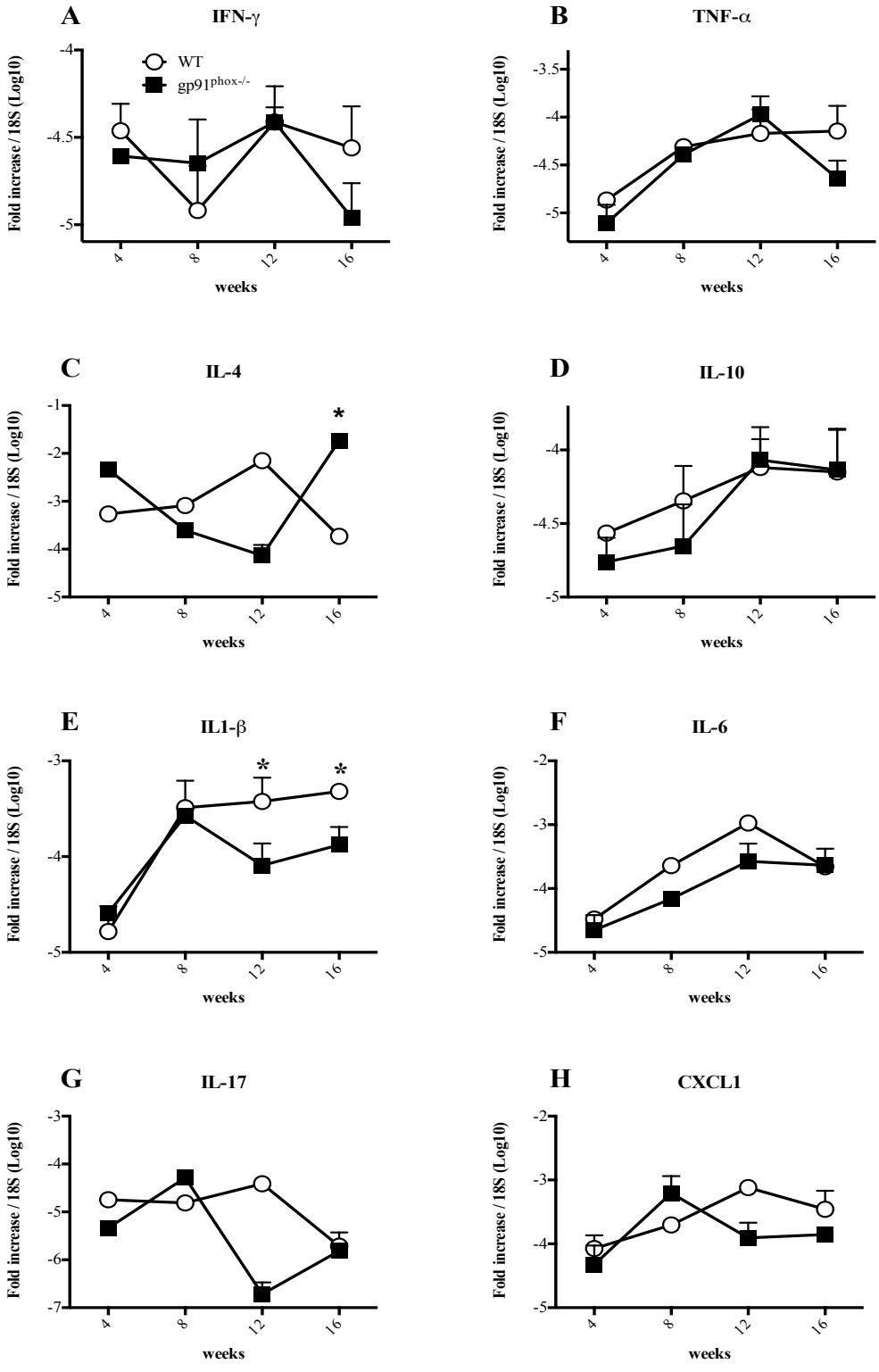

Figure 11. mRNA expression levels of cytokines in *L. Amazonensis*-infected footpads measured by qPCR. Mice were infected with 1 x 10^6 *L. amazonensis* metacyclic promastigotes in the right hind footpad and followed until 16 weeks. A, B, C, D, E, F, G and H represent the mRNA expression of IFN-γ, TNF-α, IL-4, IL-10, IL-1β, IL-6, IL-17 and CXCL1 respectively, normalized by 18S mRNA expression 4, 8, 12 and 16 weeks post infection. The results were expressed by mean ± SD, n=3-5, *p<0.05.

4.3.4. Mice lacking gp91^{phox} induces a higher Th17 response in acute phase of *L. amazonensis* infection

The Th1 response is necessary to eliminate *Leishmania* and the major sources of production of these types of cytokines are $CD4^+$ T lymphocytes (Scott et al., 1988). We measured the production of cytokines in dLNs of mice infected with *L. amazonensis* 8, 12 and 16 weeks post infection to verify the type of response triggered in gp91$^{phox-/-}$ mice in the course of infection by *L. amazonensis*.

We collected the draining lymph nodes from mice 8, 12 and 16 weeks post infection and stimulated with LA*La*. The mitogen concanavalin-A was used as a positive control for cells stimulation and cells without stimulation were used as negative control (data not shown). The secreted IFN-γ, IL-12p70, IL-17, IL-10 and IL-6 were measured and presented in the Figure 12.

We did not observe differences in IFN-γ or IL-12p70 production by draining lymph nodes 8, 12 and 16 weeks post infection (Figure 12A and B). As observed in figures 12A and 12B, the same kinetics patterns were found for the cytokine secretion. There is a peak of IFN-γ secretion by dLNs at 8 weeks and a strong drop in its levels 12 and even more at 16 weeks post infection, $p<0.0001$ (Figure 12A). Curiously, the IL12p70 secretion did not follow the IFN-γ production reaching a peak at 16 weeks of infection, $p=0.0014$ (Figure 12B).

We found no differences in the amount of IL-10 at 8 and 12 weeks, but at 16 weeks post infection, lymph node cells from WT mice secreted more IL-10 than gp91$^{phox-/-}$ (figure 12B). In addition, no differences in secreted IL-6 were found (Figure 12D).

Gp91$^{phox-/-}$ mice presented with higher IL-17 production in draining lymph nodes 8 weeks post infection. However, at 12 and 16 weeks p.i. we cannot detect differences between the two groups (Figure 12E).

Interestingly, almost all inflammatory cytokines (figure 12A, D and E, $p<0.01$) presented peaks of production at 8 weeks and those cytokines were practically suppressed at 12 and 16 weeks post infection, except for IL-12p70, which reach a peak of secretion at 16 weeks.

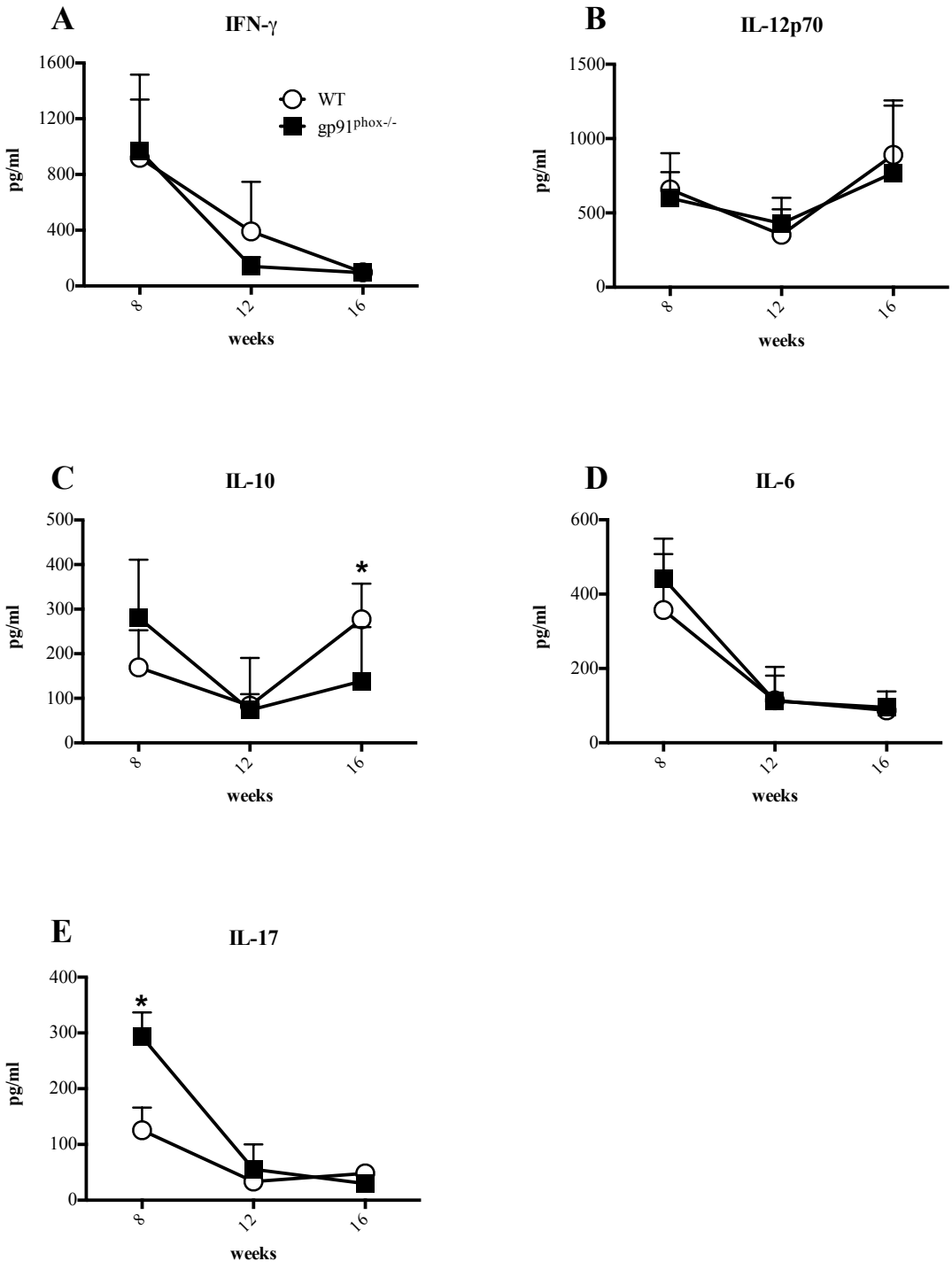

Figure 12. Cytokine production by re-stimulated dLNs of *L. amazonensis* infected mice performed by ELISA. The dLNs of infected mice were culture and re-stimulated with 50µg/ml of *L. amazonensis* antigen. After 72h, the supernatants were harvested and used to quantify cytokines by ELISA. A, B, C, D and E represent the IFN-γ, IL-12p70, IL-10, IL-6 and IL-17 secretion by dLNs of infected mice, respectively. The results were expressed by mean ± SD, n=5, *p<0.05 between WT and gp91$^{phox-/-}$.

4.3.5. Deficiency in ROS production is not compensated by increase in iNOS expression

ROS and reactive nitrogen species (RNS) are involved in killing various intracellular parasites (Ferrari et al., 2011). Since phagocytes from gp91$^{phox-/-}$ mice do not produce ROS after phagocytosis, we asked if these mice could compensate this lack of ROS by producing higher amounts of RNS. So we decided to assess mRNA expression of inducible nitric oxide synthase (iNOS) at the lesion site and the production of nitric oxide (•NO) by peritoneal macrophages in gp91$^{phox-/-}$ mice infected with *L. amazonensis*.

The mRNA levels of nitric oxide in lesions did not change between groups at the times measured (Figure 13A). So, the deficiency in ROS production does not increase the translation of iNOS gene.

After finding the same mRNA levels of iNOS in gp91$^{phox-/-}$ and WT mice during *L. amazonensis* infection in lesions, we asked if iNOS would be more active in gp91$^{phox-/-}$ mice and therefore produced more nitric oxide, in an attempt to compensate for the lack of ROS. To address this issue we infected 2 x 10^6 peritoneal macrophages *in vitro* with *L. amazonensis* at 10 parasites per macrophage and after 48h the nitrite production was measured in the supernatant by Griess reaction. When stimulated with IFN-γ, both groups of mice produced the same amount of nitrite, indicating normal production of nitric oxide in gp91$^{phox-/-}$ mice. (Figure 13B). The *L. amazonensis* itself was not capable of inducing nitric oxide production by macrophages

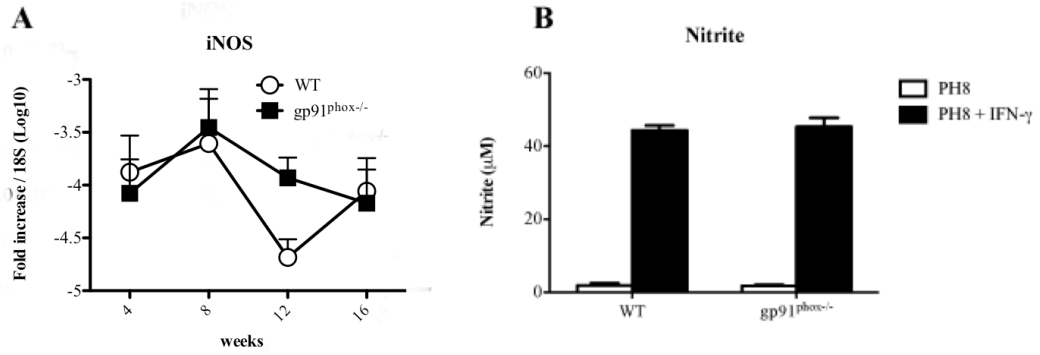

Figure 13. iNOS mRNA expression levels in footpad and nitrite production by infected thioglycolate-elicited macrophages. (A) Mice were infected with 1 x 10^6 metacyclic promastigotes forms of *L. amazonensis* in the right hind footpad and followed for 16 weeks. iNOS mRNA levels were normalized by 18S mRNA expression 4, 8, 12 and 16 weeks post infection. (B) Thioglycolate-elicited macrophages were harvested from WT or gp91$^{phox-/-}$ mice peritoneum 3 days after stimulation. Macrophages were infected with *L. amazonensis* metacyclic promastigotes at 10:1 for 4 hours, in the presence or absence of IFN-γ. After 48h of infection, the supernatants were collected and used to measure nitrite levels by Griess reaction. Data are shown as mean ± SD from one representative experiment of 4, n=5 for each experiment.

4.3.6. ROS alter the influx of innate and adaptive immune cells to the site of infection and the dynamics of dLNS expansion in mice subcutaneously infected with *L. amazonensis*

We saw clear differences in lesion sizes between WT and gp91$^{phox-/-}$ mice infected with *L. amazonensis*. Since no differences were found in parasite numbers, we investigated the cell population in these lesions. We collected footpad and dLNs from infected mice and performed flow cytometry of the cells stained them for innate and adaptive cell markers.

Lesions in gp91$^{phox-/-}$ mice presented a significant increase in the percentage of granulocytes (here denominated by Ly6G^{+}F4/80^{-}) 8 weeks post infection (Figure 14A and B). However, 12 weeks post infection there is a shift in this granulocyte accumulation: WT mice presented more granulocytes at the site of infection. This phenomenon could be correlated with the dynamics of the lesion size (Figure 10A), where we observed a higher footpad swelling in gp91$^{phox-/-}$ mice in the first weeks post infection and a lesser inflammation observed in these mice at later times of infection.

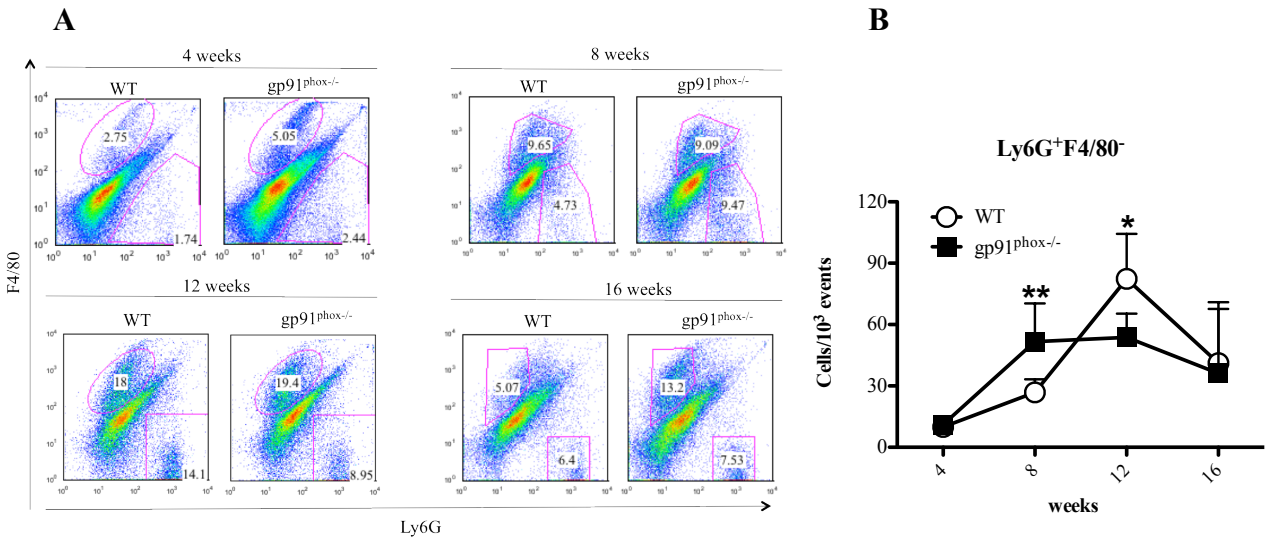

Figure 14. Flow cytometry of granulocytes present at the site of infection with *L. amazonensis*. (A) representative dot plots of the cell frequencies 4, 8, 12 and 16 weeks post infection. The figures represent the dot plots of events inside granulocyte and monocyte gate set by size and granularity of the cells. (B) graphic representation of the relative numbers of Ly6G^{+}F4/80^{-} cells (mean ± SD, n=6 for each time point). * $p<0.05$ and ** $p<0.01$.

We also evaluated lymphoid cells at the site of infection during to try to establish possible connections between the inflammation observed and lymphoid cell numbers in the lesions.

Differently than what was observed for granulocytic cells, $CD4^+$ cells present in lesions did not seem to correlate directly with lesion sizes. At 8 and 12 weeks post infection gp91$^{phox-/-}$ mice presented smaller percentage of $CD4^+$ cells. (Figure 15A and B).

In contrast the data for $CD4^+$ cells, $CD8^+$ cells did not show alterations during all throughout the experiment, ranging from 20 to 50% of gated lymphoid gated events (Figure 15A and C). No differences were found between groups.

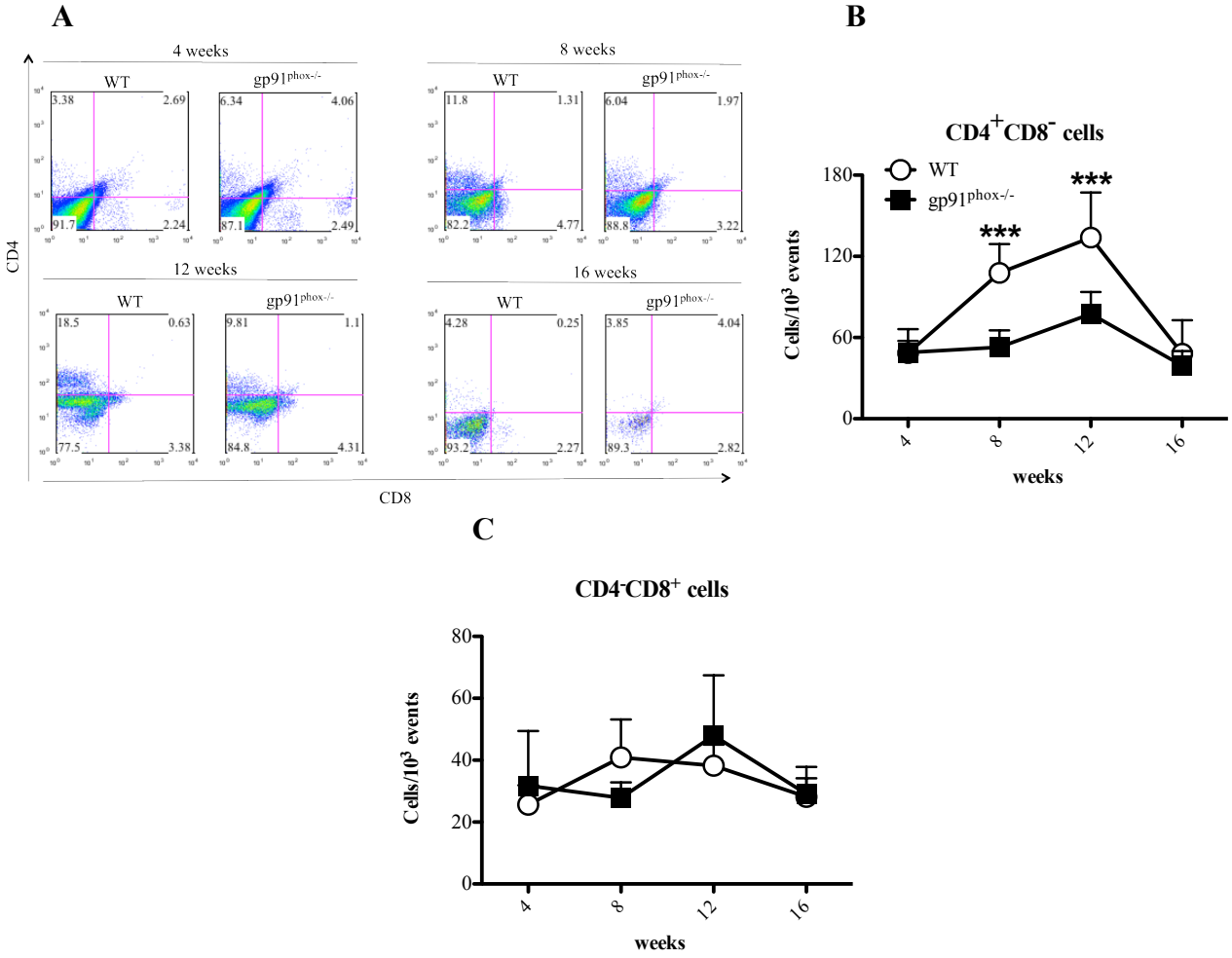

Figure 15. Flow cytometry of lymphoid cells present at the site of infection with *L. amazonensis*. (A) representative dot plots of the cell frequencies 4, 8, 12 and 16 weeks post infection. The figures represent the dot plots of events inside the lymphoid gate set by size and granularity of the cells. (B) and (C) graphic representation of the relative numbers of $Ly6G^+F4/80^-$ cells (mean ± SD, n=6 for each time point). *** $p<0.001$.

The draining lymph nodes are very important secondary lymphoid organs for the priming of immune responses to infections in peripheral sites (Sojka et al., 2009). Moreover, *in Leishmania* infections, they are a site for parasite growth and a location from which parasites can disseminate (Sojka et al., 2009). So, we analysed the expansion of dLNs in the mice subcutaneously infected with *L. amazonensis*.

Despite the fact that both mouse strains had the same parasite loads in dLNs at all time points (Figure 10C), WT and gp91$^{phox-/-}$ mice presented differences in dLNs cell expansion. At 12 weeks post infection, the gp91$^{phox-/-}$ mice presented half the cell number found in WT dLNs (5 x 10^7 cells in gp91$^{phox-/-}$ and 1 x 10^8 cells in WT (Figure 16). This datum agrees with the peak of CD4$^+$ cells found in the footpads 12 weeks post infection (Figure 15B). Hence, lymph node expansion was similar between groups at 4 and 8 weeks, after this time point WT dLNs continued expanding while cell numbers in dLNs from gp91$^{phox-/-}$ mice started to drop. At sixteen weeks post infection, dLNs cell numbers are again similar in both groups.

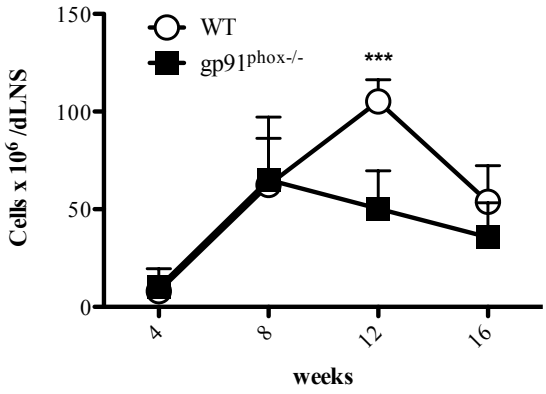

Figure 16. Total dLNs cell count during *L. amazonensis* infection. After 4, 8, 12 and 16 weeks of infection, dLNs were removed, macerated and the cells were resuspended in 1ml of complete RPMI medium and counted. The results are expressed as mean ± SD. *** $p<0.001$ (n=6 for each time point).

We analysed the proportion of CD4$^+$ and CD8$^+$ presented in this lymphoid organ. Despite alterations of cells number at 12 weeks post infection, we cannot observe changes in proportion of CD4$^+$ or CD8$^+$ cells during all times measured (Figure 17).

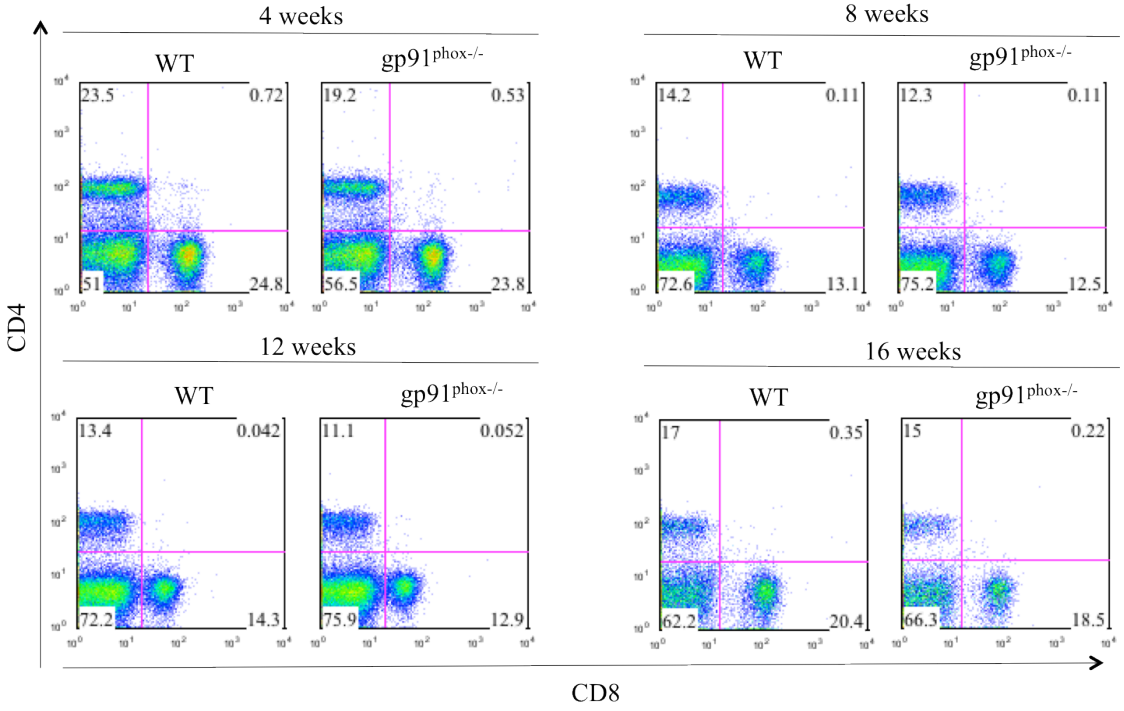

Figure 17. Flow cytometry of CD4$^+$ and CD8$^+$ cells in dLNs from mice during the *L. amazonensis* infection. After 4, 8, 12 and 16 weeks of infection, dLNs were removed, macerated and the cells were resuspended in 1ml of complete RPMI medium and counted. The cells were stained for CD4 and CD8 and read by flow cytometry. The figures represent the dot plots of events inside of lymphoid gate set by size and granularity (n=6 for each time point).

The spleen has central role in visceral forms of leishmaniasis (Goto and Prianti, 2009). In contrast, splenectomy does not change the course of *L. major* infection (Maioli et al., 2007). The role of the spleen in *L. amazonensis* infection is unknown. Therefore, we decided analyze the immune responses generated in the spleen of the animals.

Despite the fact that we did not find parasites in spleens from either group, we could detect important differences in cell numbers in this organ during the infection. We found higher numbers of cells 4 weeks post infection in the spleen of gp91$^{phox-/-}$ mice (Figure 18). In addition, gp91$^{phox-/-}$ mice had a decrease in cell number at later times of infection (12 and 16 weeks post infection, $p<0.0001$). Both groups reached the peak of cell expansion in the spleen at 8 weeks post infection followed by a drop in cell numbers by 16 weeks, $p<0.0001$. These data suggest a strong correlation between footpad swelling (Figure 10A) and the number of cells in the spleen. During the development of the infection, the gp91$^{phox-/-}$ mice had higher inflammation in footpads and higher total cell numbers in spleen at early stages of the infection and lesser inflammation and number of immune cells at later stages of the infection in the footpad and spleen, respectively.

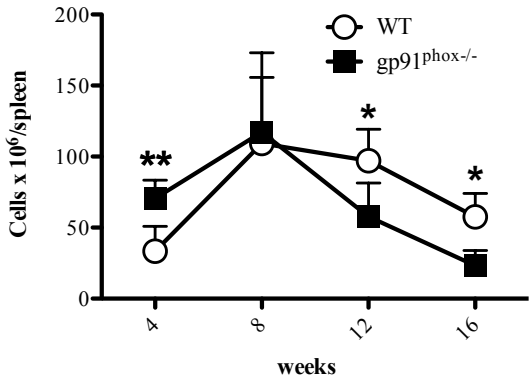

Figure 18. Number of cells in white pulp of spleens during *L. amazonensis* infection. After 4, 8, 12 and 16 weeks of infection, the spleen from mice was removed, macerated with red blood cell lysis treatment and the immune cells were resuspended in 1ml of RPMI complete medium and counted. The results are expressed in average ± SD. *p<0.05 and **p<0.01 (n=6 for each time point).

The analysis of $CD4^+$ and $CD8^+$ populations showed the same behaviour as seen in dLNs of infected mice (Figure 17 and 19). We did not observe differences between gp91$^{phox-/-}$ and WT mice as to $CD4^+$ or $CD8^+$ populations at all times analysed (Figure 19). Therefore, despite the increase in the number of cells in the spleens, there were no alterations in the percentage of $CD4^+$ or $CD8^+$ cells.

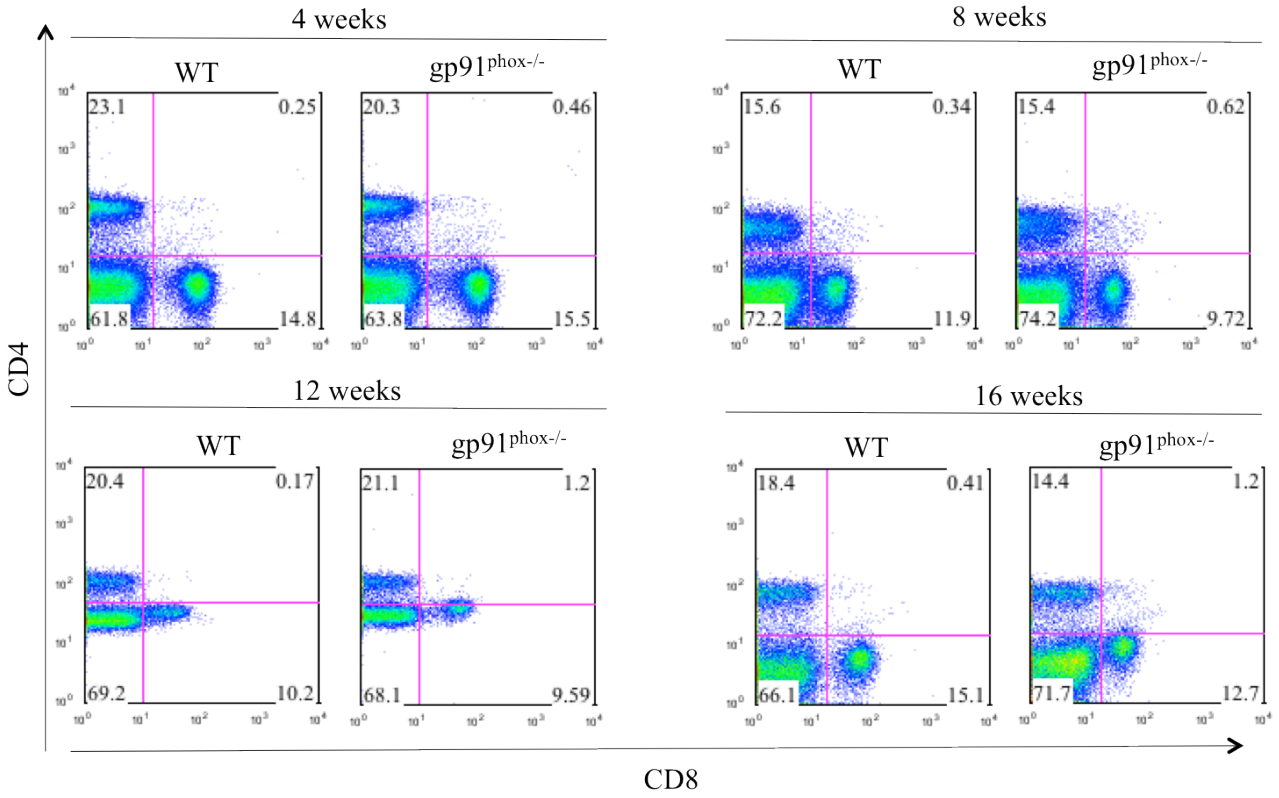

Figure 19. Flow cytometry of CD4$^+$ and CD8$^+$ cells in spleen from mice during the *L. amazonensis* infection. After 4, 8, 12 and 16 weeks of infection, the spleen from mice was removed, macerated with red blood cell lysis buffer, the remaining cells were resuspended in 1ml of RPMI complete medium and counted. Cells were stained for CD4 and CD8 molecules and read in flow cytometry. The figures represent the dot plots of events inside of lymphoid gate set by size and granularity (n=6 for each time point).

4.3.7. ROS increased the migration and decreased clearance of neutrophils immediately after infection with *L. amazonensis*

Neutrophils are important to eliminate invading microorganisms, especially by ROS production (Decoursey and Ligeti, 2005). Due this importance of neutrophils, we decided to investigate the behaviour of neutrophils deficient of ROS production.

Firstly, we infected mice with *L. amazonensis* (PH8 strain) in the footpads and analysed the accumulation of neutrophils indirectly by mieloperoxidase (MPO) 6h and 72h after infection. MPO is an abundant enzyme, especially found in granulocytic cells lines. Due the higher expression of MPO in granulocytes is possible to estimate the quantity of neutrophils presented in the tissue by assaying MPO activity.

Six hours post infection, there is a peak of neutrophil accumulation in footpads and a drop

after 72h of infection in the WT group (Figure 20). In gp91$^{phox-/-}$ mice, this first accumulation at 6h is higher compared to WT. Differently from what was observed in WT mice, gp91$^{phox-/-}$ did not display a drop in MPO activity after 72h of infection (Figure 20), suggesting a more sustained neutrophil accumulation in gp91$^{phox-/-}$ mice.

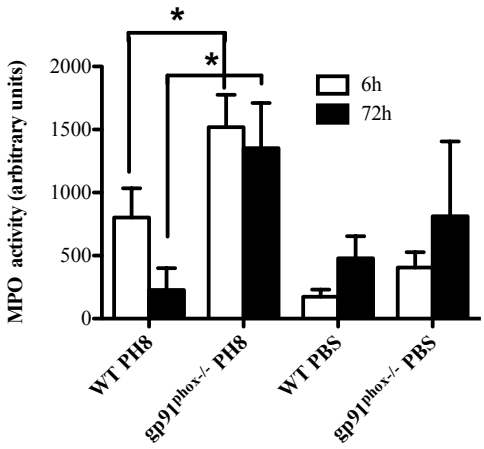

Figure 20. MPO activity in mice infected with *L. amazonensis*. Mice were infected with 1 x 10^6 metacyclic promastigotes forms of *L. amazonensis* in the right hind footpad. After 6h or 72h of infection, mice were euthanized, the footpads were removed and used to perform MPO activity assay to estimate the neutrophil numbers. Data are shown as mean ± SD from one representative experiment of 2, n=5 for each experiment, *p<0.05.

4.3.8. ROS influence anti-*Leishmania* IgG antibodies secretion during *L. amazonensis* infection

The humoral response is essential for many infectious diseases, especially those by extracellular pathogens. The humoral response is also important to eliminate intracellular pathogens promoting opsonization via antibodies and facilitating the phagocytosis of these pathogens by innate immune cells during extracellular stages (Joller et al., 2011). Moreover, the type of antibody secreted in the infection might indicate the type of T cell response (Th1 or Th2) developed by the host (Joller et al., 2011).

At present, it is not known if the absence of ROS could interfere with antibody secretion during infection with *L. amazonensis*. So, we decided to analyze possible changes in anti-*L. amazonensis* IgG sub-types during the 16 weeks of infection. We collected blood, separated the serum, and performed ELISAs to verify the IgG response against the *L. amazonensis*. During this

time, we performed ELISAs to determine the optimal sera dilution to use in the experiments using serial 1:2 dilutions ranging from 1:100 until 1:800 (data not shown). The dilution of 1:200 was used as the best dilution for antibody detection since it presented the largest difference between infected versus non-infected serum.

Four weeks post infection, WT mice started the production of IgG antibodies against *L. amazonensis* and even in low levels this production was higher compared to gp91$^{phox-/-}$ mice (Figure 21A). The concentration of anti-*Leishmania* IgG increased throughout the time of infection reaching the peak of concentration in 16 weeks in WT group ($p<0.0001$). In contrast, we did not observe an increase in secretion of total IgG during infection in the gp91$^{phox-/-}$ group. At all times measured (except 8 weeks), the gp91$^{phox-/-}$ mice produced lower levels of anti-*L. amazonensis* total IgG. Indeed, we detected around half of IgG ABS signal in gp91^{phox} compared to WT at 12 and 16 weeks post infection.

IgG_{2a} is an important antibody involved in the protective Th1 response to *Leishmania* parasites (Chu et al., 2010). We detected higher levels of IgG_{2a} anti-*L. amazonensis* in gp91$^{phox-/-}$ mice at 4 and 8 weeks post-infection (Figure 21B). This was especially true at 4 weeks post-infection when WT mice did not produce any anti-*Leishmania* $IgG_{2a.}$ In WT mice, the production of anti-*L. amazonensis* IgG_{2a} was first detected at 8 weeks post infection. At this time point, gp91$^{phox-/-}$ mice sera had a two-fold increase in anti-*L. amazonensis* IgG_{2a} signal compared to WT. At 12 and 16 weeks levels of antibodies were similar in WT and gp91$^{phox-/-}$ mice, and dropped in both groups at 16 weeks.

Contrary to IgG_{2a}, IgG_1 antibodies are related to a worsening of infection caused by *L. mexicana* (Chu et al., 2010). Interestingly, the levels of anti-*L. amazonensis* IgG_1 followed the same patterns observed for the lesion sizes in WT and gp91$^{phox-/-}$ mice (Figure 10A and 21C). Gp91$^{phox-/-}$ mice produced higher levels of IgG_1 4 and 8 weeks post infection and at these times WT did not produce considerable levels of this antibody. However, by 12 weeks post infection WT mice had a remarkable increase in IgG_1 anti-*L. amazonensis* levels contrasting with the accentuated drop in gp91$^{phox-/-}$ mice IgG_1 such that levels of IgG_1 in WT mice was two-fold greater than gp91$^{phox-/-}$ mice. Between 12 and 16 weeks post infection, the gp91$^{phox-/-}$ mice maintained lower levels of IgG_1 despite the considerable drop in the levels of this antibody seen in the WT mice.

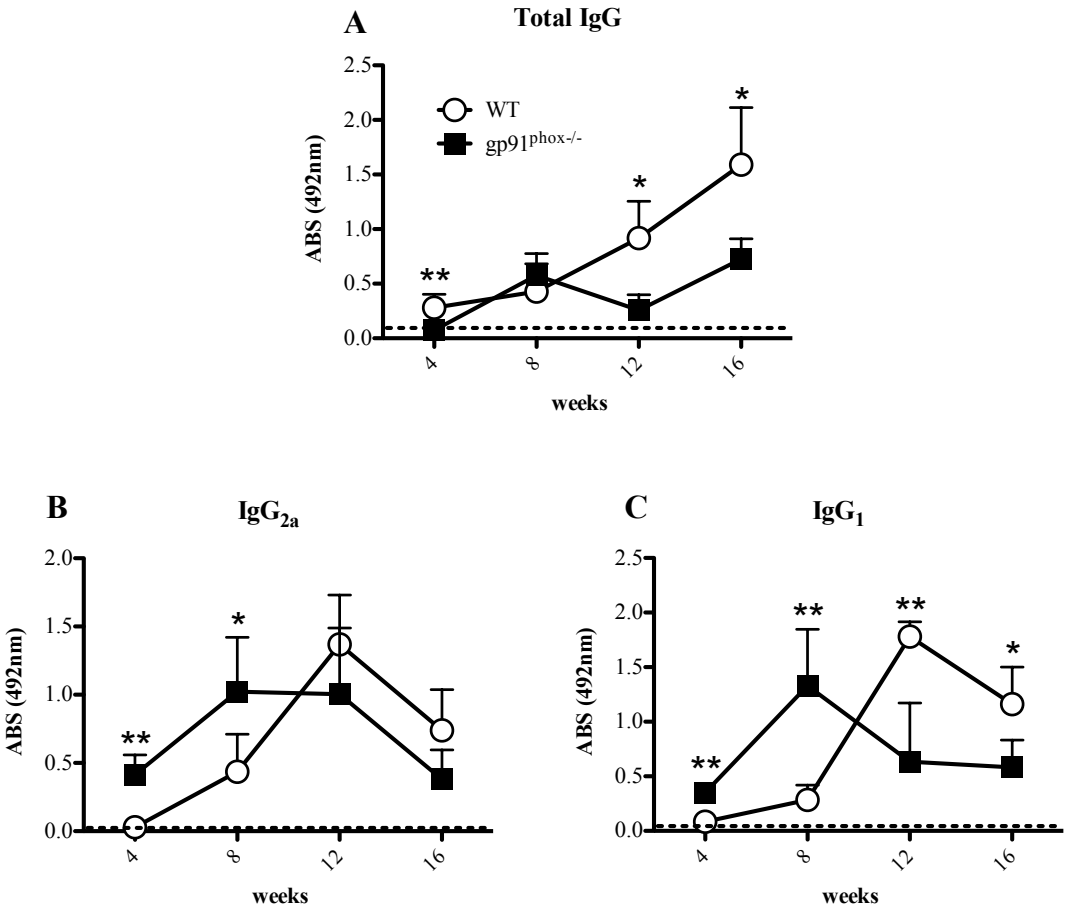

Figure 21. Production of anti-*Leishmania* IgG in NADPH oxidase deficient mice infected with *L. amazonensis*. Mice were infected with 1 x 10^6 metacyclic promastigote forms of *L. amazonensis* in the right hind footpad and followed until 16 weeks. After 4, 8, 12 and 16 weeks of infection, the serum was collected and ELISA to detect anti-*Leishmania* IgG was performed. A, B and C represent the absorbance found for anti-*Leishmania* IgG, IgG_1 and IgG_{2a}, respectively. The dotted lines represent the absorbance of serum of non-infected mice in dilution of 1:200, the same dilution used for the serum of the infected mice. Data are shown as mean ± SD from one representative experiment of 2, n=6 for each experiment.

4.3.9. Activated gp91$^{phox-/-}$ macrophages secrete higher levels of inflammatory cytokines in *L. amazonensis* infection *in vitro*

Macrophages are pivotal cells during *Leishmania* infection, being both the primary long-term host cell and the most important cell for parasite elimination. Due the importance of macrophages in the infection, we examined the interaction of macrophages from WT or gp91$^{phox-/-}$ mice with parasites *in vitro.*

We infected peritoneal macrophages with stationary-phase *L. amazonensis* promastigotes at

10 parasites per 1 macrophage. The macrophages were activated with IFN-γ plus LPS and after 72h of infection the supernatants were collected and ELISAs were performed to quantify cytokines and chemokines. IFN-γ and LPS were added to cultures because *L. amazonensis* itself is not a good macrophages activator in isolated *in vitro* systems. The LPS acts as a primary signal binding TLRs (specifically TLR-4) initiating the activation signal cascade. The IFN-γ acts as a second signal synergizing with LPS to induce the production of inflammatory cytokines as well as ROS and RNS in macrophages. So, we could analyze probable differences linked to ROS in activated infected macrophages. Despite the lack of macrophages activation by *L. amazonensis* in *in vitro* conditions, we added the group of cells not stimulated with IFN-γ plus LPS to observe possible changes in cytokines production influenced just by *L. amazonensis* infection.

Gp91$^{phox-/-}$ macrophages produce higher levels of the inflammatory cytokines IL-6 and TNF-α versus WT mice when infected with *L. amazonensis* and stimulated with IFN-γ plus LPS (Figure 22A and B). In contrast to WT mice, gp91^{phox} deficiency also resulted in enhanced IL-6 production by infected macrophages versus IFN-γ plus LPS stimulated controls (Figure 22A). Interestingly, TNF-α production by IFN-γ plus LPS activated WT macrophages dropped when infected with *L. amazonensis* ($p<0.0079$), this was not observed in gp91$^{phox-/-}$ mice.

Since we detected a larger neutrophil accumulation at the site of infection in in gp91$^{phox-/-}$ mice during the acute phase of infection, we decided to verify if infected macrophages could contribute to this increase in neutrophil numbers producing cytokines or chemokines neutrophils attractants. Indeed, we observed a larger secretion of IL-17 in activated macrophages infected with *L. amazonensis* (Figure 22C). Curiously, *Leishmania* itself induced IL-17 production ($p<0.05$), contrary to IFN-γ/LPS, however there is a synergism between these stimuli in gp91$^{phox-/-}$ mice ($p<0.05$).

We also analyzed the production of CXCL-1, one of the most important chemoattractants for neutrophils (Lira et al., 1994). *Leishmania* itself was not able to induce secretion of CXCL-1 in either group, being secreted only in response to macrophage activation (Figure 22D). Activated macrophages from both mouse strains presented similar secretion of CXCL-1, regardless of infection.

MCP-1 is involved in monocyte recruitment to the site of infection (Kunkel et al., 1991). Surprisingly, the levels of MCP-1 secreted by gp91$^{phox-/-}$ stimulated macrophages was lower compared to WT cells (Figure 22E). Infection by *L. amazonensis* itself had no influence in MCP-1 secretion, since we did not detect differences between basal levels and *L. amazonensis* infected cells. Moreover, we could not observe differences in activated versus infected and activated

macrophages between groups.

Inflammation triggers IL-10 secretion in order to control the inflammatory response and protect the inflamed tissues from damage (Cassatella et al., 1993). We detected higher levels of IL-10 secreted by gp91$^{phox-/-}$ macrophages stimulated with IFN-γ/LPS versus WT macrophages (Figure 22F). Moreover, there was a synergism between the stimuli and infection promoting an increase in IL-10 secretion in both groups. This effect was more evident in gp91$^{phox-/-}$ macrophages. IL-10 is not induced by *L. amazonensis* itself.

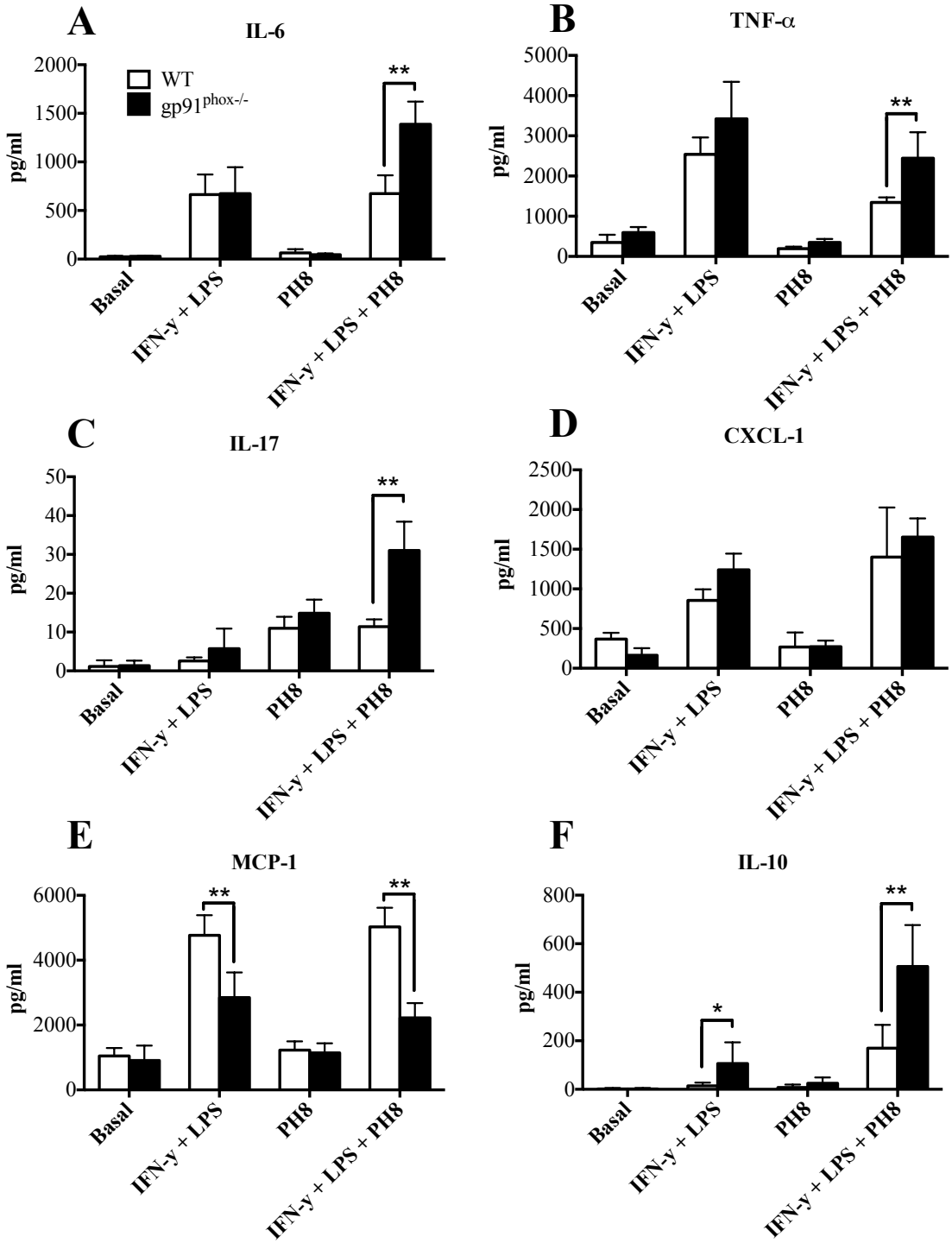

Figure 22. Production of cytokines and chemokines in gp91$^{phox-/-}$ macrophages infected with *L. amazonensis*. Thioglycolate-elicited macrophages were infected with stationary-phase *L. amazonensis* promastigotes at 10 parasites per macrophage. Macrophages were activated 50U/ml of IFN-γ plus 100ng/ml of LPS. After 72h of infection with *L. amazonensis* or activation the supernatants were collected and ELISAs were performed to quantify cytokines and chemokines. For TNF-α assays, aliquots from cell cultures were collected at 24h of infection. Controls without stimuli and infection were used to quantify the basal levels of cytokines. A, B, C, D, E and F represent the concentration showed in pg/ml of the IL-6, TNF-α, IL-17, CXCL-1, MCP-1 and IL-10 respectively. Data are shown as mean ± SD from one representative experiment of 2, n=6 for each experiment.

4.3.10. ROS promotes increased parasite loads in macrophages infected with *L. amazonensis in vitro*

Gp91$^{phox-/-}$ macrophages produced higher levels of inflammatory cytokines, as well as the anti-inflammatory cytokine IL-10. We investigated if ROS deficiency interfered with the ability of macrophages to kill *L. amazonensis* parasites. We infected thioglycolate-elicited macrophages with *L. amazonensis* at 10 parasites per macrophage and treated the cells with inhibitors of pathways of ROS and nitric oxide production.

L-NMMA is an analog of the amino acid L-arginine and is a pan-blocker of nitric oxide synthase activity (all isoforms) (Palmer et al., 1988). Treatment with L-NMMA impairs nitric oxide production and the effect of ROS alone would be isolated.

Apocynin (Apo) is an inhibitor of NADPH oxidase of phagocytes, acting by impairing the assembly of its cytosolic components p47^{phox} and p67^{phox} to the membrane fraction of the enzyme (Stolk et al., 1994). Therefore, the treatment with apocynin impairs the activity of the NADPH oxidase, consequently ROS production and promotes a phenotype similar to that of gp91$^{phox-/-}$ macrophages.

The treatment with L-NMMA plus apocynin abrogates the production of ROS and nitric oxide allowing verification of the total effect of these reactive species in *Leishmania* infection. Analogous to this treatment, we added L-NMMA to gp91$^{phox-/-}$ macrophages expecting similar results.

The treatment of WT macrophages with L-NMMA plus superoxide dismutase (SOD) allows the impairment of peroxide and nitric oxide production, and accumulation of superoxide. Therefore, we can analyze, by accumulation of superoxide, what is the role of this reactive species in the infection. On the other hand, the treatment of WT macrophages with L-NMMA plus catalase allows us to address what the impact of the absence of nitric oxide and hydrogen peroxide is on macrophage infection.

Treatment with L-NMMA increases the number of parasites/macrophage in WT animals (Figure 23). Addition of SOD or catalase did not affect this increase, but inhibition of NADPH oxidase with apocynin in L-NMMA-treated macrophages decreased infection to control levels. Interestingly, the L-NMMA did not affect gp91$^{phox-/-}$ macrophages. However, gp91$^{phox-/-}$ macrophages were less susceptible to infection with *L. amazonensis* than wild-type macrophages. In addition, WT macrophages treated with apocynin presented similar parasite numbers to gp91$^{phox-/-}$ macrophages. These data suggest that ROS play important role in parasite survival. It seems that

the ROS influenced positively the parasite growth, since all treatments to inhibit gp91^{phox} promotes decrease in parasite loads. However, we could not discard a more efficient unknown compensatory mechanism in parasite killing due to the absence of ROS. In addition, it is evident that some nitric oxide is produced at very low, undetectable levels by WT macrophages and that this $^{\bullet}$NO could play a role in partial resistance to infection.

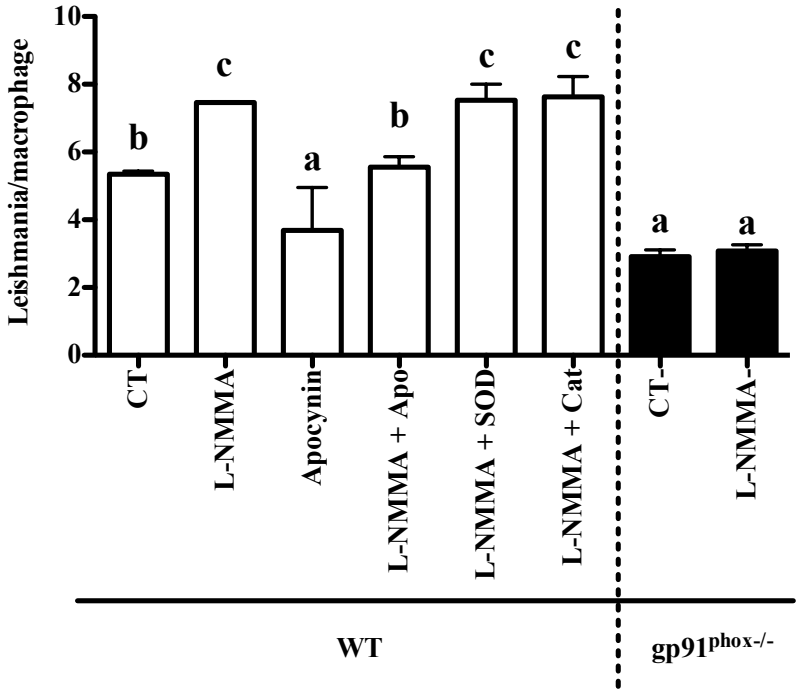

Figure 23. Quantification of parasite loads in macrophages treated with ROS and nitric oxide inhibitors in infection caused by *L. amazonensis in vitro*. Peritoneal macrophages were infected with metacyclic promastigote forms of *L. amazonensis* in proportion 10 parasites per macrophage for 4h. During the infection, the cells were treated with several inhibitors (WT macrophages treated with L-NMMA alone; apocynin alone; L-NMMA plus apocynin; L-NMMA plus SOD; L-NMMA plus catalase; WT infection without treatment; and gp91$^{phox-/-}$ macrophages treated or not with L-NMMA. After 72h of infection the cells were stained counted under light microscope.

5. PART TWO: SITE OF *L. MAJOR* INFECTION DETERMINES DOMINANT HOST CELL PHENOTYPE

5.1. Objectives

5.1.1. General objective

To analyze alterations in immune response at early times of infection of resistant mice with *L. major* by two different routes of parasite inoculation.

5.1.2. Specific objectives

- To determine the innate immune cells recruited to the site of infection at early time points;
- To verify the major cells involved in the initial uptake of *Leishmania* at intradermal and subcutaneous sites of infection;
- To analyze the adaptive immune responses developed by injection of parasites by different routes in dLNs of infected mice in acute phase of infection;

5.2. Material and Methods (the following text is taken from a manuscript in preparation)

5.2.1. Mice

This study was carried out in strict accordance with the recommendations in the Guide for the Care and Use of Laboratory Animals of the National Institutes of Health. The protocol was approved by the Animal Care and Use Committee of the NIAID, NIH (protocol number LPD 68E). Female C57BL/6 mice were purchased from Taconic Laboratories and all animals were maintained at the NIAID animal care facility under specific pathogen-free conditions without restrictions of water or food.

5.2.2. Parasites

Infection experiments were performed employing two strains of *Leishmania*: the *L. major* Friedlin strain from the Jordan Valley, National Institutes of Health (NIH)/FV1 (MHOM/IL/80/FN)

and *L. major* FV1-RFP, the FV1 strain transfected with a plasmid containing a red fluorescent protein (RFP) gene, generated by the dr. Alain Debrabant of the Division of Emerging and Transfusion Transmitted Diseases, OBRR, CBER, U.S. Food and Drug Administration (FDA, Bethesda USA) as follows: the DsRed gene was amplified by PCR using the pCMV-DsRed-Express plasmid (BD Biosciences/Clontech) as template and the forward primer 5′-TGG ACT AGT ATG GCC TCC TCC GAG GAC GTC-3′ and reverse primer 5′-CCA ACT AGT CTA CAG GAA CAG GTG GTG GCG-3′. The PCR product was first cloned into the pCR2.1 plasmid (Invitrogen) and the sequence verified by nucleotide sequencing. The SpeI insert from a selected clone was subsequently ligated into the SpeI site of the pKSNEO *Leishmania* expression plasmid (Zhang et al., 1996). FV1 promastigotes were transfected with the resulting expression plasmid construct pKSNEO-DsRed described as follow: the cells were resuspended in electroporation buffer (Hepes (ICN Biomedicals Inc., Aurora, OH), 137mM NaCl, 5mM KCl, 0.7mM Na_2HPO_4, 6mM glucose, pH 7.0) to 10^8 cells/ml. Five hundred microliters of cell suspension were added to 2mm gap electroporation cuvettes (BTX Inc., San Diego, CA) to which 20µl of purified plasmid DNA (1mg/ml in sterile 10mM Tris, 2mM Ethylenediamine tetraacetic acid (EDTA) (Quality Biological, Inc., Gaithersburg, MD), pH 8.0) was added. Cells were electroporated using a BTX ECM-600 electroporation system (BTX) and the conditions for electroporation were: 475V, 800 microfarads, 13ohms, single pulse. Electroporated cells were incubated on ice for 10 min and then transferred into 5ml of culture medium (medium 199 supplemented with 20% heat-inactivated FCS (Gemini Bio-Products), 100U/ml penicillin, 100µg/ml streptomycin, 2mM L-Glutamine, 40mM 4-(2-hydroxyethyl)-1-piperazineethanesulfonic acid (Hepes) and incubated at 26 °C for 24h. Subsequently, the cells were harvested by centrifugation 2100 × *g* for 10 min at 4°C and resuspended in fresh culture medium containing 15µg/ml of Geneticin (G418, Life Technologies, Inc.). These cells were selected for growth in increasing concentrations of G418 over a period of several weeks and then maintained at 250µg/ml drug. These drug-resistant cells were used in all subsequent experiments. For the experiments the parasites were growth in the presence of 50µg/ml Geneticin (G418) (Sigma).

5.2.3. Parasite preparation and inoculations

Parasites were grown at 26°C in medium 199 supplemented with 20% heat-inactivated FCS (Gemini Bio-Products), 100U/ml penicillin, 100µg/ml streptomycin, 2mM L-Glutamine and 40mM Hepes. For the *L. major* RFP parasite growth, we added 50µg/ml of Geneticin (Gibco) in the

medium. Infective-stage, metacyclic promastigotes of *L. major* were isolated from stationary cultures (4–5 days old) by negative selection using peanut agglutinin (PNA, Vector Laboratories Inc). The cells in the culture were washed, centrifuged at 2600 x *g* for 15 min, resuspended in 2ml of DMEM containing 100µg/ml peanut agglutinin (Vector Laboratories), incubated for 5 min, then spun for 5 min at 80 × *g* to remove the agglutinated, non-metacyclic forms. The metacyclic cells in the supernatant were washed, counted, and volumes adjusted for 10µl to intradermal ears and 40µl to subcutaneous hind footpad injections into mice.

5.2.4. Processing of tissues

Briefly, the two sheets of infected ear dermis were separated, deposited in DMEM containing 100U/ml penicillin, 100µg/ml streptomycin, and 0.2mg/ml Liberase CI purified enzyme blend (Roche Diagnostics Corp.), and incubated for 1 h and 30 min at 37°C. Digested tissue was placed in a grinder and processed in a tissue homogenizer (Medimachine; Becton Dickenson). Then, the tissue washed with 10ml of RPMI 0.05% DNAse (Sigma-Aldrich, Inc, St. Louis, MO, USA), centrifuged at 1,500 x *g* for 15 min and resuspended in 1ml complete RPMI.

The footpads were cut in small parts and placed in DMEM containing 100U/ml penicillin, 100µg/ml streptomycin, and 0.2 mg/ml Liberase CI purified enzyme blend (Roche Diagnostics Corp.), and incubated for 2h at 37°C. The digested tissue was mechanically disrupted in 70µm cell strainer filter (BD Falcon, USA) with a plunger and washed with 10ml of RPMI 0.05% DNAse (Sigma-Aldrich, Inc, St. Louis, MO, USA). The homogenates were centrifuged at 50 x *g* for 4 min to remove large tissue debris and the supernatants were collected and centrifuged at 1,500 x *g* for 15 min. The sediment was resuspended in 1mL of RPMI (GIBCO, Grand Island, NY, USA) supplemented with 10% heat-inactivated fetal bovine serum (FBS) (Gemini Bio-Products, Sacramento, CA, USA), 100U/mL penicillin, 100µg/mL streptomycin and 2mM L-Glutamine (GIBCO, USA).

5.2.5. Immunolabeling and flow cytometry

Single-cell suspensions were incubated with an anti-Fc-γ III/II (CD16/32) receptor antibody (2.4G2, BD Biosciences) in RPMI without phenol red (Gibco) containing 1% FCS and stained with fluorochrome-conjugated antibodies. The following antibodies were used: APC anti-mouse CD11c (HL3, BD Biosciences); PE-Cy7 anti-mouse CD11b (M1/70, eBioscience); PerCP-Cy5.5 anti-

mouse Ly6C (HK1.4, eBioscience); FITC anti-mouse Ly6G (1A8, eBioscience); eFluor 450 anti-mouse F4/80 (BM8, eBioscience); Alexafluor-700 anti-mouse MHC II (M5/114.15.2, eBioscience);

The acquisition of the samples was made in an eight colors FACS CANTO II cytometer (Becton Dickinson, Mountain View, California, USA) using the software Diva (Becton Dickinson, Mountain View, California, USA).

The percentage of positive cells and the median of fluorescence intensity were analyzed with the software FlowJo (Tree Star, Ashland, Oregon, USA).

The immunolabeling was organized and described: APC anti-mouse CD11c, PE-Cy7 anti-mouse CD11b, PerCP-Cy5.5 anti-mouse Ly6C, FITC anti-mouse Ly6G eFluor 450 anti-mouse F4/80; Alexafluor-700 anti-mouse MHC II.

5.2.6. Statistical analysis

The statistical analysis between the experimental groups was realized with student *t-test*, nonparametric test with Mann-Withney test and the software GraphPad Prism 5.0 (GraphPad, La Jolla, CA, USA) was utilized for the analysis. To reach significance, we considered $p<0.05$ and the data are expressed as mean and standard deviation.

5.3. Results

5.3.1. The patterns of cell migration changes according to the site of *L. major* infection

In this part of the work, we analysed the cell parameters to identify possible changes in *L. major* infection cell recruitment depending of inoculation site. As mentioned before, the route of inoculation of *Leishmania* can generate different infection outcomes. Therefore, it would be important to analyse the possible differences in the immune response according to the site of parasite inoculation. Moreover, these experiments could give us more rationale to determine the influence of ROS in a more physiological infection site when compared to subcutaneous challenge. So, we infected the resistant C57BL/6 mice intradermally in pinna ear or subcutaneously in footpads with 5×10^5 metacyclic promastigote forms of *L. major* transfected with red fluorescent protein (rfp) and followed the infection at 2h, 48h and 9 days after inoculation.

We performed flow cytometry to identify recruited cells in the first hours post infection. The

gating strategy for all times and tissues are represented in Figure 24.

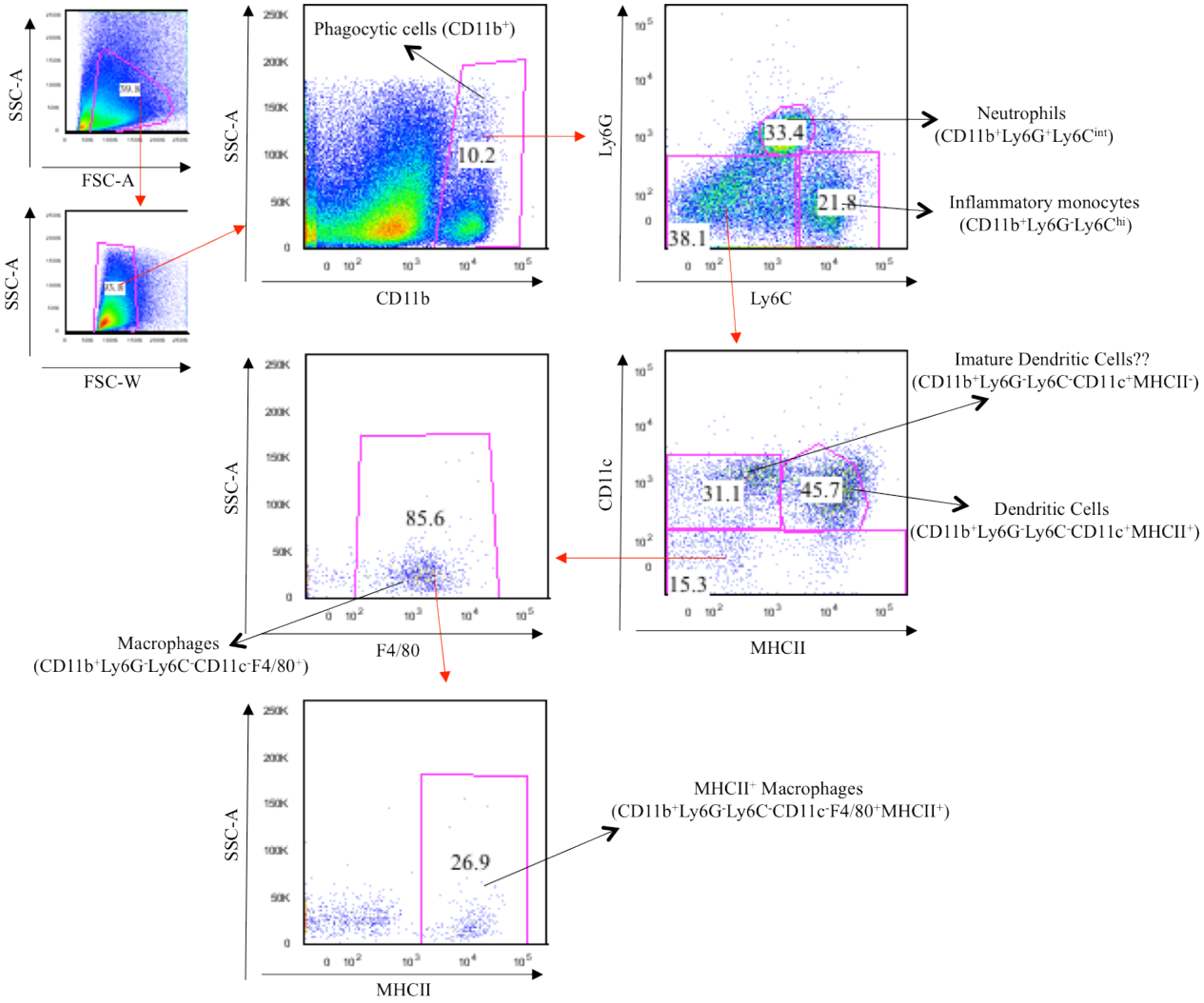

Figure 24. Flow cytometry gate strategy adopted to analyse the recruited cells after *L. major* infection. Mice ears or footpads were infected with 5 x 10^5 promastigote forms of *L. major* and 2h, 48h and 9 days post infection the tissues were processed and stained to surface markers. The same gate strategy was used in both tissues and all times. The red arrows indicate the pathways to split populations and identify subsequent sub-populations. The gates represent one sample of ears 48h post infection. A population that was $CD11b^+Ly6G^+Ly6C^-CD11c^+MHCII^-$ was suggested to be an immature dendritic cell population.

Briefly, we gated cells according their granularity and size. We excluded duplets or triplets by selection with side scatter areas versus forward scatter weight and proceeded to cell marker identification. We analysed the phagocytic cells using the CD11b marker, also known as complement receptor 3 (CR3), present on phagocytic cells. After identification of phagocytic cells, we split the population according to Ly6G and Ly6C expression to identify neutrophils and inflammatory monocytes. We considered the neutrophils as $CD11b^+Ly6G^+Ly6C^{int}$ and

inflammatory monocytes as $CD11b^{+}Ly6G^{-}Ly6C^{hi}$ (Ribeiro-Gomes et al., 2012). The double negative population to Ly6G and Ly6C ($CD11b^{+}Ly6G^{-}Ly6C^{-}$) was split to identify macrophages and dendritic cells. The dendritic cells were identified based on CD11c and MHCII expression and were considered as $CD11b^{+}Ly6G^{-}Ly6C^{-}CD11c^{+}MHCII^{+}$ cells (Ribeiro-Gomes et al., 2012). The population $CD11b^{+}Ly6G^{-}Ly6C^{-}CD11c^{+}MHCII^{-}$ was observed, but was hard to identify because immature DCs or even some populations of macrophages express the same markers. Indeed, some macrophages can be detected expressing CD11c depending the clone used for the stain (Ghosn et al., 2010). Within the $CD11b^{+}Ly6G^{-}Ly6C^{-}CD11c^{-}$ population, we identified cells expressing F4/80 and considered them as $CD11b^{+}Ly6G^{-}Ly6C^{-}CD11c^{-}F4/80^{+}$ macrophages (Ribeiro-Gomes et al., 2012). Those macrophages expressing MHCII were also identified as being $CD11b^{+}Ly6G^{-}Ly6C^{-}CD11c^{-}F4/80^{+}MHCII^{+}$.

After identification of the cells, we compared intradermal (ears) versus subcutaneous (footpad) infections and analysed the patterns of cell migration according to the inoculation site.

Analysing the subpopulations of $CD11b^{+}$ cells, we observed a robust increase in neutrophil percentage as early as 2h after the challenge in the intradermal infected mice. The percentage of this subpopulation was about five times more pronounced at the dermal site of infection after 2h of infection than in footpads. However, 48h post infection neutrophil percentage dropped and 9 days post infection the percentage of neutrophils the intradermally infected mice was comparable to non-infected mice, $p<0.05$ (Figure 25A). Curiously, the percentage of neutrophils at the subcutaneous site of infection did not change during the infection, suggesting that neutrophils are poorly recruited to the subcutaneous site.

Following the drop in neutrophils, we found an increase of the inflammatory monocyte population at the dermal site of infection. However, this phenomenon was not observed in the infected footpads. As observed for neutrophils, the inflammatory monocytes seemed to be not recruited to site of infection (Figure 25B).

The percentage of resident macrophages in the footpad was higher compared to ears in non-infected tissues (Figure 25C). After the infections this population remained at a low proportion. In contrast, the percentage of DCs in the ear was much higher compared to footpads in non-infected tissues (Figure 25D). Despite this robust difference, the percentage of DCs dropped dramatically in ears over the time of infection, contrary to the behaviour of this cell population in the footpad, $p<0.001$. This drop in DCs percentage is related to the massive increase in inflammatory monocytes over the time. Between 48h and 9 days, we observed an increase in DCs percentages in footpads. When we analysed the activated macrophages, it was possible to observe that this population of cells is more frequent in the uninfected ear than in the footpad (Figure 25E). However, we do not

know if this small difference could interfere with the infection, since 2h after infection we had not observed a significant difference anymore. Nevertheless, 9 days after infection we could detect an increase of these activated macrophages percentage in the ear-infected group. Moreover, we did not detect any alterations in percentage of this population in footpads.

We identified interesting differences in the $CD11b^{+}Ly6G^{-}Ly6C^{-}CD11c^{+}MHCII^{-}$ cell populations, however we could not characterize these cells based just on surface markers because macrophages and immature DCs express this combination of markers. Curiously, this population is the most frequent $CD11b^{+}$ population in the footpads and did not change at 2h and 48h post infection (Figure 25F). In all times analysed, this cell population was higher in the footpad compared to ears (Figure 25D). This fact suggests that $CD11b^{+}Ly6G^{-}Ly6C^{-}CD11c^{+}MHCII^{-}$ cells could be immature dendritic cells becoming mature during the infection.

In addition to the percentage analysis, we also counted the total cell populations and compared the effect of intradermal or subcutaneous infection in total cell recruitment to the site of inoculation.

The numbers of $CD11b^{+}$ were the same in both groups before infection. The numbers of this cell type increased at the same rate in both groups until 48h post infection (Figure 26A). At 9 days after infection $CD11b^{+}$ population numbers were over three-fold higher in the ears than in footpads. At the same time point, this population had increased 12-fold compared to naïve ears. Since both groups had the same numbers of $CD11b^{+}$ cells before infection, we can conclude that intradermal site had a higher inflammatory state caused by intradermal infection.

Based on the differences found in phagocytic cell recruitment, we decided to analyse which cell type was involved in this higher inflammatory state in ears. We identified a rapid influx of neutrophils just 2h after infection in ears of mice and these levels were kept high after 48h post infection (Figure 26B). At 9 days, the number of neutrophils was even higher reaching about 8,000 cells in the ears, which could contribute to recruitment of more inflammatory cells. In contrast, we could not observe increase in neutrophils numbers in footpads in any of the times measured, suggesting that this cell type is not involved in response to subcutaneous infection with *L. major*.

We also noticed an increase of inflammatory monocytes at the site of infection. The influx of these cells was observed in both groups until 9 days post infection, but was much more intense at the intradermal site (Figure 26C). Both groups of mice non-infected mice presented the same numbers of these cells and 2h post infection. However, 48h and 9 days post infection the recruitment of these cells increase dramatically at the intradermal site. At day 9 post infection, the inflammatory monocytes were increased more than 15-fold at the intradermal site, compared to the subcutaneous site. Indeed, these inflammatory monocytes were responsible for the majority of cells

recruited to the intradermal site of infection.

When we analysed the DC population, we identified the same patterns of cell migration between both routes of infection. At 9 days post infection, the numbers of cells had a considerable increase in both groups, but was higher in the ears (Figure 26D). Indeed, in all time points analysed the cell numbers were slightly higher in ear even in non-infected mice.

The number of macrophages in both groups slightly increased after the first hours post infection as observed 2h and 48h were the cell numbers increased three-fold compared to non-infected tissues (Figure 26F). However, 9 days post infection the number of macrophages found in the ear was substantially higher reaching around 15,000 cells at this time while in the footpads around 4,000 cells were detected.

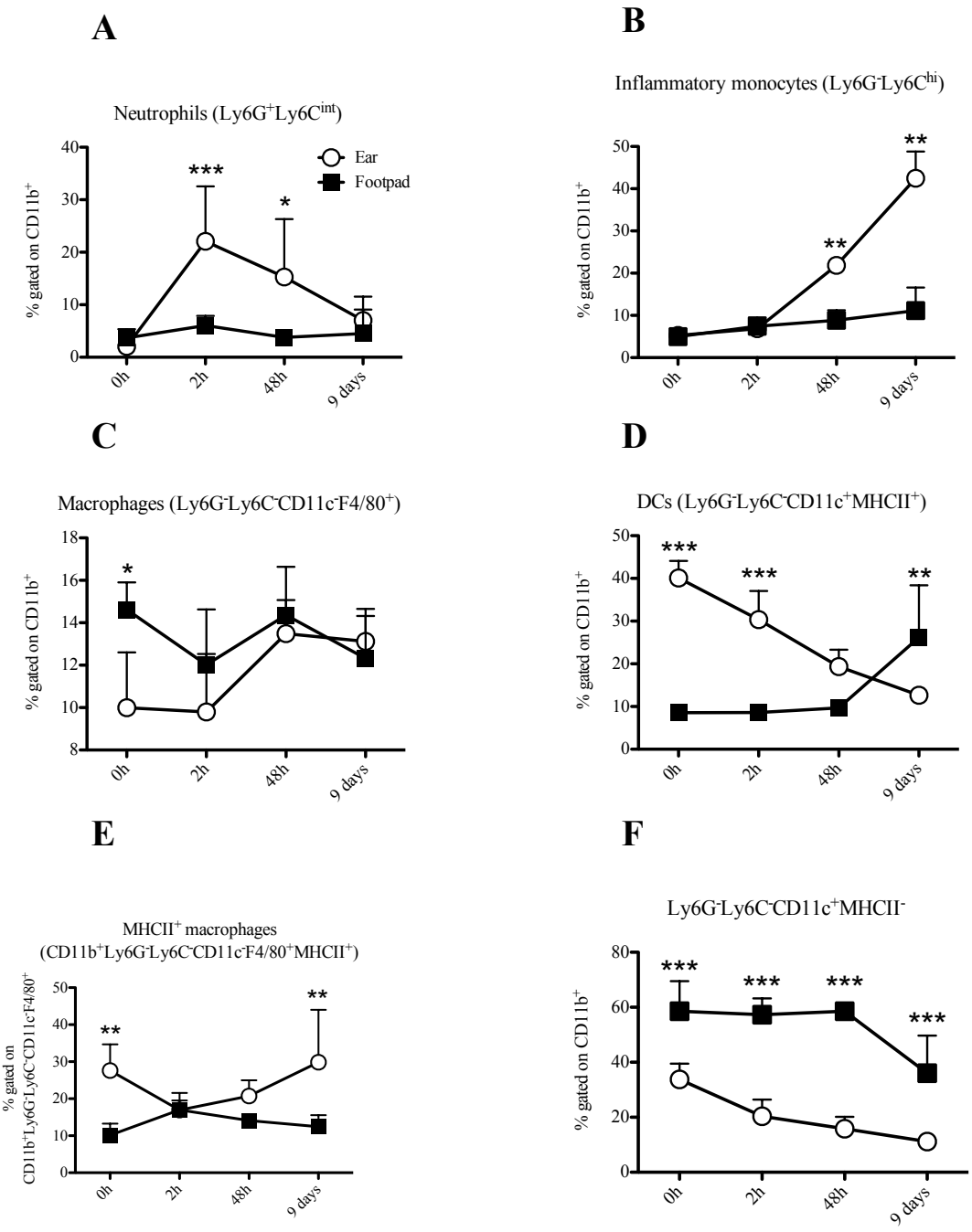

Figure 25. Percentage of subpopulations gated on CD11b$^+$ cells recruited to the inoculation site following *L. major* infection. Mouse ears or footpads were infected with 5 x 10^5 promastigote forms of *L. major* and 2h, 48h and 9 days post infection and the 0h time point represents the non-infected controls. The tissues were processed and stained to surface markers. A, B, C, D, E and F represent the kinetics of recruitment of neutrophils, inflammatory monocytes, macrophages, dendritic cells (DCs), activated macrophages and CD11c$^+$MHCII$^-$ cells, respectively. The data are represented as mean ±SD of one experiment representative of two performed, n=5 for each group. *=p<0.05, **=p<0.01 and ***=p<0.001.

Despite the fact that we did not observe significant differences 2h and 48h post infection on the total macrophage numbers (Figure 26F), the infection caused more activation of these cells at the intradermal site (Figure 26E). Before infection, footpads and ears presented the same number of $MHCII^+$ macrophages. However, 2h post infection these levels increased significantly in ears compared to footpads. Indeed, the number of these cells in footpads did not alter at 2h post infection, increased at 48h reaching the highest level 9 days post infection. At the same times analysed (48h and 9 days post infection), the macrophages in ears had same pattern of activation, but were in higher numbers.

We identified the non-characterized cell type ($CD11b^+Ly6G^-Ly6C^-CD11^+MHCII^-$) in both sites. The observation of the kinetics of DC appearing at the site of infection, as mentioned before, these cells probably are immature DCs that became mature DCs as infection progressed (Figures 25D and F). Despite the fact that the percentage of these cells was very different between ears and footpads, we did not detect differences in total cell numbers, except at 48h post infection, when we detect more of these cells present in footpads (Figure 26G). There is a shift in the kinetics of differentiation in this population. While we observed a rapid increase in footpads 2h to 48h post infection, in the ears this behaviour was just observed between 48h to 9 days post infection. At the end of 9 days, both groups of mice showed the same numbers of this specific cell sub-type.

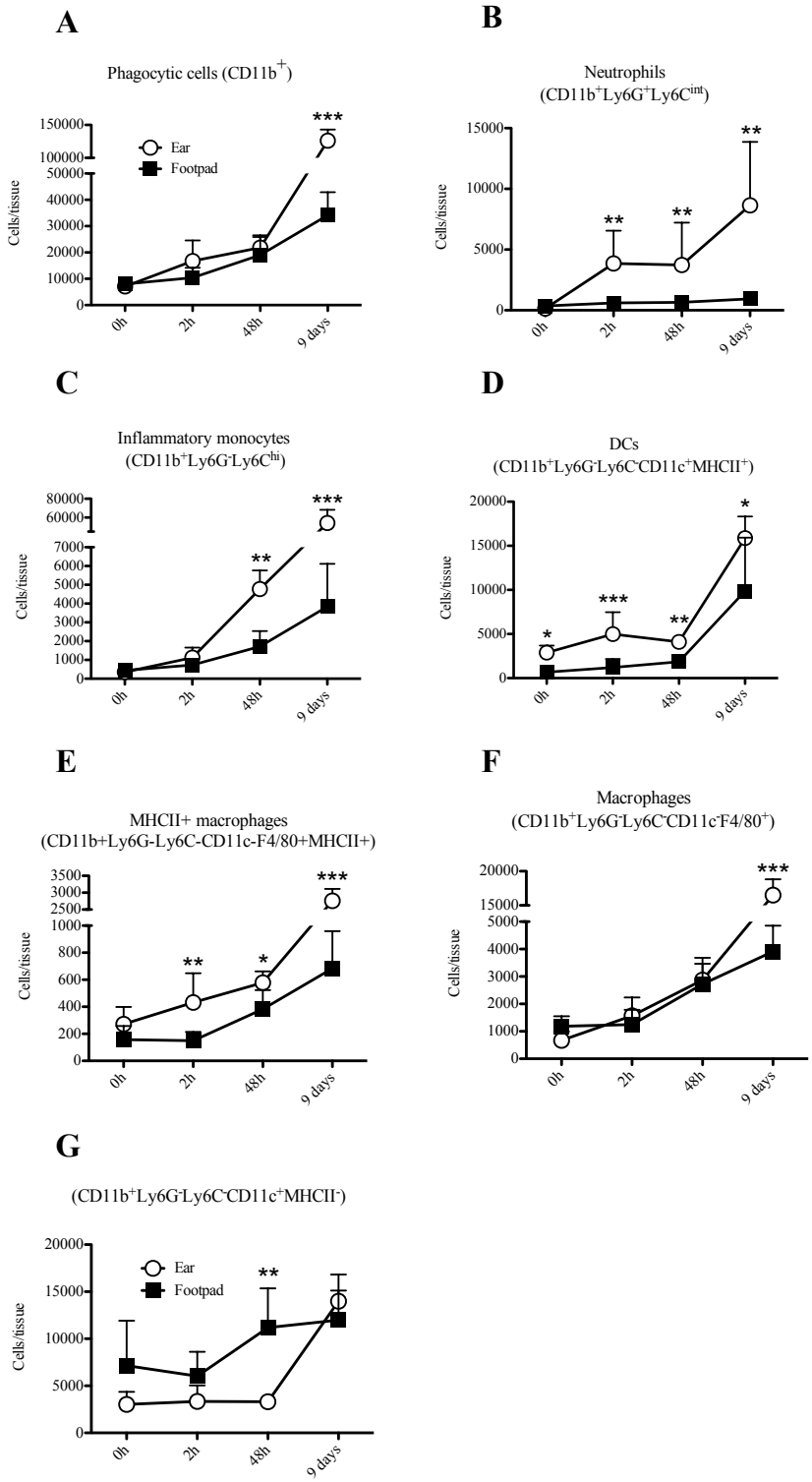

Figure 26. Total cell numbers of subpopulations gated on CD11b$^+$ recruited to the inoculation site after *L. major* infection. Mouse ears or footpads were infected with 5 x 10^5 promastigote forms of *L. major* and 2h, 48h and 9 days post infection and the 0h time point represents the non-infected controls. The tissues were processed and stained to surface markers. A, B, C, D, E and F represent the kinetics of cell recruitment of neutrophils, inflammatory monocytes, macrophages, DCs, activated macrophages and CD11c$^+$MHCII$^-$ cells, respectively. The data are represented as mean ±SD of one experiment representative of two, n=5 for each group. *=p<0.05, **=p<0.01 and ***=p<0.001.

5.3.2. The site of inoculation determines the cells involved in the initial uptake of *L. major*

As demonstrated in the past section, the site of inoculation changed the migration patterns of cells during the infection. So, it was important to verify if the cells which uptook *Leishmania* would be different. We inoculated, at intradermal and subcutaneous site, 5 x 10^5 metacyclic promastigote forms of *L. major* transfected with the rfp gene. This way, we could follow the parasites by flow cytometry during the infection.

The gate strategy was designed in same way described before (Figure 24) except for the $CD11b^+$ cells that were gated first in the rfp^+ subpopulation. Figure 25 demonstrates the new gate strategy for the identification of infected cells.

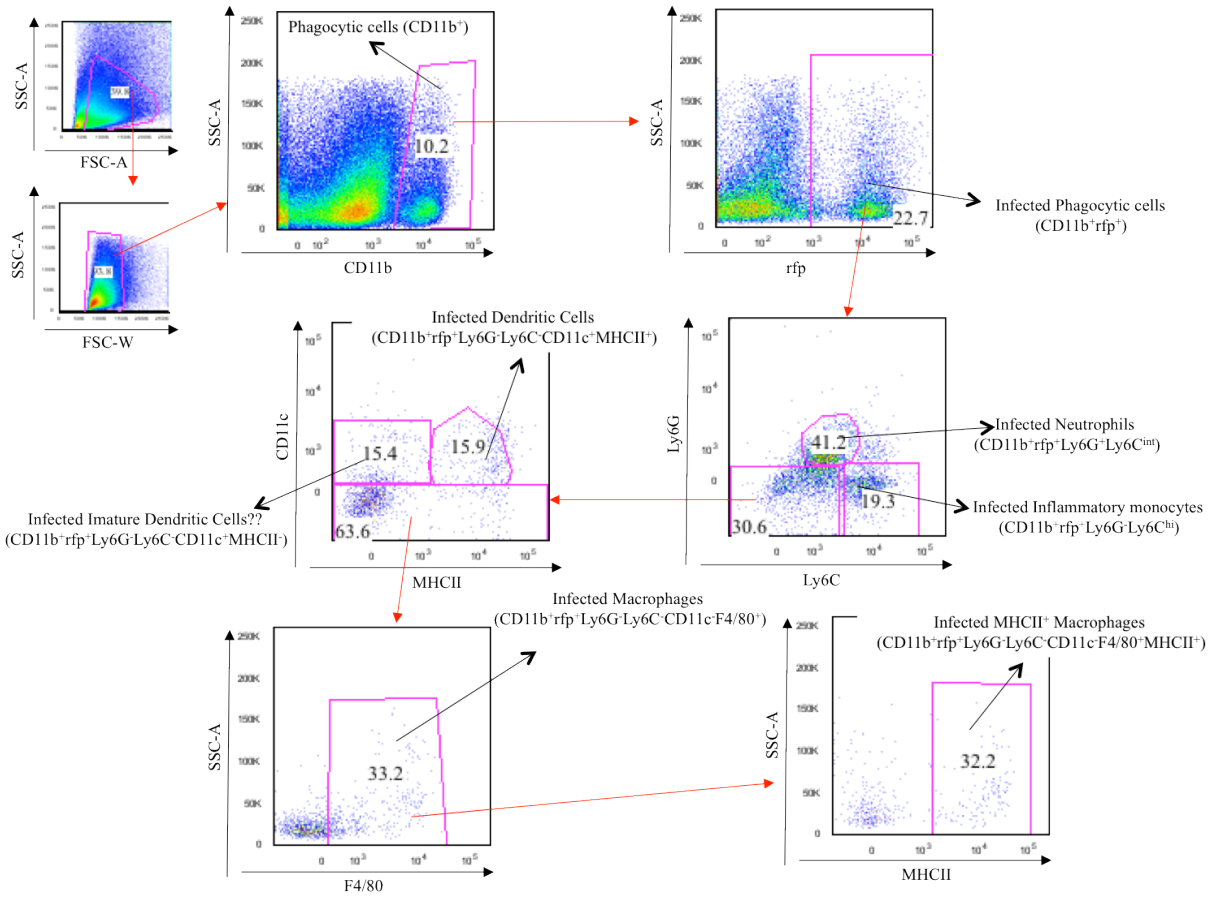

Figure 27. Flow cytometry gate strategy adopted to analyse the infected cells after *L. major* inoculation. Mouse ears or footpads were infected with 5 x 10^5 promastigote forms of *L. major* transfected with rfp gene and 2h, 48h and 9 days post infection the tissues were processed and stained for surface markers. The same gate strategy was used in both tissues and all times. The red arrows indicate the pathways to split populations and identify subsequent sub-populations. The gates represent one sample of ears 48h post infection.

After selection of the $CD11b^+rfp^+$ cells, we analysed the subpopulations generated by this gating to observe which phagocytic cell subtypes was responsible for the uptake of *Leishmania*.

We identified a higher percentage of $CD11b^+$ infected cells in the intradermal site than in the subcutaneous site, at all times measured. Indeed, the footpads presented low percentage of infected cells, about 5% at 48h and 9 days post infection and around 2% 2 h post infection (Figure 28A). We could not identify rfp^+ cells outside of the CD11b gate. At 48h post infection, we observed a peak in the percentage of infected $CD11b^+$ cells, reaching 30% of the phagocytic cells population in the intradermal site, $p<0.0001$. There is a subsequent drop in the percentage of $CD11b^+$ infected cells, probably caused by the influx of these cells to the site of infection (Figure 28A).

At 2h after intradermal infection, we found that *Leishmania* were taken up mainly by neutrophils: around 50% of infected $CD11b^+$ cells were neutrophils (Figure 28B). However, this percentage dropped dramatically to 25% at 48h and less than 10% after 9 days. In contrast, a low percentage of infected $CD11b^+$ cells were neutrophils 2h after the infection at the subcutaneous site. Indeed, the percentage of infected cell in the neutrophil gate was substantially low in all times measured.

While neutrophils are the most important cell involved in the uptake of *Leishmania* at 2 h hours of infection at the intradermal site, the inflammatory monocytes takes their neutrophils from 48h post infection. As infected neutrophil percentages drop (Figure 28B), there is an increase in $CD11b^+rfp^+$ cells that are inflammatory monocytes from 2h to 9 days. Despite the low percentage of inflammatory monocytes 2h post infection, we observed an important increase in the subsequent time points (Figure 28C). After 9 days, the inflammatory monocytes were the majority of $CD11b^+$ cells infected with *L. major*, reaching 50% of this population. In contrast, we observed a slight increase of $CD11b^+rfp^+$ inflammatory monocytes as the infection at subcutaneous site progressed. As found in ears, the footpad also practically did not presented infected inflammatory monocytes at 2h post infection. However, there was a discrete increase in this specific subpopulation 48h and even 9 days post infection reaching around 10% of infected cells at these times measured.

When we analysed the contribution of resident phagocytic cells, we observed the major contribution of these cell populations to subcutaneous infection. After 2h of infection, the resident macrophages in ears or footpads presented the same percentage of $CD11b^+rfp^+$ cells (Figure 28D). However, the percentage of these cells in footpads increased significantly compared to ears 48h and 9 days post infection.

The percentage of infected DCs was lower at subcutaneous site 2h and 48h post infection, but after 9 days this percentage was substantially higher in footpads compared to ears (Figure 28E). At this point of 9 days, resident macrophages and DCs are the major cells involved in the infection of *L. major* at the subcutaneous site.

Interestingly, the non-characterized $CD11c^{+}MHCII^{-}$ population was the most important cell population involved in *Leishmania* uptake at subcutaneous site of infection. At 2h post infection, this population was responsible for 60% of all $CD11b^{+}rfp^{+}$ cells at the subcutaneous site. This high percentage persisted after 48h and dropped considerably after 9 days of infection. In contrast, this $CD11b^{+}rfp^{+}$population was present at a significantly lower percentage in ears at 2h and 48h post infection compared to footpads. Indeed, this $CD11b^{+}rfp^{+}$ population presented lower percentage of at all times measured.

The remarkable point observed when comparing these two kinds of inoculations was: the predominance of inflammatory cells from blood being responsible for the *Leishmania* uptake the at intradermal site in the ear and the predominance of resident phagocytic cells ($CD11b^{+}Ly6G^{-}Ly6C^{-}$ cell populations) responsible for this uptake at the subcutaneous site of inoculation.

The analysis of the absolute numbers of the different cell populations in infected ears and footpads showed significant differences between the sites of inoculation.

At all times analysed, the number of $CD11b^{+}rfp^{+}$ cells was higher in the intradermal site of infection (Figure 29A). Since 2h post infection the number of phagocytic cells infected was about 2,000 against the approximate 200 cells found in the footpads at same time. This remarkable difference was also found at 48h and 9 days post infection, when we detect (as observed at 2h post infection) 10 times more parasites in cells of the ears compared to footpads. Therefore, cells at the intradermal site were much more efficient in uptaking parasite compared to subcutaneous site of inoculation in the acute phase of the infection caused by *L. major*.

Analysing the numbers of $CD11b^{+}rfp^{+}$ cell subpopulations we could conclude the non-involvement of neutrophils the in acute phase *Leishmania* infection at the subcutaneous site. In all times analysed, the number of infected neutrophils was lesser than 50, evidencing the irrelevant role of this cell type in the subcutaneous infection (Figure 29B). Indeed, the total number of neutrophils migrating to the inoculation site was substantially lower (Figure 26B), which could contribute to irrelevance of this cell in *Leishmania* uptake. In contrast, we found a higher number of neutrophils infected in the intradermal site of inoculation in all times measured. We observed around 1,000 cells infected, corresponding to 50% of all cells infected 2h hours post infection (Figures 28B, 29A and B). Despite the decrease in the percentage of neutrophils gated on $CD11b^{+}rfp^{+}$ during the

infection (Figure 28B), the total number of these cells sustained considerable rates of infection until 9 days post-infection.

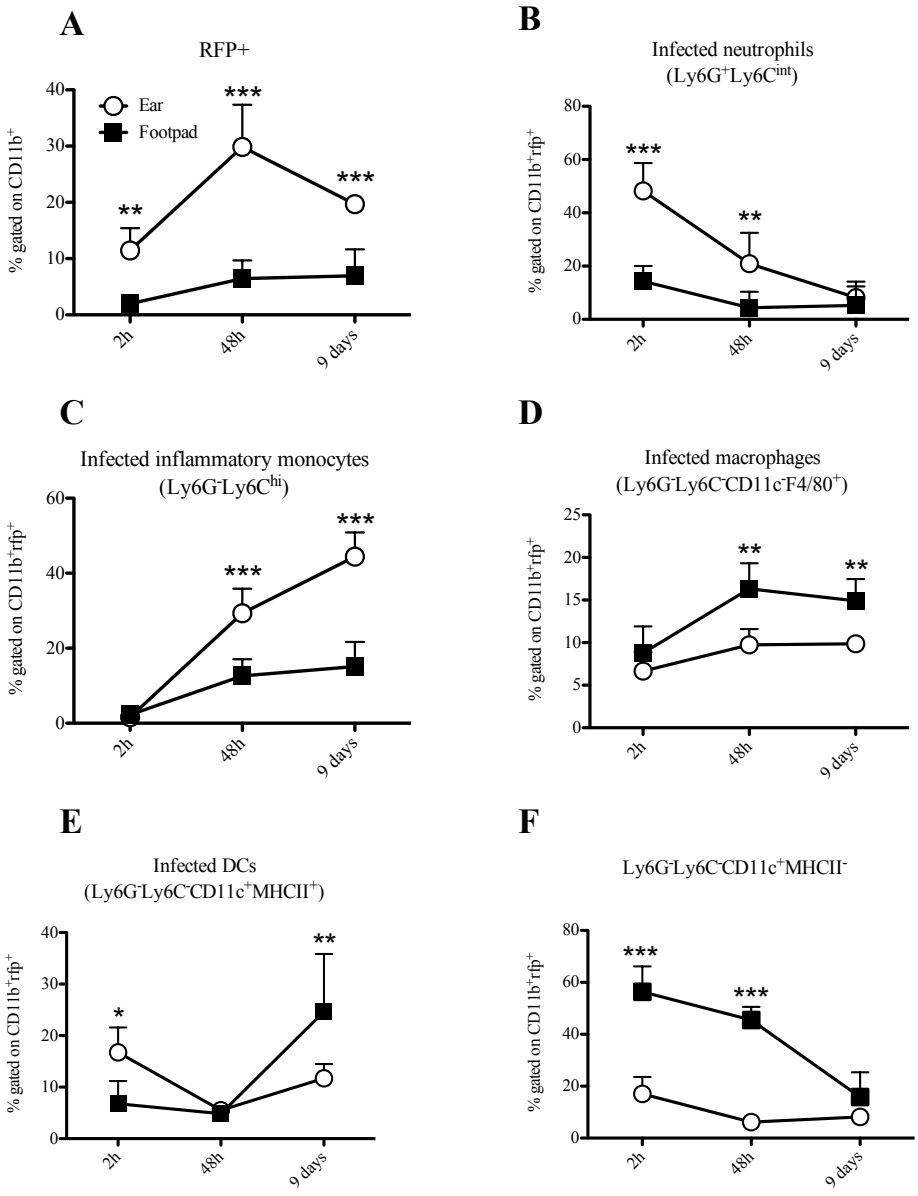

Figure 28. Percentage of subpopulations gated on infected CD11b$^+$rfp$^+$ cells recruited to the *L. major* inoculation site. Mouse ears or footpads were infected with 5 x 10^5 *L. major* promastigote forms and 2h, 48h and 9 days post infection the tissues were processed and stained to surface markers. A, B, C, D, E and F represent the kinetics of phagocytic cells, neutrophils, inflammatory monocytes, macrophages, DCs and CD11c$^+$MHCII$^-$ cells, respectively. The data are represented as mean ±SD of 1 experiment representative of 2, n=5 for each group. *=p<0.05, **=p<0.01 and ***=p<0.001.

Following the observation of an elevated number of inflammatory monocytes at the intradermal site of infection, we observed a significant increase in inflammatory monocytes infected over the time at this particular site of inoculation (Figure 29C). As noted before, 2h after the infection we did not detect significant numbers of inflammatory monocytes at the site of lesion (Figure 26C). Consequently, the number of infected cells at the same time was almost zero. At 48h, the inflammatory monocytes increased in a high ratio where they start to be the most important cell at the intradermal site of infection. Finally, 9 days post infection the number of inflammatory monocytes infected was so high compared to footpads at the same time that the ratio ear/footpad was around 10,000x.

Despite the fact that parasites infected preferentially tissue resident cells observed in footpads, we found more macrophages infected in the ears (Figure 29D) in all times measured. This fact could be related to few phagocytic cells infected in footpads, which would contribute for this observation. Indeed, there is a substantial increase in these macrophage numbers over time, when compared with infected neutrophils or inflammatory monocytes in footpads during the infection. Moreover, the inclination of the curve representing the course of infection in the ears was higher, showing higher efficiency in parasites uptake by ears macrophages.

Similar results were obtained related to *Leishmania* phagocytosis by DCs. Both routes of inoculation promote the same pattern of *Leishmania* uptake by DCs, we could detect relative increase in DCs infected 9 days post infection in both groups (Figure 29E). Since 2h, the ears presented more infected DCs compared to footpads and this pattern was not changed until 48h post infection. However, there is a large increase in the number of infected DCs between 48h and 9 days post infection in the ears and a slight increase in footpads of subcutaneously infected mice.

Despite the higher percentage of infected $CD11b^{+}CD11c^{+}MHCII^{-}$ cells in the footpads 2h and 48h post infection (Figure 28F), we did not detect differences in total number of this specific cell type between intradermal or subcutaneous infection at same time (Figure 29F). At 9 days post inoculation, the infection in this population increased, being significantly different from that in the footpad, which did not change throughout infection.

Practically in all times measured, the number of infected cells were higher in the ears demonstrating a more efficient phagocytosis of *Leishmania* when the parasite is inoculated by intradermal route.

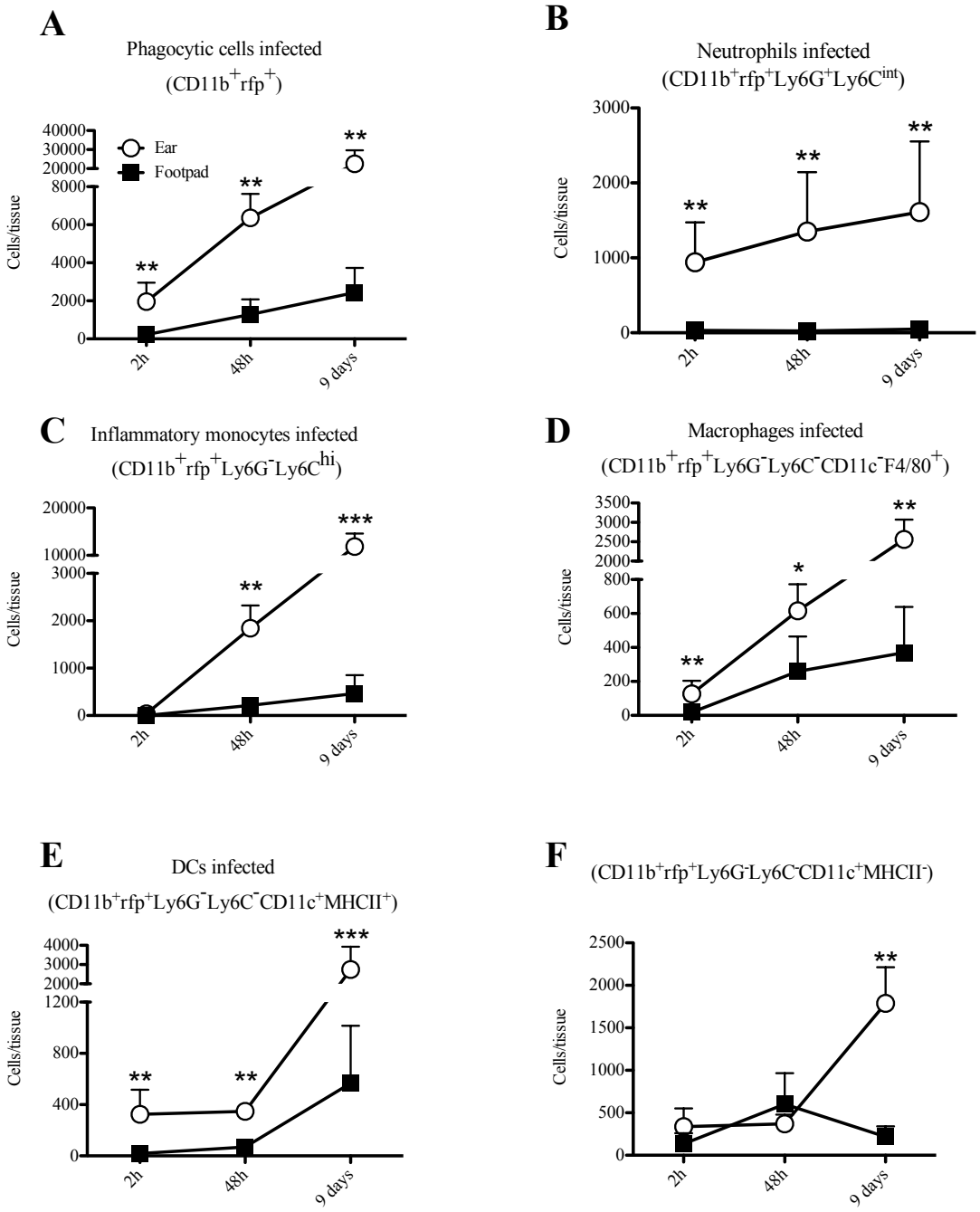

Figure 29. Total numbers of infected CD11b$^+$ cells recruited to the *L. major* inoculation site. Mouse ears or footpads were infected with 5 x 10^5 promastigote forms of *L. major* and 2h, 48h and 9 days post infection the tissues were processed and stained for surface markers. A, B, C, D, E and F represent phagocytic cells, neutrophils, inflammatory monocytes, macrophages, DCs and CD11c$^+$MHCII$^-$ cells, respectively. The data are represented as mean ±SD of 1 experiment representative of 2, n=5 for each group. *=p<0.05, **=p<0.01 and ***=p<0.001.

5.3.3. Infection at the intradermal site elicited higher cell activation and inflammatory response in the acute phase of *L. major* infection

Since we detected a higher influx of the phagocytic cells to the intradermal site of inoculation, we decided to analyse the activation status of APCs in the tissues by assessing the expression of MHCII on the cell surface.

We analysed the expression of MHCII on macrophages and DCs 2h, 48h and 9 days post infection on the total population or just on infected cells and we observed a more robust expression of MHCII on cells from ears.

There are no differences in the activation state as measured by MHCII expression before infection between the two tissues. Both tissues expressed similar levels of this molecule before the infection (Figure 30A). However, just 2h post infection the $MHCII^+$ macrophages in the ears expressed almost 2 times more MHCII compared those from footpads. This significant difference in the MHCII expression persisted at 48h and 9 days post infection. Indeed, the expression of MHCII did not changed in footpads during infection, being comparable to non-infected counterparts. In contrast to what we observed in $MHCII^+$ macrophages, non-infected ears presented higher levels of MHCII expression in DCs (Figure 30B). Moreover, 2h after infection, DCs increased the expression of MHCII, while in the footpads the expression of this activation marker was not altered. After 9 days of infection, MHCII expression fell slightly, indicating a possible downregulation of this marker in DCs from footpads or migration of these cells to dLNs. In the ears, this fall in the expression of MHCII was more accentuated and started at 48h and dropped even more 9 days post infection.

When we analysed MHC expression on infected cells we also noted a higher expression of this molecule on macrophages as well DCs at 2h and 48h post infection (Figure 30C and D). Both infected cell types expressed similar levels of MHCII at 2h and 48h post infection in both groups. While the levels of MHCII did not change in macrophages and DCs from footpads in all times measured, there is a strong reduction of this marker 9 days post infection in cells from ears ($p=0.0079$ for macrophages and DCs). At this time, both cells types and tissues presented with the same levels of MHCII.

The higher number of inflammatory cells and the higher activation state of macrophages and DCs found in the ears of mice are signals indicating that infection with *L. major* causes strong inflammation when inoculated in the dermis. To better characterize this inflammation, we analysed the mRNA levels of inflammatory cytokines, IL-10 and CXCL1 at the different sites of infection.

The levels of IL-1β mRNA at 2h and 48h post infection of the ear increased when compared to the naïve controls. However, the mRNA levels of this cytokine in ears 9 days post infection presented a 15-fold increase relative to naïve control (Figure 31A). On the other hand, when we looked at footpads, no changes in this IL-1β mRNA were detected compared to naïve controls. IL-1β is a known inflammatory cytokine involved in the recruitment of inflammatory monocytes and the increase in IL-1β mRNA 9 days post infection is in accordance with the larger number of inflammatory monocytes at intradermal site at same time (Figure 26C).

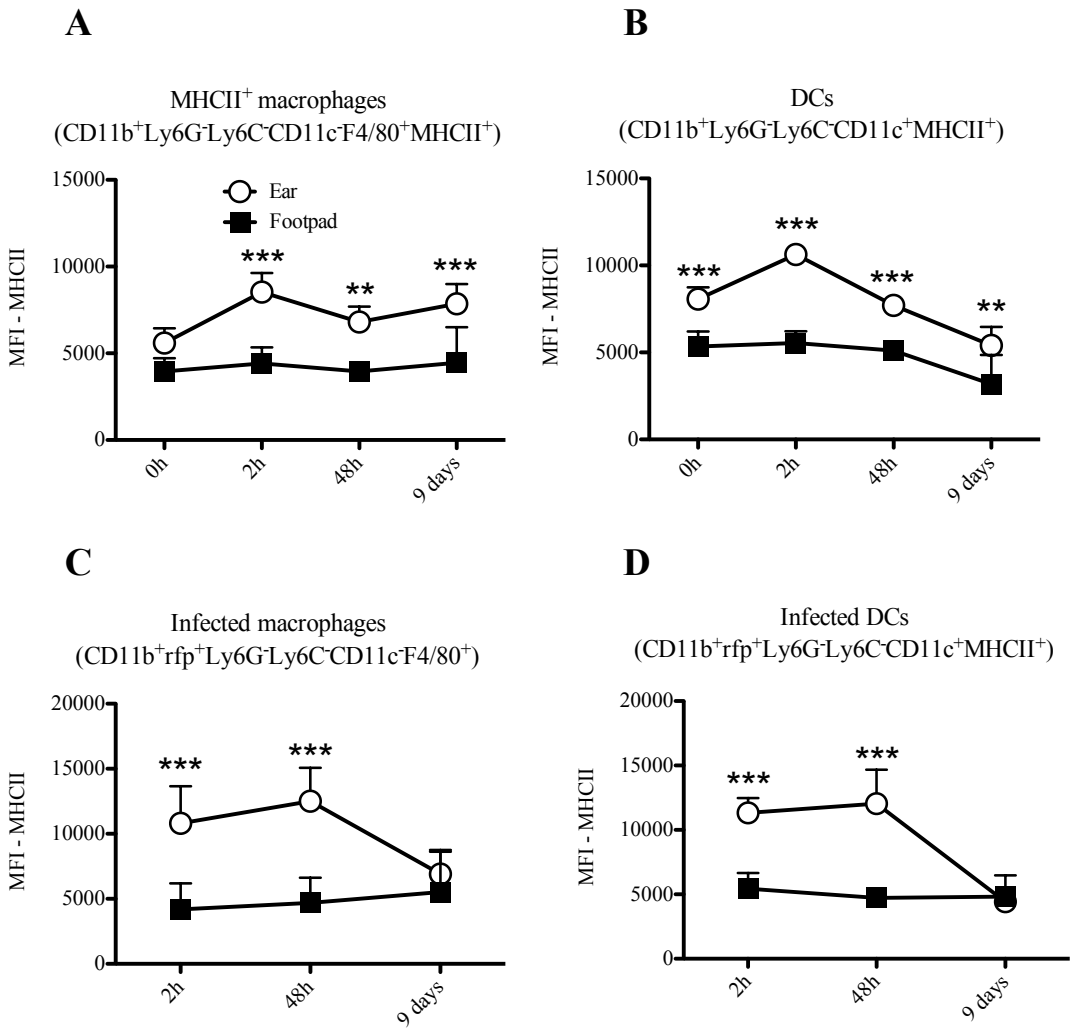

Figure 30. Mean fluorescence intensity (MFI) of MHCII on macrophages or DCs infected with *L. major*. Mouse ears or footpads were infected with 5 x 10^5 promastigote forms of *L. major* and 2h, 48h and 9 days post infection and the 0h time point represents the non-infected controls. The tissues were processed and stained for surface markers. A, B, C and D represent the MFI of MHCII$^+$ macrophages, DCs, infected macrophages and infected DCs, respectively. The data are represented as mean ±SD of 1 experiment representative of 2, n=5 for each group. **=p<0.01 and ***=p<0.001.

We also analysed the mRNA levels of CXCL1, an important chemokine involved in neutrophil recruitment in response to several pathogens. We observed a 5-fold increase in mRNA levels of CXCL1 in the ears from 2h post infection and no changes in footpads were detected at this time point (Figure 31B). The levels of CXCL1 mRNA were significant higher in the ears compared to footpads at 2h post infection. At 48h post infection, there was no difference between groups at this time. At 9 days post infection, the levels of this cytokine dropped in the ears, reaching almost the levels found in non-infected mice. The higher levels of CXCL1 mRNA at 2h post infection correlates with the peak of neutrophil percentage found in the ears of infected mice (Figure 25A). We also could correlate the lower levels of CXCL1 mRNA found 2h post infection in the footpads with the low percentage of neutrophils found in this tissue at the same time (Figure 25A). Moreover, the drop in mRNA CXCL1 levels after 9 days of infection in ears followed the low percentage of this cell type found at the same time in this tissue.

We also analysed the mRNA levels of IL-6, a cytokine involved in the production of neutrophils by the bone marrow. Despite the significant differences in neutrophil recruitment to the inoculation site (Figures 25A and 26B), we did not detect differences in IL-6 mRNA expression between groups at any time measured (Figure 31C).

IL-10 is one of most important anti-inflammatory cytokines and its expression is increased in inflammatory conditions, to regulate inflammation. We detected higher levels of IL-10 mRNA levels in the ears in all times measured (Figure 31D). Especially at 9 days post infection, the levels of IL-10 mRNA were about 20-fold increased in the ears compared to naïve counterparts. In contrast, we could not detect alterations in IL-10 mRNA expression during the infection at subcutaneous site. The higher levels of mRNA IL-10 found since the first hours post infection in the ears correlates with higher inflammatory cell infiltrate 2h and 48h hours post infection (Figure 26B and C). Moreover, the significant increase in the IL-10 mRNA levels at the intradermal site of inoculation is in agreement with cell influx, especially inflammatory monocytes, observed in the ears at same time (Figure 26A and C).

Since we observed a high inflammatory response at the intradermal site and the Th1 response is deeply linked to inflammation, we analysed Th1 cytokine mRNA levels expressed in both tissues during the acute phase of infection.

Both tissues presented the same kinetics of TNF-α mRNA expression during the infection. The levels of TNF-α detected at 2h, 48h and 9 days post infection did not change between the groups and during the time (Figure 31E).

We performed a RT-PCR in naïve ears and footpads to normalize the mRNA expression in these tissues, however we could not detect any amplification of IFN-γ mRNA in either naïve

tissues. Because IFN-γ is an inducible gene in infections, the naïve ears and footpads probably express few copies of this mRNA and consequently not enough for RT-PCR amplification. So, we normalized the IFN-γ expression using -ΔCT method to relative quantification based in the expression of the constitutive gene ribosomal 18S. We detected an increase in the expression of IFN-γ mRNA over time in both groups measured (Figure 31F). However, the expression of this cytokine was higher in the ears 9 days after the infection when compared with footpads at same time.

IL-17 is an important cytokine related to neutrophilic response. We asked if IL-17 could be altered in ears due the high numbers of neutrophils detected in the acute phase of the infection. We could not detect expression of IL-17 mRNA in footpads or ears from naïve mice, so we also used the -ΔCT method to quantify the relative mRNA expression of IL-17. We detected higher expression of IL-17 in the ears 2h and 9 days after infection (Figure 31G). Moreover, no mRNA levels of IL-17 were detected 48h post infection in the footpads implying very low IL-17 production at this time. This higher expression of IL-17 together with CXCL1 augmented levels (Figure 31B) could contribute to increased numbers of neutrophils found in the ears during the infection (Figure 26B).

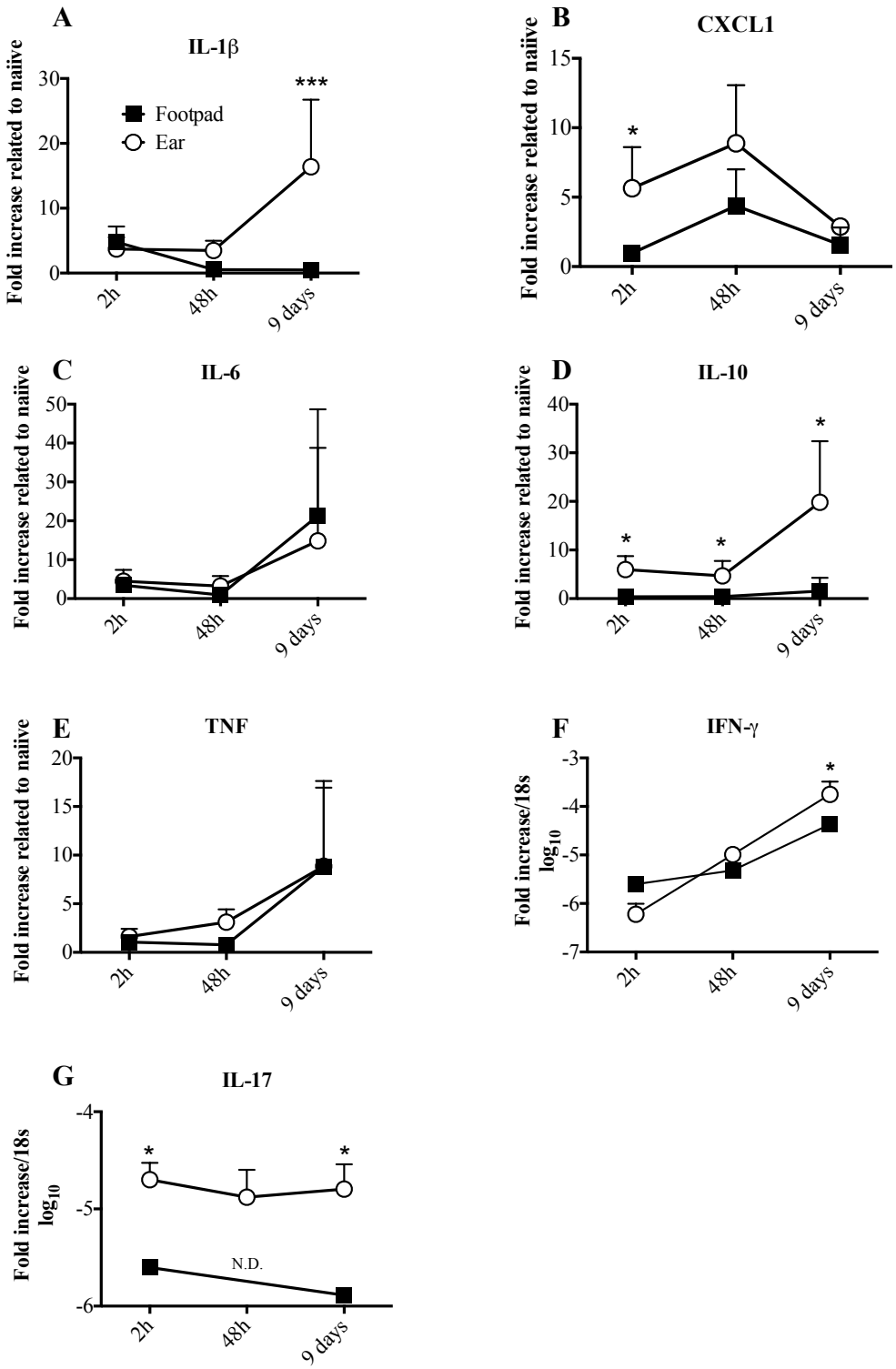

Figure 31. qRT-PCR of cytokines and chemokines expressed during acute phase of *L. major* infection. Mouse ears or footpads were infected with 5 x 10^5 promastigote forms of *L. major* and 2h, 48h and 9 days post infection the tissues were processed and a qRT-PCR was performed to verify the mRNA levels of cytokines and chemokines. A, B, C, D and D represent the mRNA expression 2h, 48h and 9 days post infection of IL-1β, CXCL-1, IL-6, IL-10 and TNF-α, respectively and normalized by mRNA expression of the cytokines in naïve tissues. E and F represent the mRNA expression 2h, 48h and 9 days post infection of IFN-γ and IL-17, respectively and normalized by constitutive expression of 18S mRNA. N.D. indicates not determined. The data are represented as mean ±SD, n=5 for each group. *=$p<0.05$ and ***=$p<0.001$.

6. PART THREE: REACTIVE OXYGEN SPECIES (ROS) CONTROL THE INFLAMMATION IN *L. AMAZONENSIS* INTRADERMAL INFECTION IMPAIRING NEUTROPHIL NECROSIS

6.1. Objectives

6.1.1. General objective

To verify the role of ROS in the control of inflammation caused by *L. amazonensis* infection employing the intradermal route of infection.

6.1.2. Specific objectives

- To follow the development of lesions in gp91$^{phox-/-}$ and C57BL/6 mice (WT) intradermally infected with *Leishmania amazonesis* until 16 weeks post-infection;
- To compare the parasite loads found in gp91$^{phox-/-}$ and WT after 4, 8, 12 and 16 weeks at the site of infection and dLNs;
- To analyze the innate and adaptive immune cellular population phenotypes in several times of the infection at the lesion site as well draining lymph nodes;
- To analyze the expression of inflammatory and anti-inflammatory cytokines as well chemokines (as protein or mRNA levels) at the site of infection and draining lymph nodes during the infection development;
- To verify the major cells involved in the initial uptake of *Leishmania* at intradermal site of infection;
- To compare the neutrophil migration profile to the lesion site 10h, 36h and 60h in gp91$^{phox-/-}$ and WT infected with *L. amazonensis*;
- To analyze the apoptotic profile of the cells in gp91$^{phox-/-}$ and WT mice infected with *L. amazonensis*;

6.2. Material and Methods

6.2.1. Mice

Mice (n=5 for all experiments for each repetition) which genes for the gp91^{phox} chain of NADPH oxidase were deleted by homologous recombination (C57BL/6.129S6-Cybb^{tm1Din}/J, here named gp91$^{phox-/-}$) (Pollock et al., 1995) were purchased from Jackson Farms and bred in NIAID animal care facility. The control mice used in the experiments were C57BL/6 also purchased from Jackson Farms. All animals were maintained at the NIAID animal care facility under specific pathogen-free conditions, controlled 12h dark-light cycles and without restrictions of water or food. The animals used in this study had four to twelve weeks old.

This study was carried out in strict accordance with the recommendations in the Guide for the Care and Use of Laboratory Animals of the National Institutes of Health. The protocol was approved by the Animal Care and Use Committee of the NIAID, NIH (protocol number LPD 68E). BALB/c mice were purchased from Taconic Laboratories and all animals were maintained at the NIAID animal care facility under specific pathogen-free conditions without restrictions of water or food.

6.2.2. Parasites

We utilized the PH8 strain of *Leishmania amazonensis* (IFLA/BR/1967/PH8). Parasites were grown at 26°C in 199 medium supplemented with 20% heat-inactivated FCS (Gemini Bio-Products, Sacramento, CA, USA), 100U/ml penicillin, 100µg/ml streptomycin, 2mM L-Glutamine and 40mM Hepes. Parasites with less than 10 passages in culture were used for all experiments and new isolates were obtained form BALB/c mice lesions.

Alternatively, we used PH8 strain of *L. amazonensis* (IFLA/BR/1967/PH8) transfected with a plasmid containing a red fluorescent protein (RFP) gene, generated as follows. The DsRed gene was amplified by PCR using the pCMV-DsRed-Express plasmid (BD Biosciences/Clontech) as template and the forward primer 5′-TGG ACT AGT ATG GCC TCC TCC GAG GAC GTC-3′ and reverse primer 5′-CCA ACT AGT CTA CAG GAA CAG GTG GTG GCG-3′. The PCR product was first cloned into the pCR2.1 plasmid (Invitrogen) and the sequence verified by nucleotide

sequencing. The SpeI insert from a selected clone was subsequently ligated into the SpeI site of the pKSNEO *Leishmania* expression plasmid (Zhang et al., 1996). PH8 promastigotes were transfected with the resulting expression plasmid construct pKSNEO-DsRed described as follow: the cells were resuspended in electroporation buffer Hepes (ICN Biomedicals Inc., Aurora, OH), 137mM NaCl, 5mM KCl, 0.7mM Na_2HPO_4, 6mM glucose, pH 7.0) to 10^8 cells/ml. Five hundred microliters of cell suspension were added to 2mm gap electroporation cuvettes (BTX Inc., San Diego, CA) to which 20µl of purified plasmid DNA (1mg/ml in sterile 10mM Tris, 2mM Ethylenediamine tetraacetic acid (EDTA) (Quality Biological, Inc., Gaithersburg, MD, USA), pH 8.0) was added. Cells were electroporated using a BTX ECM-600 electroporation system (BTX) and the conditions for electroporation were: 475V, 800 microfarads, 13ohms, single pulse. Electroporated cells were incubated on ice for 10 min and then transferred into 5ml of culture medium (medium 199 supplemented with 20% heat-inactivated FCS (Gemini Bio-Products), 100U/ml penicillin, 100µg/ml streptomycin, 2mM L-Glutamine, 40mM 4-(2-hydroxyethyl)-1-piperazineethanesulfonic acid (Hepes) and incubated at 26 °C for 24h. Subsequently, the cells were harvested by centrifugation 2100 × *g* for 10 min at 4°C and resuspended in fresh culture medium containing 15µg/ml of Geneticin (G418, Life Technologies, Inc.). These cells were selected for growth in increasing concentrations of G418 over a period of several weeks and then maintained at 250µg/ml drug. These drug-resistant cells were used in all subsequent experiments. For the experiments the parasites were growth in the presence of 15µg/ml Geneticin (G418, Life Technologies, Inc).

6.2.3. Infection with *L. amazonensis*

Mice were infected with 5 x 10^3 metacyclic promastigote forms of *L. amazonensis* diluted in 10µl of DMEM in the pinna ears. For the mice infection, metacyclic promastigote forms were used and obtained by centrifugation in Ficoll gradient (Spath et al., 2003). The course of the infection was followed for 16 weeks with weekly ears measurements of the lesions diameter using a digital calliper. We also determined tissue loss due advanced inflammation caused by infection. The frequency of ears with tissue loss was expressed as a percentage of the total number of infected ears.

For short-term experiments, we infected mice intradermally in pinna ear with 5 x 10^5 metacyclic promastigote forms of *L. amazonensis* transfected with rfp gene (*La*-rfp) diluted in 10µl of DMEM and follow the infection until 60h after the challenge.

6.2.4. Euthanasia and tissue processing

Mice of each group were euthanized in CO_2 gas chamber 4, 8, 12 and 16 weeks post infection. Then, the ears and draining lymph nodes were removed and processed as follows: the two sheets of infected ear dermis were separated, deposited in DMEM containing 100U/ml penicillin, 100µg/ml streptomycin, and 0.2mg/ml Liberase CI purified enzyme blend (Roche Diagnostics Corp.), and incubated for 1 h and 30 min at 37°C. Digested tissue was placed in a grinder and processed in a tissue homogenizer (Medimachine; Becton Dickenson). Then, the tissue washed with 10ml of RPMI 0,05% DNAse (Sigma-Aldrich, Inc, St. Louis, MO, USA), centrifuged at 1,500 x *g* for 15 min and resuspended in 1ml complete RPMI. Retromaxillary lymph nodes were removed, and mechanically dissociated using tweezers and a syringe plunger and resuspended in 1ml of complete RPMI.

The draining lymph nodes were excised from the animals, smashed in 40µm cell strainer filter (BD Falcon, USA) and washed by 10ml of RPMI 0,05% DNAse (Sigma-Aldrich, Inc). The homogenates were centrifuged at 1,500 x *g* for 15 min. and the pellet was resuspended in 1mL of RPMI (GIBCO USA) supplemented with 10% heat-inactivated fetal bovine serum (FBS) (Gemini Bio-Products), 100U/mL penicillin, 100µg/mL streptomycin and 2mM L-Glutamine (GIBCO USA) and counted in a hemocytometer.

6.2.5. Parasite load quantification

Parasite load was quantified by limiting dilution assay. After euthanasia, the ears were removed and washed in ethanol 70%. The ears and dLNs were disrupted as described in item 6.2.4 and an aliquot of 50µl was used for parasite quantification. These samples were diluted 1:2 successively in medium 199 supplemented with 20% heat-inactivated FCS (Gemini Bio-Products), 100U/ml penicillin, 100µg/ml streptomycin, 2mM L-Glutamine and 40mM Hepes in 96-well blood agar plates for each ear and draining lymph node. After 10 days of incubation at 25ºC, the cultures were examined for parasite detection. The results were expressed as described (Santiago et al., 2004).

6.2.6. Quantitative Real time PCR

Total RNA, obtained from lesions at 4, 8, 12 and 16 weeks post-infection, was extracted using RNeasy Mini Kit (Qiagen Dusseldorf, Germany) according to the manufacturer's instructions. Next, 1 µg of total RNA obtained from the lesions or lymph nodes was reverse transcribed using Reverse Transcriptase (Promega, Southampton, UK) and oligo (dT) 15 primers (Promega). PCR amplification was performed with a programmable thermal cycler (Perkin–Elmer 2400, USA). The cDNA amplification protocol was as follows: 2 minutes at 50°C, activation of AmpliTaq at 95°C for 10 minutes, melting at 95°C for 15 seconds. For the annealing and final extension, the samples were heated at 60°C for 1 minute for 45 cycles. For dissociation curve, the samples were heated at 95°C for 15 seconds, following cooling at 60°C for 5 seconds. Finally, the samples were cooled for 1 minute at 4°C.

The amplification of cDNA was made using specific primers as represented in the table 1:

Table 2. Primers used in qPCR to quantify the expression of mRNA from ears in the infection

Gene	Primer	Sequence
IFN-γ	Forward	5' -TCAAGTGGCATAGATGTGGAAGAA- 3'
	Reverse	5' -TGGCTCTGCAGGATTTTCATG- 3'
IL-10	Forward	5' -GGTTGCCAATTATCGGA- 3'
	Reverse	5' -ACCTGCTCCACTGCCTTGCT- 3'
TNF-α	Forward	5' -TTCTGTCTACTGAACTTCGGGGTGATCGGTCC- 3'
	Reverse	5' -GTATGAGATAGCAAATCGGCTGACGGTGTGGG- 3
IL1-β	Forward	5' -CAACCAACAAGTGATATTCTCCAT- 3'
	Reverse	5' -GATCCACACTCTCCAGCTGCA- 3
CXCL2	Forward	5' -TGACTTCAAGAACATCCAGAGCTT- 3'
	Reverse	5' -CTTGAGAGTGGCTATGACTTCTGTCT- 3
IL-17	Forward	5' -ATCCCTCAAAGCTCAGCGTGTC- 3'
	Reverse	5' -GGGTCTTCATTGCGGTGGAGAG- 3'
CXCL1	Forward	5' -TGTCCCCAAGTAACGGAGAAA- 3'
	Reverse	5' -TGTCAGAAGCCAGCGTTCAC- 3'
18S rRNA	Forward	5' -TACCACATCCAAGAAGGCAG- 3'
	Reverse	5' -TGCCCTCCAATGGATCCTC- 3'

The reactions were developed in the ABI PRISM®7900HT (Applied Biosystems, Foster City, CA, USA) using 20% of reaction in cDNA volume and 15µl of total PCR mixture. All reactions were made in duplicates using TaqMan® system (Applied Biosystems) according manufacturer instructions. Finally, the samples were cooled by 1 minute at 4°C. The specific cDNAs were normalized according the expression of ribosomal 18S gene based in ΔCT calculation.

6.2.6. Generation of *L. amazonensis* antigen (LA*La*)

Antigens were prepared from log phase promastigotes, washed in PBS and submitted to seven cycles of freezing in liquid nitrogen and thawing in water bath (37ºC). Suspensions were adjusted to a final concentration of 1 mg of protein/ml and kept at -70ºC until use. Protein concentration was assessed by the Lowry assay (Lowry et al., 1951).

6.2.8. Flow cytometry

Single-cell suspensions were incubated with an anti-Fc-γ III/II (CD16/32) receptor antibody (2.4G2, BD Biosciences) in RPMI without phenol red (Gibco) containing 1% FCS and stained with fluorochrome-conjugated antibodies. The following antibodies were used: APC anti-mouse CD11c (HL3, BD Biosciences); PE-Cy7 anti-mouse CD11b (M1/70, eBioscience); PerCP-Cy5.5 anti-mouse Ly6C (HK1.4, eBioscience); FITC anti-mouse Ly6G (1A8, eBioscience); eFluor 450 anti-mouse F4/80 (BM8, eBioscience); Alexafluor-700 anti-mouse MHC II (M5/114.15.2, eBioscience); PE-cy7 anti-mouse CD4 (L3T4, eBioscience); pacific blue anti-mouse TCRβ (H57-597, eBioscience); FITC anti-human ki67 (B56, BD Pharmigen), APC anti-mouse IFN-γ (XMG1.2, eBioscience); PE anti-mouse IL-10 (JES5-16E3, eBioscience); PerCP-Cy5.5 anti-mouse IL-17 (eBio17B7, eBioscience); efluor 660 anti-mouse TNF-α (TN3-19, eBioscience) and acqua live dead probe (Invitrogen). The isotype controls used (all obtained from BD Biosciences) were rat IgG1 (R3–34) and rat IgG2b (A95-1). For intracellular detection of cytokines, cells were first stimulated with LA*Lm* for 6h at 37°C 5% CO_2 and them incubated with 1µg/ml brefeldin (BFA) (Sigma-Aldrich) for 4 h at 37°C 5% CO_2. Following surface staining and permeabilization, cells were then stained with a combination of anti-mouse antibodies for cytokines and the transcriptional factor ki-

67 in foxp3 permeabilization buffer (BD Bioscience). Intracellular staining was carried out for 60 minutes on ice.

The acquisition of the samples was made in an eight colors FACS CANTO II cytometer (Becton Dickinson, Mountain View, California, USA) using the software Diva (Becton Dickinson, Mountain View, California, USA).

The percentage of positive cells and the mean fluorescence intensity were analyzed with the software FlowJo (Tree Star, Ashland, Oregon, USA).

The immunolabeling was organized and described as follow: tube 1 (APC anti-mouse CD11c, PE-Cy7 anti-mouse CD11b, PerCP-Cy5.5 anti-mouse Ly6C, FITC anti-mouse Ly6G eFluor 450 anti-mouse F4/80; Alexafluor-700 anti-mouse MHCII); tube 2 (PE-cy7 anti-mouse CD4, pacific blue anti-mouse TCRβ, FITC anti-human ki67, APC anti-mouse IFN-γ, PE anti-mouse IL-10, PerCP-Cy5.5 anti-mouse IL-17, efluor 660 anti-mouse TNF-α and acqua live dead probe).

6.2.9. Apoptosis assessment

We assessed the apoptosis in neutrophils in acute and chronic phase of infection by flow cytometry as described as follow. After infection with *La*-rfp, the cells from ears were processed as described in item 6.2.4. Single-cell suspensions were incubated with an anti-Fc-γ III/II (CD16/32) receptor antibody (2.4G2, BD Biosciences) in RPMI without phenol red (Gibco) containing 1% FCS and stained with fluorochrome-conjugated antibodies. The following antibodies were used: PE-Cy7 anti-mouse CD11b (M1/70, eBioscience); APC-Cy7 anti-mouse Ly6C (HK1.4, eBioscience) and FITC anti-mouse Ly6G (1A8, eBioscience). After the surface stain, the cells were stained with Annexin-V-APC and 7-AAD (BD Biosciences) as recommended by the manufacturer.

The acquisition of the samples was made in an eight colors FACS CANTO II cytometer (Becton Dickinson, Mountain View, California, USA) using the software Diva (Becton Dickinson, Mountain View, California, USA).

6.2.10. Statistical analysis

The statistical analysis was performed by with two-tailed Student's *t*-test, Mann-Withney nonparametric test or two-way ANOVA with Bonferroni post-test depending on the experiment. The software GraphPad Prism 5.0 (GraphPad, La Jolla, CA, USA) was utilized for the analysis. Differences were considered significant if $p<0.05$, data are expressed as mean and standard deviation.

6.3. Results

6.3.1. Intradermally inoculated gp91$^{phox-/-}$ mice exhibit higher inflammation in *L. amazonensis* infection

All *in vivo* studies in the literature addressing the role of ROS in *Leishmania* infections were made utilizing subcutaneous challenge. However, as shown in section 5, subcutaneous infection differs from intradermal infection mainly due to the accumulation of neutrophils observed in the latter. So, we thought it would be important to determine the influence of ROS during intradermal infection, since neutrophils might be the major cells involved in oxidative stress. Moreover, ROS have a direct influence in neutrophil death through apoptotic mechanisms. The intradermal model is also more representative of natural infection.

We infected WT and gp91$^{phox-/-}$ mice intradermally in ear pinna with 5 x 10^3 promastigote forms of *L. amazonensis* and followed the infection for 16 weeks measuring the diameter of lesions weekly.

Lesions in both groups of mice increased in size over the course of infection, demonstrating the susceptibility of both WT and gp91$^{phox-/-}$ mice to *L. amazonensis.* After 3 weeks of infection we observed lesions in gp91$^{phox-/-}$ mice, and one week later lesions appeared in the WT group (Figure 32A). While we observed a concurrent increase in lesion size in WT mice (Figure 32A), lesions were significantly smaller and with greatly reduced early necrosis. Starting at 5 weeks post infection, lesions in gp91$^{phox-/-}$ group became significantly larger compared to WT mice. Remarkably, the site of infection influenced disease outcome. Infection in the footpad resulted in non-healing but stable lesions whereas infection in the ear led to progressive lesion growth and

eventual necrosis (Figure 10A and 32, A-C). We followed the lesions until 16 weeks p.i.. However, starting at 10 weeks post infection the ears from gp91$^{phox-/-}$ mice started to become heavily necrotic and a considerable percentage of the mice eventually lost portions of their ears. Therefore, for the purposes of comparing lesions sizes we disregarded all time points after 11 weeks, at which time a comparison of the frequency of ears with tissue loss was a better measure of disease progression. Twelve weeks post infection, the ears of gp91$^{phox-/-}$ mice were in advanced necrotic state, while the WT ears presented consistent lesions with a discrete tissue loss (Figure 32C). At 16 weeks, the gp91$^{phox-/-}$ group had extended tissue loss. In contrast, the WT ears had only just started to present with tissue loss, although in a less extended way. Because of the extended necrosis found in gp91$^{phox-/-}$, we disregarded all data from 16 weeks post infection in the ears of mice because a reduction in the total amount of ear tissue is likely to influence our analysis. We followed this tissue loss and converted it to a percentage of mice that had some part of ear eroded by the infection. The percentage of ears with necrotic areas was higher in gp91$^{phox-/-}$ group starting at 7 weeks, reaching 90% of ears with tissue loss at 14 weeks post infection (Figure 32B). In contrast, the WT mice reached 50% of tissue loss at same time suggesting an advanced necrotic state in gp91$^{phox-/-}$ mice during *L. amazonensis* infection. The percentage of ears with tissue loss represented in Figure 32B does not consider the extension of this tissue loss. Therefore, we photographed ears from each group to depict the severe extend of tissue destruction in gp91$^{phox-/-}$ mice at 16 weeks p.i., as seen in Figure 32C.

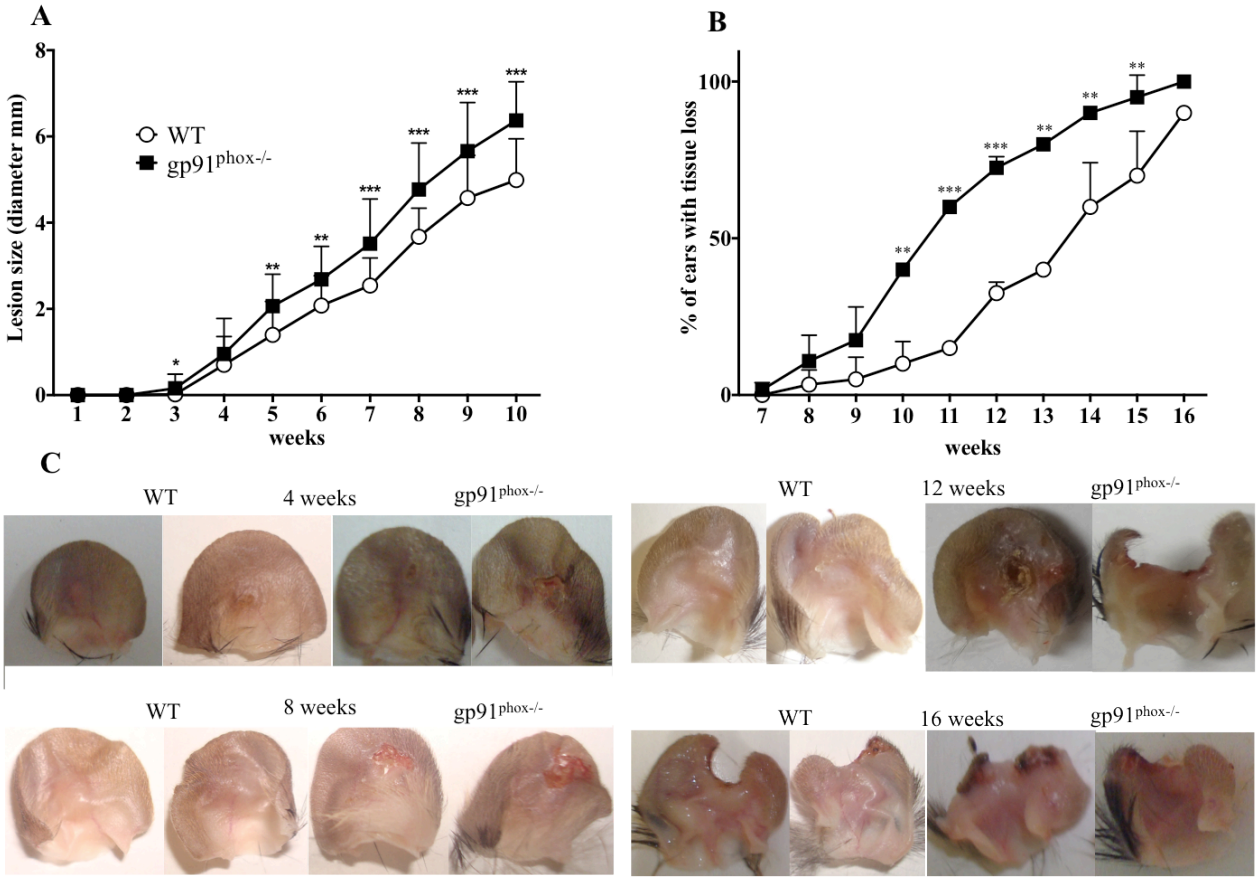

Figure 32. Lesion size of mice infected with *L. amazonensis*. Mice were infected with 5 x 10^3 *L. amazonensis* metacyclic promastigotes in pinna ears and followed until 16 weeks. (A) The lesion diameter was measured week by week with a calliper, *p<0.05, **p<0.01 and ***p<0.001 Data are shown as mean ± standard deviation (± SD). (B) Percentage of mice that had some tissue loss from 7 to 16 weeks post infection. (C) Representative pictures of ears from mice infected with *L. amazonesis* 4, 8, 12 and 16 weeks post infection. The figure represents one representative experiment of 2, n=5 for each experiment.

6.3.2. ROS do not influence the killing of *L. amazonensis in vivo* at the site of infection, but is required to control parasite loads in dLNs

ROS have a strong influence in the control of inflammation generated by *L. amazonensis* intradermal infection (Figure 32). So, it was important to verify if this higher inflammatory state could be explained by possible alterations in parasite loads in gp91$^{phox-/-}$.

As observed for subcutaneous infection (Figure 10B), we could not detect differences in the parasite loads at the site of infection WT versus gp91$^{phox-/-}$ mice (Figure 33A) and the parasite loads

increased over the course of infection. Since we did not observe differences in parasite loads between groups, we cannot attribute the higher inflammatory response seen in gp91$^{phox-/-}$ mice (Figure 32) to parasite growth at the site of infection.

Despite the equal numbers of parasites at the lesion site in gp91$^{phox-/-}$ and WT mice (Figure 33A), we detected small but significant differences in dLNs at 4, 12, and 16 weeks post-infection (Figure 33B). Because the dLN did not suffer from the same loss of tissue that we experienced in the ear we were able to include the 16 week data. The observed difference in dLN parasite loads was in contrast to dLNs after subcutaneous infection, which were the same (Figure 10C). Eight weeks post infection, we found equal parasite numbers, but at 12 and 16 weeks post infection the gp91$^{phox-/-}$ mice had significantly increased parasite loads in dLNs. These results suggest that ROS are important for parasite control in dLNs.

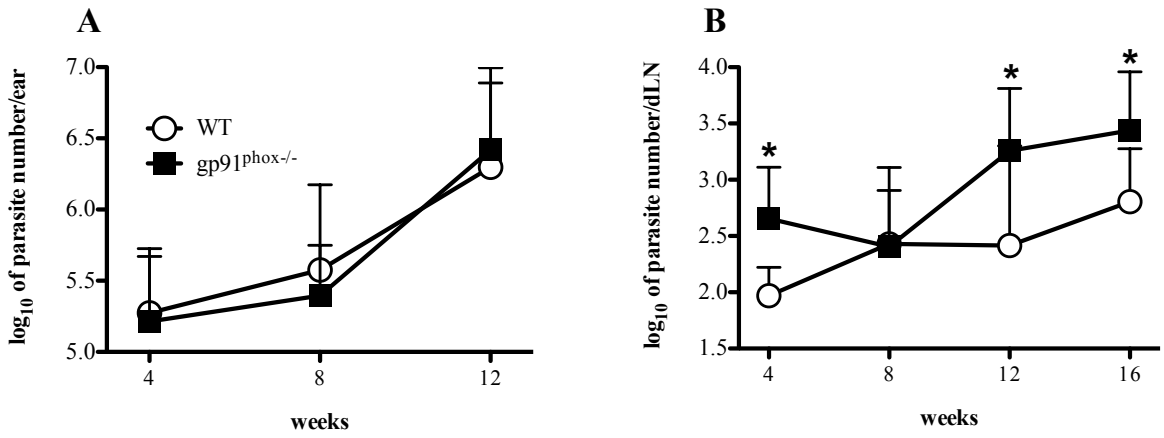

Figure 33. Parasite loads found in *L. Amazonensis*-infected mice 4, 8, 12 and 16 weeks post infection. Mice were infected with 5 x 10^3 *L. amazonensis* metacyclic promastigotes in pinna ears and followed for 16 weeks. (A) Parasite loads found in ears of infected mice 4, 8, 12 and 16 weeks post infection. (B) Parasite loads found in draining lymph nodes of infected mice 4, 8, 12 and 16 weeks post infection. Data are shown as mean ± SD from one representative experiment of 2, n=5 for each experiment.

6.3.3. ROS impairs neutrophil accumulation at the site of inoculation with *L. amazonensis*

Since ROS is principally involved in innate cellular immunity, we analysed innate cells by flow cytometry 4, 8, and 12 weeks post infection. The strategy to define the cell populations was the same as shown in the Figure 24. The total number of CD11b$^+$ cells increased in both groups

over time. However, at 8 and 12 weeks post infection, the numbers of $CD11b^+$ cells per ear was significantly higher in $gp91^{phox-/-}$ mice (Figure 34). The higher number of $CD11b^+$ cells accumulation corroborates the increase in lesion size (Figure 32A) seen in both groups during the infection.

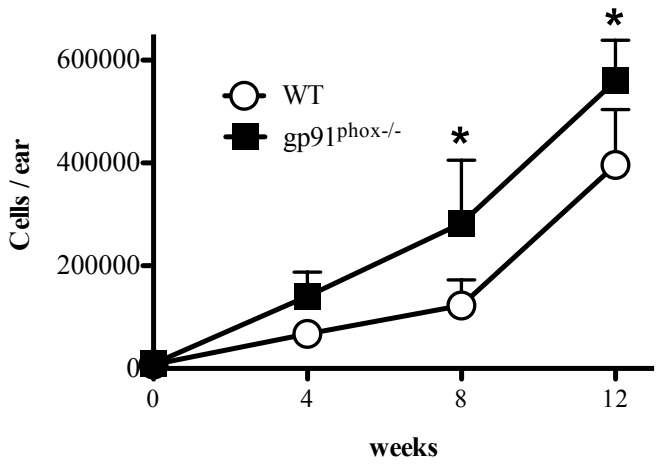

Figure 34. Number of $CD11b^+$ cells recruited to the site of inoculation with *L. amazonensis* 4, 8 and 12 weeks post infection. Mice were infected with 5 x 10^3 *L. amazonensis* metacyclic promastigotes in pinna ears and followed for 16 weeks. The data represents the total numbers of CD11b+ cells in ears 4, 8 and 12 weeks post infection. Data are shown as mean ± SD from one representative experiment of 2, n=5 for each experiment.

We also analysed $CD11b^+$ subpopulations to determine if the overall increase in $CD11b^+$ cells was attributed to a specific population. Interestingly, we observed a remarkable increase in the neutrophil population at 8 and 12 weeks post infection in $gp91^{phox-/-}$ mice (Figure 35A). The increase in this population was three times more pronounced compared to WT mice at 12 weeks post infection. This higher population of neutrophils coincides with an advanced necrotic state seen in $gp91^{phox-/-}$ mice (Figure 32C). Despite the significant differences in neutrophil numbers between the groups, we could not detect differences in other $CD11b^+$ populations. Inflammatory monocytes, macrophages and dendritic cells found at the lesion in the same numbers in both groups (Figure 35 B, C and D). Therefore, the increase in $CD11b^+$ total cells in $gp91^{phox-/-}$ mice (Figure 34) is attributable to increased numbers of neutrophils at the site of inoculation.

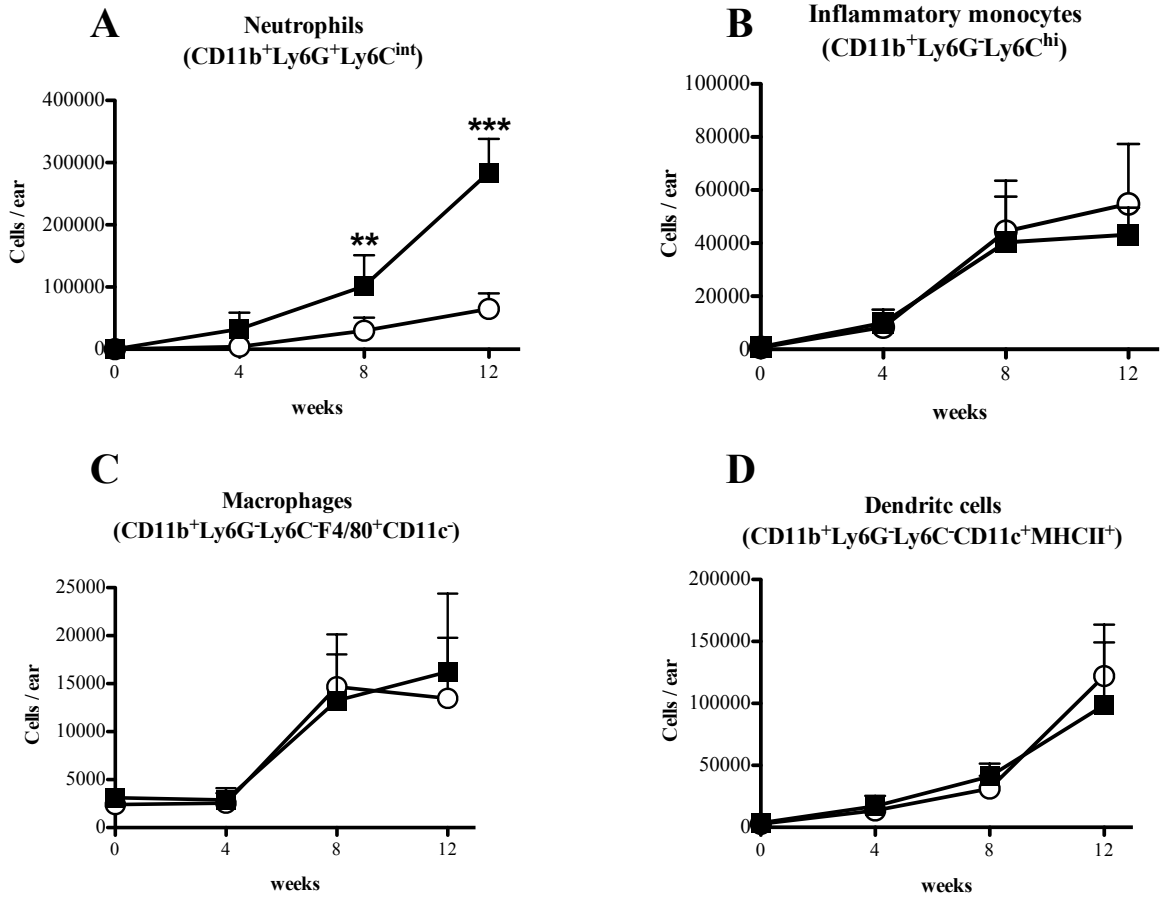

Figure 35. CD11b$^+$ subpopulations recruited to the site of inoculation with *L. amazonensis* 4, 8 and 12 weeks post infection. The mice were infected with 5 x 10^3 of *L. amazonensis* metacyclic promastigotes in pinna ears and followed for 16 weeks. A, B C and D represent the total numbers of neutrophils, inflammatory monocytes, macrophages and dendritic cells in ears 4, 8 and 12 weeks post infection, respectively. Data are shown as mean ± SD from one representative experiment of 2, n=5 for each experiment.

We also analysed the percentage of CD11b$^+$ subpopulations to determine which populations predominated at the site of infection. The percentage of neutrophils increased over time in both groups, but at 8 and 12 weeks post infection this percentage was higher in gp91$^{phox-/-}$ mice (Figure 36A and B). Indeed, at all times analysed, the majority of CD11b$^+$ found in gp91$^{phox-/-}$ mice were neutrophils, which represented 30, 40 and 55% of migrating cells to site of lesion at 4, 8 and 12 weeks post infection, respectively. In contrast, the majority of cells found in the infection site in WT mice were dendritic cells, which reached almost 40% of CD11b$^+$ cell population at 8 and 12 weeks post infection (Figure 36E). The high percentage of neutrophils present during infection

resulted in a corresponding drop in the frequency of other $CD11b^+$ populations. We observed a decrease of inflammatory monocytes and dendritic cells percentage at 8 and 12 weeks post infection in $gp91^{phox-/-}$ mice (Figure 36C and E), suggesting a deficiency in ROS production during *L. amazonensis* the infection alters the composition of $CD11b^+$ cells at the site of infection. Despite the alterations observed in $CD11b^+$ subpopulations, we could not detect differences between the groups in the percentage of macrophages (Figure 36D) although the overall percentage of macrophages decreased substantially after infection and was maintained at low levels at 4, 8 and 12 weeks post infection.

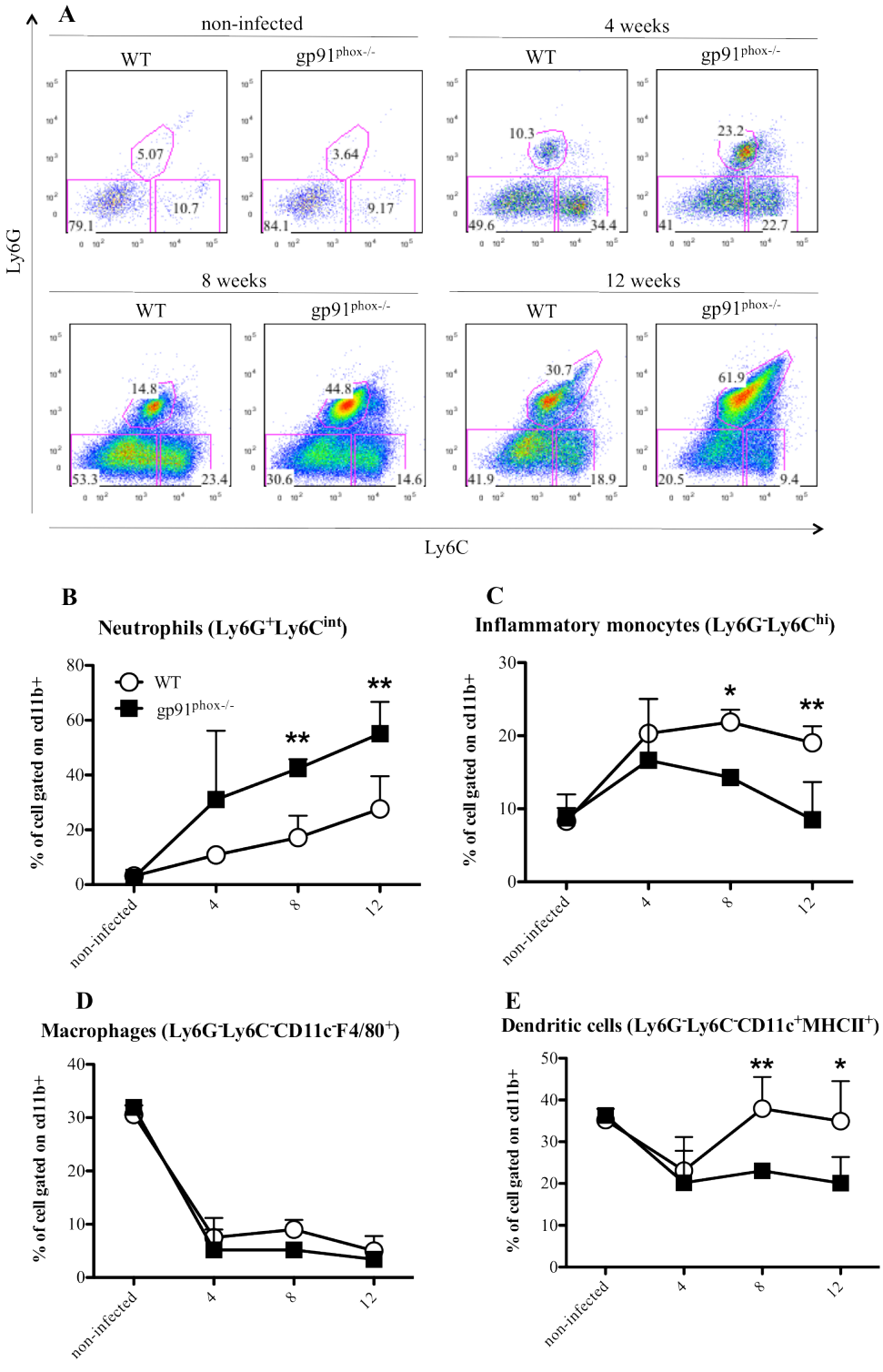

Figure 36. Percentage of CD11b$^+$ subpopulations recruited to the site of inoculation with *L. amazonensis* 4, 8 and 12 weeks post infection. Mice were infected with 5 x 10^3 *L. amazonensis* metacyclic promastigotes in pinna ears and followed for 16 weeks. A represents the dot plots of the subpopulations gated on Ly6G and Ly6C markers. B C, D and E represent the percentage of neutrophils, inflammatory monocytes, macrophages and dendritic cells in ears 4, 8 and 12 weeks post infection, respectively. Data are shown as mean ± SD from one representative experiment of 2, n=5 for each experiment.

6.3.4. Gp91$^{phox-/-}$ mice do not presented with alterations in T lymphocytes during *L. amazonensis* infection

We found that ROS deficiency influences the dynamics of innate immune cell accumulation in the site of infection (Figure 36). We wished to analyse whether this resulted in an alteration in the adaptive immune response.

We analysed the total number of $CD4^+$ and $CD8^+$ T lymphocytes recruited to the ears over the course of infection. Regard we observed a tendency in higher number of $CD4^+$ T cells we did not find statistical differences in the number of $CD4^+$ or $CD8^+$ T cells (this last one presenting a significant increase at 8 weeks p.i. in gp91$^{phox-/-}$ group) at any of the time points analysed (Figure 37A and E). Both groups had the same response profile, with increasing numbers of cells recruited to the site of infection up to12 weeks p.i., the last time before which necrosis began to compromise the interpretation of the data.

We analysed numerous markers related to T cell function CD44 is a receptor for hyaluronic acid involved in cell migration and adhesion to inflamed tissues and the expression of this marker indicates cell activation (Huet et al., 1989). We did not detect alterations in $CD44^+$ cell numbers in the $CD4^+$ T lymphocyte population indicating that the recruitment of highly activated $CD4^+$ T cells was similar between groups (Figure 37B).

We also analysed the transcriptional factor foxp3, which is expressed by regulatory $CD4^+$ T cells (T_{regs}) and is responsible for the activation of regulatory genes in T cells and subsequent control of the inflammatory response (Schubert et al., 2001). Despite the larger cellular infiltrate in gp91$^{phox-/-}$ mice (Figure 32), the numbers of T_{regs} cells did not change between the groups. The number of T_{regs} recruited to lesions in WT and gp91$^{phox-/-}$ mice was low at 4 and 8 weeks post infection (Figure 37C). However, likely due to the intense inflammation observed in both groups at 12 weeks post infection, we observed a significant increase of T_{regs} number at this time.

Ki67 is a transcription factor involved in cell proliferation. The fact that the Ki67 protein is present during all active phases of the cell cycle (G_1, S, G_2, and mitosis), but is absent from resting cells (G_0), makes it an excellent marker for determining the proliferating fraction of a given cell population (Gerdes et al., 1984). So, we analyzed $ki67^+CD4^+$ T cells to evaluate the proliferation of these cells at the site of infection. We observed a gradual increase of $ki67^+CD4^+$ T cells over the time of infection (Figure 37D). Both groups seemed to reach a peak of T cell proliferation at 12

weeks post infection, however, at all times analyzed, we could not detect significant differences between groups related to the ki67 marker.

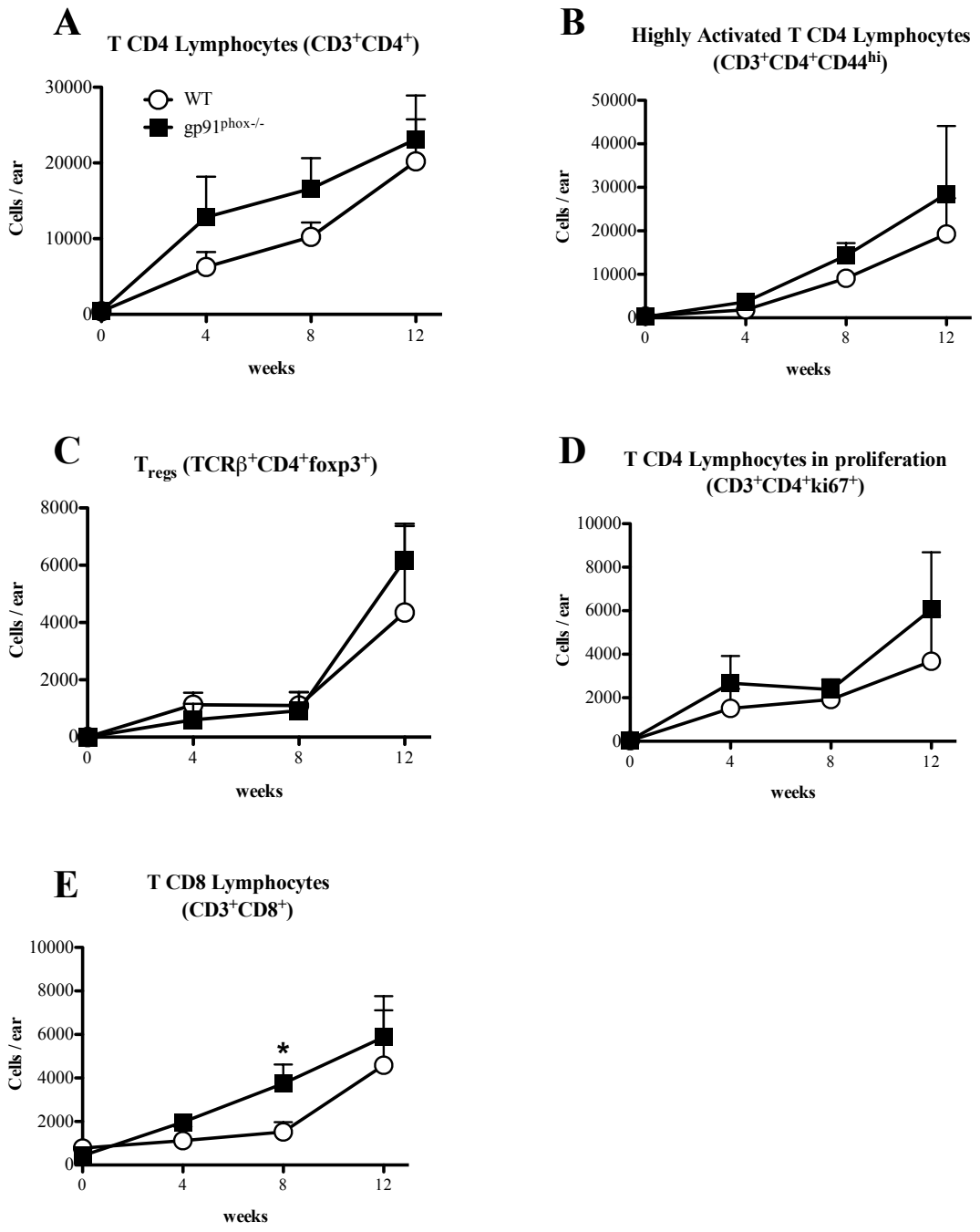

Figure 37. Total number of CD4$^+$ T cell sub-populations recruited to site of inoculation with *L. amazonensis* 4, 8 and 12 weeks post infection. Mice were infected with 5 x 10^3 *L. amazonensis* metacyclic promastigotes in pinna ears and followed for 16 weeks. A, B C, D and E represent the total numbers of CD4$^+$ T cells, activated CD4$^+$ T cells, regulatory CD4$^+$ T cells, proliferating CD4$^+$ T cells and CD8$^+$ T cells in ears, respectively. T cell populations were analysed 4, 8 and 12 weeks post infection. Data are shown as mean ± SD from one representative experiment of 2, n=5 for each experiment.

6.3.5. Gp91$^{phox-/-}$ and WT mice produce similar levels of cytokines by T lymphocytes during *L. amazonensis* infection

Despite no differences found in the activation state of T cells during the infection between the groups, it would be important verify if these cells had differences in cytokine production. So, 4, 8 and 12 weeks post infection we performed flow cytometry to evaluate the production of cytokines by T cells.

We re-stimulated the ear cells with LA*La* for 6h and stained for intracellular cytokines following treatment with brefeldin. At the times post infection analysed, we did not observe differences in cytokine production by T lymphocytes from the WT or KO group. We observed a slight, but non-significant increase in the number of cells producing IFN-γ (Figure 38A), TNF-α (Figure 38B), IL-2 (Figure 38D), IL-10 (Figure 38F) and IL-17 (Figure 38G) from 4 to 8 weeks p.i. in both groups. Twelve weeks p.i. there are a significant increase in the production of these cytokines, when compared to 4 weeks p.i., $p<0.05$. Despite the absence of ROS in gp91$^{phox-/-}$ mice, both groups showed a similar profile in cytokine production. Therefore, ROS production by gp91^{phox} does not seem to affect cytokine production by T lymphocytes during the infection. One exception was IL-10 production, which was higher in the WT group at 12 weeks post infection (Figure 38F). This higher production of IL-10 could contribute to the smaller cellular infiltrate seen in WT mice during the infection.

Despite the elevated number of neutrophils migrating to ears in gp91$^{phox-/-}$ mice during the infection (Figure 35A), there was no correlation with IL-17 production (Figure 38G). We did not observe differences in the production of this cytokine during infection between the two groups.

We also analysed T cells double positive for IFN-γ and TNF-α (Figure 38C) or triple positive for IFN-γ, TNF-α and IL-2 (Figure 38E). These cells are very important for the control of parasites in infections caused by *Leishmania*, since they help in macrophage activation and consequent killing of the parasite. More than single IFN-γ producers, the IFN-γ, TNF-α and IL-2 triple producers are the required T cells involved in the protection against *Leishmania.* They can synergize the effects of IFN-γ with TNF-α to increase the intensity and efficacy of anti-leishmanial response. Moreover, the IL-2 secreted enhances the expansion of these cells promoting a better immune response (Darrah et al., 2007). We detected low numbers of these cell types in both groups (Figure 38 C and E), suggesting an irrelevant role of ROS in functionality of these cells.

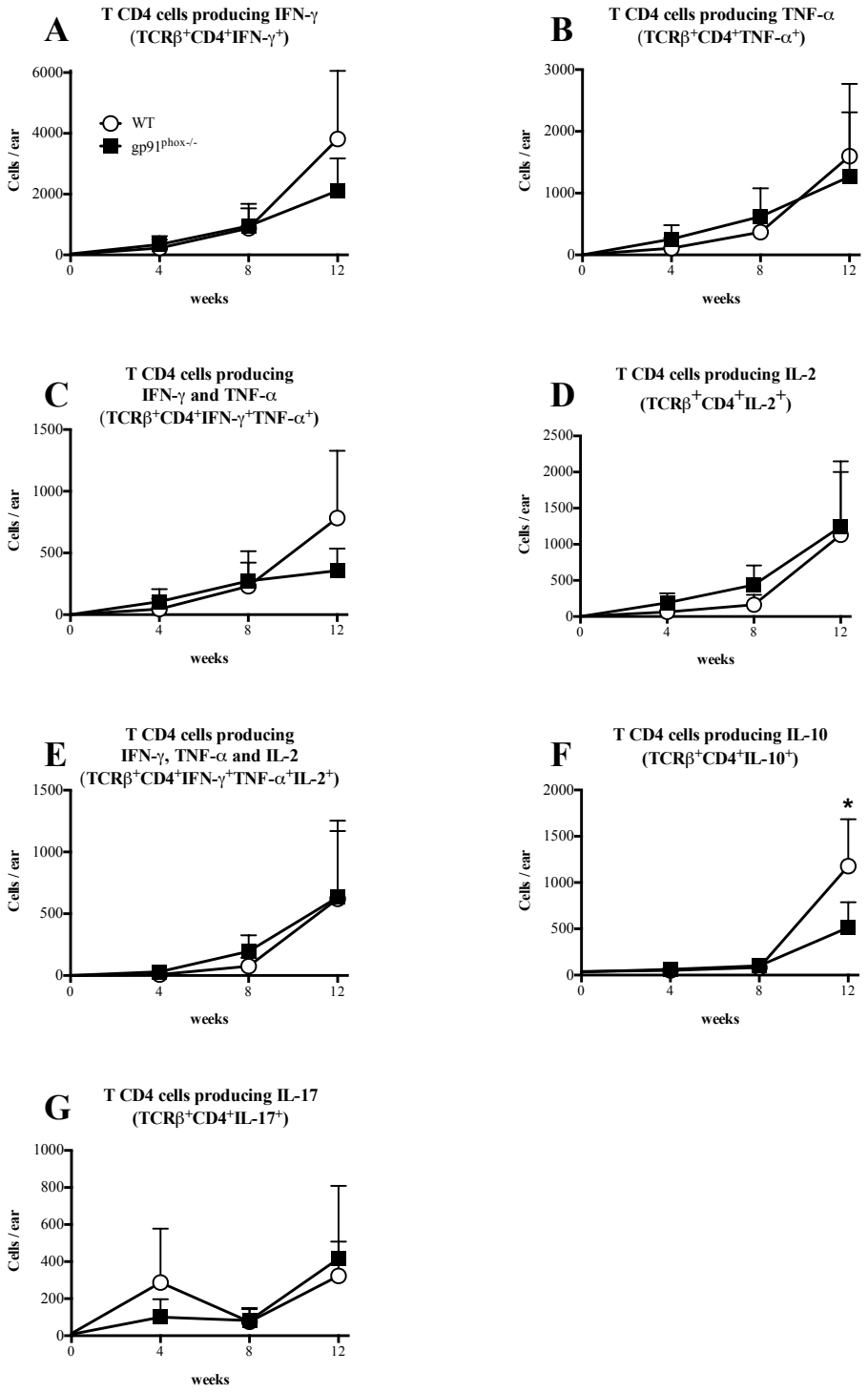

Figure 38. Production of cytokines by CD4$^+$ T cells at the site of *L. amazonensis* inoculation 4, 8 and 12 weeks post infection. Mice were infected with 5 x 10^3 *L. amazonensis* metacyclic promastigotes in pinna ears and followed for 16 weeks. A represents CD4$^+$ T cells producing IFN-γ, B represents CD4$^+$ T cells producing TNF-α, C represents CD4$^+$ T cells producing IFN-γ and TNF-α, D represents CD4$^+$ T cells producing IL-2, E represents CD4$^+$ T cells producing IFN-γ, TNF-α and IL-2, F represents CD4$^+$ T cells producing IL-10 and G represents CD4$^+$ T cells producing IL-17 in ears 4, 8 and 12 weeks post infection. Data are shown as mean ± SD from one representative experiment of 2, n=5 for each experiment.

6.3.6. ROS influence expansion of dLN cells during *L. amazonensis* infection

The gp91$^{phox-/-}$ mice presented with a higher inflammatory response in the skin compared to WT mice during *L. amazonensis* (Figure 32). Because of this remarkable characteristic we also analysed dLN cells in in detail.

We observed a significant cell expansion in dLNs from gp91$^{phox-/-}$ mice until 16 weeks post infection (Figure 39). In contrast, WT mice just presented an initial expansion of dLNs cells at 4 weeks post infection. Subsequently, cell numbers were stable until the end of the experiment. Indeed, 12 and 16 weeks post infection the number of cells found in dLNs of gp91$^{phox-/-}$ mice was almost three times higher than WT mice. This augmented cell number in gp91$^{phox-/-}$ mice 12 and 16 weeks post infection can be correlated with higher dLN parasite loads in these mice at same time (Figure 33B), which suggests an important role of ROS in control of parasite growth in the dLN.

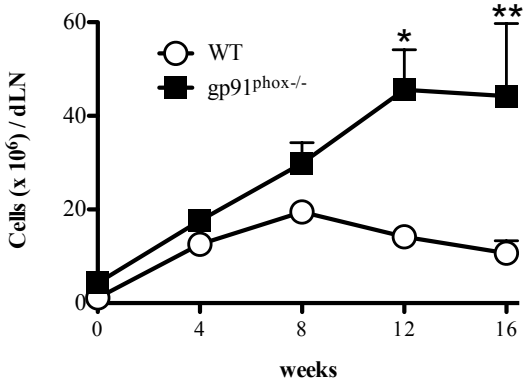

Figure 39. Total number of cells in draining lymph nodes in *L. amazonensis* infected mice 4, 8, 12 and 16 weeks post infection. Mice were infected with 5 x 10^3 *L. amazonensis* metacyclic promastigotes in pinna ears and followed for 16 weeks. At 4, 8, 12 and 16 the dLNs were harvested and cells counted. Data are shown as mean ± SD from one representative experiment of two, n=5 for each experiment.

We analysed the major subpopulations in dLNs. Despite the significant difference in dLN total cell numbers between the groups (Figure 39), we did not find differences in the cell composition between groups. They presented the same percentage of CD11b$^+$ cells in all times analysed (Figure 40A), with a significant increase of this population percentage at 12 weeks post infection. Indeed, the CD11b$^+$ population did not alter even after 8 weeks post infection compared to naïve mice. We also analysed the T lymphocyte population and we could not observe differences

between groups. Indeed, the percentage of $CD4^+$ and $CD8^+$ T cells in dLNs slightly decreased with the infection, $p<0.0001$ (Figure 40B and 40C). Together, these results indicate general proliferation of T cells in dLNs.

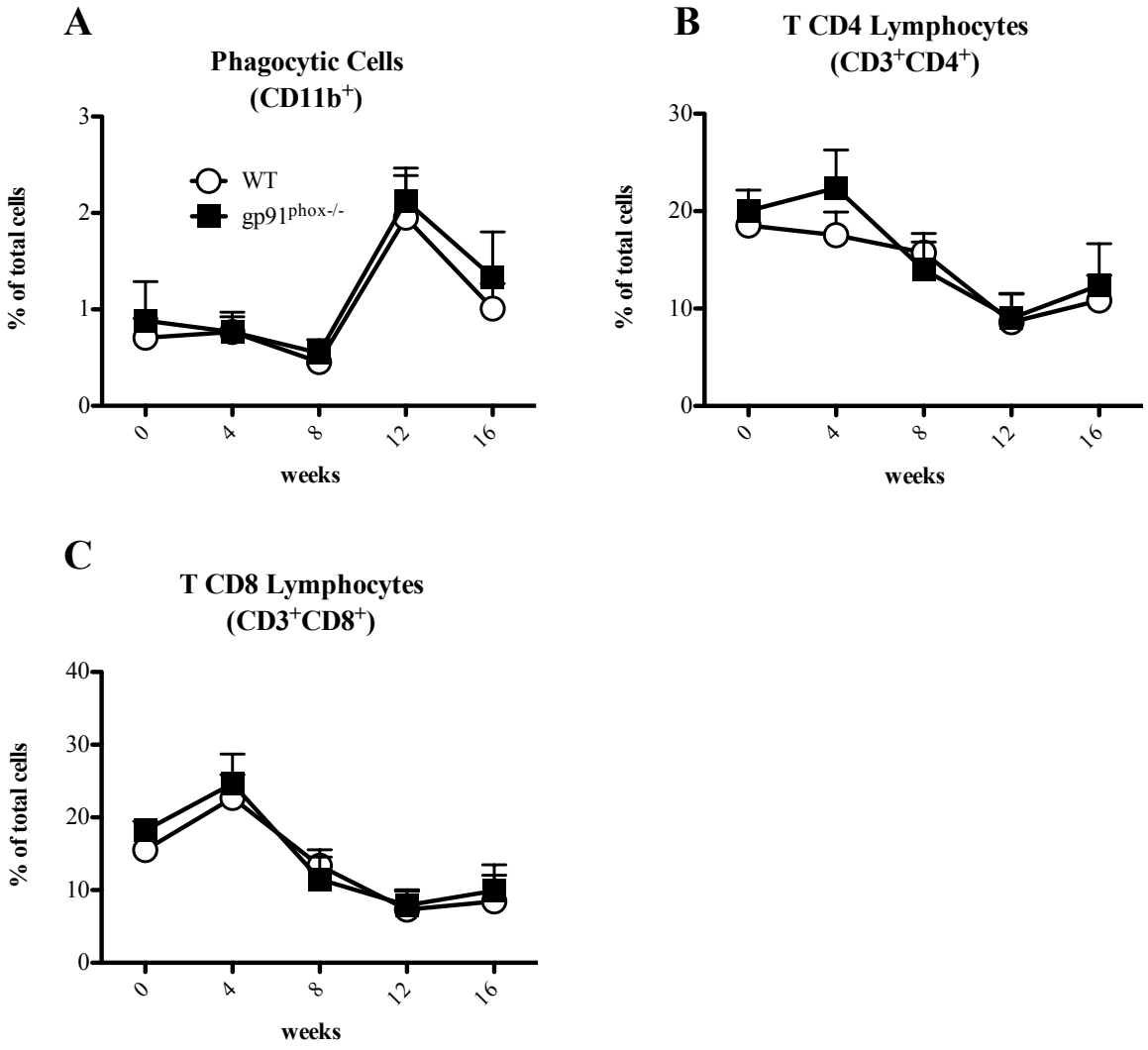

Figure 40. Percentage phagocytic and T cells in draining lymph nodes in *L. amazonensis* infected mice 4, 8, 12 and 16 weeks post infection. Mice were infected with 5 x 10^3 *L. amazonensis* metacyclic promastigotes forms of in pinna ears and followed for 16 weeks. At 4, 8, 12 and 16 the dLNs were disrupted and the total cells counted. A, B and C represent the percentage of phagocytic, $CD4^+$ and $CD8^+$ T cells ranging from non-infected mice (week 0) until 16 weeks post infection. Data are shown as mean ± SD from one representative experiment of 2, n=5 for each experiment.

When we analysed the subpopulations of $CD11b^+$ cells we also did not detect differences in the dLN between WT and KO groups. Even the proportion of neutrophils did not change with the infection (Figure 41A). The percentage of neutrophils was maintained at the same levels as naïve mice, suggesting that these cells do not migrate to dLNs during the infection. In contrast, we observed an important migration of inflammatory monocytes to dLNs (Figure 41B). After 4 weeks post infection, a significant increase in inflammatory monocyte percentage was detected in dLNs and these levels were maintained during all period of infection.

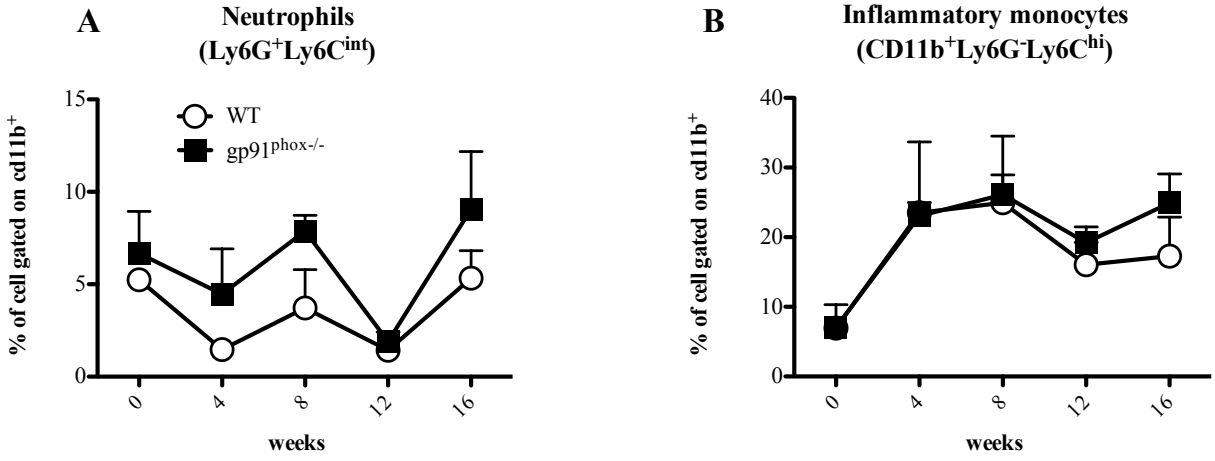

Figure 41. Percentage phagocytic subpopulations in draining lymph nodes in *L. amazonensis* infected mice 4, 8, 12 and 16 weeks post infection. Mice were infected with 5 x 10^3 *L. amazonensis* metacyclic promastigotes in pinna ears and followed for 16 weeks. At 4, 8, 12 and 16 the dLNs were harvested, disrupted and the total cells counted. A and B represent the percentage of neutrophils and inflammatory monocytes in lymph nodes from non-infected mice (week 0) until 16 weeks post infection. Data are shown as mean ± SD from one representative experiment of 2, n=5 for each experiment.

To analyse possible changes in $CD4^+$ T cell subpopulations, we stained the cells for intra-nuclear markers of T cell differentiation in dLNs during infection with *L. amazonensis* in $gp91^{phox-/-}$ mice. As mentioned before, CD44 is an activation marker highly expressed during inflammatory processes. We identified an increase in the percentage of $CD4^+$ activated T cells from 8 weeks post infection that was maintained until 16 weeks post infection, this increase was seen in both groups (Figure 42A).

We could not detect differences in percentages of regulatory T cells in dLNs, as determined by the foxp3 marker, during the infection, or when compared to non-infected controls (Figure 42B).

As mentioned before, ki67 is an important marker of recent cell proliferation. So, we analysed possible alterations in this marker, since we found higher numbers of $CD4^+$ T cells in $gp91^{phox-/-}$ mice during the infection (Figure 39). Indeed, we observed a slight increase in the percentage of recently proliferated cells in the dLNs of infected mice for up to 8 weeks of infection in both groups, p=0.0002 (Figure 42C).

T-bet is a transcriptional factor involved in Th cell differentiation into the Th1 subtype during infections. This transcriptional factor regulates the expression of inflammatory cytokines such as IFN-γ (Szabo et al., 2002), therefore promoting the required immune response to eliminate *Leishmania*. The percentages of T-bet^+ $CD4^+$ T cells were the same in both groups, decreasing at the initial stages of infection (until 8 weeks post infection) and increasing at final stages (until 16 weeks post infection) (Figure 42D).

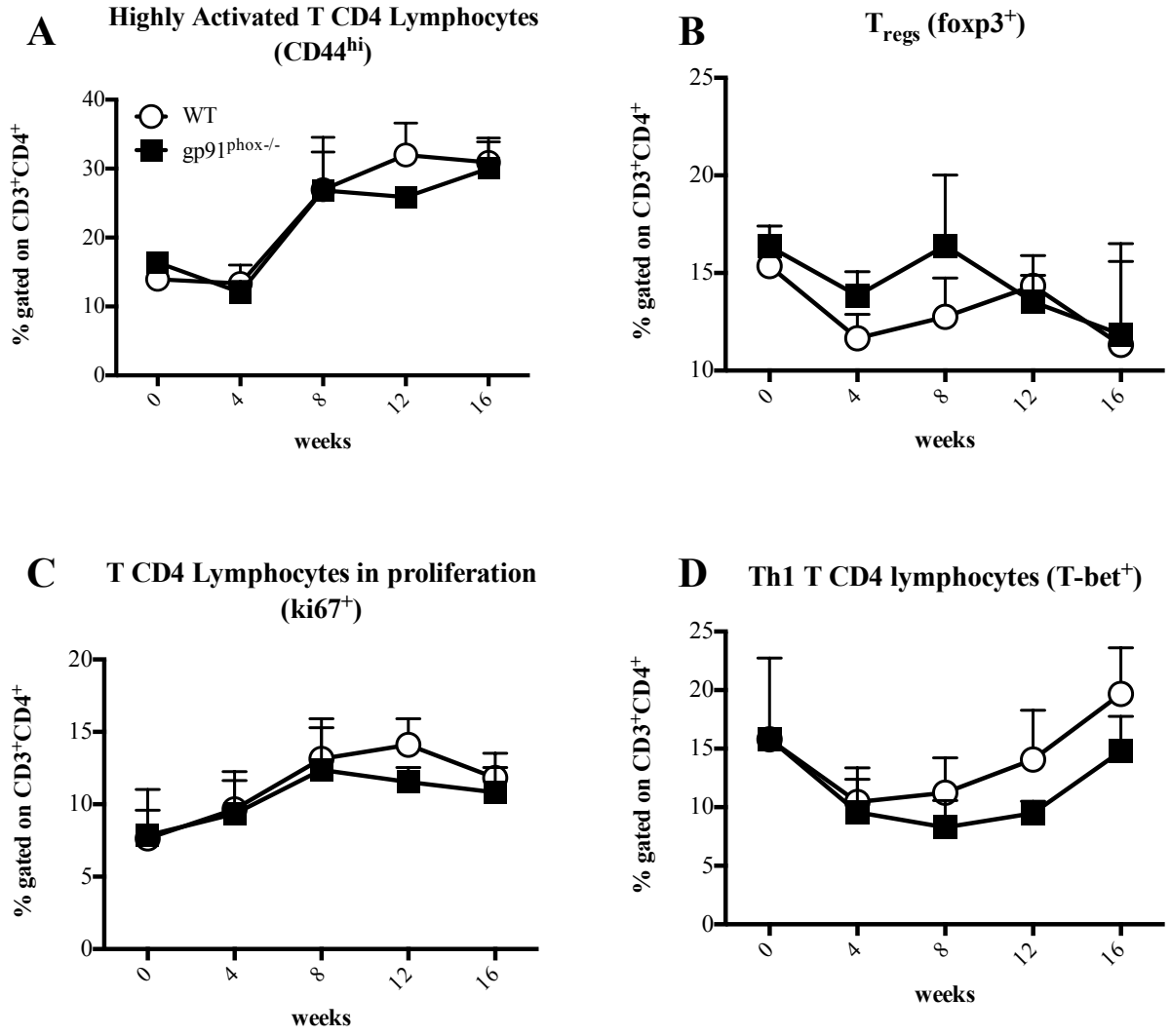

Figure 42. Percentage CD4$^+$ T cell subpopulations in draining lymph nodes in *L. amazonensis* infected mice 4, 8, 12 and 16 weeks post infection. Mice were infected with 5 x *L. amazonensis* 10^3 metacyclic promastigotes in pinna ears and followed until 16 weeks. At 4, 8, 12 and 16 the dLNs were harvested, disrupted and the total cells counted. A, B, C and D represent the percentage of activated, regulatory, proliferated and Th1 differentiated CD4$^+$ T cells, respectively, in DLNs from non-infected mice (week 0) until 16 weeks post infection. Data are shown as mean ± SD from one representative experiment of 2, n=5 for each experiment.

We analysed possible changes in cytokine production in gp91$^{phox-/-}$ mice. We re-stimulated dLNs cells with LA*La* for 6h to identify possible differences in the cytokine production by infected mice.

We observed low percentages of CD4$^+$ T cells producing cytokines in dLNs of mice infected with *L. amazonensis* suggesting a strong immune regulation by this parasite. Indeed, we

detected a peak of cytokine production 4 weeks post infection, however the percentage of cells producing cytokines dropped almost to naïve levels from 8 to 16 weeks post infection (Figure 43).

The percentage of $CD4^+$ T cells producing IFN-γ (Figure 43A), TNF-α (Figure 43B), IFN-γ and TNF-α (Figure 43C), IL-2 (Figure 43D), IFN-γ, TNF-α and IL-2 (Figure 43E), IL-10 (Figure 43F) and IL-17 (Figure 43G) followed the same pattern during the infection, and no differences between the groups were observed.

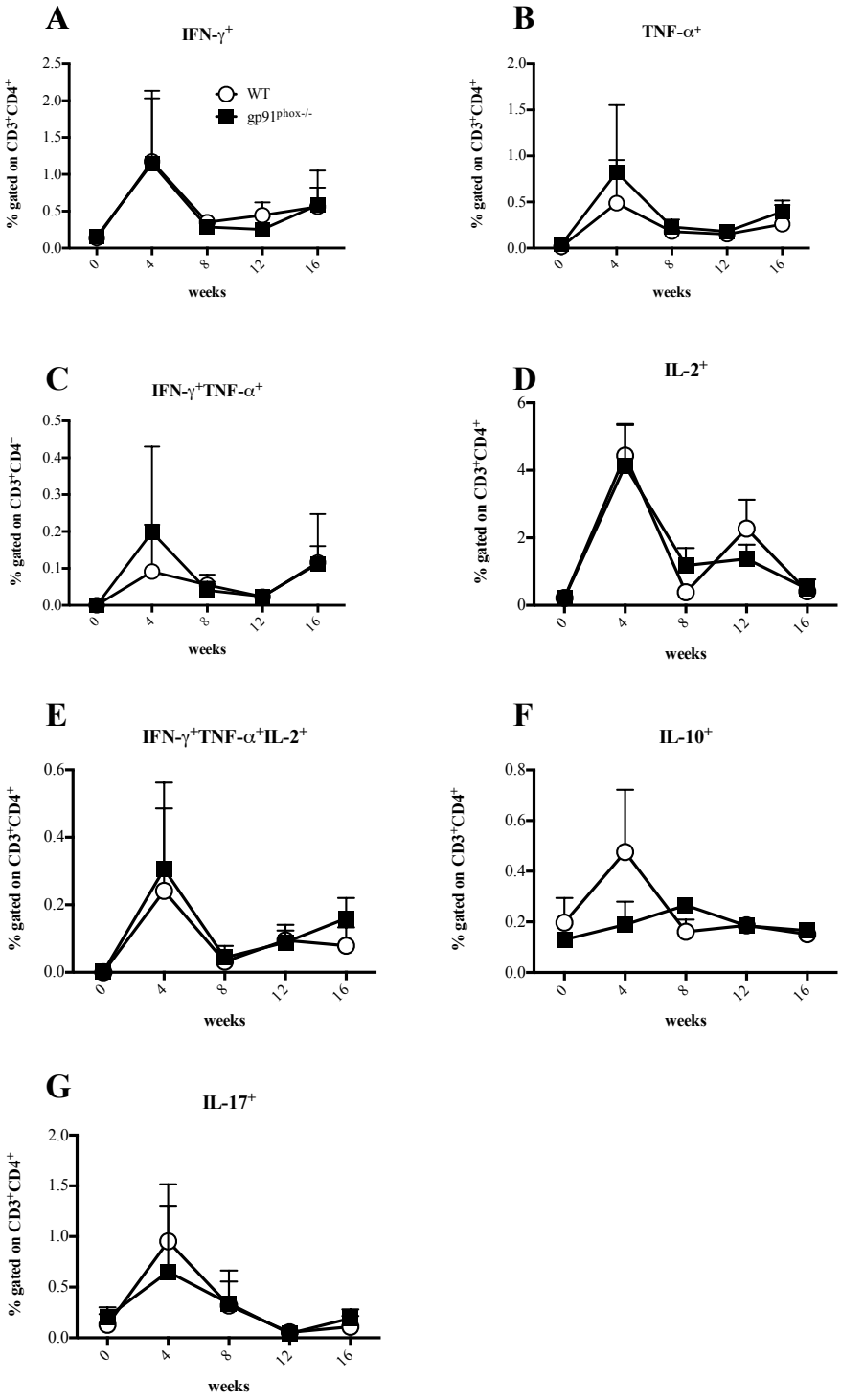

Figure 43. Percentage of CD4$^+$ T cells producing cytokines in draining lymph nodes in *L. amazonensis*-infected mice 4, 8, 12 and 16 weeks post infection. Mice were infected with 5 x 10^3 metacyclic promastigotes forms of *L. amazonensis* in pinna ears and followed until 16 weeks. 4, 8, 12 and 16 the dLNs were disrupted and the total cells counted. A, B, C, D, E, F and G represent the percentage of IFN-γ, TNF-α, double (IFN-γ and TNF-α), IL-2, triple (IFN-γ, TNF-α and IL-2), IL-10 and IL-17 CD4$^+$ T producing cells, respectively, ranging from non-infected mice (week 0) until 16 weeks post infection. Data are shown as mean ± SD from one representative experiment of 2, n=5 for each experiment.

6.3.7. Gp91$^{phox-/-}$ mice *L. amazonensis* induces higher expression of CXCL2 at initial stages of infection in gp91$^{phox-/-}$ mice

We identified very significant differences in neutrophil infiltration in gp91$^{phox-/-}$ mice during infection with *L. amazonensis*, however we could not detect any differences in other cell populations in the ear that could explain the larger lesions observed in these mice. So, we hypothesised that neutrophils would be the major factor that led to larger lesions seen in gp91$^{phox-/-}$ mice. Therefore, we looked for differences in chemokines that attract neutrophils between the two groups.

We analysed the mRNA expression of chemokines (CXCL1 and CXCL2) and inflammatory cytokines (IL-1β) involved in the recruitment of neutrophils. We measured the mRNA expression levels of CXCL1, CXCL2 and IL-1β at early stages of infection (4 and 8 weeks post infection) since we identify these points as the beginning of the inflammatory process (Figure 32).

As mentioned before, CXCL1 is one of most important chemokines involved in neutrophil recruitment to sites of infection (Kobayashi, 2008). However, we could not detect differences in CXCL1 mRNA expression 4 and 8 weeks post infection in the skin (Figure 44A). Moreover, the levels of mRNA of this chemokine was just about 8 fold higher compared to naïve mice in both groups at 4 weeks post infection, suggesting a small participation of this chemokine in the ongoing recruitment of neutrophils. We could not detect differences in CXCL1 expression compared to gp91$^{phox-/-}$ mice even at 8 weeks of infection.

There is a redundancy in the chemokines involved in neutrophil recruitment (Kobayashi, 2008). CXCL2 is also involved in neutrophil recruitment and may bind to the same receptor on neutrophils (CXCR-1/2) as CXCL1 (Dunstan et al., 1996). We observed a significant increase of CXCL2 mRNA expression in gp91$^{phox-/-}$ mice 4 weeks post infection (Figure 44B). Ears from gp91$^{phox-/-}$ mice had a more than 200-fold increase in CXCL2 mRNA over non-infected controls, while WT mice had a 50-fold increase at the same time point, when compared to their naïve counterparts. Eight weeks post infection there was a drop in the mRNA levels of this chemokine. IL-1β is involved in recruitment of inflammatory cells to site of infections, including neutrophils and inflammatory monocytes (Patton et al., 1995; Wang et al., 1995). However, we did not observe changes in IL-1β mRNA levels between the groups (Figure 44C). We observed a significant fold increase in IL-1β mRNA levels compared to naïve mice 4 weeks post infection, suggesting a participation of this cytokine in the recruitment of inflammatory cells at this time point.

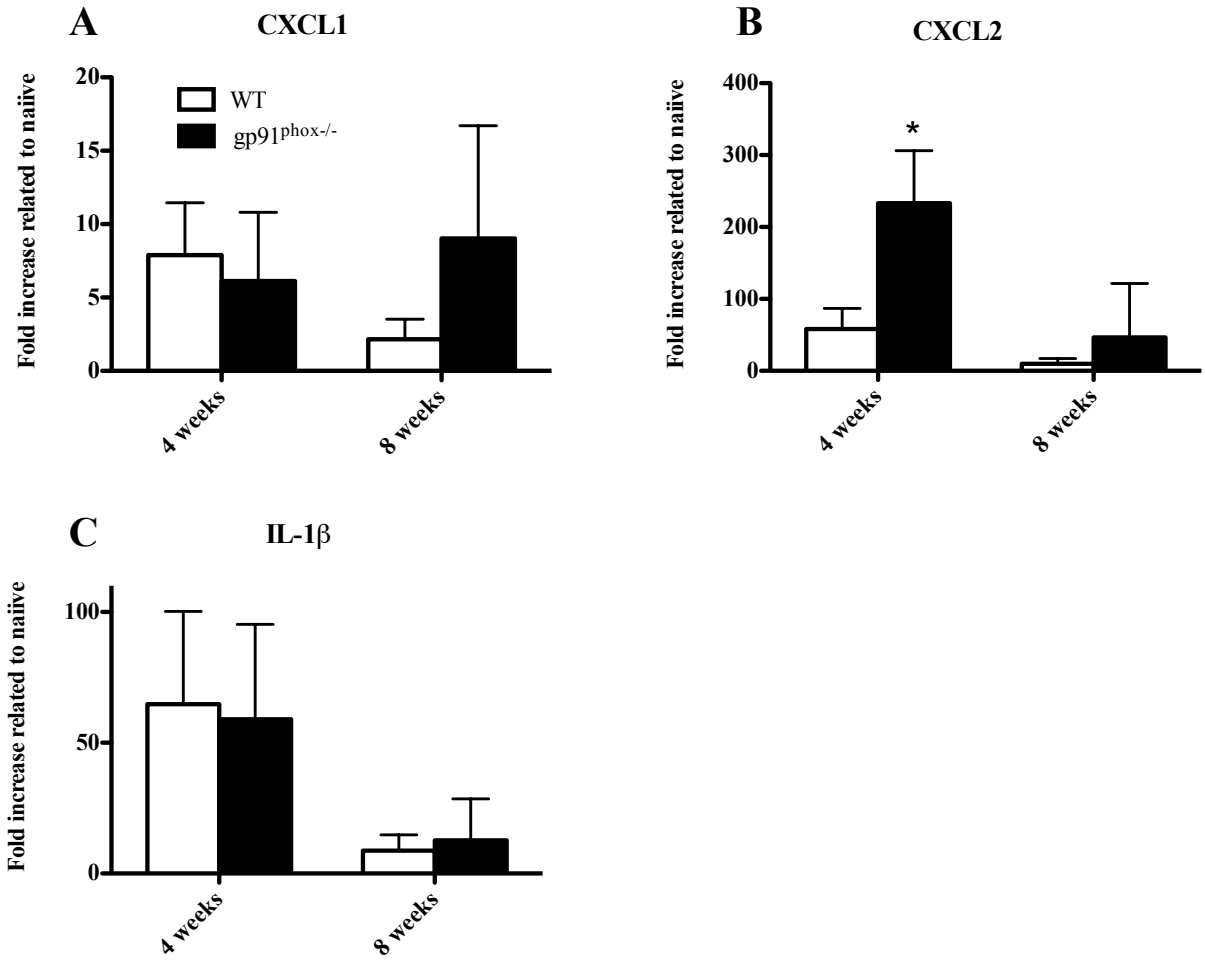

Figure 44. mRNA expression levels of CXCL1, CXCL2 and IL-1β from *L. amazonensis* infected ears measured by qPCR. Mice were infected with 5 x 10^3 metacyclic promastigotes forms of *L. amazonensis* in pinna ears and followed until 16 weeks. A, B and C represent the mRNA expression of CXCL1, CXCL2 and IL-1β, respectively, normalized to mRNA expression in naïve mice 4 and 8 weeks post infection. Data are shown as mean ± SD from one representative experiment of 2, n=5 for each experiment.

6.3.8. In the absence of ROS neutrophils die by necrosis at the site of infection with *L. amazonensis*

Despite the important role of ROS in many infections, acting as oxidizer molecules to cause damage to microbes, these ions also are involved in cell signalling and other processes like apoptosis under stress conditions.

To try to understand if the accumulation of neutrophils seen in the gp91$^{phox-/-}$ mice could be related to a deficiency in neutrophil programmed cell death, we performed an assay for neutrophil apoptosis and necrosis. We infected mice with 5 x 10^3 *L. amazonensis* metacyclic promastigotes transfected with RFP gene and followed the infection for 8 weeks, time before the ears start necrotic process. We infected the mice with an RFP expressing parasite so that we could track the infected cells and observe any influence of the parasite on neutrophil programed cell death.

We used the nuclear dye 7-aminoactinomycin D (7-AAD) and annexin V to identify apoptotic or necrotic neutrophils. 7-AAD has strong affinity for DNA molecules, but does not have the capacity to transpose intact and functional cell membranes (Lecoeur et al., 1997). Thus, it will stain DNA when the cell is dying and the cellular membrane is compromised. Annexin V binds to phosphatidylserine molecules presented on cell membranes in the early stages of apoptosis. Generally, the membrane phospholipids containing phosphatidylserine are present in the cytoplasmatic side of the cell. One of the initial signs of apoptosis is the presence of these phospholipids to the exterior side of the membrane (Lecoeur et al., 1997). At this point the cellular membrane is still selective and prevents the incorporation of 7-AAD by the cells. Therefore, in flow cytometry, annexin V$^+$7-AAD$^-$ cells are considered apoptotic and 7-AAD$^+$ cells are considered necrotic even if positive for annexin V, since necrotic cells loose membrane integrity.

We first confirmed the high percentage of neutrophils observed in gp91$^{phox-/-}$ mice during the infection. As observed before (Figure 36), we found a high percentage and number of neutrophils migrating to ears (Figure 45B and C) 8 weeks post infection in gp91$^{phox-/-}$ mice.

Since we infected the mice with rfp-transfected parasites, it was possible to follow the parasites and determine the role of *Leishmania* in neutrophil death process. We first analysed the percentage of infected neutrophils to determine if there were differences between the groups of mice. We observed a higher percentage of infected neutrophils in WT mice (Figure 46B) possibly because of excess neutrophils in gp91$^{phox-/-}$ mice (Figure 45B). Indeed, we found similar number of neutrophils infected in both groups (Figure 46C) confirming that the percentage of infected neutrophils was influenced by the high number of these cells present in gp91$^{phox-/-}$ mice.

We did not detect differences in the percentage of apoptotic cells 8 weeks post infection (Figure 47B) between the groups. Both groups presented around 15% of neutrophils in apoptotic process and the infection did not change the apoptosis ratio in these cells (Figure 47B, right panel). Indeed, since the percentage of infected neutrophils was quite low (Figure 46B), the number of infected cells did not seem to be relevant in the context of the total number of apoptotic neutrophils

(Figure 47D). Interestingly, we found a higher number of apoptotic cells in gp91$^{phox-/-}$ mice, but since we could not detect differences in the percentage of this population (Figure 47B), this increase likely reflects the high number of neutrophils found at 8 weeks post infection at the site of inoculation.

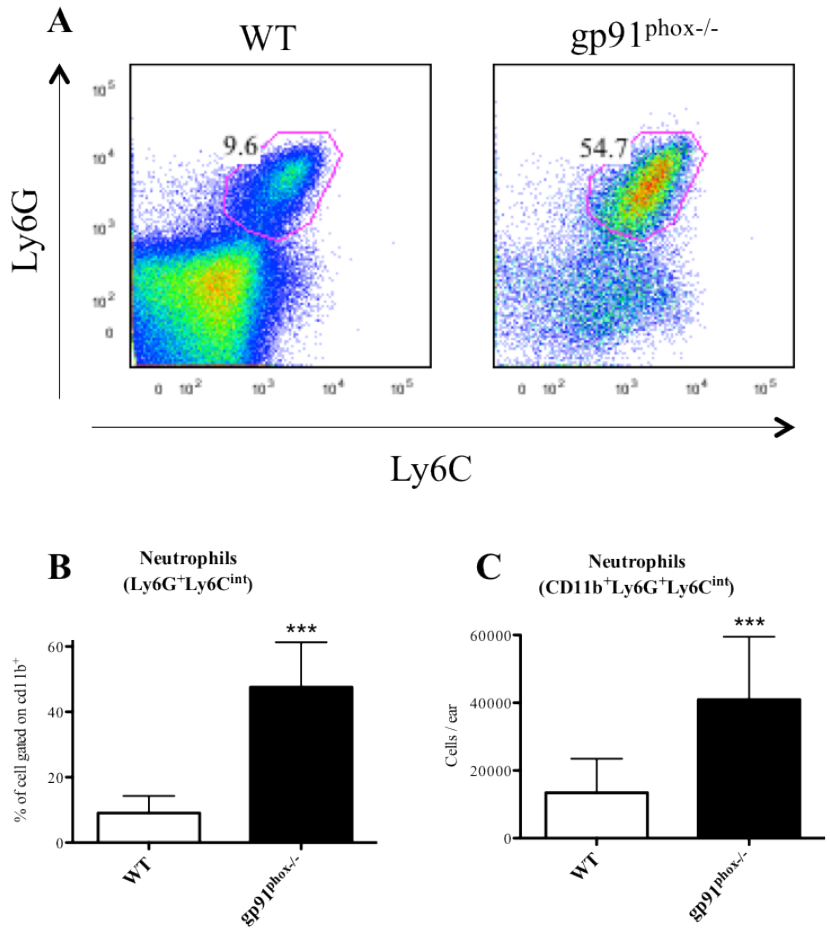

Figure 45. Percentage and total number of neutrophils recruited to the site of inoculation in *L. amazonensis* 8 weeks post infection. Mice were infected with 5 x 10^3 *L. amazonensis* metacyclic promastigotes transfected with rfp gene in pinna ears and followed for 8 weeks. A represents the dot plots of subpopulations gated on Ly6G and Ly6C markers. B and C represent the percentage and total numbers of neutrophils, respectively. Data are shown as mean ± SD from one experiment, n=13.

Gp91$^{phox-/-}$ mice presented higher frequency of necrotic neutrophils 8 weeks post infection (Figure 47C). At this time, the percentage of necrotic neutrophils was doubled in gp91$^{phox-/-}$ mice when compared to WT group. If we consider the increased absolute number of neutrophils in gp91$^{phox-/-}$ mice, there are four times more necrotic neutrophils in gp91$^{phox-/-}$ mice (Figure 47E). As

noted for apoptotic cells, we could not detect an influence on necrosis by *L. amazonensis* infection (Figure 47E).

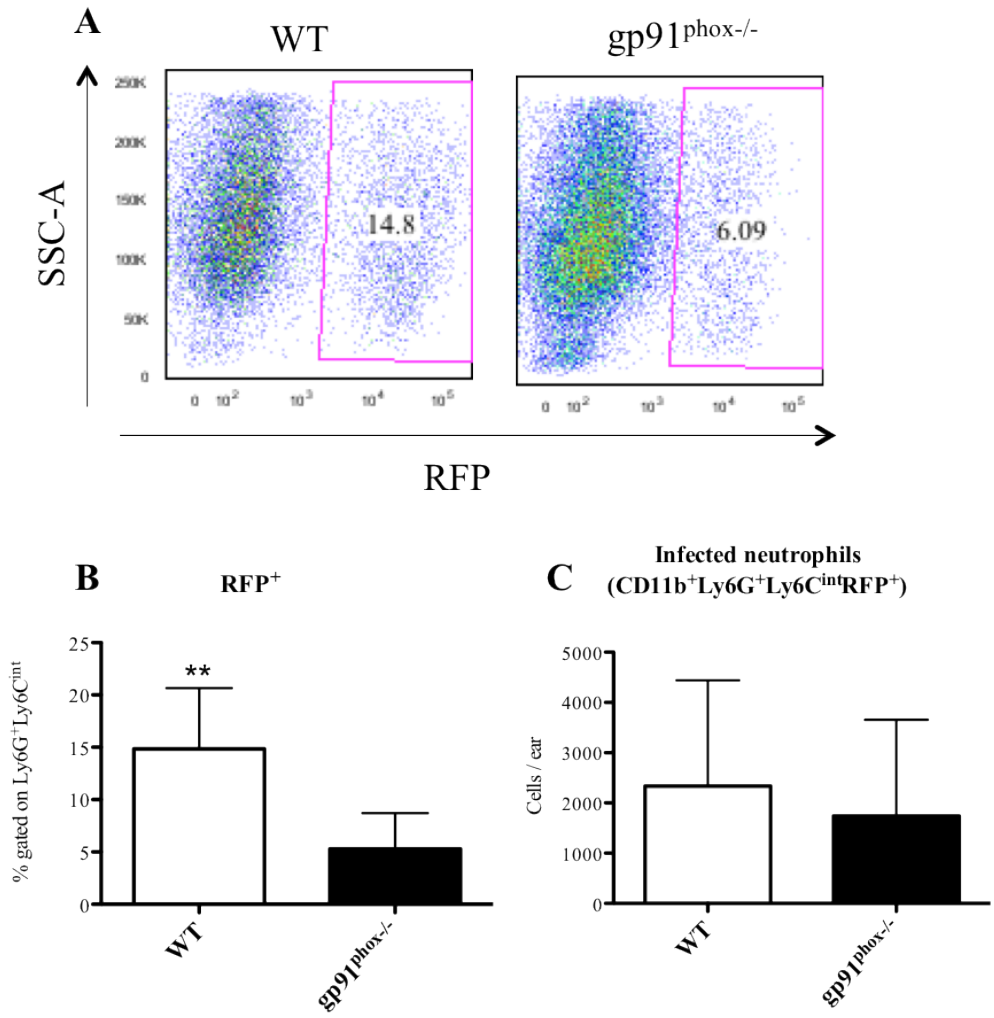

Figure 46. Percentage and total number of infected neutrophils at site of *L. amazonensis* inoculation 8 weeks post infection. Mice were infected with 5 x 10^3 *L. amazonensis* metacyclic promastigotes transfected with rfp gene in pinna ears and followed for 8 weeks. A represents the dot plots of the percentage of neutrophils gated on RFP. B and C represent the percentage and total numbers of infected neutrophils, respectively. Data are shown as mean ± SD from one experiment, n=13.

Taken together, these results strongly suggest an alteration in programmed cell death or clearance of dead and dying cells in gp91$^{phox-/-}$ mice resulting in the accumulation of necrotic cells during *L. amazonensis* infection. The exaggerated neutrophil death by necrosis strongly correlated with the increase in inflammatory cell number seen in gp91$^{phox-/-}$ mice and proceeded visible

destruction of the tissue. These observations suggest neutrophil necrosis may be involved in the accelerated destruction of skin tissue observed in gp91$^{phox-/-}$ mice.

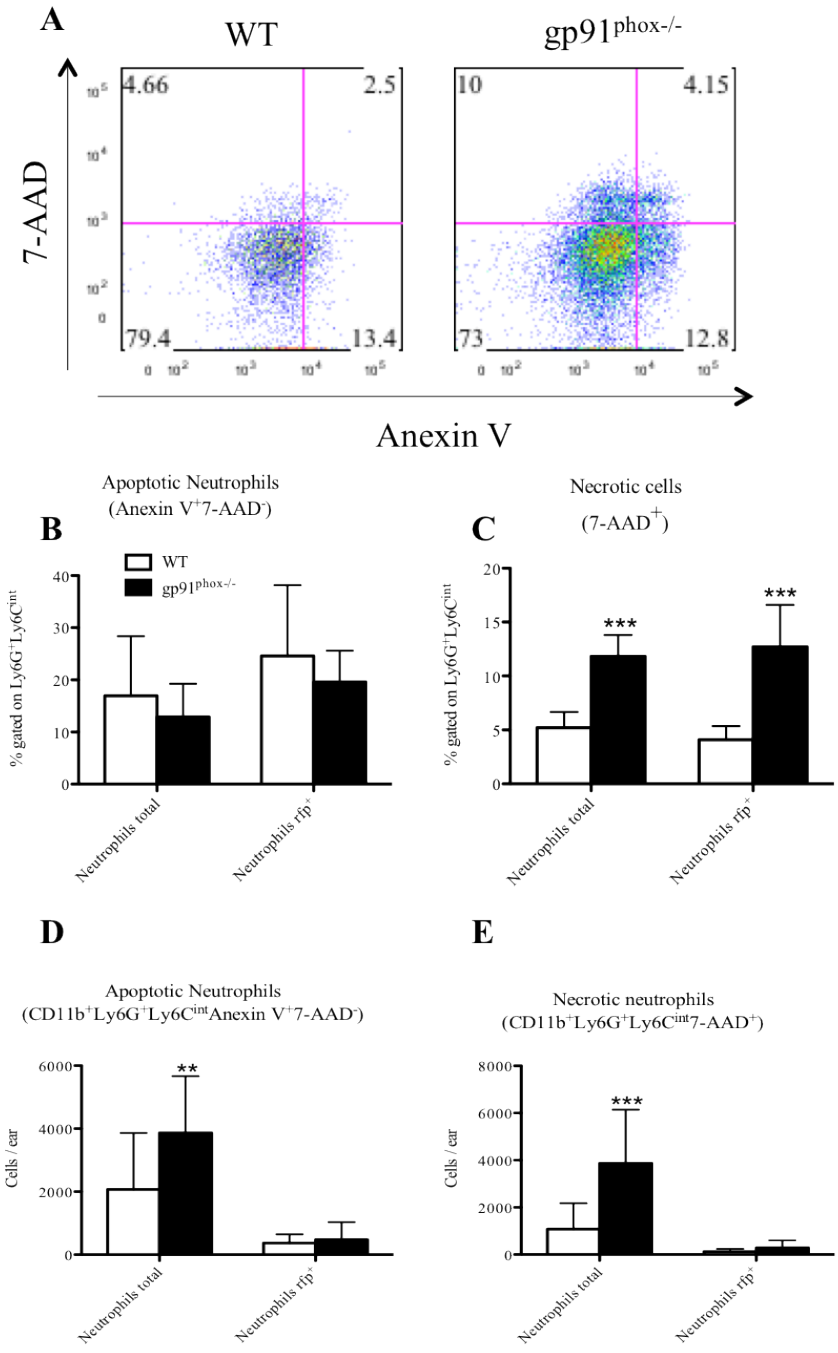

Figure 47. Percentage and total number of dying neutrophils at the site of inoculation with *L. amazonensis* 8 weeks post infection. Mice were infected with 5 x 10^3 *L. amazonensis* metacyclic promastigotes transfected with rfp gene in pinna ears and followed for 8 weeks. A represents the dot plots of the percentage of neutrophils in necrotic or apoptotic death process. B and C represent the percentage of apoptotic or necrotic cells, respectively, in total or infected neutrophils. D and E represent the total number of apoptotic or necrotic cells, respectively, in total or infected neutrophils. Data are shown as mean ± SD from one experiment, n=13.

6.3.9. Enhanced migration of inflammatory cells to the site of inoculation in gp91$^{phox-/-}$ during acute infection

Since we observed significant differences in gp91$^{phox-/-}$ mice related to inflammation and tissue necrosis at 4 weeks post infection (Figure 32C), we decided to analyse cell migration within the first hours of infection to determine if increased neutrophil recruitment preceded tissue damage. We infected mice with a high dose (5 x 10^5 parasites) of metacyclic promastigote forms of *L. amazonensis*-RFP and followed the initial recruitment of cells to the site of inoculation and the phenotype of infected cells.

We identified a higher number of phagocytic cells (CD11b$^+$) at 10h and 36h post infection in gp91$^{phox-/-}$ mice (Figure 48A). However, 60h after the challenge the numbers of these cells equalled that of WT mice. The numbers of neutrophils dropped from 10 to 36h and 60h after challenge in both groups (Figure 48B). Despite the drop seen in both groups, at all times the gp91$^{phox-/-}$ mice presented higher numbers of neutrophils compared to WT. We also observed a high number of migrating inflammatory monocytes to ears 10h and 36h hours post infection in the gp91$^{phox-/-}$ mice (Figure 48C). However, contrasting with neutrophil behaviour, the number of inflammatory monocytes increased over time during the infection. We could not detect differences in resident macrophages (Figure 48D) or dendritic cells during acute infection in either group. Thus, the increase in CD11b$^+$ cells numbers can be attributed to inflammatory cells migration. Therefore, from the first hours post infection there is a higher inflammatory infiltrate present in gp91$^{phox-/-}$ mice that could contribute to the enhanced necrotic phenotype observed weeks after challenge (Figure 32).

Assessment of the frequency of CD11b$^+$ subpopulations revealed that there was a higher percentage of neutrophils in gp91$^{phox-/-}$ mice at 10h and 36h post infection (Figure 49B) while the frequency of inflammatory monocytes was the same (Figure 49C). Because of the high percentage of neutrophils observed in gp91$^{phox-/-}$ mice, there was corresponding drop in the percentage of resident macrophages at 10h p.i. (Figure 49D) and resident DCs at 10h and 36h post infection (Figure 49E). It is important to mention that at these time points, the Ly6C denotes recruited (Ly6C^{hi} cells) and resident (Ly6C$^-$) cells.

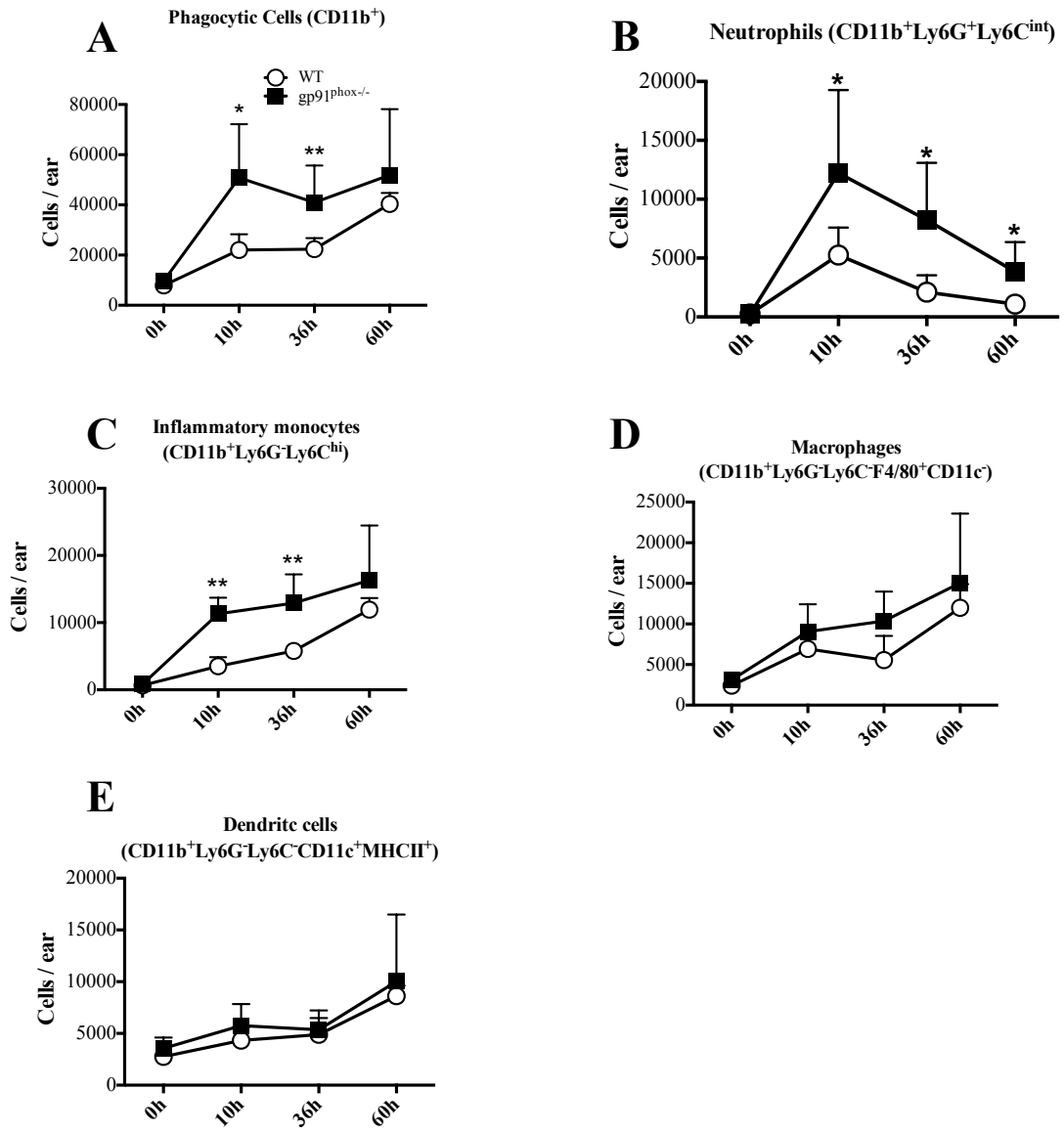

Figure 48. Total number of recruited phagocytic CD11b$^+$ cells at site of inoculation of *L. amazonensis* 10h, 36h and 60h post infection. Mice were infected with 5 x 10^5 *L. amazonensis* metacyclic promastigotes transfected with rfp gene in pinna ears. A, B, C, D and E represent the total number of phagocytic cells, neutrophils, inflammatory monocytes, macrophages and DCs, respectively, recruited to ears 10h, 36h and 60h post infection. Data are shown as mean ± SD from one representative experiment of 3, n=5 for each experiment.

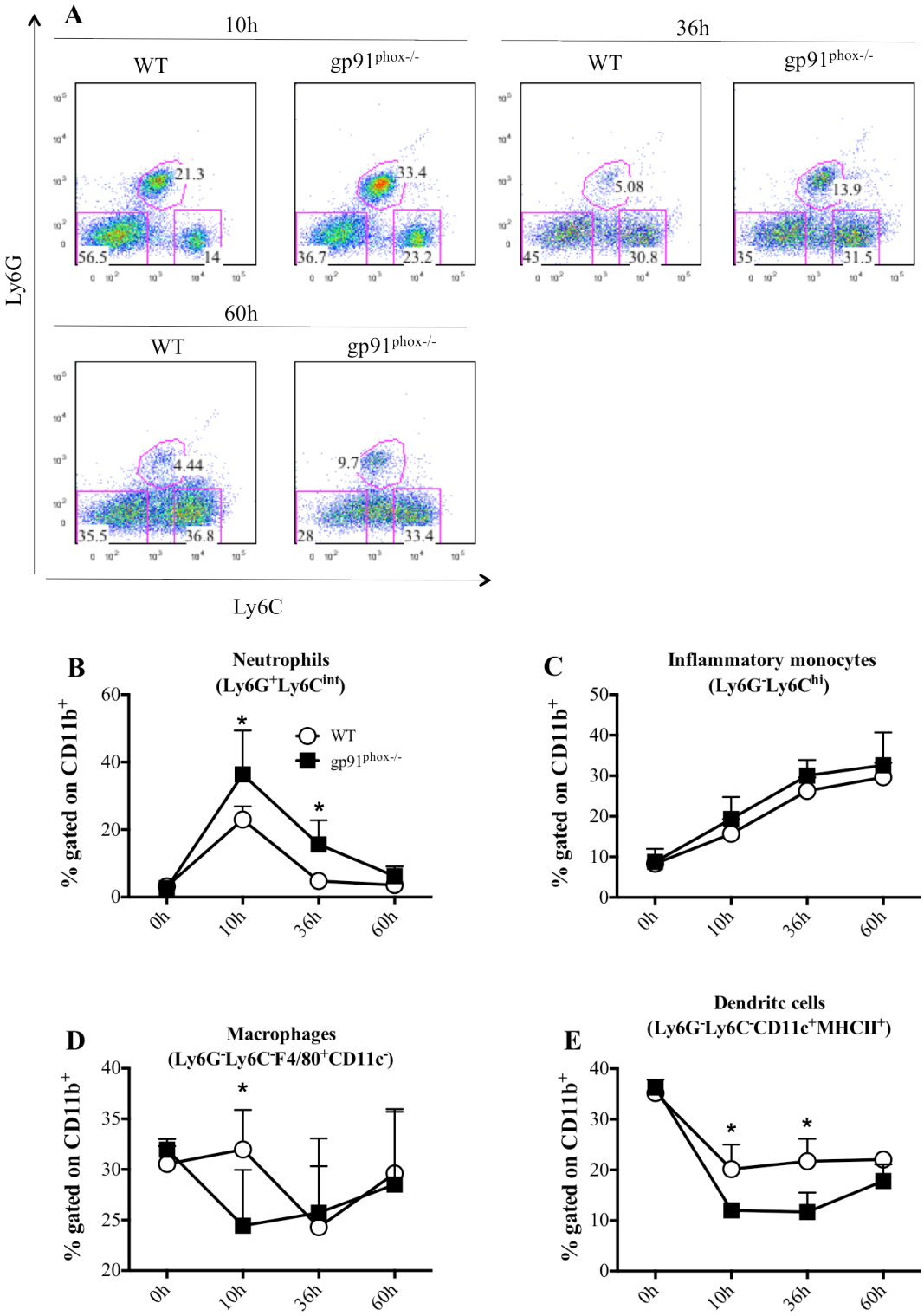

Figure 49. Percentage CD11b$^+$ subpopulations at site of inoculation of *L. amazonensis* 10h, 36h and 60h post infection. Mice were infected with 5 x 10^5 *L. amazonensis* metacyclic promastigotes transfected with rfp gene in pinna ears. A represents the dot plots of the percentage of CD11b$^+$ cells subpopulations during first hours of infection. B, C D and E represent the percentage of neutrophils, inflammatory monocytes, macrophages and DCs present in ears 10h, 36h and 60h post infection. Data are shown as mean ± SD from one representative experiment of 3, n=5 for each experiment.

6.3.10. The absence of gp91^{phox} changes the dynamics of *L. amazonensis* infected cells early during infection

We analysed possible alterations in infected cells in gp91$^{phox-/-}$ mice. Indeed, the inflammatory cells that migrated from blood are the major cells involved in *L. amazonensis* uptake (Figure 50). We observed a shift in infected cells: first, the neutrophils are responsible for *Leishmania* uptake, however, at later time points, inflammatory monocytes represent a large proportion of infected cells (Figures 49B, C, 50B and C). This transition likely occurs via the release of live parasite by apoptosing or dying neutrophils and subsequent uptake by inflammatory monocytes (Peters et al., 2008). At 10h post infection, about 60 to 80% of infected CD11b^{+} cells were neutrophils (Figure 50B), however this percentage was even higher in gp91$^{phox-/-}$ mice. This difference persisted at 36h, but values were similar between the groups at 60h.

Resident macrophages and DCs are present in the Ly6G^{-}Ly6C^{-} subpopulations of CD11b^{+} cells. Due to the higher percentage of infected phagocytic cells expressing neutrophil markers at 10h and 36h post infection seen in gp91$^{phox-/-}$ mice, there was a decrease in the percentage of infected resident cells infected in these mice at 10h and 36h (Figure 50D and E). The increased frequency of infected neutrophils observed in gp91$^{phox-/-}$ mice could contribute to the higher inflammatory state in gp91$^{phox-/-}$ mice.

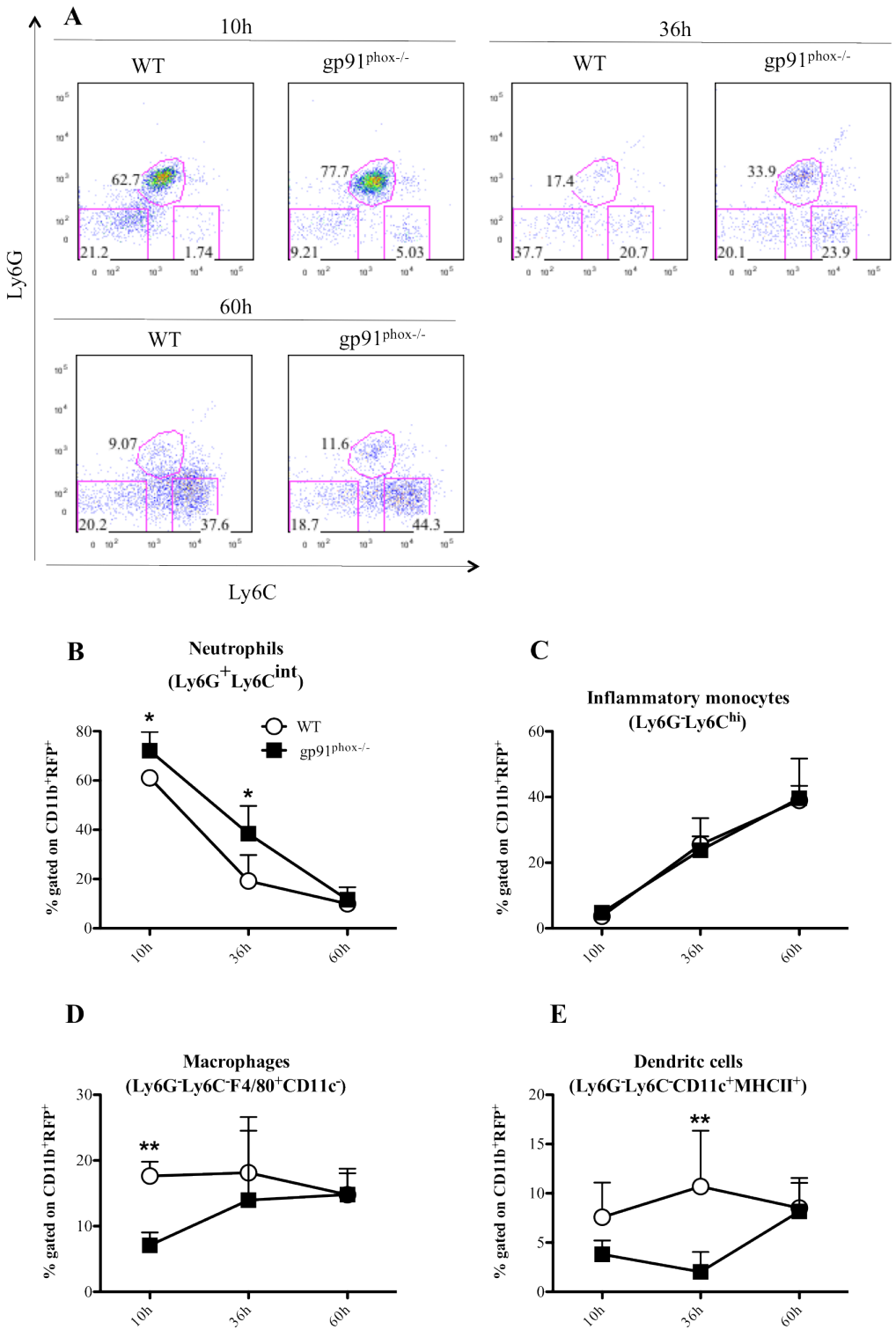

Figure 50. Percentage of infected CD11b$^+$RFP$^+$ subpopulations at the site of inoculation with *L. amazonensis* 10h, 36h and 60h post infection. Mice were infected with 5 x 10^5 metacyclic promastigotes forms of *L. amazonensis* transfected with rfp gene in pinna ears and followed since 10h to 60h post infection. A represents the dot plots of the percentage of infected CD11b$^+$ cells subpopulations. B, C D and E represent the percentage of neutrophils, inflammatory monocytes, macrophages and DCs presented in ears. Data are shown as mean ± SD from one representative experiment of 3, n=5 for each experiment.

6.3.11. Gp91$^{phox-/-}$ mice have deficiency in apoptotic neutrophil death at early stages of *L. amazonensis* infection

We found a higher number of neutrophils in gp91$^{phox-/-}$ mice at the early stages of *L. amazonensis* infection (Figure 48B). Neutrophils are largely damaged during the oxidative burst promoted by themselves in the infection, and because of this process, they start apoptotic programs. Due to the absence of ROS to contribute to apoptosis in gp91$^{phox-/-}$ neutrophils, we speculate that these cells could have problems with ROS-dependent apoptosis and eventually dye by inflammatory mechanisms such as necrosis. So, we analysed the neutrophils for apoptotic and necrotic markers to observe possible differences in the mechanism of cell death during acute infection.

At 36h and 60h post infection, we identified a lower percentage of apoptotic neutrophils in gp91$^{phox-/-}$ mice (Figure 51B). The percentage of apoptotic neutrophils found in WT mice was almost 3 times higher at 36h post infection when compared to gp91$^{phox-/-}$ mice. This higher frequency of apoptotic neutrophils was maintained in WT mice even after 60h post infection. This could suggest impairment in the apoptosis program of neutrophils in gp91$^{phox-/-}$ mice during the early stages of infection caused by *L. amazonensis*.

Despite the fact that we observed these changes in neutrophil apoptosis at early stages, we could not detect differences in necrotic cells (Figure 51C) as found at 8 weeks post infection (Figure 47). However, when we analysed the infected cells, we detected differences in neutrophil necrosis 36h post infection (Figure 51E). We found around 40% of infected neutrophils dying due to necrosis, while about 20% of neutrophils from WT died of necrosis. As we did not find differences in total neutrophil necrosis (Figure 51C), we do not know the importance of these infected necrotic neutrophils in inflammation development. In the same way, the percentage of apoptotic infected neutrophils was similar in both groups at all times measured (Figure 51D), contrasting with what we had observed in total neutrophils apoptosis (Figure 51B). Despite the fact that we have not seen differences in infected cells, the total cells revealed a clear alteration in apoptosis in gp91$^{phox-/-}$ mice.

Taken together, these results demonstrate impairment in neutrophil apoptosis at early time points that could contribute to the higher initial inflammatory response seen in gp91$^{phox-/-}$ mice.

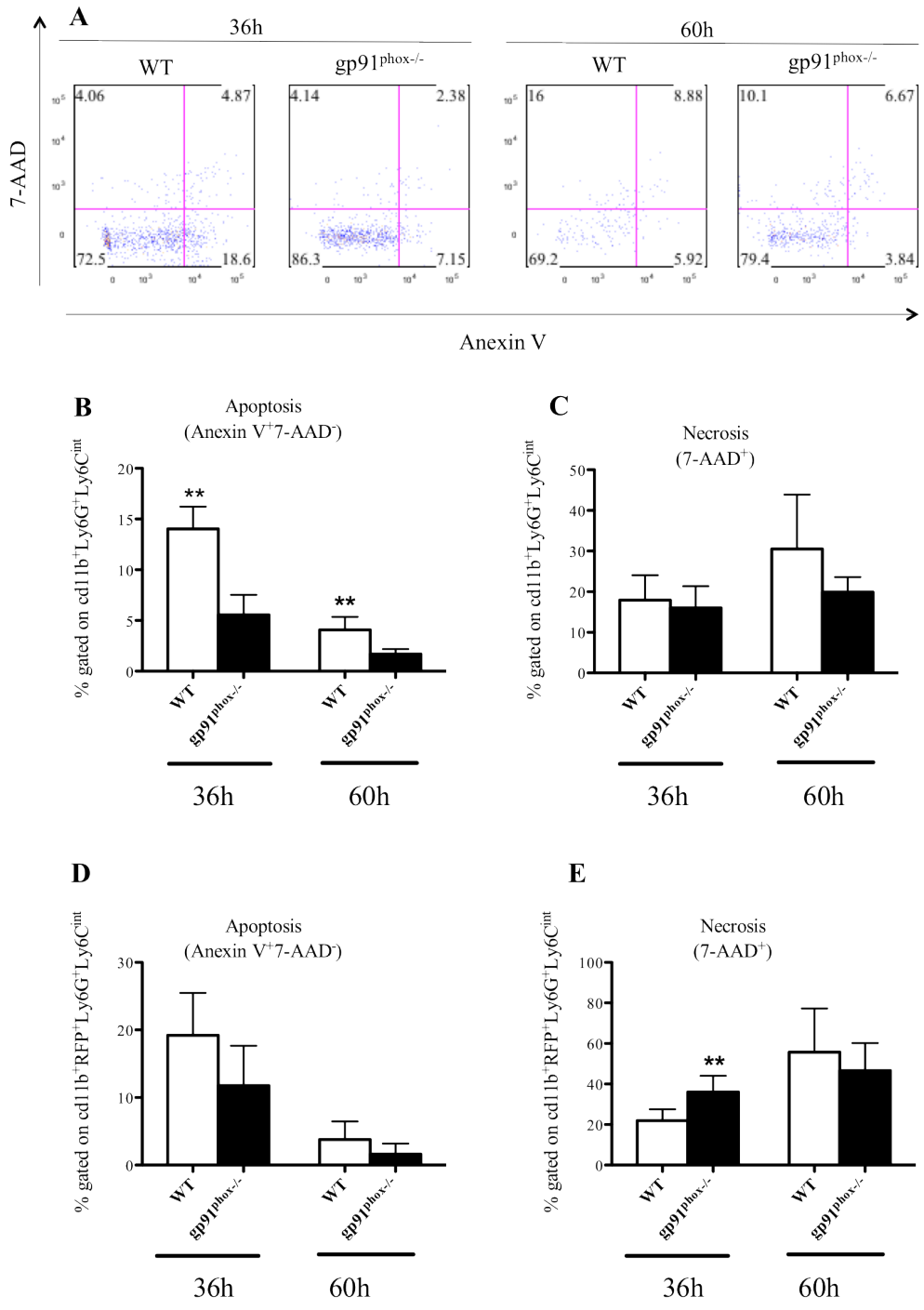

Figure 51. Percentage of dying neutrophils at the site of inoculation with *L. amazonensis* 36h and 60h post infection. Mice were infected with 5 x 10^5 metacyclic promastigotes forms of *L. amazonensis* transfected with rfp gene in pinna ears and followed until 60h post infection. A represents the dot plots of the percentage of neutrophils in necrotic or apoptotic death process 36h and 60h post infection. B and C represent the percentage of apoptotic or necrotic cells, respectively, in total recruited neutrophils 36h or 60h post infection. D and E represent the percentage of apoptotic or necrotic cells, respectively, in infected neutrophils 36h or 60h post infection. Data are shown as mean ± SD from one representative experiment of 2, n=5 for each experiment.

7. DISCUSSION

In this work, we analysed the role of ROS during *L. amazonensis* infection and the implications of the site of infection in disease. We used the two most common sites of *Leishmania* infection, the subcutaneous infection of the footpad and intradermal infection of the ears. We found substantial differences in the effect of ROS depending of the inoculation site involved. While C57BL/6 mice are susceptible to *L. amazonensis* infection at either site, the intradermal site led to more severe disease. This site presented progressive lesions development (Figure 32) and increasing parasite loads overtime in both WT and gp91$^{phox-/-}$ groups (Figure 33A). In contrast, inoculation at the subcutaneous site promotes a limited lesion growth with stabilization of these lesions sizes at late times p.i. (Figure 10A). Moreover, the mice of both groups do not present with increasing parasite loads, rather they maintain similar numbers of parasites during all times measured (Figure 10B), and even showing a tendency to decrease parasite numbers at late stages of infection. One of the possible explanations for these differences is neutrophil recruitment. We found a massive and progressive recruitment of neutrophils to the ear dermis with increased tissue destruction (Figure 32) and these events were much more intense in gp91$^{phox-/-}$ mice. ROS plays an important role in neutrophil biology, with ROS being one the major factors responsible for neutrophils apoptosis. We observed that neutrophils from gp91$^{phox-/-}$ mice had impaired apoptosis (Figure 51) and a significant higher necrosis (Figure 47), suggesting that ROS could control inflammation in *L. amazonensis* infection via its role in neutrophil apoptosis. There are many controversial data sets in the literature (also in our ROS models of infection) about the role of different cell types, especially neutrophils, and molecules in *Leishmania* infection. We suggested that these controversial results could be related to different sites of inoculation used in these studies. Therefore we compared the differences between subcutaneous and intradermal infections with special emphasis on the recruitment of innate immune cells in the early stages of infection using a more established model of *Leishmania* infection, the infection caused by *L. major*. We found substantial differences in cell recruitment (Figures 25 and 26) and the cells involved in *Leishmania* uptake (Figure 28). The intradermal site of infection is markedly characterized by the recruitment of inflammatory cells such as neutrophils followed by inflammatory monocytes. This high inflammatory environment culminates in a more efficient uptake of *Leishmania* (Figure 29), with neutrophils being the most important cells involved in this initial uptake. The intradermal site of infection is a more physiological site of inoculation since it better approximates the natural mode of infection by infected sand fly bite both in terms of the intradermal localization of parasites and the recruitment of inflammatory cells. As neutrophils are a major cell population involved in oxidative burst thereby generating ROS to

combat pathogens and since these cells are massively recruited to the intradermal site in contrast to the subcutaneous site, it would be beneficial to use the intradermal route of inoculation to study the effect of the NADPH-dependent oxidase of phagocytes, through ROS production, following intradermal *Leishmania* infection.

In general, we observed similar cell recruitment kinetics in mice infected intradermally with *L. major* (Figure 25) or *L. amazonensis* (Figure 49) at early stages of infection. Although we did not use the exact same time points in all of the studies reported here, those experiments where the time points employed were the same revealed similar results. Therefore we inferred from our *L. major* studies employing direct comparisons of different sites of infection to help explain the differences in the effect of ROS at intradermal and subcutaneous site of infection.

The complex of NADPH-dependent oxidase (Nox2 or $gp91^{phox}$) is a multimeric protein responsible for generation of ROS in phagocytes and has been well characterized (Nauseef, 2004). The genetic deficiency of specific NADPH subunits promotes enhanced susceptibility to infection, a condition known as chronic granulomatous disease (CGD). In CGD patients it was possible to demonstrate the importance of ROS production in host defense (Dinauer, 2005). Individuals with CGD show elevated susceptibility to opportunistic pathogens such as *Salmonella enterica*, *Staphylococcus aureus*, *Serratia marcescens*, and *Aspergillus spp*. (Chang et al., 1998; van den Berg et al., 2009; Winkelstein et al., 2000). In addition, mouse models with disruption of $gp91^{phox}$ components present impaired host resistance comparable to humans with CGD (Pollock et al., 1995). These mice present with difficulties in controlling bacterial and fungal infections as well as increased neutrophil migration in peritonitis.

Despite the importance of ROS to kill intracellular pathogens, some species of the genus *Leishmania* developed strategies to avoid the damage induced by ROS. The $^{\bullet}NO$ and ROS are recognized molecules with microbicidal activities against *Leishmania* (Liew et al., 1990; Murray, 1982). $^{\bullet}NO$ is critical for parasite killing, since mice lacking inducible nitric oxide synthase ($iNOS^{-/-}$ or $NOS2^{-/-}$) present uncontrolled infection and increasing parasite replication. Moreover, $iNOS^{-/-}$ macrophages are incapable of eliminating amastigotes in culture (Wei et al., 1995). Infected macrophages or macrophages incubated with purified *Leishmania* surface molecules LPG or GIPL lose their ability to express iNOS or to generate $^{\bullet}NO$ in response to IFN-γ and lipopolysaccharide (LPS) (Proudfoot et al., 1996; Proudfoot et al., 1995). On the other hand, IFN-γ and LPG can synergize to generate $^{\bullet}NO$ when given simultaneously to naïve macrophages (Proudfoot et al., 1996; Proudfoot et al., 1995) suggesting that previous contact between parasites and macrophages prevents the macrophage response when subsequently exposed to IFN-γ produced by lymphoid

cells. In contrast to iNOS$^{-/-}$ mice, gp91$^{phox-/-}$ mice can normally control infection with *L. donovani* after an initial period of increased susceptibility (Murray and Nathan, 1999), indicating that ROS plays a less important role in the parasite clearance. In addition, Blos et al. (2003) showed that gp91$^{phox-/-}$ mice control infection with *L. major* similarly to wild-type mice, however, prompt control of spleen parasitism and draining lymph nodes were dependent of gp91^{phox}. In that work, the authors also demonstrated that ROS is essential to impair the relapse of the disease after long periods post infection.

ROS generation by macrophages is inhibited by *L. donovani* infection (Buchmuller-Rouiller and Mauel, 1987; Olivier et al., 1992a; Olivier et al., 1992b). This inhibition seems to be caused by the molecules LPG and gp63, present on the surface of the parasite (Descoteaux and Turco, 1999; Sorensen et al., 1994) and this interaction would be correlated with abnormal PKC activity (Olivier et al., 1992b). In contrast, we were able to detect production of ROS by macrophages stimulated with *L. amazonensis* promastigotes by luminometry assay (Figure 9), which agrees with data published by Reybier et al. (2010), who also demonstrated intracellular ROS produced by *L. amazonensis*-infected cells. Data from our group shows that the degree of ROS production by infected cells varies with the *Leishmania* species, suggesting specific mechanisms of ROS release impairment by each species. Indeed, our group has shown that *L. amazonensis*-infected macrophages produce less ROS in response to zymosan than non-infected macrophages, suggesting that infection partially impairs the respiratory burst in these cells.

Holzmuller et al. (2002) demonstrated $^{\bullet}$NO-dependent killing of *L. amazonensis* in peritoneal activated macrophages as measured by enhanced parasite DNA fragmentation. However, Mukbel et al. (2007) showed that bone marrow macrophages infected with *L. amazonensis* require both nitric oxide and superoxide production to kill intracellular parasites. The relative resistance of *L. amazonensis* amastigotes to IFN-γ and LPS–mediated macrophage activation would not be due to the suppression of $^{\bullet}$NO production or of iNOS expression by the parasite. In this specific case, the superoxide anion combines with nitric oxide to generate peroxynitrite, which would be the potent killer of *L. amazonensis* amastigotes *in vitro*, contrary to $^{\bullet}$NO alone that would have just a cytostatic effect in the parasite (Bogdan et al., 2000; Linares et al., 2001). Khouri et al. (2009) demonstrated dependency of superoxide generation for *L. amazonensis* or *L. braziliensis* killing in human cases of chronic disease. These authors demonstrated that IFN-β impairs the superoxide action by increasing the SOD intracellular levels, thus increasing the parasite burden independently of $^{\bullet}$NO production.

Despite this attribution of a significant importance of ROS in *L. amazonensis* killing, our

results in the experimental model indicate an irrelevant role of ROS in control of parasitism in both sites of infection used in our study, the footpad and the ear dermis (Figures 10B and 33A). The majority of the studies addressing the role of ROS in *L. amazonensis* killing were done in *in vitro* systems. As important as *in vitro* systems are for the discovery of specific pathways involved in *Leishmania* infections, they fail to consider the interference of other cell types or factors during the disease. We did not observe differences between WT and gp91$^{phox-/-}$ mice in iNOS expression during infection and in nitric oxide production *in vitro* (Figure 13A and B). Hence, the importance of ROS determined previously in *in vitro* studies does not seem to hold *in vivo.* This discrepancy may be due to other factors present *in vivo* that are not present in *in vitro* macrophage infections. Indeed, immune components deeply influence the parasite loads and disease progression. According with Stefani et al. (1994), CD8 T cells might be one source of IFN-γ that activates infected macrophages to release •NO to kill the *L. major*. The •NO released by macrophages during the infection could act also in the down-regulation of the CD8 T cells, impairing their IFN-γ production. In addition, the phagocytosis of apoptotic neutrophils by *L. amazonensis*-infected human macrophages increases parasite burden by promoting enhancement of TGF-β1 and prostaglandin E2 production in the macrophages (Afonso et al., 2008). In contrast, Ribeiro-Gomes et al. (2007) demonstrated that elastase produced by neutrophils enhances the intracellular killing of *L. major*-infected macrophages by a mechanism dependent of TLR4. Even B cells have influence in progression of the disease. C3HeB/FeJ mice co-infected with *L. major* and *L. amazonensis* heal the disease in contrast to C57BL/6 in the same conditions. The higher production of specific antibodies against the parasites by C3HeB/FeJ mice could indicate an important role of B cells in the healing processes (Gibson-Corley et al., 2010). The ablation of C3 receptor ameliorates the progression on lesions in BALB/c mice infected with *L. major*. The C3 molecule inhibits partially the production of IL-12, which is essential to promote a Th1 response (Carter et al., 2009). Therefore, isolated immune components could not represent the real phenotype of the disease, although they are important for the knowledge of how specific factors influence in the parasite killing and possibly disease control.

In vitro data from Mukbel et al. (2007) disagree with our data, since we detected smaller numbers of parasites in gp91$^{phox-/-}$ macrophages infected *in vitro* (Figure 23). Consistently, gp91$^{phox-/-}$ and WT apocynin-treated macrophages bore less parasites than WT controls (Figure 23). The inhibition of NADPH oxidase may activate other powerful mechanisms for parasite killing. Alternatively, parasites need signals provided by the production of ROS by the host cell that allow its successful growth as shown by Paiva et al. (2012) and our unpublished observations with *T.*

cruzi. It is possible that the differences observed between our data and those of Mukbel et al. (2007) are due to differences in experimental design between the assays. We used peritoneal macrophages infected for 4h with metacyclic promastigote forms of *L. amazonensis* in the proportion of 5 parasites to 1 macrophage. In Mukbell´s work, bone marrow macrophages were infected by amastigote forms of *L. amazonensis* in the proportion of 3 parasites to 1 macrophage for 24h. These differences could explain the discordant results found in our experiments.

Gibson-Corley et al. (2010) suggested that any effective immune response against *L. amazonensis* must include specific and productive anti-*Leishmania* response by B cells that can promote macrophage-mediated parasite killing at later stages of infection. Macrophages expressing FcγR on their surface bind the Fc portion of antibodies becoming activated to produce effector molecules including ROS, trough NADPH-oxidase via immunoreceptor tyrosine-based activation motifs (ITAMs) (Hulett and Hogarth, 1994). In the C3H mouse model, B cells and IgG antibodies together with $CD4^+$ T cells from an established *L. major* infection are necessary to provide effective stimulation of macrophages for superoxide-dependent killing of *L. amazonensis* (Mukbel et al., 2006). In this case, the binding of IgG_{2a} in FCγR1 triggers the production of RNS and superoxide trough ITAMs domains. These findings indicate that antibodies might be necessary, but not sufficient, for *L. amazonensis* killing and antibodies are just one of several critical immune components required for killing. The higher production of IgG_1 and IgG_{2a} seen in $gp91^{phox-/-}$ mice (Figure 21B and C) could be a consequence of the compensation of absence in ROS production. Indeed, Wheeler and Defranco (2012) demonstrated an increased production of antibodies after B cell receptor stimulation in $gp91^{phox}$ deficient mice in *in vivo* conditions.

When infected subcutaneously, $gp91^{phox-/-}$ mice presented a higher inflammatory response in the first weeks of infection and a strong decrease in footpad swelling at later times of the infection compared to WT mice (Figure 10A). Despite this shift in lesion development, we could not detect differences in parasites loads in between groups during the evolution of the infection. This suggests that lesions size differences are not due to parasite growth, but rather to inflammatory response in the site of infection. Indeed, the role of ROS in inflammation control is extensively reported in the literature (Brown et al., 2003; Fukai and Ushio-Fukai, 2011; Gonzalez et al., 2011; Harrison et al., 1999; Hattori et al., 2010; Hiraoka et al., 1998; Marriott et al., 2008; Purushothaman and Sarin, 2009; Schappi et al., 2008; Segal et al., 2010; Zhang et al., 2003).

Inflammation is a pathway highly regulated, being mediated by pro- and anti-inflammatory biochemical signals. In particular, some authors demonstrated evidences that the resolution of inflammation is an active process that requires the activation of endogenous programs (Serhan et

al., 2007). In the various hyper-inflammatory states observed in CGD, ROS production by NADPH oxidase seems have an active role in this resolution. One of the important roles of ROS in the resolution of inflammation is the degradation of phagocytosed material, thereby assisting in antigen clearance. Therefore, the proposed mechanism of CGD hyperinflammation is a decreased degradation of phagocyted material due to deficient generation of superoxide in CGD phagocytes. Phagocyted material could accumulate in NADPH oxidase deficient phagocytes leading to persistent cell activation (Metcalfe et al., 1990; Schappi et al., 2008). Deficient degradation could implicate either the remaining phagocyted microbial material (Schappi et al., 2008) or phagocyted apoptotic neutrophils by macrophages. Harbord et al. (2002) demonstrated that eosinophilic crystals observed in CGD patients and mice could be residues of poorly degraded apoptotic neutrophils. In fact, the proteins within these observed crystals are, at least in part derived from neutrophils (Harbord et al., 2002). The molecular mechanisms involved in these processes are in the initial phase of investigation and the possibilities of knowledge remain open. Therefore, non-degraded *Leishmania* could be persistent, favoring an extended time of antigen presence and consequently the inflammation.

In addition, ROS could also contribute to the termination of inflammation suppressing pro-inflammatory signals or impairing the survival of pro-inflammatory cells. Any defect in these processes might aggravate the inflammation. There are increasing reports addressing ROS acting in the regulation of intracellular signaling, particularly through the oxidation of cysteine residues in phosphatases and in transcription factors (Bedard and Krause, 2007). Thus, the absence of $gp91^{phox}$ -derived ROS in CGD leukocytes could create alterations in cell signaling that favor pro-inflammatory responses. Indeed, there are numerous publications suggesting that the inflammatory response can be more pronounced in CGD phagocytes with higher release of TNF-α and IL-8 (Geiszt et al., 1997; Hatanaka et al., 2004; Lekstrom-Himes et al., 2005; Rada et al., 2003). Another explanation for hyperinflammation observed in CGD patients or mice deficient relies in the inability of CGD immune cells to inactivate inflammatory mediators. CGD phagocytes have an impaired ability to produce anti-inflammatory mediators, such as TGF-β and PGE2 (Brown et al., 2003). In the other hands, Harrison et al. (1999) suggested that impaired oxidative inactivation of pro-inflammatory mediators may prolong the inflammatory response. *In vitro* oxidation and consequently clearance of inflammatory mediators such as leukotrienes (Clark and Klebanoff, 1979; Hamasaki et al., 1989; Henderson and Klebanoff, 1983) and S100 (chemotactic stimulating factor for the recruitment of myeloid cells to inflammatory sites) proteins (Harrison et al., 1999) has been shown to be dependent on ROS production. Studies *in vivo* and in isolated macrophages have

demonstrated that in the absence of functional NADPH oxidase, there are flaws in redox-sensitive anti-inflammatory regulators. Consistent with these findings, zymosan-treated peripheral blood mononuclear cells from X-linked CGD patients show impaired Nrf2 (a key redox-sensitive anti-inflammatory regulator) activity and increased NF-κB activation (Segal et al., 2010).

The stimulus sensed by the cell is also an important factor. The fungal wall component β-glucan, but not bacterial cell wall components, induces hyperinflammation. So, it is possible that ROS provide a feedback inhibition to inflammatory signaling through β-glucan receptors (Schappi et al., 2008). In same way, human CGD leukocytes stimulated by sterile *Aspergillus* cell wall extracts release either pro- or anti-inflammatory cytokines, depending on the source of the extract: conidial stimulation tips favor the production of pro-inflammatory cytokines, such as TNF-α and IL-6, while hyphal stimulation induces the release of higher levels of regulatory cytokines, such as IL-10 (Warris et al., 2003).

Indeed, these results agree with our findings since we detected an increase in IL-6 and TNF-α production by macrophages infected with *L. amazonensis in vitro* (Figure 22A and B). When we compare macrophages stimulated with IFN-γ/LPS and *L. amazonensis* to controls stimulated just with IFN-γ/LPS, we can see that there is an increased production of IL-6 by *L. amazonensis*-infected gp91$^{phox-/-}$ macrophages. This increased production can be attributed to presence of the parasite since we did not detected differences in macrophages stimulated just with IFN-γ/LPS. We also detected an increased release of IL-10 in gp91$^{phox-/-}$ macrophages. This effect could be explained by the attempt to reduce the higher inflammatory state caused by the infection in gp91$^{phox-/-}$ macrophages. Curiously, we did not detect an increase in CXCL1 expression in these macrophages (Figure 22D). Indeed, data from our group shows that CXCL1$^{-/-}$ mice do not present alterations in neutrophil migration after *L. major* challenge in the ear, implying a possible irrelevant function of this chemokine in the infection. This result has to be analyzed carefully since we do not know if CXCL1$^{-/-}$ mice could compensate for the lack of CXCL1 by a possible overexpression of CXCL2. In contrast to other cytokines, MCP-1 was produced at lower levels by gp91$^{phox-/-}$ macrophages infected with *L. amazonensis* compared to WT cells. Kinoshita et al. (2013) showed an inhibition of inflammatory cytokines mRNA expression, including MCP-1, in macrophages treated with apocynin (a potent NADPH oxidase inhibitor) stimulated with oxidized LDL. So, the absence of ROS combined with the external signals could influence the profile of inflammatory cytokine expression.

Recently, IL-17-producing effector cells (Th17 cells and *γδ* T cells) have been found to be involved in chronic inflammatory processes and several autoimmune diseases, for example,

multiple sclerosis or rheumatoid arthritis. These highly pro-inflammatory cells are essential for the defense against pathogens (Annunziato et al., 2007; Bettelli et al., 2007) and would be controlled by regulatory T cells (Sakaguchi et al., 2008). A fine regulation by both of these T cell subsets is crucial for controlling infections, inflammation, autoimmunity, and malignancies (Bettelli et al., 2006; Stevens and Bradfield, 2008). Recent work published by Romani et al. (2008) and Segal et al. (2010) demonstrated the contribution of IL-17 in CGD hyperinflammation in an animal model. According with Segal et al. (2010), NADPH oxidase-deficient $p47^{phox-/-}$ mice and $gp91^{phox-/-}$ mice challenged with either intra-tracheal zymosan or LPS, presented exaggerated and progressive lung inflammation, augmented NF-kappa B activation, and elevated production of pro-inflammatory cytokines (TNF-α, IL-17, and G-CSF) compared to WT mice. However, the replacement of functional NADPH oxidase in bone marrow-derived cells restores the normal lung inflammatory response. The immune response mediated by IL-17 starts just few hours after epithelial cell injury or activation of PAMPs, however there is not enough time for the development of Th17 cells. IL-17 produced 4–8 h after microbial infection was shown to enhance neutrophil chemotaxis promoting the production of IL-6, G-CSF, and CXC-chemokine ligand-8 (CXCL8 or IL-8) and to triggering rapid, nonspecific immunity to infectious agents (Happel et al., 2005). IL-17-producing cells can induce epithelial cells to secrete granulopoietic factors such as G-CSF, recruiting large numbers of neutrophils that are crucial for effective and rapid control of bacterial and fungal pathogens. IL-17 also synergizes with other cytokines, such as IL-1, IL-6 and TNF-α, promoting activation of neutrophils to migrate to tissue and effectively eliminate extracellular pathogens, such as *Klebsiella pneumoniae* (Ye et al., 2001), *Staphylococcus aureus* (Cho et al., 2010), and *Candida albicans* (Huang et al., 2004). We found higher release of IL-17 from *L. amazonensis*-infected $gp91^{phox-/-}$ macrophages (Figure 22C) and from dLNs from $gp91^{phox-/-}$ mice 8 weeks post infection (Figure 12E). Indeed, some authors related the production of IL-17 by macrophages in special circumstances, but the mechanisms implied in this secretion has not been elucidated at the moment (Da Silva et al., 2008; Song et al., 2008; Zhu et al., 2008). Therefore, *L. amazonensis* could stimulate the production of IL-17 especially in the absence of ROS and synergizing with additional signals such as LPS. The presence of higher levels of IL-17 in these mice could contribute for the initial recruitment of neutrophils to the infection site within the first hours post infection (Figure 20). This higher inflammatory environment seen in $gp91^{phox-/-}$ mice a few hours after subcutaneous infection could persist in the first weeks post infection causing a sustained recruitment of neutrophils to the infection site (Figure 14B) and subsequently more inflammation in these mice during the first weeks (Figure 10).

Oxygen, besides its role in ATP generation in aerobic cellular metabolism, is also critical in wound-healing processes. Oxygen protects wounds from infection, induces angiogenesis, increases keratinocyte differentiation, migration, and re-epithelialization, enhances fibroblast proliferation and collagen synthesis, and promotes wound contraction (Bishop, 2008; Rodriguez et al., 2008). Moreover, the increased superoxide release by PMN is dependent on suitable oxygen quantities. Vascular rupture and the augmented consumption of oxygen by active cells in the microenvironment of the early wound deplete oxygen and makes this environment hypoxic. According with Tandara and Mustoe (2004), the tensions of oxygen in chronic wounds measured transcutaneously is hypoxic and ranges between about 5 and 20 mm Hg, while in healthy tissues these values vary from 30 to 50 mm Hg.

In regular wound healing processes, ROS such as H_2O_2 and $O_2^{\bullet -}$ might act as cellular messengers promoting cell motility, cytokine release (including PDGF signal transduction) and angiogenesis, among others key processes related to wound healing. Niethammer et al. (2009) recently demonstrated, using the zebrafish as a model, a sustained increase in H_2O_2 production at the margins of the wound, reaching the peak of production at 20 minutes after the wounding. Using a reporter gene encoding H_2O_2-sensitive fluorescent protein as ROS indicator, it was demonstrated that H_2O_2 production at the wound margin occurred before the recruitment of leukocytes, suggesting that the source of H_2O_2 was epithelial cells and not leukocytes. This finding contrasts with the idea that ROS found at the wound site would come principally from inflammatory leukocytes during their oxidative bursts.

In the past decade, several isoforms of NADPH oxidase were discovered that were found to be active independently of phagocytosis. Until now, six isoforms (Nox-1, -3, -4, -5, and Duox1, -2), one $p47^{phox}$ isoform (Noxo1) and one $p67^{phox}$ isoform (Noxa1) were identified in mammalian cells (Banfi et al., 2003; Banfi et al., 2001; Cheng et al., 2001; De Deken et al., 2000; Dupuy et al., 1999; Geiszt et al., 2000; Suh et al., 1999). Moreover, it seems that the patterns of expression observed in these isoforms are tissue-specific. Unlike $gp91^{phox}$ in phagocytic cells, where the complex is anchored to the phagocytic membrane, the subcellular localization of other Nox isoforms in non-phagocytic cells is not restricted to the cell membrane.

Koff et al. (2006) demonstrated that artificial wounds generated by scrapping of human airway epithelial cell monolayer cultures closed faster when the cells were treated with non toxic concentrations of LPS. However, the effect of accelerated wound healing by LPS was inhibited by ROS scavengers, Nox inhibitors, and siRNA against Duox1, which suggests that this specific repairing process is dependent on NADPH oxidase redox signaling. Jiang et al. (2011) have also

shown a positive effect of NADPH oxidase using artificial wounding of *in vitro* vascular endothelial cell monolayers. In addition, it was demonstrated that Nox4, but not $gp91^{phox}$, was markedly upregulated and that silencing of the Nox4 gene suppressed wound healing of the cultured cells (Datla et al., 2007; Peshavariya et al., 2009). Qian et al. (2005) also demonstrated that DPI (an unspecific inhibitor of Nox) suppressed arsenite-induced wound healing in monolayers of an immortal mouse endothelial cell line. In this study, the ablation of Rac1 was sufficient to abolish the superoxide production induced by arsenite, which suggests a specific involvement of Nox in the healing process. In the work by Niethammer et al. (2009) on zebrafish larvae mentioned above, the authors demonstrated that Duox1 was the Nox isoform responsible for the early ROS generation after tissue wounding by those epithelial cells. The authors observed that when ROS reach the peak of production, a gradient of H_2O_2 was identified around 100 to 200μm of the wound margin. In, addition, the ablation of Duox by knockdown of the gene reduced significantly the production of H_2O_2 in the wound, suppressing the consequent recruitment of leukocytes to the injured site. All these reports together point to the possibility that ROS could act in cellular functions beyond those single cell contexts, and could also have an important role as a paracrine signal during the wound repair processes (Niethammer et al., 2009; Wong and Shimamoto, 2009).

Taken together, these reports show that oxygenation and ROS production are essential for wound healing. However, the ROS produced to generate healing seem to come from other isoforms of Nox, such as Duox1 and Nox4, which are functional in $gp91^{phox-/-}$ mice. As mentioned before, the superoxide production by polymorphonuclear leukocytes is critically dependent on oxygen levels. Therefore, $gp91^{phox}$ from leukocytes consume high quantities of oxygen to produce superoxide and consequently deplete oxygen, making the microenvironment quite hypoxic. We suggest that the absence of $gp91^{phox}$ in $gp91^{phox-/-}$ mice increases the availability of oxygen to other Nox isoforms and the metabolic processes important for wound healing. This could explain why $gp91^{phox-/-}$ mice presented an eventual partial resolution of the inflammation when infected subcutaneously with *L. amazonensis* (Figure 10A) in the chronic phase of the infection.

There are no reports addressing cell recruitment and the immune response during the early stages of infection at different sites of *Leishmania* inoculation. This is despite the fact that many controversies exist regarding the role of different cell types and molecular components in leishmaniasis studied employing different routes of inoculation (Lima et al., 1998; Peters et al., 2008; Smelt et al., 2000; Tacchini-Cottier et al., 2000; Thalhofer et al., 2011). Moreover, the majority of the studies about the immune responses developed at different sites of inoculation were based on vaccine studies where just the secondary challenge is studied in more detail. Indeed, the

primary site of challenge influences the secondary challenge, and the response is quite different depending on which site was used in primary inoculation (Tabbara et al., 2005). The effect of the route in infection on the outcome of infection has been reported for *L. major* (Nabors and Farrell, 1994), *L. donovani* (Kaur et al., 2008) and *L. tropica* (Mahmoudzadeh-Niknam et al., 2013).

Nabors and Farrell (1994) showed that SWR mice infected with *L. major* in the rump developed rapidly progressive disease, which culminates on the death of the animals. However, when SWR mice were inoculated in the footpad, a mild disease was observed and the mice were able to control lesions and even progress toward healing. The authors attribute these different outcomes to the different levels of cell activation during the early stages of the diseases. This differential activation of the cells could involve non-immunological factors like skin temperature, which would influence parasite growth directly. Kaur et al. (2008) demonstrated that CB6F1 mice (C57BL/6 x BALB/c) infected with *L. donovani* developed progressive disease when inoculated in the dorsal skin, but healed of the infection in the footpad. Surprisingly, the site of the inoculation appeared to influence the immune response to the parasite, since the infection in the footpad ultimately led to the development of a Th1 response, known to be required for healing, while a Th2 response developed in mice inoculated in the dorsal skin.

In their study on *L. tropica* infection in BALB/c mice, Mahmoudzadeh-Niknam et al. (2013) demonstrated that the intradermal ear route of infection results in a non-healing outcome, while subcutaneous footpad route of infection with the same parasite results in a self-healing outcome. In addition, the intradermal ear route of *L. tropica* infection induces significantly less protective immune responses against secondary *L. major* challenge in comparison to the subcutaneous footpad route. Moreover, lower delayed-type hypersensitivity response and higher levels of IL-10 were observed at intradermal site one week after *L. major* challenge (Tabbara et al., 2005).

The subcutaneous site of injection into the footpad has been frequently reported in the literature for initiation of cutaneous lesions in mice, as reviewed by Sacks and Melby (2001). This site is frequently used because of some advantages that include easy sequential measurement of lesion development through footpad swelling, without euthanizing the animals, and the easy mode of inoculation itself. However, infection of the ear dermis seems to be closer to the natural route of infection, and consequently is a better model for leishmaniasis studies (Belkaid et al., 1998). In addition, murine infection models have consistently inoculated 10^4 to 10^7 parasites, which are much higher numbers than the ones inoculated by the parasite vector (Kimblin et al., 2008).

The differences between papers that addressed experimental models using subcutaneous and intradermal sites of inoculation start with the number of parasites that are used by the different

groups. While at the subcutaneous sites (such as the footpads or base of the tail) the usual numbers vary from 10^4 to 10^7 parasites (Sacks and Noben-Trauth, 2002), the numbers used for intradermal infections in the ears range between 10^2-10^6 parasites (Belkaid et al., 1998; Belkaid et al., 2000). Indeed, the intradermal model of infection used by Belkaid et al. (1998) simulates better the natural infection since low doses of parasites are inoculated by sand flies bites, around 10^2-10^3 parasites (Sacks and Noben-Trauth, 2002).

The inoculation of high dose of parasites by needle is associated with an increasing number of parasites at the site of infection in early stages of lesion formation (Hill, 1984; Hill et al., 1983; Titus et al., 1985). Belkaid et al. (2000) showed that the maximum number of parasites at intradermal site was observed (through the quantification of *L. major* loads at different time points) during the subclinical stage of infection. Therefore, the maximum number of parasites at intradermal site seems to occur before the lesion formation. This quiescent parasite growth at the intradermal site is supported by the unchanged number and types of leukocytes during the first 4 weeks post-infection, despite the rapid and transient increase in the influx of neutrophils immediately after needle injection. The use of low doses of inoculation at intradermal site in the ears induces a "silent phase" in the infection that is characterized by apparent absence of active immune response and increase in parasite charge. On the other hand, the high dose of parasites inoculated during the infection at the subcutaneous site in the footpads promotes the uptake of these parasites by other cell types such as dendritic cells, which in contrast to macrophages, are stimulated to produce IL-12 in response to *Leishmania* infection (Gorak et al., 1998; von Stebut et al., 1998). Therefore, the inoculation of high numbers of parasites provides a potent source of APC for cell activation (Moll et al., 1993; Will et al., 1992).

Similar results were observed by Cortes et al. (2010) related to low and high dose of inoculation with *L. amazonensis* parasites. The authors demostrated that low doses of *L. amazonensis* injected in the ears of C57BL/6 mice were followed by responsiveness of immune cells such as macrophages and T cells and silent growth of the parasite in the first weeks post challenge.

Our findings demonstrate clear differences in cells responsible for *Leishmania* uptake in the two different inoculation sites. At the intradermal site of infection, neutrophils are the major cells involved in phagocytosis of the parasites in the first hours of infection (Figure 28B). However, inflammatory monocytes migrated from blood take the place of neutrophils, as neutrophils start to die (Figure 28C). Therefore, inflammatory cells that came from the blood are responsible for the establishment of the disease. Indeed, data from Sacks´ laboratory show that Ly6C^{hi} inflammatory

monocytes decrease the expression of Ly6C becoming $Ly6C^{low}$ during early infection, being indistinguishable from the resident $Ly6C^{low}$ macrophages or DCs (data not published). However, these cells continue to express CX_3CR_1, a hallmark of $Gr1^+$ monocytes migrated from blood (Auffray et al., 2009). CX_3CR_1 expression is associated with the commitment of CSF-$1R^+$ myeloid precursors to the macrophage/dendritic cell (DC) lineage (Auffray et al., 2009). Therefore, once these cells reach the infected tissue, they can differentiate into macrophages or DCs, contributing to the immune response in leishmaniasis. Using the CX_3CR_1-GFP reporter mice, we observed that $Ly6C^{hi}$ inflammatory monocytes migrated from blood are the major cells infected in tissue 48h after challenge and a considerable part of these cells decrease the expression of Ly6C (data not shown).

The subcutaneous site of infection is widely used in the studies of *Leishmania* infection. However, we demonstrated that cells involved in infection are quite different from those from intradermal infection. The cells involved in the subcutaneous site of infection are primarily non-activated cells. The major cells responsible for *Leishmania* uptake are resident immature DCs and macrophages without participation of cells migrated from blood in the uptake process. We did not detect the infiltration of neutrophils after the challenge at subcutaneous site. Indeed, the injection at subcutaneous site is caused by just a little puncture in footpad contrasting with the intradermal site, which is caused by a parallel injection causing a considerable damage in the tissue.

The shift in the infected cell population (from neutrophils to inflammatory macrophages) did not happen in the subcutaneous site of infection. Instead, resident $Ly6G^-Ly6C^-$ cells were responsible for the initial *Leishmania* uptake from 2h post infection (Figure 28). Inside of resident cells, we identified an unnamed population, $CD11c^+MHCII^-$, which are the major cells involved *Leishmania* uptake from 2h to 48h post infection. We believe that these cells are DCs in an immature stage, since this population drops coincidently with an increase in typical DC population during the times measured (Figure 28E and F).

Indeed, the subpopulations of $CD11b^+$ cells in both sites of inoculation at steady state are different when we compared the subcutaneous site in footpads and intradermal site in ears. DCs and macrophages are the major $CD11b^+$ cells present in naïve ears (Figure 25). However, the immature DCs are the major cells present in the footpads. These different cell populations at the different sites could change completely the immune response in *Leishmania* infection. One of most important observations in this case was the sequential recruitment of inflammatory leukocytes that happened only at the intradermal dermal site of infection. Indeed, we found a more activated environment in the ears with high proportion of activated $MHCII^+$ macrophages (Figure 25E) and mature DCs (Figure 25D). This environment could favour the recruitment of inflammatory cells to ears through

chemoattractant release after tissue damage by needle. These chemoattractants may have caused the initial recruitment of neutrophils to ears, and this recruitment was reinforced by augmented expression of CXCL1 and IL-17 from 2h post infection (Figure 31B and G).

A portion of neutrophils patrol the postcapillary venules, through temporary interactions, via rolling in endothelial cells, surveying connective tissue, mucosal membranes, skeletal muscle, and lymphatic organs for signs of tissue damage, inflammation, or invading microorganisms (Lawrence and Springer, 1991; Richter et al., 2004; Zarbock and Ley, 2009). These rolling marginating neutrophils search the host looking for chemotactic signals or chemoattractants derived from the host or pathogens. Following damage or invasion by pathogens, diverse types of host cells, which include monocytes, macrophages, mast cells, fibroblasts, keratinocytes, endothelial and epithelial cells start to induce the production and secretion of inflammatory mediators such as neutrophil attractants. Among others, we can cite interleukin-8 (IL-8, CXCL8), GROα (CXCL1), granulocyte chemotactic protein 2 (GCP2, CXCL6), and leukotriene B4 (LTB 4). These chemokines and chemoattractants bind in specific receptors found in neutrophils improving their adhesion capacity and consequent migration into the tissue. These signals provided by the attractants lead the neutrophils out of the circulation to the damage or infected sites, which promote rapid influx of these cells and consequent accumulation in the tissue. In infection caused by *Leishmania*, the damage promoted by the needle injection or even the damage induced by the sand fly bite is sufficient to cause neutrophil migration. However, the damage induced by the sand fly bite seems to promote a more sustained migration and accumulation of neutrophils at site of the bite (Peters et al., 2008).

The needle injection causes considerable damage in the layers of ear skin. Consequently, this damage causes rupture of cells and release of intracellular contents in the extracellular matrix. These cytoplasmatic components might bind to danger associated molecular patterns (DAMPs) localized on the surface of skin cells initiating the inflammatory response. Apart from the damage caused by the inoculation, the injected vehicle containing the parasites increases the pressure against the skin layers, which contribute to tissue rupture and consequent inflammation. In the case of natural infection, the sand fly bite causes considerable wounding of the microvasculature creating a blood pool necessary to sand fly feeding. This process initiates a strong local inflammatory response compared to needle injection (Belkaid et al., 1998; Peters and Sacks, 2009). Results from our group show that even if the needle damage causes considerable neutrophils recruitment, there is a contribution of the parasite to neutrophil recruitment. The increasing doses of parasite inoculation promote increase in number of neutrophils recruited to intradermal site of

infection.

The puncture at the subcutaneous site by the injection does not seem to be enough to cause a massive recruitment of neutrophils to the site of infection. Moreover, the subcutaneous space does not seem to be damaged in the process, suggesting that the parasites would be the main factor responsible for the inflammation. Accordingly, there is no production of inflammatory cytokines early after the parasite inoculation (Figure 31) subcutaneously. Contrary to the pressure exerted by intradermal inoculation, the subcutaneous space seems to permit a spread of the liquid containing the parasite without important tissue damage. Interestingly, the number of infected cells at the subcutaneous site is quite low compared to intradermal site (Figure 29A) even the tissues presenting the same number of phagocytic cells during the first hours of infection (Figure 26A). Probably the large space of the subcutaneous site compared to intradermal site makes it difficult for the phagocytes to encounter *Leishmania*, consequently decreasing the phagocytosis of parasites and lowering the effective parasite dose.

Certainly, the different immune cells involved in the subcutaneous or intradermal site *L. amazonensis* infection interfere with the immune response against this parasite. An indirect comparison shows that while the *L. amazonensis* infection in the footpads promotes a controlled lesion growth with no changes in parasite loads until 16 weeks (Figure 10), the intradermal infection in the ears cause a progressive lesion with tissue destruction (Figure 32) and increase in parasite loads over the course of infection in both mice (Figure 33A). Moreover, the intradermal site of infection seems to influence even more the $gp91^{phox-/-}$ mice, since we detected higher parasite loads in dLNs of these mice over the course of infection (Figure 33B) and no difference was observed in these organs after subcutaneous challenge (Figure 10C).

The $gp91^{phox-/-}$ mice seem to have difficulties in controlling parasites in dLNs since they presented higher dLNs expansion (Figure 39) and higher parasite loads (Figure 33B) during the infection. Indeed, the importance of ROS to control parasites at internal organs has been documented. Blos et al. (2003) showed that the NADPH oxidase activity is most critical for the control of *L. major* in the spleen, where it appears to substitute for the hardly detectable anti-leishmanial function of iNOS in that organ. According to those authors, NADPH oxidase acts in concert with iNOS in the skin and lymph node, but cannot replace the function of iNOS in these compartments. These results agree with our findings and ROS could be required to control parasites in dLNs in intradermally *L. amazonensis*-infected mice. Moreover, Acestor et al. (2006) demonstrated that the resistance of the parasites to H_2O_2 might influence the metastatic behavior of species of *Leishmania* that cause the mucocutaneous disease. Therefore, ROS would be important

to impair the parasite spread to other sites via dLNs. So, we suggest the high parasite loads in gp91$^{phox-/-}$ mice dLNs could facilitate the dissemination of the disease. Indeed, data from our group show augmented number of *L. major* parasites in liver of gp91$^{phox-/-}$ mice treated with aminoguanidine ($^{\bullet}$NO production inhibitor) compared to WT with the same treatment.

The remarkable difference noted in both models of infection caused by *L. amazonensis* is the sustained presence of neutrophils after intradermal injection of parasites, as observed when we compared intradermal versus subcutaneous in *L. major* infection model. Moreover, the gp91$^{phox-/-}$ mice presented even higher levels of neutrophils over the course of the infection (Figure 35A). Since we did not detect any difference in other immunological parameters between WT and gp91$^{phox-/-}$ mice during the *L. amazonensis* infection, we could attribute the exacerbated inflammation and tissue destruction seen in gp91$^{phox-/-}$ mice (Figure 32) to neutrophils. Since we detected significant increased numbers in neutrophils recruitment to site of infection in gp91$^{phox-/-}$ mice, we focused in the alterations related to neutrophil function to try to explain this augmented infiltration. We measured the mRNA levels of inflammatory chemokines and cytokines involved in neutrophils recruitment during the first weeks post infection. We detected higher levels of CXCL2 in gp91$^{phox-/-}$ mice 4 weeks after the infection without alteration in CXCL1 or IL-1β. Our results suggest that CXCL2 could be involved at initial stages of neutrophil recruitment in gp91$^{phox-/-}$ mice during the infection. At 8 weeks post infection, we detected a tendency of increased mRNA expression of CXCL1 and CXCL2 in gp91$^{phox-/-}$ mice. It is possible that the combined increase of these two chemokines could contribute for the increase in neutrophil numbers seen in gp91$^{phox-/-}$ mice. Indeed, increase in chemokine production and neutrophil recruitment during infections was already documented in mice deficient in ROS production, principally in bacterial infections (Acestor et al., 2006; Boots et al., 2012; Gonzalez et al., 2011; Miyairi et al., 2007).

Despite the contribution of chemokines to neutrophil recruitment during the infection, this factor by itself would not be sufficient to explain the heavy necrosis and tissue destruction seen in gp91$^{phox-/-}$ mice. Analyzing the first hours after the challenge we noticed impairment in neutrophil apoptosis in gp91$^{phox-/-}$ mice (Figure 51B). This phenomenon could interfere in neutrophil death culminating on the accumulation of this cell type since the beginning of the infection. Indeed, several reports demonstrated significant influence of ROS in apoptotic processes in neutrophils. A role for the NADPH oxidase as the principal inductor of ROS production during spontaneous apoptosis came from observations in neutrophils derived from patients with chronic granulomatous disease (CGD) that do not possess a functional NADPH oxidase. Several reports have shown that CGD neutrophils possess increased survival when compared with neutrophils from healthy donors

(Conus et al., 2008; Fadeel et al., 1998; Kasahara et al., 1997; von Gunten et al., 2005).

Pierce et al. (1991) demonstrated that hydrogen peroxide is able to induce apoptosis, having the effect reverted by catalase in blastocysts. Besides catalase, high levels of the intracellular antioxidant glutathione oppose the apoptosis triggered by ROS. Moreover, many authors have shown that ROS can induce apoptosis in many different cell systems. As described for blastocysts, H_2O_2 induced apoptosis in neutrophils, which also can be prevented by catalase (Kasahara et al., 1997). Since catalase impairs the spontaneous apoptosis of neutrophils, it is suggested that H_2O_2 might be an important trigger mechanism of neutrophil death and, consequently, responsible for their short life spam in the mature stage. In addition, according with Watson et al. (1997), the augmented intracellular glutathione levels prevented Fas receptor-mediated apoptosis in neutrophils.

Receptors of the tumor necrosis factor (TNF)/nerve growth factor (NGF) family display multiple functions, ranging from cell growth and differentiation to cell death (Ashkenazi and Dixit, 1998; Wallach et al., 1999). A particular subgroup of this family has been shown to induce apoptosis in several models and they are termed death receptors. Despite the presence of cystein-rich motifs found in the extracellular domain in all members of the TNF/NGF receptors family, these receptors contain an additional common sequence in their cytoplasmic domain called death domain. This death domain is required and sufficient to induce death via caspase-dependent mechanisms (Ashkenazi and Dixit, 1998; Wallach et al., 1999). The death receptors promote cell death by caspase-dependent mechanism, however it seem that ROS generation is equally important in this process although the mechanism has not been fully elucidated. In addition, it has been already described that the antioxidant N-acetylcysteine blocks TNF-induced apoptosis in human neuronal cells (Talley et al., 1995) and U937 cell line (Cossarizza et al., 1995), which suggests a functional participation of ROS during the apoptotic process.

Clearly, not all ROS target in cells have been identified. ROS activate acid sphingomyelinase in neutrophils, which results in increased ceramide levels (Scheel-Toellner et al., 2004). Ceramides contributes to apoptosis in neutrophils, since these molecules increases caspase-3/-8, -9 activity. Moreover, ROS also induce release of cathepsin D from azurophilic granules, which would lead to caspase-8 activation (Conus et al., 2008). Other example of ROS contribution to apoptosis is through inhibition of class IB PI3K p110γ, which results in reduced PIP_3 levels and Akt phosphorylation. Therefore, ROS have important roles in neutrophils apoptosis during inflammatory processes, since they participate and interfere in an intimately and integrated ways with apoptotic signalling cascades.

In order to follow the neutrophils during the chronic stages of infection, we performed an apoptosis/necrosis assay at 8 weeks of infection to verify the functional state of these cells at this time. We detect more than 10% of neutrophils in gp91$^{phox-/-}$ mice in necrotic death process and just 5% in same situation in WT group (Figure 47C). Due the higher number of neutrophils in gp91$^{phox-/-}$ mice (Figure 45C), these mice presented about 4 times more necrotic cells at 8 weeks post infection compared WT animals (Figure 47E). Indeed, because a problem in the apoptotic process of neutrophils clearance, in gp91$^{phox-/-}$ mice the neutrophil migration might culminate in necrosis.

The leakage of cell contents during the necrotic processes causes the release of cytoplasmatic proteins in the extracellular environment. In the specific case of neutrophils, the necrotic processes releases, among others proteins, proteases that are highly harmful, destroy the extracellular matrix and cause necrosis. The necrotic process seen in gp91$^{phox-/-}$ mice could lead a strong release of proteases in the extracellular matrix causing intense tissue destruction as seen in the ears of gp91$^{phox-/-}$ mice infected with *L. amazonensis* (Figure 32C).

Other cytoplasmatic and nuclear cell compounds are also released in the extracellular environment. These intracellular compounds have been named alarmins and are able to activate innate immune cells (Scaffidi et al., 2002). The nuclear high mobility group box protein 1 (HMGB1) was one of the first alarmins identified that was related to endogenous tissue trauma (Bianchi, 2007; Scaffidi et al., 2002). However, it is now known that a large number of other additional cell compounds act as DAMPs, such as heat shock proteins, DNA, RNA, ATP, among others (Bianchi, 2007). In addition, the association of HMGB1 and other DAMPs particularly cause a strong activation of inflammatory genes (Bianchi, 2009). This specific activation of innate immunity by DAMPs is triggered through binding of these molecules to toll-like receptors (Schwabe et al., 2006).

Taken together, the release of proteases and alarmins in the extracellular environment could lead to destruction of the tissue and increase in the inflammation, promoting the tissue loss (Figure 32C) and the significant accumulation of neutrophils (Figure 35A) seen in gp91$^{phox-/-}$ mice during *L. amazonensis* infection.

We observed a deficient mechanism of apoptosis in gp91$^{phox-/-}$ mice at early stages of infection (Figure 51B). In addition, we noted an increase in necrosis 8 weeks post infection also in gp91$^{phox-/-}$ mice (Figure 47C). Neutrophils are short-lived cells, however, as mentioned above, these cells, if deficient in ROS production, are more resistant to apoptosis. We suggest that the impairment of neutrophil clearance via apoptosis in the acute phase of the *L. amazonensis* infection

promotes inflammatory death of these cells via necrotic mechanisms in the chronic phase of infection leading high tissue loss seen in gp91$^{phox-/-}$ mice (Figure 32C).

Despite the fact that we observed the same parasite loads in WT and gp91$^{phox-/-}$ mice during the infection, we asked if an alteration of the cell types involved in *Leishmania* harboring could occur in the absence of NADPH oxidase at the intradermal site. We observed a higher percentage of neutrophils infected 10h and 36h post-infection in gp91$^{phox-/-}$ mice, resulting in a decreased number of infected resident macrophages after 10h and DCs after 36h in these mice (Figure 50). These changes in dynamics of infected cells did not alter the late times of the infection since just 60h post-infection, the percentage of all innate immune cells analyzed were equaled. So, the absence of ROS could not determine alterations in the population of infected cells 60h post-infection with *L. amazonensis*.

Neutrophils have been extensively studied in the context of *Leishmania* infection in the last years. However, contradictory results have been found on the role of neutrophils in the disease control (Peters and Sacks, 2009). These contradictory results can be attributed to many variables such as the use of different mouse strains, the site of infection, the size of the parasite inoculum among others. In the study on role of neutrophils in sand flies transmitted infections, parasites deposited into the skin of neutrophil-depleted C57BL/6 mice were only half as successful at establishing infection when compared to the parasites transmitted to neutrophil sufficient mice (Peters et al., 2008). The enhanced host resistance was associated with an increase in pro-inflammatory cytokines. There are no reports in literature about the role of neutrophils in *L. amazonensis* infection. However, data from our group determined an irrelevant role of neutrophils in intradermal infection caused by *L. amazonensis* in C57BL/6 mice. The depletion of neutrophils in these mice did not have effects in the infection. Despite the irrelevant role of neutrophils in parasite loads in C57BL/6 mice, the depletion of neutrophils in infected BALB/c mice promoted augmented susceptibility in these animals. Our results show no differences in parasite loads of WT and gp91$^{phox-/-}$ mice during the infection even with higher numbers of neutrophils seen in gp91$^{phox-/-}$ mice, although it is necessary to take into consideration that absence of ROS directly influences the functions of these cells.

In conclusion, the effect of ROS in *Leishmania* infections could be strongly influenced by the site of inoculation. Almost all *in vivo* studies about the role of ROS in *Leishmania* infection employed the subcutaneous site of infection. Because neutrophils have a more limited role in infection at this site these observations could generate inaccurate conclusions regarding the role of ROS during infection, since neutrophils are one of most important cells involved in oxidative burst.

Moreover, the use of models that better approximate natural infection should be prioritized since they show more similarities with natural infection. Therefore, we hope to have elucidated the importance of ROS in the *L. amazonensis* infection in a context closest to natural infection model.

8. BIBLIOGRAPHIC REFERENCES

Acestor, N., Masina, S., Ives, A., Walker, J., Saravia, N.G., Fasel, N., 2006. Resistance to oxidative stress is associated with metastasis in mucocutaneous leishmaniasis. The Journal of infectious diseases 194, 1160-1167.

Afonso, L., Borges, V.M., Cruz, H., Ribeiro-Gomes, F.L., DosReis, G.A., Dutra, A.N., Clarencio, J., de Oliveira, C.I., Barral, A., Barral-Netto, M., Brodskyn, C.I., 2008. Interactions with apoptotic but not with necrotic neutrophils increase parasite burden in human macrophages infected with Leishmania amazonensis. Journal of leukocyte biology 84, 389-396.

Afonso, L.C., Scott, P., 1993. Immune responses associated with susceptibility of C57BL/10 mice to Leishmania amazonensis. Infection and immunity 61, 2952-2959.

Allen, R.C., Loose, L.D., 1976. Phagocytic activation of a luminol-dependent chemiluminescence in rabbit alveolar and peritoneal macrophages. Biochemical and biophysical research communications 69, 245-252.

Alvarez, B., Radi, R., 2003. Peroxynitrite reactivity with amino acids and proteins. Amino acids 25, 295-311.

Annunziato, F., Cosmi, L., Santarlasci, V., Maggi, L., Liotta, F., Mazzinghi, B., Parente, E., Fili, L., Ferri, S., Frosali, F., Giudici, F., Romagnani, P., Parronchi, P., Tonelli, F., Maggi, E., Romagnani, S., 2007. Phenotypic and functional features of human Th17 cells. The Journal of experimental medicine 204, 1849-1861.

Ashkenazi, A., Dixit, V.M., 1998. Death receptors: signaling and modulation. Science 281, 1305-1308.

Assreuy, J., Cunha, F.Q., Epperlein, M., Noronha-Dutra, A., O'Donnell, C.A., Liew, F.Y., Moncada, S., 1994. Production of nitric oxide and superoxide by activated macrophages and killing of Leishmania major. European journal of immunology 24, 672-676.

Auffray, C., Fogg, D.K., Narni-Mancinelli, E., Senechal, B., Trouillet, C., Saederup, N., Leemput, J., Bigot, K., Campisi, L., Abitbol, M., Molina, T., Charo, I., Hume, D.A., Cumano, A., Lauvau, G., Geissmann, F., 2009. CX3CR1+ CD115+ CD135+ common macrophage/DC precursors and the role of CX3CR1 in their response to inflammation. The Journal of experimental medicine 206, 595-606.

Babior, B.M., 1999. NADPH oxidase: an update. Blood 93, 1464-1476.

Babior, B.M., 2004. NADPH oxidase. Current opinion in immunology 16, 42-47.

Bahrami, S., Hatam, G.R., Razavi, M., Nazifi, S., 2011. In vitro cultivation of axenic amastigotes and the comparison of antioxidant enzymes at different stages of Leishmania tropica. Tropical biomedicine 28, 411-417.

Banfi, B., Clark, R.A., Steger, K., Krause, K.H., 2003. Two novel proteins activate superoxide generation by the NADPH oxidase NOX1. The Journal of biological chemistry 278, 3510-3513

Banfi, B., Molnar, G., Maturana, A., Steger, K., Hegedus, B., Demaurex, N., Krause, K.H., 2001. A Ca(2+)-activated NADPH oxidase in testis, spleen, and lymph nodes. The Journal of biological chemistry 276, 37594-37601.

Banuls, A.L., Hide, M., Prugnolle, F., 2007. Leishmania and the leishmaniases: a parasite genetic update and advances in taxonomy, epidemiology and pathogenicity in humans. Advances in parasitology 64, 1-109.

Barral, A., Costa, J.M., Bittencourt, A.L., Barral-Netto, M., Carvalho, E.M., 1995. Polar and subpolar diffuse cutaneous leishmaniasis in Brazil: clinical and immunopathologic aspects. International journal of dermatology 34, 474-479.

Barral, A., Petersen, E.A., Sacks, D.L., Neva, F.A., 1983. Late metastatic Leishmaniasis in the mouse. A model for mucocutaneous disease. The American journal of tropical medicine and hygiene 32, 277-285.

Basu Ball, W., Kar, S., Mukherjee, M., Chande, A.G., Mukhopadhyaya, R., Das, P.K., 2011. Uncoupling protein 2 negatively regulates mitochondrial reactive oxygen species generation and induces phosphatase-mediated anti-inflammatory response in experimental visceral leishmaniasis. J Immunol 187, 1322-1332.

Bedard, K., Krause, K.H., 2007. The NOX family of ROS-generating NADPH oxidases: physiology and pathophysiology. Physiological reviews 87, 245-313.

Belkaid, Y., Kamhawi, S., Modi, G., Valenzuela, J., Noben-Trauth, N., Rowton, E., Ribeiro, J., Sacks, D.L., 1998. Development of a natural model of cutaneous leishmaniasis: powerful effects of vector saliva and saliva preexposure on the long-term outcome of Leishmania major infection in the mouse ear dermis. The Journal of experimental medicine 188, 1941-1953.

Belkaid, Y., Mendez, S., Lira, R., Kadambi, N., Milon, G., Sacks, D., 2000. A natural model of Leishmania major infection reveals a prolonged "silent" phase of parasite amplification in the skin before the onset of lesion formation and immunity. J Immunol 165, 969-977.

Bettelli, E., Carrier, Y., Gao, W., Korn, T., Strom, T.B., Oukka, M., Weiner, H.L., Kuchroo, V.K., 2006. Reciprocal developmental pathways for the generation of pathogenic effector TH17 and regulatory T cells. Nature 441, 235-238.

Bettelli, E., Oukka, M., Kuchroo, V.K., 2007. T(H)-17 cells in the circle of immunity and autoimmunity. Nature immunology 8, 345-350.

Bianchi, M.E., 2007. DAMPs, PAMPs and alarmins: all we need to know about danger. Journal of leukocyte biology 81, 1-5.

Bianchi, M.E., 2009. HMGB1 loves company. Journal of leukocyte biology 86, 573-576.

Bishop, A., 2008. Role of oxygen in wound healing. Journal of wound care 17, 399-402.

Blos, M., Schleicher, U., Soares Rocha, F.J., Meissner, U., Rollinghoff, M., Bogdan, C., 2003. Organ-specific and stage-dependent control of Leishmania major infection by inducible nitric oxide synthase and phagocyte NADPH oxidase. European journal of immunology 33, 1224-1234.

Bogdan, C., Moll, H., Solbach, W., Rollinghoff, M., 1990. Tumor necrosis factor-alpha in combination with interferon-gamma, but not with interleukin 4 activates murine macrophages for elimination of Leishmania major amastigotes. European journal of immunology 20, 1131-1135.

Bogdan, C., Rollinghoff, M., Diefenbach, A., 2000. Reactive oxygen and reactive nitrogen intermediates in innate and specific immunity. Current opinion in immunology 12, 64-76.

Bomfim, G., Nascimento, C., Costa, J., Carvalho, E.M., Barral-Netto, M., Barral, A., 1996. Variation of cytokine patterns related to therapeutic response in diffuse cutaneous leishmaniasis. Experimental parasitology 84, 188-194.

Boots, A.W., Gerloff, K., Bartholome, R., van Berlo, D., Ledermann, K., Haenen, G.R., Bast, A., van Schooten, F.J., Albrecht, C., Schins, R.P., 2012. Neutrophils augment LPS-mediated pro-inflammatory signaling in human lung epithelial cells. Biochimica et biophysica acta 1823, 1151-1162.

Bovaird, J.H., Ngo, T.T., Lenhoff, H.M., 1982. Optimizing the o-phenylenediamine assay for horseradish peroxidase: effects of phosphate and pH, substrate and enzyme concentrations, and stopping reagents. Clinical chemistry 28, 2423-2426.

Bray, R.S., 1974. Leishmania. Annual review of microbiology 28, 189-217.

Brown, J.R., Goldblatt, D., Buddle, J., Morton, L., Thrasher, A.J., 2003. Diminished production of anti-inflammatory mediators during neutrophil apoptosis and macrophage phagocytosis in chronic granulomatous disease (CGD). Journal of leukocyte biology 73, 591-599.

Buchmuller-Rouiller, Y., Mauel, J., 1987. Impairment of the oxidative metabolism of mouse peritoneal macrophages by intracellular Leishmania spp. Infection and immunity 55, 587-593.

Calabrese, K.S., da Costa, S.C., 1992. Enhancement of Leishmania amazonensis infection in BCG non-responder mice by BCG-antigen specific vaccine. Memorias do Instituto Oswaldo Cruz 87 Suppl 1, 49-56.

Calegari-Silva, T.C., Pereira, R.M., De-Melo, L.D., Saraiva, E.M., Soares, D.C., Bellio, M., Lopes, U.G., 2009. NF-kappaB-mediated repression of iNOS expression in Leishmania amazonensis macrophage infection. Immunology letters 127, 19-26.

Carter, C.R., Whitcomb, J.P., Campbell, J.A., Mukbel, R.M., McDowell, M.A., 2009. Complement receptor 3 deficiency influences lesion progression during Leishmania major infection in BALB/c mice. Infection and immunity 77, 5668-5675.

Carter, K.C., Hutchison, S., Boitelle, A., Murray, H.W., Sundar, S., Mullen, A.B., 2005. Sodium stibogluconate resistance in Leishmania donovani correlates with greater tolerance to macrophage antileishmanial responses and trivalent antimony therapy. Parasitology 131, 747-757.

Carvalho, E.M., Barral, A., Costa, J.M., Bittencourt, A., Marsden, P., 1994. Clinical and immunopathological aspects of disseminated cutaneous leishmaniasis. Acta tropica 56, 315-325.

Cassatella, M.A., Meda, L., Bonora, S., Ceska, M., Constantin, G., 1993. Interleukin 10 (IL-10) inhibits the release of proinflammatory cytokines from human polymorphonuclear leukocytes. Evidence for an autocrine role of tumor necrosis factor and IL-1 beta in mediating the production of IL-8 triggered by lipopolysaccharide. The Journal of experimental medicine 178, 2207-2211.

Chang, Y.C., Segal, B.H., Holland, S.M., Miller, G.F., Kwon-Chung, K.J., 1998. Virulence of catalase-deficient aspergillus nidulans in p47(phox)-/- mice. Implications for fungal pathogenicity and host defense in chronic granulomatous disease. The Journal of clinical investigation 101, 1843-1850.

Cheng, G., Cao, Z., Xu, X., van Meir, E.G., Lambeth, J.D., 2001. Homologs of gp91phox: cloning and tissue expression of Nox3, Nox4, and Nox5. Gene 269, 131-140.

Chessa, T.A., Anderson, K.E., Hu, Y., Xu, Q., Rausch, O., Stephens, L.R., Hawkins, P.T., 2010. Phosphorylation of threonine 154 in p40phox is an important physiological signal for activation of the neutrophil NADPH oxidase. Blood 116, 6027-6036.

Cho, J.S., Pietras, E.M., Garcia, N.C., Ramos, R.I., Farzam, D.M., Monroe, H.R., Magorien, J.E., Blauvelt, A., Kolls, J.K., Cheung, A.L., Cheng, G., Modlin, R.L., Miller, L.S., 2010. IL-17 is essential for host defense against cutaneous Staphylococcus aureus infection in mice. The Journal of clinical investigation 120, 1762-1773.

Chu, N., Thomas, B.N., Patel, S.R., Buxbaum, L.U., 2010. IgG1 is pathogenic in Leishmania mexicana infection. J Immunol 185, 6939-6946.

Clark, R.A., Klebanoff, S.J., 1979. Chemotactic factor inactivation by the myeloperoxidase-hydrogen peroxide-halide system. J Clin Invest 64, 913-920.

Conus, S., Perozzo, R., Reinheckel, T., Peters, C., Scapozza, L., Yousefi, S., Simon, H.U., 2008. Caspase-8 is activated by cathepsin D initiating neutrophil apoptosis during the resolution of inflammation. The Journal of experimental medicine 205, 685-698.

Cortes, D.F., Carneiro, M.B., Santos, L.M., Souza, T.C., Maioli, T.U., Duz, A.L., Ramos-Jorge, M.L., Afonso, L.C., Carneiro, C., Vieira, L.Q., 2010. Low and high-dose intradermal infection with Leishmania major and Leishmania amazonensis in C57BL/6 mice. Memorias do Instituto Oswaldo Cruz 105, 736-745.

Cossarizza, A., Franceschi, C., Monti, D., Salvioli, S., Bellesia, E., Rivabene, R., Biondo, L., Rainaldi, G., Tinari, A., Malorni, W., 1995. Protective effect of N-acetylcysteine in tumor necrosis factor-alpha-induced apoptosis in U937 cells: the role of mitochondria. Experimental cell research 220, 232-240.

Costa, J.M., Marsden, P.D., Llanos-Cuentas, E.A., Netto, E.M., Carvalho, E.M., Barral, A., Rosa, A.C., Cuba, C.C., Magalhaes, A.V., Barreto, A.C., 1986. Disseminated cutaneous leishmaniasis in a field clinic in Bahia, Brazil: a report of eight cases. The Journal of tropical medicine and hygiene 89, 319-323.

Coxon, A., Rieu, P., Barkalow, F.J., Askari, S., Sharpe, A.H., von Andrian, U.H., Arnaout, M.A., Mayadas, T.N., 1996. A novel role for the beta 2 integrin CD11b/CD18 in neutrophil apoptosis: a homeostatic mechanism in inflammation. Immunity 5, 653-666.

Cupolillo, E., Medina-Acosta, E., Noyes, H., Momen, H., Grimaldi, G., Jr., 2000. A revised classification for Leishmania and Endotrypanum. Parasitol Today 16, 142-144.

Da Silva, C.A., Hartl, D., Liu, W., Lee, C.G., Elias, J.A., 2008. TLR-2 and IL-17A in chitin-induced macrophage activation and acute inflammation. J Immunol 181, 4279-4286.

Darrah, P.A., Patel, D.T., De Luca, P.M., Lindsay, R.W., Davey, D.F., Flynn, B.J., Hoff, S.T., Andersen, P., Reed, S.G., Morris, S.L., Roederer, M., Seder, R.A., 2007. Multifunctional TH1 cells define a correlate of vaccine-mediated protection against Leishmania major. Nature medicine 13, 843-850.

Datla, S.R., Peshavariya, H., Dusting, G.J., Mahadev, K., Goldstein, B.J., Jiang, F., 2007. Important role of Nox4 type NADPH oxidase in angiogenic responses in human microvascular endothelial cells in vitro. Arteriosclerosis, thrombosis, and vascular biology 27, 2319-2324.

De Deken, X., Wang, D., Many, M.C., Costagliola, S., Libert, F., Vassart, G., Dumont, J.E., Miot, F., 2000. Cloning of two human thyroid cDNAs encoding new members of the NADPH oxidase family. The Journal of biological chemistry 275, 23227-23233.

Decoursey, T.E., Ligeti, E., 2005. Regulation and termination of NADPH oxidase activity. Cellular and molecular life sciences : CMLS 62, 2173-2193.

Degrossoli, A., Arrais-Silva, W.W., Colhone, M.C., Gadelha, F.R., Joazeiro, P.P., Giorgio, S., 2011. The influence of low oxygen on macrophage response to Leishmania infection. Scandinavian journal of immunology 74, 165-175.

DeLeo, F.R., Burritt, J.B., Yu, L., Jesaitis, A.J., Dinauer, M.C., Nauseef, W.M., 2000. Processing and maturation of flavocytochrome b558 include incorporation of heme as a prerequisite for heterodimer assembly. The Journal of biological chemistry 275, 13986-13993.

Descoteaux, A., Turco, S.J., 1999. Glycoconjugates in Leishmania infectivity. Biochimica et biophysica acta 1455, 341-352.

Desjeux, P., 2001. The increase in risk factors for leishmaniasis worldwide. Transactions of the Royal Society of Tropical Medicine and Hygiene 95, 239-243.

Dinauer, M.C., 2005. Chronic granulomatous disease and other disorders of phagocyte function. Hematology / the Education Program of the American Society of Hematology. American Society of Hematology. Education Program, 89-95.

Dumas, C., Ouellette, M., Tovar, J., Cunningham, M.L., Fairlamb, A.H., Tamar, S., Olivier, M., Papadopoulou, B., 1997. Disruption of the trypanothione reductase gene of Leishmania decreases its ability to survive oxidative stress in macrophages. The EMBO journal 16, 2590-2598.

Dunstan, C.A., Salafranca, M.N., Adhikari, S., Xia, Y., Feng, L., Harrison, J.K., 1996. Identification of two rat genes orthologous to the human interleukin-8 receptors. The Journal of biological chemistry 271, 32770-32776.

Dupuy, C., Ohayon, R., Valent, A., Noel-Hudson, M.S., Deme, D., Virion, A., 1999. Purification of a novel flavoprotein involved in the thyroid NADPH oxidase. Cloning of the porcine and human cdnas. The Journal of biological chemistry 274, 37265-37269.

Ellson, C., Davidson, K., Anderson, K., Stephens, L.R., Hawkins, P.T., 2006. PtdIns3P binding to the PX domain of p40phox is a physiological signal in NADPH oxidase activation. The EMBO journal 25, 4468-4478.

Evans, P., Halliwell, B., 2001. Micronutrients: oxidant/antioxidant status. The British journal of nutrition 85 Suppl 2, S67-74.

Evans, T.G., 1993. Leishmaniasis. Infectious disease clinics of North America 7, 527-546.

Fadeel, B., Ahlin, A., Henter, J.I., Orrenius, S., Hampton, M.B., 1998. Involvement of caspases in neutrophil apoptosis: regulation by reactive oxygen species. Blood 92, 4808-4818.

Fenton, H.J.H., 1894. Oxidation of tartaric acid in presence of iron. J. Chem. Soc., Trans, 11.

Ferrari, C.K., Souto, P.C., Franca, E.L., Honorio-Franca, A.C., 2011. Oxidative and nitrosative stress on phagocytes' function: from effective defense to immunity evasion mechanisms. Archivum immunologiae et therapiae experimentalis 59, 441-448.

Fukai, T., Ushio-Fukai, M., 2011. Superoxide dismutases: role in redox signaling, vascular function, and diseases. Antioxidants & redox signaling 15, 1583-1606.

Gamberale, R., Giordano, M., Trevani, A.S., Andonegui, G., Geffner, J.R., 1998. Modulation of human neutrophil apoptosis by immune complexes. J Immunol 161, 3666-3674.

Geiszt, M., Kapus, A., Nemet, K., Farkas, L., Ligeti, E., 1997. Regulation of capacitative Ca2+ influx in human neutrophil granulocytes. Alterations in chronic granulomatous disease. The Journal of biological chemistry 272, 26471-26478.

Geiszt, M., Kopp, J.B., Varnai, P., Leto, T.L., 2000. Identification of renox, an NAD(P)H oxidase in kidney. Proceedings of the National Academy of Sciences of the United States of America 97, 8010-8014.

Gerdes, J., Lemke, H., Baisch, H., Wacker, H.H., Schwab, U., Stein, H., 1984. Cell cycle analysis of a cell proliferation-associated human nuclear antigen defined by the monoclonal antibody Ki-67. J Immunol 133, 1710-1715.

Gessner, A., Blum, H., Rollinghoff, M., 1993. Differential regulation of IL-9-expression after infection with Leishmania major in susceptible and resistant mice. Immunobiology 189, 419-435.

Ghosh, S., Goswami, S., Adhya, S., 2003. Role of superoxide dismutase in survival of Leishmania within the macrophage. The Biochemical journal 369, 447-452.

Ghosn, E.E., Cassado, A.A., Govoni, G.R., Fukuhara, T., Yang, Y., Monack, D.M., Bortoluci, K.R., Almeida, S.R., Herzenberg, L.A., Herzenberg, L.A., 2010. Two physically, functionally, and developmentally distinct peritoneal macrophage subsets. Proceedings of the National Academy of Sciences of the United States of America 107, 2568-2573.

Gibson-Corley, K.N., Boggiatto, P.M., Mukbel, R.M., Petersen, C.A., Jones, D.E., 2010. A deficiency in the B cell response of C57BL/6 mice correlates with loss of macrophage-mediated killing of Leishmania amazonensis. International journal for parasitology 40, 157-161.

Giorgio, S., Linares, E., Capurro Mde, L., de Bianchi, A.G., Augusto, O., 1996. Formation of nitrosyl hemoglobin and nitrotyrosine during murine leishmaniasis. Photochemistry and photobiology 63, 750-754.

Gollob, K.J., Antonelli, L.R., Faria, D.R., Keesen, T.S., Dutra, W.O., 2008. Immunoregulatory mechanisms and CD4-CD8- (double negative) T cell subpopulations in human cutaneous leishmaniasis: a balancing act between protection and pathology. International immunopharmacology 8, 1338-1343.

Gonzalez, A., Hung, C.Y., Cole, G.T., 2011. Absence of phagocyte NADPH oxidase 2 leads to severe inflammatory response in lungs of mice infected with Coccidioides. Microbial pathogenesis 51, 432-441.

Gorak, P.M., Engwerda, C.R., Kaye, P.M., 1998. Dendritic cells, but not macrophages, produce IL-12 immediately following Leishmania donovani infection. European journal of immunology 28, 687-695.

Goto, H., Prianti, M., 2009. Immunoactivation and immunopathogeny during active visceral leishmaniasis. Revista do Instituto de Medicina Tropical de Sao Paulo 51, 241-246.

Green, L.C., Wagner, D.A., Glogowski, J., Skipper, P.L., Wishnok, J.S., Tannenbaum, S.R., 1982. Analysis of nitrate, nitrite, and [15N]nitrate in biological fluids. Analytical biochemistry 126, 131-138.

Green, S.J., Meltzer, M.S., Hibbs, J.B., Jr., Nacy, C.A., 1990. Activated macrophages destroy intracellular Leishmania major amastigotes by an L-arginine-dependent killing mechanism. J Immunol 144, 278-283.

Guimaraes, E.T., Santos, L.A., Ribeiro dos Santos, R., Teixeira, M.M., dos Santos, W.L., Soares, M.B., 2006. Role of interleukin-4 and prostaglandin E2 in Leishmania amazonensis infection of BALB/c mice. Microbes and infection / Institut Pasteur 8, 1219-1226.

Gutteridge, J.M., Halliwell, B., 1992. Comments on review of Free Radicals in Biology and Medicine, second edition, by Barry Halliwell and John M. C. Gutteridge. Free radical biology & medicine 12, 93-95.

Gyurko, R., Boustany, G., Huang, P.L., Kantarci, A., Van Dyke, T.E., Genco, C.A., Gibson, F.C., 3rd, 2003. Mice lacking inducible nitric oxide synthase demonstrate impaired killing of Porphyromonas gingivalis. Infection and immunity 71, 4917-4924.

Haanen, C., Vermes, I., 1995. Apoptosis and inflammation. Mediators of inflammation 4, 5-15.

Halliwell, B., 2006. Phagocyte-derived reactive species: salvation or suicide? Trends in biochemical sciences 31, 509-515.

Hamasaki, T., Sakano, T., Kobayashi, M., Sakura, N., Ueda, K., Usui, T., 1989. Leukotriene B4 metabolism in neutrophils of patients with chronic granulomatous disease: phorbol myristate acetate decreases endogenous leukotriene B4 via NADPH oxidase-dependent mechanism. European journal of clinical investigation 19, 404-411.

Hampton, M.B., Fadeel, B., Orrenius, S., 1998. Redox regulation of the caspases during apoptosis. Annals of the New York Academy of Sciences 854, 328-335.

Hampton, M.B., Vissers, M.C., Keenan, J.I., Winterbourn, C.C., 2002. Oxidant-mediated phosphatidylserine exposure and macrophage uptake of activated neutrophils: possible impairment in chronic granulomatous disease. Journal of leukocyte biology 71, 775-781.

Handman, E., 1999. Cell biology of Leishmania. Advances in parasitology 44, 1-39.

Happel, K.I., Dubin, P.J., Zheng, M., Ghilardi, N., Lockhart, C., Quinton, L.J., Odden, A.R., Shellito, J.E., Bagby, G.J., Nelson, S., Kolls, J.K., 2005. Divergent roles of IL-23 and IL-12 in host defense against Klebsiella pneumoniae. The Journal of experimental medicine 202, 761-769.

Harbord, M., Novelli, M., Canas, B., Power, D., Davis, C., Godovac-Zimmermann, J., Roes, J., Segal, A.W., 2002. Ym1 is a neutrophil granule protein that crystallizes in p47phox-deficient mice. The Journal of biological chemistry 277, 5468-5475.

Harrison, C.A., Raftery, M.J., Walsh, J., Alewood, P., Iismaa, S.E., Thliveris, S., Geczy, C.L., 1999. Oxidation regulates the inflammatory properties of the murine S100 protein S100A8. The Journal of biological chemistry 274, 8561-8569.

Hatanaka, E., Carvalho, B.T., Condino-Neto, A., Campa, A., 2004. Hyperresponsiveness of neutrophils from gp 91phox deficient patients to lipopolysaccharide and serum amyloid A. Immunology letters 94, 43-46.

Hattori, H., Subramanian, K.K., Sakai, J., Luo, H.R., 2010. Reactive oxygen species as signaling molecules in neutrophil chemotaxis. Communicative & integrative biology 3, 278-281.

Heinzel, F.P., Sadick, M.D., Mutha, S.S., Locksley, R.M., 1991. Production of interferon gamma, interleukin 2, interleukin 4, and interleukin 10 by CD4+ lymphocytes in vivo during healing and progressive murine leishmaniasis. Proceedings of the National Academy of Sciences of the United States of America 88, 7011-7015.

Henderson, W.R., Klebanoff, S.J., 1983. Leukotriene production and inactivation by normal, chronic granulomatous disease and myeloperoxidase-deficient neutrophils. The Journal of biological chemistry 258, 13522-13527.

Herwaldt, B.L., 1999. Leishmaniasis. Lancet 354, 1191-1199.

Heyworth, P.G., Cross, A.R., Curnutte, J.T., 2003. Chronic granulomatous disease. Current opinion in immunology 15, 578-584.

Hill, J.O., 1984. Resistance to cutaneous leishmaniasis: acquired ability of the host to kill parasites at the site of infection. Infection and immunity 45, 127-132.

Hill, J.O., North, R.J., Collins, F.M., 1983. Advantages of measuring changes in the number of viable parasites in murine models of experimental cutaneous leishmaniasis. Infection and immunity 39, 1087-1094.

Hiraoka, W., Vazquez, N., Nieves-Neira, W., Chanock, S.J., Pommier, Y., 1998. Role of oxygen radicals generated by NADPH oxidase in apoptosis induced in human leukemia cells. The Journal of clinical investigation 102, 1961-1968.

Holzmuller, P., Sereno, D., Cavaleyra, M., Mangot, I., Daulouede, S., Vincendeau, P., Lemesre, J.L., 2002. Nitric oxide-mediated proteasome-dependent oligonucleosomal DNA fragmentation in Leishmania amazonensis amastigotes. Infection and immunity 70, 3727-3735.

Hommel, M., 1999. Visceral leishmaniasis: biology of the parasite. The Journal of infection 39, 101-111.

Hooker, J.D., Nguyen, V.H., Taylor, V.M., Cedeno, D.L., Lash, T.D., Jones, M.A., Robledo, S.M., Velez, I.D., 2012. New application for expanded porphyrins: sapphyrin and heterosapphyrins as inhibitors of Leishmania parasites. Photochemistry and photobiology 88, 194-200.

Horta, M.F., Mendes, B.P., Roma, E.H., Noronha, F.S., Macedo, J.P., Oliveira, L.S., Duarte, M.M., Vieira, L.Q., 2012. Reactive oxygen species and nitric oxide in cutaneous leishmaniasis. J Parasitol Res 2012, 203818.

Hoshino, H., Laan, M., Sjostrand, M., Lotvall, J., Skoogh, B.E., Linden, A., 2000. Increased elastase and myeloperoxidase activity associated with neutrophil recruitment by IL-17 in airways in vivo. The Journal of allergy and clinical immunology 105, 143-149.

Huang, W., Na, L., Fidel, P.L., Schwarzenberger, P., 2004. Requirement of interleukin-17A for systemic anti-Candida albicans host defense in mice. The Journal of infectious diseases 190, 624-631.

Huet, S., Groux, H., Caillou, B., Valentin, H., Prieur, A.M., Bernard, A., 1989. CD44 contributes to T cell activation. J Immunol 143, 798-801.

Hulett, M.D., Hogarth, P.M., 1994. Molecular basis of Fc receptor function. Advances in immunology 57, 1-127.

Ji, J., Sun, J., Qi, H., Soong, L., 2002. Analysis of T helper cell responses during infection with Leishmania amazonensis. The American journal of tropical medicine and hygiene 66, 338-345.

Ji, J., Sun, J., Soong, L., 2003. Impaired expression of inflammatory cytokines and chemokines at early stages of infection with Leishmania amazonensis. Infection and immunity 71, 4278-4288.

Jiang, F., Zhang, Y., Dusting, G.J., 2011. NADPH oxidase-mediated redox signaling: roles in cellular stress response, stress tolerance, and tissue repair. Pharmacological reviews 63, 218-242.

Joller, N., Weber, S.S., Oxenius, A., 2011. Antibody-Fc receptor interactions in protection against intracellular pathogens. European journal of immunology 41, 889-897.

Jones, D.E., Ackermann, M.R., Wille, U., Hunter, C.A., Scott, P., 2002. Early enhanced Th1 response after Leishmania amazonensis infection of C57BL/6 interleukin-10-deficient mice does not lead to resolution of infection. Infection and immunity 70, 2151-2158.

Jones, D.E., Buxbaum, L.U., Scott, P., 2000. IL-4-independent inhibition of IL-12 responsiveness during Leishmania amazonensis infection. J Immunol 165, 364-372.

Kane, M.M., Mosser, D.M., 2001. The role of IL-10 in promoting disease progression in leishmaniasis. J Immunol 166, 1141-1147.

Kasahara, Y., Iwai, K., Yachie, A., Ohta, K., Konno, A., Seki, H., Miyawaki, T., Taniguchi, N., 1997. Involvement of reactive oxygen intermediates in spontaneous and CD95 (Fas/APO-1)-mediated apoptosis of neutrophils. Blood 89, 1748-1753.

Kaur, S., Kaur, T., Garg, N., Mukherjee, S., Raina, P., Athokpam, V., 2008. Effect of dose and route of inoculation on the generation of CD4+ Th1/Th2 type of immune response in murine visceral leishmaniasis. Parasitology research 103, 1413-1419.

Kavoosi, G., Ardestani, S.K., Kariminia, A., 2009. The involvement of TLR2 in cytokine and reactive oxygen species (ROS) production by PBMCs in response to Leishmania major phosphoglycans (PGs). Parasitology 136, 1193-1199.

Kedzierski, L., Zhu, Y., Handman, E., 2006. Leishmania vaccines: progress and problems. Parasitology 133 Suppl, S87-112.

Khouri, R., Bafica, A., Silva Mda, P., Noronha, A., Kolb, J.P., Wietzerbin, J., Barral, A., Barral-Netto, M., Van Weyenbergh, J., 2009. IFN-beta impairs superoxide-dependent parasite killing in human macrophages: evidence for a deleterious role of SOD1 in cutaneous leishmaniasis. J Immunol 182, 2525-2531.

Khouri, R., Novais, F., Santana, G., de Oliveira, C.I., Vannier dos Santos, M.A., Barral, A., Barral-Netto, M., Van Weyenbergh, J., 2010. DETC induces Leishmania parasite killing in human in vitro and murine in vivo models: a promising therapeutic alternative in Leishmaniasis. PloS one 5, e14394.

Killick-Kendrick, R., 1990. Phlebotomine vectors of the leishmaniases: a review. Medical and veterinary entomology 4, 1-24.

Kimblin, N., Peters, N., Debrabant, A., Secundino, N., Egen, J., Lawyer, P., Fay, M.P., Kamhawi, S., Sacks, D., 2008. Quantification of the infectious dose of Leishmania major transmitted to the skin by single sand flies. Proceedings of the National Academy of Sciences of the United States of America 105, 10125-10130.

Kinoshita, H., Matsumura, T., Ishii, N., Fukuda, K., Senokuchi, T., Motoshima, H., Kondo, T., Taketa, K., Kawasaki, S., Hanatani, S., Takeya, M., Nishikawa, T., Araki, E., 2013. Apocynin suppresses the progression of atherosclerosis in apoE-deficient mice by inactivation of macrophages. Biochemical and biophysical research communications 431, 124-130.

Kobayashi, S.D., Voyich, J.M., Braughton, K.R., Whitney, A.R., Nauseef, W.M., Malech, H.L., DeLeo, F.R., 2004. Gene expression profiling provides insight into the pathophysiology of chronic granulomatous disease. J Immunol 172, 636-643.

Kobayashi, Y., 2006. Neutrophil infiltration and chemokines. Critical reviews in immunology 26, 307-316.

Kobayashi, Y., 2008. The role of chemokines in neutrophil biology. Frontiers in bioscience : a journal and virtual library 13, 2400-2407.

Koff, J.L., Shao, M.X., Kim, S., Ueki, I.F., Nadel, J.A., 2006. Pseudomonas lipopolysaccharide accelerates wound repair via activation of a novel epithelial cell signaling cascade. J Immunol 177, 8693-8700.

Kunkel, S.L., Standiford, T., Kasahara, K., Strieter, R.M., 1991. Stimulus specific induction of monocyte chemotactic protein-1 (MCP-1) gene expression. Advances in experimental medicine and biology 305, 65-71.

Laroux, F.S., Romero, X., Wetzler, L., Engel, P., Terhorst, C., 2005. Cutting edge: MyD88 controls phagocyte NADPH oxidase function and killing of gram-negative bacteria. J Immunol 175, 5596-5600.

Lawrence, M.B., Springer, T.A., 1991. Leukocytes roll on a selectin at physiologic flow rates: distinction from and prerequisite for adhesion through integrins. Cell 65, 859-873.

Lecoeur, H., Ledru, E., Prevost, M.C., Gougeon, M.L., 1997. Strategies for phenotyping apoptotic peripheral human lymphocytes comparing ISNT, annexin-V and 7-AAD cytofluorometric staining methods. Journal of immunological methods 209, 111-123.

Lekstrom-Himes, J.A., Kuhns, D.B., Alvord, W.G., Gallin, J.I., 2005. Inhibition of human neutrophil IL-8 production by hydrogen peroxide and dysregulation in chronic granulomatous disease. J Immunol 174, 411-417.

Lemos de Souza, V., Ascencao Souza, J., Correia Silva, T.M., Sampaio Tavares Veras, P., Rodrigues de-Freitas, L.A., 2000. Different Leishmania species determine distinct profiles of immune and histopathological responses in CBA mice. Microbes and infection / Institut Pasteur 2, 1807-1815.

Leto, T.L., Adams, A.G., de Mendez, I., 1994. Assembly of the phagocyte NADPH oxidase: binding of Src homology 3 domains to proline-rich targets. Proceedings of the National Academy of Sciences of the United States of America 91, 10650-10654.

Li, Y., Huang, T.T., Carlson, E.J., Melov, S., Ursell, P.C., Olson, J.L., Noble, L.J., Yoshimura, M.P., Berger, C., Chan, P.H., Wallace, D.C., Epstein, C.J., 1995. Dilated cardiomyopathy and neonatal lethality in mutant mice lacking manganese superoxide dismutase. Nature genetics 11, 376-381.

Liew, F.Y., Millott, S., Parkinson, C., Palmer, R.M., Moncada, S., 1990. Macrophage killing of Leishmania parasite in vivo is mediated by nitric oxide from L-arginine. J Immunol 144, 4794-4797.

Lima, G.M., Vallochi, A.L., Silva, U.R., Bevilacqua, E.M., Kiffer, M.M., Abrahamsohn, I.A., 1998. The role of polymorphonuclear leukocytes in the resistance to cutaneous Leishmaniasis. Immunology letters 64, 145-151.

Linares, E., Giorgio, S., Augusto, O., 2008. Inhibition of in vivo leishmanicidal mechanisms by tempol: nitric oxide down-regulation and oxidant scavenging. Free radical biology & medicine 44, 1668-1676.

Linares, E., Giorgio, S., Mortara, R.A., Santos, C.X., Yamada, A.T., Augusto, O., 2001. Role of peroxynitrite in macrophage microbicidal mechanisms in vivo revealed by protein nitration and hydroxylation. Free radical biology & medicine 30, 1234-1242.

Lira, S.A., Zalamea, P., Heinrich, J.N., Fuentes, M.E., Carrasco, D., Lewin, A.C., Barton, D.S., Durham, S., Bravo, R., 1994. Expression of the chemokine N51/KC in the thymus and epidermis of transgenic mice results in marked infiltration of a single class of inflammatory cells. The Journal of experimental medicine 180, 2039-2048.

Locksley, R.M., Heinzel, F.P., Sadick, M.D., Holaday, B.J., Gardner, K.D., Jr., 1987. Murine cutaneous leishmaniasis: susceptibility correlates with differential expansion of helper T-cell subsets. Annales de l'Institut Pasteur. Immunology 138, 744-749.

Lodge, R., Diallo, T.O., Descoteaux, A., 2006. Leishmania donovani lipophosphoglycan blocks NADPH oxidase assembly at the phagosome membrane. Cellular microbiology 8, 1922-1931.

Lopes, M.V., Desoti, V.C., Caleare Ade, O., Ueda-Nakamura, T., Silva, S.O., Nakamura, C.V., 2012. Mitochondria Superoxide Anion Production Contributes to Geranylgeraniol-Induced Death in Leishmania amazonensis. Evidence-based complementary and alternative medicine : eCAM 2012, 298320.

Lowry, O.H., Rosebrough, N.J., Farr, A.L., Randall, R.J., 1951. Protein measurement with the Folin phenol reagent. J Biol Chem 193, 265-275.

Lumsden, W.H., 1974. Letter: Biochemical taxonomy of Leishmania. Transactions of the Royal Society of Tropical Medicine and Hygiene 68, 74-75.

Mahmoudzadeh-Niknam, H., Khalili, G., Abrishami, F., Najafy, A., Khaze, V., 2013. The Route of Leishmania tropica Infection Determines Disease Outcome and Protection against Leishmania major in BALB/c Mice. The Korean journal of parasitology 51, 69-74.

Maioli, T.U., Carneiro, C.M., Assis, F.A., Faria, A.M., 2007. Splenectomy does not interfere with immune response to Leishmania major infection in mice. Cellular immunology 249, 1-7.

Maioli, T.U., Takane, E., Arantes, R.M., Fietto, J.L., Afonso, L.C., 2004. Immune response induced by New World Leishmania species in C57BL/6 mice. Parasitology research 94, 207-212.

Marriott, H.M., Jackson, L.E., Wilkinson, T.S., Simpson, A.J., Mitchell, T.J., Buttle, D.J., Cross, S.S., Ince, P.G., Hellewell, P.G., Whyte, M.K., Dockrell, D.H., 2008. Reactive oxygen species regulate neutrophil recruitment and survival in pneumococcal pneumonia. American journal of respiratory and critical care medicine 177, 887-895.

Matthews, D.J., Emson, C.L., McKenzie, G.J., Jolin, H.E., Blackwell, J.M., McKenzie, A.N., 2000. IL-13 is a susceptibility factor for Leishmania major infection. J Immunol 164, 1458-1462.

Matute, J.D., Arias, A.A., Wright, N.A., Wrobel, I., Waterhouse, C.C., Li, X.J., Marchal, C.C., Stull, N.D., Lewis, D.B., Steele, M., Kellner, J.D., Yu, W., Meroueh, S.O., Nauseef, W.M., Dinauer, M.C., 2009. A new genetic subgroup of chronic granulomatous disease with autosomal recessive mutations in p40 phox and selective defects in neutrophil NADPH oxidase activity. Blood 114, 3309-3315.

Mauricio, I.L., Stothard, J.R., Miles, M.A., 2000. The strange case of Leishmania chagasi. Parasitol Today 16, 188-189.

Metcalfe, D.D., Thompson, H.L., Klebanoff, S.J., Henderson, W.R., Jr., 1990. Oxidative degradation of rat mast-cell heparin proteoglycan. The Biochemical journal 272, 51-57.

Miyairi, I., Tatireddigari, V.R., Mahdi, O.S., Rose, L.A., Belland, R.J., Lu, L., Williams, R.W., Byrne, G.I., 2007. The p47 GTPases Iigp2 and Irgb10 regulate innate immunity and inflammation to murine Chlamydia psittaci infection. J Immunol 179, 1814-1824.

Mizrahi, A., Berdichevsky, Y., Ugolev, Y., Molshanski-Mor, S., Nakash, Y., Dahan, I., Alloul, N., Gorzalczany, Y., Sarfstein, R., Hirshberg, M., Pick, E., 2006. Assembly of the phagocyte NADPH oxidase complex: chimeric constructs derived from the cytosolic components as tools for exploring structure-function relationships. Journal of leukocyte biology 79, 881-895.

Moll, H., Fuchs, H., Blank, C., Rollinghoff, M., 1993. Langerhans cells transport Leishmania major from the infected skin to the draining lymph node for presentation to antigen-specific T cells. European journal of immunology 23, 1595-1601.

Mosser, D.M., Edelson, P.J., 1987. The third component of complement (C3) is responsible for the intracellular survival of Leishmania major. Nature 327, 329-331.

Mosser, D.M., Vlassara, H., Edelson, P.J., Cerami, A., 1987. Leishmania promastigotes are recognized by the macrophage receptor for advanced glycosylation endproducts. The Journal of experimental medicine 165, 140-145.

Mukbel, R., Petersen, C.A., Jones, D.E., 2006. Soluble factors from Leishmania major-specific CD4+T cells and B cells limit L. amazonensis amastigote survival within infected macrophages. Microbes and infection / Institut Pasteur 8, 2547-2555.

Mukbel, R.M., Patten, C., Jr., Gibson, K., Ghosh, M., Petersen, C., Jones, D.E., 2007. Macrophage killing of Leishmania amazonensis amastigotes requires both nitric oxide and superoxide. The American journal of tropical medicine and hygiene 76, 669-675.

Mukherjee, S., Bandyapadhyay, R., Basu, M.K., 1988. Leishmania donovani: superoxide dismutase level in infected macrophages. Bioscience reports 8, 131-137.

Murray, H.W., 1982. Cell-mediated immune response in experimental visceral leishmaniasis. II. Oxygen-dependent killing of intracellular Leishmania donovani amastigotes. J Immunol 129, 351-357.

Murray, H.W., 2002. Kala-azar--progress against a neglected disease. The New England journal of medicine 347, 1793-1794.

Murray, H.W., Nathan, C.F., 1999. Macrophage microbicidal mechanisms in vivo: reactive nitrogen versus oxygen intermediates in the killing of intracellular visceral Leishmania donovani. The Journal of experimental medicine 189, 741-746.

Murray, H.W., Xiang, Z., Ma, X., 2006. Responses to Leishmania donovani in mice deficient in both phagocyte oxidase and inducible nitric oxide synthase. The American journal of tropical medicine and hygiene 74, 1013-1015.

Nabors, G.S., Farrell, J.P., 1994. Site-specific immunity to Leishmania major in SWR mice: the site of infection influences susceptibility and expression of the antileishmanial immune response. Infection and immunity 62, 3655-3662.

Naderer, T., Vince, J.E., McConville, M.J., 2004. Surface determinants of Leishmania parasites and their role in infectivity in the mammalian host. Current molecular medicine 4, 649-665.

Nauseef, W.M., 2004. Assembly of the phagocyte NADPH oxidase. Histochemistry and cell biology 122, 277-291.

Neal, R.A., Bray, R.S., 1983. Leishmania enriettii. Transactions of the Royal Society of Tropical Medicine and Hygiene 77, 426.

Niethammer, P., Grabher, C., Look, A.T., Mitchison, T.J., 2009. A tissue-scale gradient of hydrogen peroxide mediates rapid wound detection in zebrafish. Nature 459, 996-999.

Olivier, M., Baimbridge, K.G., Reiner, N.E., 1992a. Stimulus-response coupling in monocytes infected with Leishmania. Attenuation of calcium transients is related to defective agonist-induced accumulation of inositol phosphates. J Immunol 148, 1188-1196.

Olivier, M., Brownsey, R.W., Reiner, N.E., 1992b. Defective stimulus-response coupling in human monocytes infected with Leishmania donovani is associated with altered activation and translocation of protein kinase C. Proceedings of the National Academy of Sciences of the United States of America 89, 7481-7485.

Ottonello, L., Frumento, G., Arduino, N., Bertolotto, M., Dapino, P., Mancini, M., Dallegri, F., 2002. Differential regulation of spontaneous and immune complex-induced neutrophil apoptosis by proinflammatory cytokines. Role of oxidants, Bax and caspase-3. Journal of leukocyte biology 72, 125-132.

Padigel, U.M., Alexander, J., Farrell, J.P., 2003. The role of interleukin-10 in susceptibility of BALB/c mice to infection with Leishmania mexicana and Leishmania amazonensis. J Immunol 171, 3705-3710.

Paiva, C.N., Feijo, D.F., Dutra, F.F., Carneiro, V.C., Freitas, G.B., Alves, L.S., Mesquita, J., Fortes, G.B., Figueiredo, R.T., Souza, H.S., Fantappie, M.R., Lannes-Vieira, J., Bozza, M.T., 2012. Oxidative stress fuels Trypanosoma cruzi infection in mice. The Journal of clinical investigation 122, 2531-2542.

Palmer, R.M., Rees, D.D., Ashton, D.S., Moncada, S., 1988. L-arginine is the physiological precursor for the formation of nitric oxide in endothelium-dependent relaxation. Biochemical and biophysical research communications 153, 1251-1256.

Patton, L.M., Saggart, B.S., Ahmed, N.K., Leff, J.A., Repine, J.E., 1995. Interleukin-1 beta-induced neutrophil recruitment and acute lung injury in hamsters. Inflammation 19, 23-29.

Pawate, S., Shen, Q., Fan, F., Bhat, N.R., 2004. Redox regulation of glial inflammatory response to lipopolysaccharide and interferongamma. Journal of neuroscience research 77, 540-551.

Pereira, B.A., Alves, C.R., 2008. Immunological characteristics of experimental murine infection with Leishmania (Leishmania) amazonensis. Veterinary parasitology 158, 239-255.

Peshavariya, H., Dusting, G.J., Jiang, F., Halmos, L.R., Sobey, C.G., Drummond, G.R., Selemidis, S., 2009. NADPH oxidase isoform selective regulation of endothelial cell proliferation and survival. Naunyn-Schmiedeberg's archives of pharmacology 380, 193-204.

Peters, N., Sacks, D., 2006. Immune privilege in sites of chronic infection: Leishmania and regulatory T cells. Immunological reviews 213, 159-179.

Peters, N.C., Egen, J.G., Secundino, N., Debrabant, A., Kimblin, N., Kamhawi, S., Lawyer, P., Fay, M.P., Germain, R.N., Sacks, D., 2008. In vivo imaging reveals an essential role for neutrophils in leishmaniasis transmitted by sand flies. Science 321, 970-974.

Peters, N.C., Sacks, D.L., 2009. The impact of vector-mediated neutrophil recruitment on cutaneous leishmaniasis. Cellular microbiology 11, 1290-1296.

Petersen, E.A., Neva, F.A., Oster, C.N., Bogaert Diaz, H., 1982. Specific inhibition of lymphocyte-proliferation responses by adherent suppressor cells in diffuse cutaneous leishmaniasis. The New England journal of medicine 306, 387-392.

Pham, N.K., Mouriz, J., Kima, P.E., 2005. Leishmania pifanoi amastigotes avoid macrophage production of superoxide by inducing heme degradation. Infection and immunity 73, 8322-8333.

Pierce, G.B., Parchment, R.E., Lewellyn, A.L., 1991. Hydrogen peroxide as a mediator of programmed cell death in the blastocyst. Differentiation; research in biological diversity 46, 181-186.

Pinheiro, R.O., Rossi-Bergmann, B., 2007. Interferon-gamma is required for the late but not early control of Leishmania amazonensis infection in C57Bl/6 mice. Memorias do Instituto Oswaldo Cruz 102, 79-82.

Plewes, K.A., Barr, S.D., Gedamu, L., 2003. Iron superoxide dismutases targeted to the glycosomes of Leishmania chagasi are important for survival. Infection and immunity 71, 5910-5920.

Pollock, J.D., Williams, D.A., Gifford, M.A., Li, L.L., Du, X., Fisherman, J., Orkin, S.H., Doerschuk, C.M., Dinauer, M.C., 1995. Mouse model of X-linked chronic granulomatous disease, an inherited defect in phagocyte superoxide production. Nature genetics 9, 202-209.

Pratt, D.M., David, J.R., 1981. Monoclonal antibodies that distinguish between New World species of Leishmania. Nature 291, 581-583.

Proudfoot, L., Nikolaev, A.V., Feng, G.J., Wei, W.Q., Ferguson, M.A., Brimacombe, J.S., Liew, F.Y., 1996. Regulation of the expression of nitric oxide synthase and leishmanicidal activity by glycoconjugates of Leishmania lipophosphoglycan in murine macrophages. Proceedings of the National Academy of Sciences of the United States of America 93, 10984-10989.

Proudfoot, L., O'Donnell, C.A., Liew, F.Y., 1995. Glycoinositolphospholipids of Leishmania major inhibit nitric oxide synthesis and reduce leishmanicidal activity in murine macrophages. European journal of immunology 25, 745-750.

Purushothaman, D., Sarin, A., 2009. Cytokine-dependent regulation of NADPH oxidase activity and the consequences for activated T cell homeostasis. The Journal of experimental medicine 206, 1515-1523.

Qi, H., Ji, J., Wanasen, N., Soong, L., 2004. Enhanced replication of Leishmania amazonensis amastigotes in gamma interferon-stimulated murine macrophages: implications for the pathogenesis of cutaneous leishmaniasis. Infection and immunity 72, 988-995.

Qian, Y., Liu, K.J., Chen, Y., Flynn, D.C., Castranova, V., Shi, X., 2005. Cdc42 regulates arsenic-induced NADPH oxidase activation and cell migration through actin filament reorganization. The Journal of biological chemistry 280, 3875-3884.

Rada, B., Leto, T.L., 2008. Oxidative innate immune defenses by Nox/Duox family NADPH oxidases. Contributions to microbiology 15, 164-187.

Rada, B.K., Geiszt, M., Van Bruggen, R., Nemet, K., Roos, D., Ligeti, E., 2003. Calcium signalling is altered in myeloid cells with a deficiency in NADPH oxidase activity. Clinical and experimental immunology 132, 53-60.

Reiner, S.L., Zheng, S., Wang, Z.E., Stowring, L., Locksley, R.M., 1994. Leishmania promastigotes evade interleukin 12 (IL-12) induction by macrophages and stimulate a broad range of cytokines from CD4+ T cells during initiation of infection. The Journal of experimental medicine 179, 447-456.

Repine, J.E., Fox, R.B., Berger, E.M., 1981. Hydrogen peroxide kills Staphylococcus aureus by reacting with staphylococcal iron to form hydroxyl radical. The Journal of biological chemistry 256, 7094-7096.

Reybier, K., Ribaut, C., Coste, A., Launay, J., Fabre, P.L., Nepveu, F., 2010. Characterization of oxidative stress in Leishmaniasis-infected or LPS-stimulated macrophages using electrochemical impedance spectroscopy. Biosensors & bioelectronics 25, 2566-2572.

Ribeiro-Gomes, F.L., Moniz-de-Souza, M.C., Alexandre-Moreira, M.S., Dias, W.B., Lopes, M.F., Nunes, M.P., Lungarella, G., DosReis, G.A., 2007. Neutrophils activate macrophages for intracellular killing of Leishmania major through recruitment of TLR4 by neutrophil elastase. J Immunol 179, 3988-3994.

Ribeiro-Gomes, F.L., Peters, N.C., Debrabant, A., Sacks, D.L., 2012. Efficient capture of infected neutrophils by dendritic cells in the skin inhibits the early anti-leishmania response. PLoS pathogens 8, e1002536.

Ribeiro-Gomes, F.L., Sacks, D., 2012. The influence of early neutrophil-Leishmania interactions on the host immune response to infection. Frontiers in cellular and infection microbiology 2, 59.

Richter, Y., Groothuis, A., Seifert, P., Edelman, E.R., 2004. Dynamic flow alterations dictate leukocyte adhesion and response to endovascular interventions. The Journal of clinical investigation 113, 1607-1614.

Rioux, J.A., Lanotte, G., Serres, E., Pratlong, F., Bastien, P., Perieres, J., 1990. Taxonomy of Leishmania. Use of isoenzymes. Suggestions for a new classification. Annales de parasitologie humaine et comparee 65, 111-125.

Rodriguez, P.G., Felix, F.N., Woodley, D.T., Shim, E.K., 2008. The role of oxygen in wound healing: a review of the literature. Dermatologic surgery : official publication for American Society for Dermatologic Surgery [et al.] 34, 1159-1169.

Romani, L., Fallarino, F., De Luca, A., Montagnoli, C., D'Angelo, C., Zelante, T., Vacca, C., Bistoni, F., Fioretti, M.C., Grohmann, U., Segal, B.H., Puccetti, P., 2008. Defective tryptophan catabolism underlies inflammation in mouse chronic granulomatous disease. Nature 451, 211-215.

Rose-John, S., Waetzig, G.H., Scheller, J., Grotzinger, J., Seegert, D., 2007. The IL-6/sIL-6R complex as a novel target for therapeutic approaches. Expert opinion on therapeutic targets 11, 613-624.

Sacks, D., Noben-Trauth, N., 2002. The immunology of susceptibility and resistance to Leishmania major in mice. Nature reviews. Immunology 2, 845-858.

Sacks, D.L., Melby, P.C., 2001. Animal models for the analysis of immune responses to leishmaniasis. Current protocols in immunology / edited by John E. Coligan ... [et al.] Chapter 19, Unit 19 12.

Sakaguchi, S., Yamaguchi, T., Nomura, T., Ono, M., 2008. Regulatory T cells and immune tolerance. Cell 133, 775-787.

Sanmun, D., Witasp, E., Jitkaew, S., Tyurina, Y.Y., Kagan, V.E., Ahlin, A., Palmblad, J., Fadeel, B., 2009. Involvement of a functional NADPH oxidase in neutrophils and macrophages during programmed cell clearance: implications for chronic granulomatous disease. American journal of physiology. Cell physiology 297, C621-631.

Santiago, H.C., Oliveira, C.F., Santiago, L., Ferraz, F.O., de Souza, D.G., de-Freitas, L.A., Afonso, L.C., Teixeira, M.M., Gazzinelli, R.T., Vieira, L.Q., 2004. Involvement of the chemokine RANTES (CCL5) in resistance to experimental infection with Leishmania major. Infection and immunity 72, 4918-4923.

Scaffidi, P., Misteli, T., Bianchi, M.E., 2002. Release of chromatin protein HMGB1 by necrotic cells triggers inflammation. Nature 418, 191-195.

Schappi, M., Deffert, C., Fiette, L., Gavazzi, G., Herrmann, F., Belli, D., Krause, K.H., 2008. Branched fungal beta-glucan causes hyperinflammation and necrosis in phagocyte NADPH oxidase-deficient mice. The Journal of pathology 214, 434-444.

Scheel-Toellner, D., Wang, K., Craddock, R., Webb, P.R., McGettrick, H.M., Assi, L.K., Parkes, N., Clough, L.E., Gulbins, E., Salmon, M., Lord, J.M., 2004. Reactive oxygen species limit neutrophil life span by activating death receptor signaling. Blood 104, 2557-2564.

Schmidt, K.N., Amstad, P., Cerutti, P., Baeuerle, P.A., 1995. The roles of hydrogen peroxide and superoxide as messengers in the activation of transcription factor NF-kappa B. Chemistry & biology 2, 13-22.

Schreck, R., Baeuerle, P.A., 1991. A role for oxygen radicals as second messengers. Trends in cell biology 1, 39-42.

Schubert, L.A., Jeffery, E., Zhang, Y., Ramsdell, F., Ziegler, S.F., 2001. Scurfin (FOXP3) acts as a repressor of transcription and regulates T cell activation. The Journal of biological chemistry 276, 37672-37679.

Schwabe, R.F., Seki, E., Brenner, D.A., 2006. Toll-like receptor signaling in the liver. Gastroenterology 130, 1886-1900.

Scott, P., 1993. IL-12: initiation cytokine for cell-mediated immunity. Science 260, 496-497.

Scott, P., Natovitz, P., Coffman, R.L., Pearce, E., Sher, A., 1988. Immunoregulation of cutaneous leishmaniasis. T cell lines that transfer protective immunity or exacerbation belong to different T helper subsets and respond to distinct parasite antigens. The Journal of experimental medicine 168, 1675-1684.

Scott, P., Sher, A., 1986. A spectrum in the susceptibility of leishmanial strains to intracellular killing by murine macrophages. J Immunol 136, 1461-1466.

Segal, A.W., 2005. How neutrophils kill microbes. Annual review of immunology 23, 197-223.

Segal, B.H., Han, W., Bushey, J.J., Joo, M., Bhatti, Z., Feminella, J., Dennis, C.G., Vethanayagam, R.R., Yull, F.E., Capitano, M., Wallace, P.K., Minderman, H., Christman, J.W., Sporn, M.B., Chan, J., Vinh, D.C., Holland, S.M., Romani, L.R., Gaffen, S.L., Freeman, M.L., Blackwell, T.S., 2010. NADPH oxidase limits innate immune responses in the lungs in mice. PloS one 5, e9631.

Serhan, C.N., Brain, S.D., Buckley, C.D., Gilroy, D.W., Haslett, C., O'Neill, L.A., Perretti, M., Rossi, A.G., Wallace, J.L., 2007. Resolution of inflammation: state of the art, definitions and terms. FASEB journal : official publication of the Federation of American Societies for Experimental Biology 21, 325-332.

Shatwell, K.P., Segal, A.W., 1996. NADPH oxidase. The international journal of biochemistry & cell biology 28, 1191-1195.

Silveira, F.T., Blackwell, J.M., Ishikawa, E.A., Braga, R., Shaw, J.J., Quinnell, R.J., Soong, L., Kima, P., McMahon-Pratt, D., Black, G.F., Shaw, M.A., 1998. T cell responses to crude and defined leishmanial antigens in patients from the lower Amazon region of Brazil infected with different species of Leishmania of the subgenera Leishmania and Viannia. Parasite immunology 20, 19-26.

Silveira, F.T., Lainson, R., Corbett, C.E., 2004. Clinical and immunopathological spectrum of American cutaneous leishmaniasis with special reference to the disease in Amazonian Brazil: a review. Memorias do Instituto Oswaldo Cruz 99, 239-251.

Silveira, F.T., Lainson, R., Corbett, C.E., 2005. Further observations on clinical, histopathological, and immunological features of borderline disseminated cutaneous leishmaniasis caused by Leishmania (Leishmania) amazonensis. Memorias do Instituto Oswaldo Cruz 100, 525-534.

Silveira, F.T., Lainson, R., De Castro Gomes, C.M., Laurenti, M.D., Corbett, C.E., 2009. Immunopathogenic competences of Leishmania (V.) braziliensis and L. (L.) amazonensis in American cutaneous leishmaniasis. Parasite immunology 31, 423-431.

Silveira, F.T., Lainson, R., Shaw, J.J., De Souza, A.A., Ishikawa, E.A., Braga, R.R., 1991. Cutaneous leishmaniasis due to Leishmania (Leishmania) amazonensis in Amazonian Brazil, and the significance of a negative Montenegro skin-test in human infections. Transactions of the Royal Society of Tropical Medicine and Hygiene 85, 735-738.

Sinha, P.K., Pandey, K., Bhattacharya, S.K., 2005. Diagnosis & management of leishmania/HIV co-infection. The Indian journal of medical research 121, 407-414.

Smelt, S.C., Cotterell, S.E., Engwerda, C.R., Kaye, P.M., 2000. B cell-deficient mice are highly resistant to Leishmania donovani infection, but develop neutrophil-mediated tissue pathology. J Immunol 164, 3681-3688.

Sojka, D.K., Lazarski, C.A., Huang, Y.H., Bromberg, I., Hughson, A., Fowell, D.J., 2009. Regulation of immunity at tissue sites of inflammation. Immunologic research 45, 239-250.

Song, C., Luo, L., Lei, Z., Li, B., Liang, Z., Liu, G., Li, D., Zhang, G., Huang, B., Feng, Z.H., 2008. IL-17-producing alveolar macrophages mediate allergic lung inflammation related to asthma. J Immunol 181, 6117-6124.

Soong, L., Chang, C.H., Sun, J., Longley, B.J., Jr., Ruddle, N.H., Flavell, R.A., McMahon-Pratt, D., 1997. Role of CD4+ T cells in pathogenesis associated with Leishmania amazonensis infection. J Immunol 158, 5374-5383.

Soong, L., Henard, C.A., Melby, P.C., 2012. Immunopathogenesis of non-healing American cutaneous leishmaniasis and progressive visceral leishmaniasis. Seminars in immunopathology 34, 735-751.

Sorensen, A.L., Hey, A.S., Kharazmi, A., 1994. Leishmania major surface protease Gp63 interferes with the function of human monocytes and neutrophils in vitro. APMIS : acta pathologica, microbiologica, et immunologica Scandinavica 102, 265-271.

Sousa-Franco, J., Araujo-Mendes, E., Silva-Jardim, I., J, L.S., Faria, D.R., Dutra, W.O., Horta, M.F., 2006. Infection-induced respiratory burst in BALB/c macrophages kills Leishmania guyanensis amastigotes through apoptosis: possible involvement in resistance to cutaneous leishmaniasis. Microbes and infection / Institut Pasteur 8, 390-400.

Spath, G.F., Garraway, L.A., Turco, S.J., Beverley, S.M., 2003. The role(s) of lipophosphoglycan (LPG) in the establishment of Leishmania major infections in mammalian hosts. Proceedings of the National Academy of Sciences of the United States of America 100, 9536-9541.

Spinner, J.L., Seo, K.S., O'Loughlin, J.L., Cundiff, J.A., Minnich, S.A., Bohach, G.A., Kobayashi, S.D., 2010. Neutrophils are resistant to Yersinia YopJ/P-induced apoptosis and are protected from ROS-mediated cell death by the type III secretion system. PloS one 5, e9279.

Stefani, M.M., Muller, I., Louis, J.A., 1994. Leishmania major-specific CD8+ T cells are inducers and targets of nitric oxide produced by parasitized macrophages. European journal of immunology 24, 746-752.

Stevens, E.A., Bradfield, C.A., 2008. Immunology: T cells hang in the balance. Nature 453, 46-47.

Stolk, J., Hiltermann, T.J., Dijkman, J.H., Verhoeven, A.J., 1994. Characteristics of the inhibition of NADPH oxidase activation in neutrophils by apocynin, a methoxy-substituted catechol. American journal of respiratory cell and molecular biology 11, 95-102.

Suh, Y.A., Arnold, R.S., Lassegue, B., Shi, J., Xu, X., Sorescu, D., Chung, A.B., Griendling, K.K., Lambeth, J.D., 1999. Cell transformation by the superoxide-generating oxidase Mox1. Nature 401, 79-82.

Sun, S.Y., 2010. N-acetylcysteine, reactive oxygen species and beyond. Cancer Biol Ther 9, 109-110.

Szabo, S.J., Sullivan, B.M., Stemmann, C., Satoskar, A.R., Sleckman, B.P., Glimcher, L.H., 2002. Distinct effects of T-bet in TH1 lineage commitment and IFN-gamma production in CD4 and CD8 T cells. Science 295, 338-342.

Tabbara, K.S., Peters, N.C., Afrin, F., Mendez, S., Bertholet, S., Belkaid, Y., Sacks, D.L., 2005. Conditions influencing the efficacy of vaccination with live organisms against Leishmania major infection. Infection and immunity 73, 4714-4722.

Tacchini-Cottier, F., Zweifel, C., Belkaid, Y., Mukankundiye, C., Vasei, M., Launois, P., Milon, G., Louis, J.A., 2000. An immunomodulatory function for neutrophils during the induction of a CD4+ Th2 response in BALB/c mice infected with Leishmania major. J Immunol 165, 2628-2636.

Talley, A.K., Dewhurst, S., Perry, S.W., Dollard, S.C., Gummuluru, S., Fine, S.M., New, D., Epstein, L.G., Gendelman, H.E., Gelbard, H.A., 1995. Tumor necrosis factor alpha-induced apoptosis in human neuronal cells: protection by the antioxidant N-acetylcysteine and the genes bcl-2 and crmA. Molecular and cellular biology 15, 2359-2366.

Tandara, A.A., Mustoe, T.A., 2004. Oxygen in wound healing--more than a nutrient. World journal of surgery 28, 294-300.

Thalhofer, C.J., Chen, Y., Sudan, B., Love-Homan, L., Wilson, M.E., 2011. Leukocytes infiltrate the skin and draining lymph nodes in response to the protozoan Leishmania infantum chagasi. Infection and immunity 79, 108-117.

Titus, R.G., Marchand, M., Boon, T., Louis, J.A., 1985. A limiting dilution assay for quantifying Leishmania major in tissues of infected mice. Parasite immunology 7, 545-555.

Tuon, F.F., Amato, V.S., Bacha, H.A., Almusawi, T., Duarte, M.I., Amato Neto, V., 2008. Toll-like receptors and leishmaniasis. Infection and immunity 76, 866-872.

Turetz, M.L., Machado, P.R., Ko, A.I., Alves, F., Bittencourt, A., Almeida, R.P., Mobashery, N., Johnson, W.D., Jr., Carvalho, E.M., 2002. Disseminated leishmaniasis: a new and emerging form of leishmaniasis observed in northeastern Brazil. The Journal of infectious diseases 186, 1829-1834.

van de Loo, F.A., Bennink, M.B., Arntz, O.J., Smeets, R.L., Lubberts, E., Joosten, L.A., van Lent, P.L., Coenen-de Roo, C.J., Cuzzocrea, S., Segal, B.H., Holland, S.M., van den Berg, W.B., 2003. Deficiency of NADPH oxidase components p47phox and gp91phox caused granulomatous synovitis and increased connective tissue destruction in experimental arthritis models. The American journal of pathology 163, 1525-1537.

van den Berg, J.M., van Koppen, E., Ahlin, A., Belohradsky, B.H., Bernatowska, E., Corbeel, L., Espanol, T., Fischer, A., Kurenko-Deptuch, M., Mouy, R., Petropoulou, T., Roesler, J., Seger, R., Stasia, M.J., Valerius, N.H., Weening, R.S., Wolach, B., Roos, D., Kuijpers, T.W., 2009. Chronic granulomatous disease: the European experience. PloS one 4, e5234.

von Gunten, S., Yousefi, S., Seitz, M., Jakob, S.M., Schaffner, T., Seger, R., Takala, J., Villiger, P.M., Simon, H.U., 2005. Siglec-9 transduces apoptotic and nonapoptotic death signals into neutrophils depending on the proinflammatory cytokine environment. Blood 106, 1423-1431.

von Stebut, E., Belkaid, Y., Jakob, T., Sacks, D.L., Udey, M.C., 1998. Uptake of Leishmania major amastigotes results in activation and interleukin 12 release from murine skin-derived dendritic cells: implications for the initiation of anti-Leishmania immunity. The Journal of experimental medicine 188, 1547-1552.

Wallach, D., Varfolomeev, E.E., Malinin, N.L., Goltsev, Y.V., Kovalenko, A.V., Boldin, M.P., 1999. Tumor necrosis factor receptor and Fas signaling mechanisms. Annual review of immunology 17, 331-367.

Wanderley, J.L., Moreira, M.E., Benjamin, A., Bonomo, A.C., Barcinski, M.A., 2006. Mimicry of apoptotic cells by exposing phosphatidylserine participates in the establishment of amastigotes of Leishmania (L) amazonensis in mammalian hosts. J Immunol 176, 1834-1839.

Wang, X., Feuerstein, G.Z., Gu, J.L., Lysko, P.G., Yue, T.L., 1995. Interleukin-1 beta induces expression of adhesion molecules in human vascular smooth muscle cells and enhances adhesion of leukocytes to smooth muscle cells. Atherosclerosis 115, 89-98.

Warris, A., Netea, M.G., Wang, J.E., Gaustad, P., Kullberg, B.J., Verweij, P.E., Abrahamsen, T.G., 2003. Cytokine release in healthy donors and patients with chronic granulomatous disease upon stimulation with Aspergillus fumigatus. Scandinavian journal of infectious diseases 35, 482-487.

Watson, R.W., Rotstein, O.D., Jimenez, M., Parodo, J., Marshall, J.C., 1997. Augmented intracellular glutathione inhibits Fas-triggered apoptosis of activated human neutrophils. Blood 89, 4175-4181.

Wei, X.Q., Charles, I.G., Smith, A., Ure, J., Feng, G.J., Huang, F.P., Xu, D., Muller, W., Moncada, S., Liew, F.Y., 1995. Altered immune responses in mice lacking inducible nitric oxide synthase. Nature 375, 408-411.

Wheeler, M.L., Defranco, A.L., 2012. Prolonged production of reactive oxygen species in response to B cell receptor stimulation promotes B cell activation and proliferation. J Immunol 189, 4405-4416.

WHO, 2013. World Heath Organization. Fact sheet #375.

Will, A., Blank, C., Rollinghoff, M., Moll, H., 1992. Murine epidermal Langerhans cells are potent stimulators of an antigen-specific T cell response to Leishmania major, the cause of cutaneous leishmaniasis. European journal of immunology 22, 1341-1347.

Wilson, M.E., Jeronimo, S.M., Pearson, R.D., 2005. Immunopathogenesis of infection with the visceralizing Leishmania species. Microbial pathogenesis 38, 147-160.

Winkelstein, J.A., Marino, M.C., Johnston, R.B., Jr., Boyle, J., Curnutte, J., Gallin, J.I., Malech, H.L., Holland, S.M., Ochs, H., Quie, P., Buckley, R.H., Foster, C.B., Chanock, S.J., Dickler, H., 2000. Chronic granulomatous disease. Report on a national registry of 368 patients. Medicine 79, 155-169.

Winterbourn, C.C., 2002. Biological reactivity and biomarkers of the neutrophil oxidant, hypochlorous acid. Toxicology 181-182, 223-227.

Wong, H.L., Shimamoto, K., 2009. Sending ROS on a bullet train. Science signaling 2, pe60.

Yamamoto, A., Taniuchi, S., Tsuji, S., Hasui, M., Kobayashi, Y., 2002. Role of reactive oxygen species in neutrophil apoptosis following ingestion of heat-killed Staphylococcus aureus. Clinical and experimental immunology 129, 479-484.

Ye, P., Rodriguez, F.H., Kanaly, S., Stocking, K.L., Schurr, J., Schwarzenberger, P., Oliver, P., Huang, W., Zhang, P., Zhang, J., Shellito, J.E., Bagby, G.J., Nelson, S., Charrier, K., Peschon, J.J., Kolls, J.K., 2001. Requirement of interleukin 17 receptor signaling for lung CXC chemokine and granulocyte colony-stimulating factor expression, neutrophil recruitment, and host defense. The Journal of experimental medicine 194, 519-527.

Yu, L., DeLeo, F.R., Biberstine-Kinkade, K.J., Renee, J., Nauseef, W.M., Dinauer, M.C., 1999. Biosynthesis of flavocytochrome b558 . gp91(phox) is synthesized as a 65-kDa precursor (p65) in the endoplasmic reticulum. The Journal of biological chemistry 274, 4364-4369.

Zarbock, A., Ley, K., 2009. Neutrophil adhesion and activation under flow. Microcirculation 16, 31-42.

Zhang, B., Hirahashi, J., Cullere, X., Mayadas, T.N., 2003. Elucidation of molecular events leading to neutrophil apoptosis following phagocytosis: cross-talk between caspase 8, reactive oxygen species, and MAPK/ERK activation. The Journal of biological chemistry 278, 28443-28454.

Zhang, W.W., Charest, H., Ghedin, E., Matlashewski, G., 1996. Identification and overexpression of the A2 amastigote-specific protein in Leishmania donovani. Molecular and biochemical parasitology 78, 79-90.

Zhu, X., Mulcahy, L.A., Mohammed, R.A., Lee, A.H., Franks, H.A., Kilpatrick, L., Yilmazer, A., Paish, E.C., Ellis, I.O., Patel, P.M., Jackson, A.M., 2008. IL-17 expression by breast-cancer-associated macrophages: IL-17 promotes invasiveness of breast cancer cell lines. Breast cancer research : BCR 10, R95.